

The Impact Response of Carbon/Epoxy Laminates

**(MSFC Center Director's Discretionary Fund Final Report,
Project No. 94-13)**

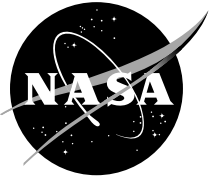
A.T. Nettles and A.J. Hodge

Marshall Space Flight Center, Marshall Space Flight Center, Alabama

Available from:

NASA Center for AeroSpace Information
800 Elkridge Landing Road
Linthicum Heights, MD 21090-2934
(301) 621-0390

National Technical Information Service
5285 Port Royal Road
Springfield, VA 22161
(703) 487-4650



The Impact Response of Carbon/Epoxy Laminates

A.T. Nettles and A.J. Hodge

Marshall Space Flight Center, Marshall Space Flight Center, Alabama

National Aeronautics and
Space Administration

Marshall Space Flight Center

TABLE OF CONTENTS

1. INTRODUCTION	2
2. PREVIOUS WORK	3
2.1 History and Background.....	3
2.2 Damage Resistance and Damage Tolerance	6
2.3 Key Findings of Past Research	6
2.4 The Effects of In-Plane Loading, N_x	19
3. ANALYTICAL.....	25
3.1 Energy Method	25
3.2 Finite Element Technique	30
3.3 Finite Element Results	31
4. EXPERIMENTAL	41
4.1 Material	41
4.2 Impact Specimens	43
4.3 Pretensioning Device	43
4.4 Impact Testing	45
4.5 Postimpact Testing	46
4.6 Static Indentation Testing	48
5. RESULTS	52
5.1 Instrumented Impact Testing	52
5.2 Visual Examination	60
5.3 X-Ray Inspection	61
5.4 Cross-Sectional Examination	63
5.5 Static Indentation Tests	73
6. DISCUSSION OF RESULTS	77
6.1 Instrumented Impact Testing	77
6.2 Visual Examination	78
6.3 X-Ray Inspection	79
6.4 Cross-Sectional Examination	81
6.5 Static Indentation Tests	81

TABLE OF CONTENTS (continued)

7. CONCLUSIONS AND RECOMMENDATIONS	86
7.1 Overview	86
7.2 Conclusions	86
7.3 Recommendations	87
8. SUMMARY	88
REFERENCES	155
APPENDIX A—Load-Deflection Data From Instrumented Impact Tests.....	89
APPENDIX B—X-Ray Signatures of Statically-Loaded and Impacted Specimens.....	104
APPENDIX C—Load-Displacement Curves From Static Indentation Tests.....	138
APPENDIX D—Strain-Gauge Readings From Static Indentation Tests.....	144

LIST OF FIGURES

1.	Top ply cracking due to contact stresses	7
2.	Cracking through other plies due to contact stresses	8
3.	Transverse cracks in adjacent 45° and 0° plies joined via delamination	8
4.	Schematic representation of cross-sectional view of transverse cracks and delaminations due to contact forces	9
5.	Schematic of cross-sectional view of bidirectional laminates	10
6.	Residual strength versus impact energy curve as predicted by Husman et al. ¹²	13
7.	Rapid reduction in residual strength as measured by Rhodes ⁵⁰	14
8.	Schematic of residual tensile strength versus impact energy for high- and low-velocity impacts	15
9.	Example plot of preload versus impact energy curve to demonstrate concept of a failure threshold curve	20
10.	Representative data from Avva ¹¹³	22
11.	Deflection, w_{max} , versus preload for constant values of transverse load, P , from equation (9)	29
12.	Load versus displacement for constant values of prestrain from equation (9)	29
13.	Plate geometry for the finite element model	31
14.	Finite element results for prestrain versus deflection at a constant transverse load	34
15.	Finite element results for displacement versus load for a constant value of prestrain	34
16.	Contour plot of transverse deflection for a transverse load of 223 N (50 lb) and no prestrain	36
17.	Contour plot of transverse deflection for a transverse load of 223 N (50 lb) and a prestrain of 6,000 $\mu\epsilon$	37
18.	Contour plot of transverse deflection for a transverse load of 2,003 N (450 lb) and no prestrain.	38

LIST OF FIGURES (continued)

19.	Contour plot of transverse deflection for a transverse load of 2,003 N (450 lb) and a prestrain of 6,000 $\mu\epsilon$	39
20.	Specimens used for impact testing	43
21.	Fixture to apply preloads	44
22.	Preload and impact apparatus	46
23.	Dam of plumber's putty to hold zinc iodide solution over damage area	47
24.	Maximum load of impact versus applied prestrain for 3.4 J (2.5 ft-lb) impacts	52
25.	Maximum load of impact versus applied prestrain for 4.5 J (3.3 ft-lb) impacts	53
26.	Maximum load of impact versus applied prestrain for 6.0 J (4.4 ft-lb) impacts	53
27.	Total time of impact versus prestrain for 3.4 J (2.5 ft-lb) impacts	54
28.	Total time of impact versus prestrain for 4.5 J (3.3 ft-lb) impacts	54
29.	Total time of impact versus prestrain for 6.0 J (4.4 ft-lb) impacts	55
30.	Maximum center deflection versus prestrain for 3.4 J (2.5 ft-lb) impacts	55
31.	Maximum center deflection versus prestrain for 4.5 J (3.3 ft-lb) impacts	56
32.	Maximum center deflection versus prestrain for 6.0 J (4.4 ft-lb) impacts	56
33.	Absorbed energy during impact versus prestrain for 3.4 J (2.5 ft-lb) impacts	57
34.	Absorbed energy during impact versus prestrain for 4.5 J (3.3 ft-lb) impacts	57
35.	Absorbed energy during impact versus prestrain for 6.0 J (4.4 ft-lb) impacts	58
36.	Load/displacement curve for lowest level impact at lowest prestrain	59
37.	Load/displacement curve for highest level impact at highest prestrain	59
38.	Typical x-ray signature for a specimen that exhibits no visible damage	61
39.	Typical x-ray signature for a specimen that contains back face matrix splitting	62
40.	Typical x-ray signature for a specimen that exhibits visible damage on the impacted side	63

LIST OF FIGURES (continued)

41.	Cross-section of specimen # Static #5	64
42.	Cross-section of specimen # 12/13B	65
43.	Cross-section of specimen # 12-14B, cut 1	66
44.	Cross-section of specimen # 12-14B, cut 2	67
45.	Cross-section of specimen # L6, cut 1	68
46.	Cross-section of specimen # L6, cut 2	69
47.	Cross-section of specimen # 12/12C, cut 1	70
48.	Cross-section of specimen # 12/12C, cut 3	71
49.	Cross-section of specimen # 12-14B, cut 2	72
50.	Load displacement from a statically loaded specimen at a low prestrain	74
51.	Load displacement from a statically loaded specimen at a high prestrain	74
52.	Load displacement from a statically loaded specimen (loaded until failure)	75
53.	Load displacement from a statically loaded specimen (loaded until failure)	76
54.	Schematic of bottom ply splitting and associated delaminations	79
55.	Stresses associated with back face matrix crack	80
56.	Load-deflection data comparison between equation (9), the finite element method, and static indentation for a prestrain of $4,000 \mu\epsilon$	82
57.	Prestrain-deflection data for a constant transverse load of 223 N (50 lb)	83
58.	Comparison of load-deflection curves for a static indentation specimen and an impact specimen both preloaded at $\approx 228 \text{ N/cm}$ (130 lb/in)	84
59.	Comparison of load-deflection curves for a static indentation specimen and an impact specimen both preloaded at $\approx 1,300 \text{ N/cm}$ (742 lb/in)	84
60.	Comparison of load-deflection curves for a static indentation specimen and an impact specimen both preloaded at $\approx 2,600 \text{ N/cm}$ (1,500 lb/in)	85

LIST OF TABLES

1	Calculated data from equation (9)	28
2	Results from the finite element analysis	33
3	Finite element results for stresses within plies	40
4	Specimens for static indentation tests	49
5	Specimens tested with associated parameters and results	60

TECHNICAL MEMORANDUM

THE IMPACT RESPONSE OF CARBON/EPOXY LAMINATES (MSFC Center Director's Discretionary Fund Final Report, Project No. 94-13)

1. INTRODUCTION

The term "composite materials" can be used to describe a host of different material forms used for a vast variety of final applications. The one common denominator for all of these materials is that two or more distinct phases of material are combined in a manner such that the resulting "composite" properties are more desirable for the application at hand than any of the constituents alone. One of these phases is usually called the matrix, which acts to hold together the composite material. The other major phase is commonly called the reinforcement. Composites generally fall into three major categories defined by the type of reinforcement phase: particulate, short fiber, and continuous fiber.

Particulate composites consist of particles (aspect ratio approximately less than 10) bound together by the matrix phase. The particles usually do not act as reinforcements for the matrix, but are commonly used as fillers (such as rocks in cement to make concrete) or to enhance properties other than strength (such as rubber particles in a brittle plastic to enhance the plastic's toughness).

Short fiber composites contain fibers with an aspect ratio of approximately 10:10,000. With the exception of most ceramic matrix composites (which use fibers for toughening), the fibers are the major load-carrying component of the composite material. This class of composites represents the most widely used and common composites, mainly due to what is commonly referred to as "fiberglass." Strictly speaking, fiberglass is glass that has been melted and drawn into fiber form, although the term "fiberglass" usually means chopped glass fiber in a polyester or other inexpensive resin matrix. This material has been widely used since the 1950's for components such as boat hulls, automobile bodies for sports cars, and recreational products such as surfboards, skis, and racket frames.

The use of continuous fiber-reinforced composites is growing at a rapid rate since the cost of materials and processing is decreasing. These types of composites make the most efficient use of the high stiffness and strength of the fibers used in them, and are usually what is being referred to when the term "advanced composites" is used. Some of the more common fibers used in this category are glass, carbon, and KevlarTM. Glass fiber-reinforced plastics (FRP's) have good tensile and compressive strengths and moduli but are heavier than carbon FRP's, which offer very high specific properties but are relatively weak in compression, limiting them to use in such tensile load-dominated structures as filament wound pressure vessels.

High strength can be achieved by aligning the fibers in the direction(s) in which the structural load(s) will be applied. However, for laminated (layered) composites (which are almost always plates or shells), there are no fibers in the through-the-thickness direction. This is the “Achilles heel” of laminated advanced composites since, on occasion, loads may get rather high in this direction.

Another problem with laminated FRP's is that the failure modes are multiple and complex. These modes rely on both true material properties as well as structural properties. A homogeneous isotropic material fails by a single flaw, propagating to failure, whereas composites fail as a result of a statistical accumulation of many flaws. Unlike composites, traditional homogeneous isotropic materials (metals, glass, unreinforced plastics, etc.) have the luxury of enjoying a mature database developed over many years for predicting the effects of damage. In addition, the homogeneous nature of these traditional engineering materials make them much easier to work with than composites, both analytically and experimentally. Further complicating the problem for composites is the large number of ply orientations that are used in composite structures. A database must be generated for each layup sequence used in a structure composed of laminated composites, which can become quite cumbersome.

Foreign object impact damage to laminated FRP is a loading condition in which all of the complex failure modes must be taken into account. Impact of laminated composites has been researched heavily in the past two decades but much remains to be understood. This research is summarized in the next chapter. The threat of foreign object impact to composites has hindered the use of laminates in many applications. Great strides have been made in developing higher strain fibers and tougher resins which are more damage-resistant and damage-tolerant than the early generation carbon fiber/resin systems. However, progress in understanding the effects of the many complex variables involved in an impact event needs to continue so that laminated composites can be used with even greater confidence. For the study presented here, continuous carbon fiber composites will be the focus, since the consequences of impact damage to these advanced composites pose the greatest threat. In addition, most primary load-bearing applications of advanced composites use continuous carbon fiber as the reinforcement in a polymer matrix resin, thus the emphasis on this class of material.

In chapter 2 a review of past studies on impact damage to composite laminates is presented. Most of the cited literature is from experimental studies so that a general consensus of the effects of foreign object impact damage to composite laminates can be made. This chapter is rather broad in range and is intended to give the reader a good basis for understanding many of the issues involved concerning impact to composite laminates. Chapter 3 presents a simple analytical assessment of the effects of in-plane loads to change impact responses of orthotropic plates with clamped-clamped/free-free boundary conditions. An energy-balance solution, along with a finite element assessment, is presented. Chapter 4 contains the experimental procedure used in this study and chapter 5 presents the results. A discussion of these results is presented in chapter 6. In chapter 7, some general conclusions from this study are presented along with some recommendations for future work. Finally, a summary is given in chapter 8.

2. PREVIOUS WORK

This chapter consists of three main parts and is intended to be a fairly thorough review of the general problem of foreign object impact to composites. Section 2.1 is a chronological presentation of some of the early work that laid the groundwork for the explosive growth of studies conducted in the past decade. Section 2.2 covers impact damage resistance/tolerance to laminated composites. Section 2.3 summarizes the most important features of past research conducted to date. Section 2.4 deals specifically with the thrust of this work and the response of impacted laminates due to a small change in boundary conditions.

2.1 History and Background

The first experiments on impact damage to composites were performed (quite naturally) on the first structural composite used—wood. In the early 19th century, ballistic-type impacts were studied by several western European naval forces in an attempt to determine the size and speed of a projectile that would maximize the damage to an oak ship hull.¹ As FRP came into use, the understanding of foreign object impact to this class of material became critical. The first experiments in the 1940's were ballistic-resistance tests since the major FRP of that time, glass reinforced polyester, was being used as secondary load-bearing components for military aircraft.² With the advent of “advanced composites” came the need to better understand the damage resistance due to a larger variety of types of impact, not just ballistic impacts.

Some of the first research into the effects of foreign object impact on advanced composites focused on the energy needed to inflict a certain level of damage, usually fracture or penetration. In the mid-1960's, glass fiber woven into cloth form, impregnated with polyester resin, was tested to determine the most efficient configuration to resist ballistic impacts.³ Lower velocity impact testing was originally performed using Charpy or Izod impact test machines, using beams made of laminated composites to determine what type of composite possessed the best damage resistance and what variables were responsible for energy absorption.⁴ This was a natural extension of the type of impact testing being conducted on metallic materials to determine a ductility index for brittleness. With this impact technique, the relative importance of the fibers, matrix, and interfaces on impact resistance and energy absorption could be determined. In using this type of test, it was found that the fiber strain to failure was of primary importance in determining a composite beam's impact resistance.⁵

As impact testing of composite laminates matured, test methods and analyses became more well defined. In particular, for test methods, instrumented impact and noncatastrophic testing became widely used and the analyses were broken down into dynamic response and quasi-static response impacts.

2.1.1 Instrumented Impact

By placing strain gauges, load cells, and/or accelerometers on the striker, load time, load deflection, and other measurements of the dynamic impact event can be made using this instrumentation. Instru-

mented impact testing has proven to be a valuable research tool in studying foreign object impact of composite laminates. The first instrumented impact tests were conducted by the British Welding Research Association to access the impact behavior of welded steel joints.⁶ Toland was among the first to use instrumented impactor techniques to study the progression of damage in a composite laminate beam.⁷ By utilizing the Charpy test, the importance in distinguishing between initial elastic failure energy and energy absorbed during the resulting failure process was noted. About the same time (early 1970's), Phillips and Tetelman published a paper demonstrating through instrumented Charpy techniques that linear elastic fracture mechanics could not be relied on for composite flaw analysis as it could in the analysis of homogeneous materials.⁸

2.1.2 Noncatastrophic Impact Testing

Through experience gained with composite laminates, it became evident that a major threat is damage that cannot be seen from the outside surface. Most of this damage is due to a foreign object impact event. Being a laminated material, the high shear stresses set up during an impact event can cause the layers to delaminate in the vicinity of the impact site. In addition, with the advent of the first generation carbon fibers (extremely brittle) as a reinforcement, FRP laminates no longer had the impact resistance of glass-reinforced laminates. Thus, noncatastrophic impact testing became increasingly prevalent in the mid-1970's. It is this type of testing that separated composite material impact studies from techniques used on metallic materials. Some of the first work involving noncatastrophic impact was performed on sandwich panels by Oplinger and Slepetz⁹ in which a steel ball was dropped onto panels with carbon/epoxy and glass/epoxy facesheets. The results clearly demonstrated the lower impact resistance of the carbon/epoxy facesheets. Other papers presenting results of the study of noncatastrophic impact to composites are found in reference.¹⁰ Of particular interest is a study that simulated turbine blade impacts with steel spheres (to represent rocks), ice (to represent hail), and gelatin (presumably to simulate birds).¹¹ This study classified the failure modes produced as transverse (matrix delamination and cracking), penetrative, or breakage of the specimen. When the damage was of the transverse type (noncatastrophic), the amount of damage was assessed using ultrasonic scans and cross-sectional photomicroscopy, two techniques used extensively today in the study of impact to composite laminates. In another study Husman et al.¹² examined the postimpact strength-carrying capabilities (residual strength) of impacted composite laminate tensile specimens. From the experimental data it was observed that the residual strength does drop as the impactor kinetic energy is increased and that glass fiber composites retained more of their initial undamaged strength than carbon fiber composites for a given impact level. Residual strength of impacted composites will be discussed further in section 2.3.3.

2.1.3 Dynamic Analysis

Since an impact event is time-dependent, that is, a load inflicted over a short period of time, it seems natural to use a time-dependent solution. This involves vibrations and stress waves set up in the material due to the impact event. This dynamic aspect of impact was examined, mostly analytically, fairly early among the impact studies. Moon¹³ used a time-dependent solution to determine the stress wave propagation due to impact in anisotropic fiber composite plates. The slowest (as well as fastest) stress waves were associated with a unidirectional layup and had a speed of slightly less than 2 mm/ μ sec (0.08 in/ μ sec), (the fastest wave was predicted to be almost 10 mm/ μ sec (0.4 in/ μ sec)). Thus, if the impact is of a short duration, the stress waves will not yet have reflected from the target boundaries and will become the driving force in determining the resulting damage. Mortimer et al.¹⁴ experimentally

measured the wave velocity in edge-impacted, cross-ply laminates as 7.38 mm/ μ sec (0.3 in/ μ sec), so the order of magnitude is that predicted by Moon. A previously mentioned reference 11 shows the duration of impact for a high-velocity event, on the order of 100 μ sec. This implies that for a 20-cm² (7.9-in²) specimen impacted at its center, the impacting projectile will be moving away from the target's surface just as the reflected stress wave returns to the center of the plate, assuming a wave velocity of 2 mm/ μ sec (0.08 in/ μ sec). In contrast, a typical low-velocity drop-weight test will be on the duration of 10,000 μ sec which gives ample time for the stress waves to decay away before the striker leaves the target.

Inertial effects, on the other hand, become important at much lower velocities than stress wave propagation effects. Inertial effects pertain to the energy needed to accelerate the out-of-plane deformations of the impacted plate's mass. During low-velocity/high-mass impact, the energy to do this is negligible compared to the strain energies involved, but at higher velocities, the plate's kinetic energy becomes more significant. Sun et al.¹⁵ developed a continuum theory for the dynamic behavior of layered composites which took into account the kinetic energy of the continuum. Greszczuk¹⁶ incorporated the mass of the target in his analytical solution of the impact of a sphere on an elastic half-plane. Results showed that a higher target mass will give rise to higher impact forces and contact deformations (deformation of the upper surface of the target right below the impactor). Global deflections were not accounted for in this model. For thick laminates, it has been shown that global deflections can be ignored since they are so small and the material response is governed almost solely by contact stresses.¹⁷ Inertial effects are also important in that the inertia of the plate and projectile can interact and cause multiple impacts.

2.1.4 Quasi-Static Analysis

For low-velocity impacts, many of the analyses are done as quasi-static, ignoring all time-dependent behavior of the event and inertial effects of the material. In essence, this analysis is that for a "static indentation" case in which the plate is loaded in increments of force over an essentially infinite period of time. Practically, this is carried out in a material loading frame. In one of the early studies, Oplinger and Slepetz⁹ performed both low-velocity drop-weight and static indentation tests on graphite/epoxy and glass/epoxy sandwich panels and found that the resulting damage was similar. Similar results were obtained more recently by Kaczmarek and Maisson¹⁸ for quasi-isotropic and bidirectional carbon/epoxy plates.

In the analytical approach discussed in reference 19, it was seen that a quasi-static event is defined by the lowest natural frequency ratio of the impactor and target, regardless of their mass ratios and impactor velocity. However, for most practical purposes, high-velocity projectiles are small objects with high natural frequencies which will produce a dynamic response; low-velocity impacts are really of interest only when the impactor mass is large and its natural frequency is low, which will produce a quasi-static response.

Swanson²⁰ has developed a procedure based on the impactor mass and the "equivalent lumped mass" of the target which is not inconsistent with the work in reference 19. He showed that if the impactor mass is more than 10 times greater than the target's "lumped mass," then the impact event can be considered quasi-static. For various plates and beams of different boundary conditions, the "lumped mass" was seen to be no more than one-half the entire plate or beam mass. Thus a crude, but effective, rule of thumb is that the impactor must be more than 20 times the target mass for the impact event to be

considered quasi-static. However, boundary conditions can affect this rule if the specimen is supported such that it is stiff in flexure. Highsmith²¹ found that quasi-static results produced slightly more damage than impact events of similar maximum load. The specimens in his study were 20 plies thick and clamped over a 6.35-cm- (2.5-in-) diameter opening.

Jackson and Poe²² demonstrated that impact force alone can be used to quantify an impact event for a given material and layup but only when the impactor mass is large and the velocity is low. In their study it was found that the maximum delamination damage area was a linear function of the force of impact whether the force was introduced by falling weight or static indentation tests. Furthermore, the support diameter of the impacted plate had no effect on the delamination size when impact force was used to quantify the event. However, for large plates, deviation from quasi-static behavior was noted since the stress waves set up by the impact event took longer to travel the length of the specimen and reflect back from the boundaries, resulting in some dynamic effects.

2.2 Damage Resistance and Damage Tolerance

Damage resistance and damage tolerance are two distinct and completely different aspects of impact damage to laminated composites. *Damage resistance* refers to the composite material's ability to minimize matrix cracking, delamination, and fiber breakage due to an impact event. *Damage tolerance* refers to a material's ability to retain its desired properties once damage has been incurred. This is usually referred to as "residual" properties.

During an impact event, many parameters determine a material's damage resistance. Structural parameters such as boundary conditions and the stress state during impact can greatly affect a laminated composite's damage resistance. It is the intent of this study to assess the damage resistance effects of a tensile stress state being applied to the target during an impact event. This will usually be referred to as a "tensile preload" throughout the remainder of this paper. Tensile prestress and tensile prestrain will also be used but implies the same physical phenomena.

2.3 Key Findings of Past Research

The following review concerns only fiber-reinforced laminated plastics being transversely impacted by a foreign object. The types of damage incurred during an impact event will be examined and the effect that the stacking sequence has on this damage will be investigated. The next extension of the impact problem involves residual load-carrying capabilities of the damaged laminate. A discussion of how different fiber/resin systems and boundary conditions can affect the amount and type of damage induced in an impacted composite will then be examined. Finally, a very important topic to those working with actual structures made of reinforced plastics, scaling from laboratory specimens to larger entities, will be discussed.

2.3.1 Damage Modes

There are three major modes of damage that can be incurred during foreign object impact events. These are matrix cracking, including fiber/matrix debonding; delamination; and fiber breakage. The formation and extent of these damage modes are heavily dependent upon specimen geometry, or more precisely, the ability of the impacted structure to deform. For relatively stiff structures, contact forces will dominate, and for flexible structures, in-plane forces will dominate due to global bending. The contact force generated by the impactor, if sufficiently large, can cause transverse matrix failure in the impacted ply and/or those beneath it parallel to the direction of fibers in each ply, due to the high shear stresses, τ_{yz} , that are set up (shown schematically in figure 1).

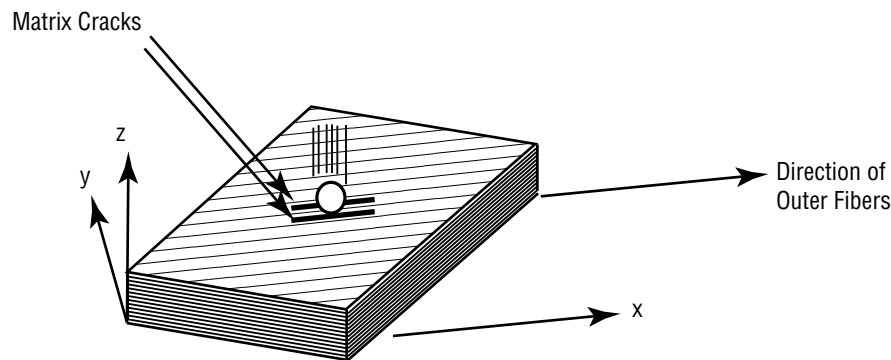


Figure 1. Top ply cracking due to contact stresses.

As the impactor drives itself into the specimen, the material from the top ply tends to spread the load over a wider diameter, producing matrix cracks slightly away from the impact site in the next-to-the-top ply. As these transverse cracks develop, they become wider apart through the thickness as shown schematically in figure 2. These transverse cracks usually join one another through the acute angle with the adjacent ply via delamination, shown schematically in figure 3. When cross-sectioned, the transverse cracks and delamination will form a characteristic cone shape as noted in references 23–27 (shown schematically in figure 4). The through-the-thickness assimilation of the delaminations will give the characteristic “stair-step” shape, noted in references 28 and 29.

For composite laminates that experience large deformations during an impact event, large in-plane stresses can cause damage to form. The intrinsic weakness of a ply perpendicular to its fibers causes the bottom plies of heavily deformed laminates to split along the fibers in that ply, due to the high tensile strains from bending. The transverse shear in the plate will be at maximum near the center of the plate and it has been observed that this region contains the planes of largest delaminations, except when spalling occurs on the nonimpacted face, after an impact event.²⁹

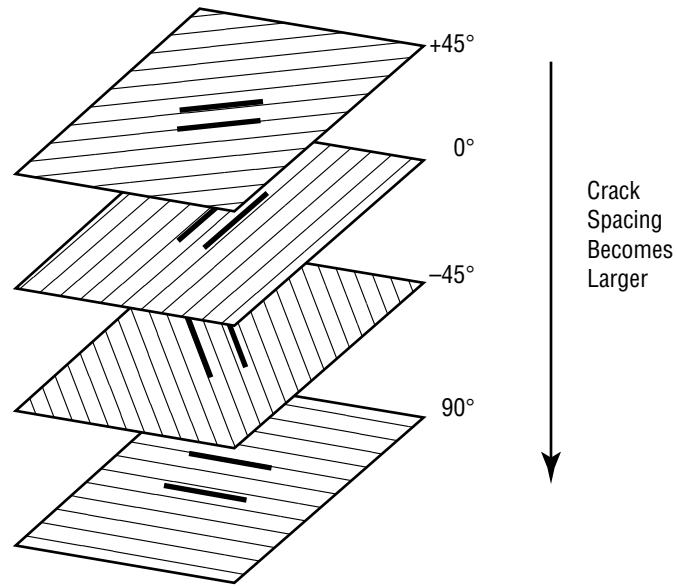


Figure 2. Cracking through other plies due to contact stresses.

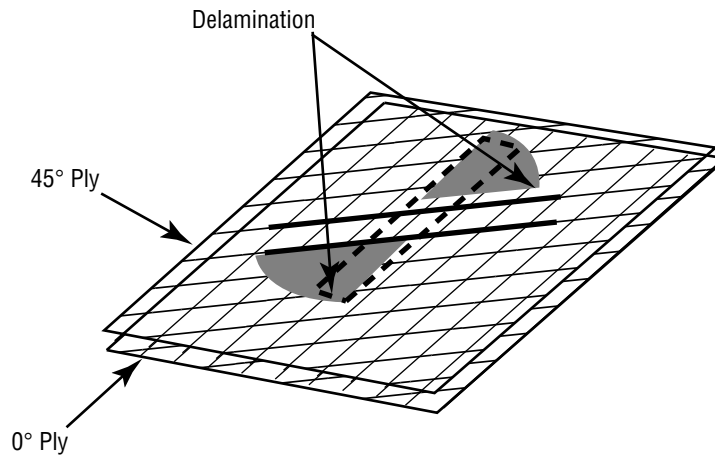


Figure 3. Transverse cracks in adjacent 45° and 0° plies joined via delamination.

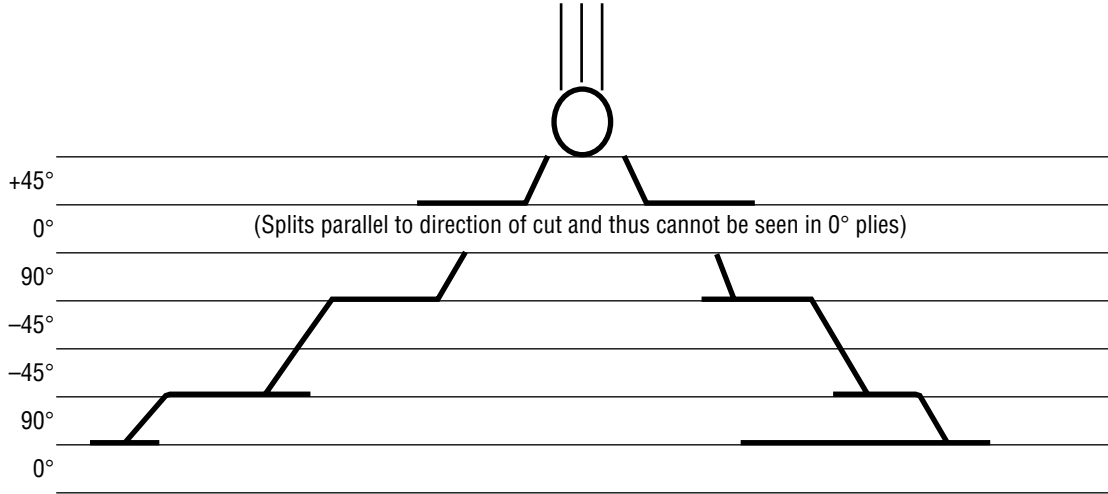


Figure 4. Schematic representation of cross-sectional view of transverse cracks and delaminations due to contact forces.

By using simple bidirectional layups (fibers aligned only in the 0° and 90° directions) and examining the resulting matrix cracking and delamination, more insight is given into the problem of damage development in impacted composite laminates. In tests by Chow et al.,³⁰ for $[0_n/90_{16-2n}/0_n]$ ($n=6$ and 7) stacking sequences, damage was seen to form as matrix cracks in the 90° plies with extensive delamination between the 0° and 90° plies (when sectioned parallel to the 0° plies). Smaller matrix cracks were observed in the 90° plies that did not join with the delamination, thus all matrix cracks do not end in delamination propagation. In these tests, delamination was observed directly under the impact site, indicating that flexural behavior is responsible for this growth. These experiments were unique in that the laminates were supported as wide beams (plates clamped-clamped/free-free) and impacted by a line nose impactor rather than the conventional spherical-shaped nose impactor. Thus, cracking in the 0° plies was limited since bending and deformation were only longitudinal to the fibers in these plies. A spherical-shaped nose impactor typically causes the laminate to deform in a “bowl” shape, causing matrix splitting between fibers in all of the plies. By dispersing the plies more in a $[0_3, 90_3, 0_3, 90_3, 0_3, 90_3, 0_3]$ layup, it was found that matrix cracking still occurred in all of the 90° plies but the delaminations between the 0° and 90° plies became progressively smaller from bottom to top.

A finite element analysis of delamination growth from matrix cracks was given in reference 31. It was demonstrated that normal stresses develop at the matrix cracks that are tensile on the *upper* interface *toward* the impacted side and tensile on the *lower* face *away* from the impact site. Thus, delaminations are predicted to grow toward the impact site on the upper interface and away from the impact site on the lower face, producing larger delaminations near the bottom plies when bending is the governing stress producer.

These findings were verified for quasi-static loading of bidirectional laminates in three-point bends while observing a polished edge in reference 32.

An experimental microstructural analysis of impacted $[0/90/0_4]_s$ and $[0/90/\bar{0}]_6$ revealed that the more $0/90$ interfaces in a laminate, the smaller the delaminations.³³ In addition, delamination growth appeared to grow only away from the impact site on the bottom interface of the $0/90$ boundary. No trans-

verse cracking was observed in the 90° plies and the delaminations were observed only at every other layer. The authors attributed this to the processing of the panel, but as demonstrated in figure 5, this is due to the nature of how the specimen was sectioned coupled with how the delaminations form as shown in figures 1–3.

For high-velocity impact loading, arguments have been given that the tensile stress waves are responsible for matrix cracking on the upper surface of an impacted composite.³⁴ Evidence was also given that matrix cracking and delaminations interact simultaneously since matrix cracking was not observed in delaminated areas in interfaces away from the impacted side of a bidirectional composite.

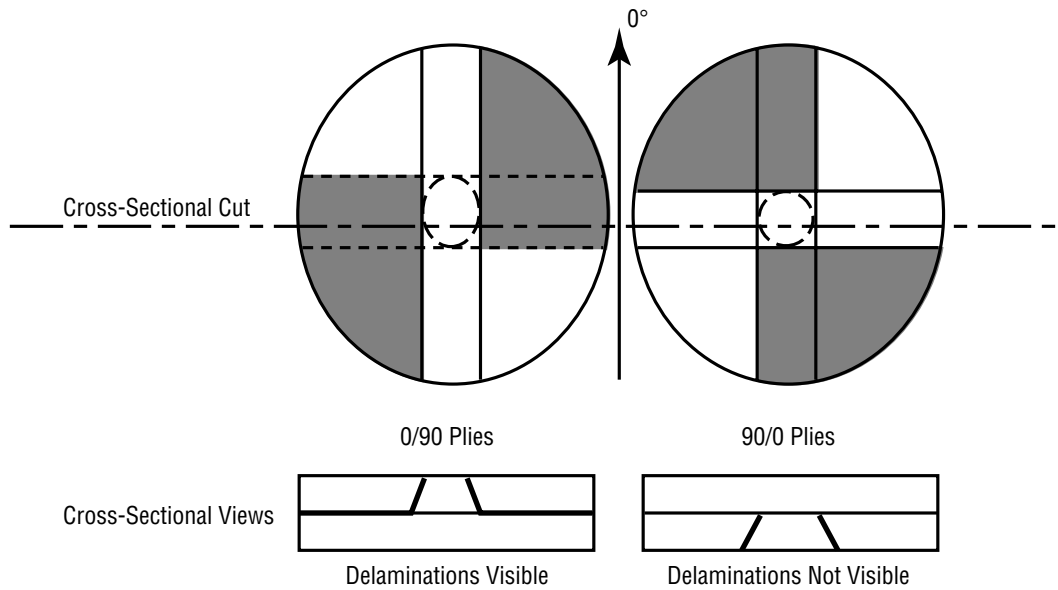


Figure 5. Schematic of cross-sectional view of bidirectional laminates.

The process of delamination formation being the result of bending stiffness mismatch between plies of different orientation was given by Liu.³⁵ He proposed a bending stiffness mismatching coefficient that would qualitatively give the size and shape of the delamination, resulting from the differences in the D_{11} terms of adjacent plies. The shape was seen to be of a “peanut” type, mathematically a lemniscate. The size was seen to increase as the angle between plies approached 90° . However, a host of empirical data^{28,29, 36–42} shows that the characteristic shape of delaminations between plies is mostly governed by matrix cracks and the lemniscate has a significant magnitude in the 45° direction, whereas it is predicted by Liu to be zero in this direction.

Fiber failure occurs in laminates experience seeing such large contact stresses that surface fibers are broken or such large bending stresses as to exceed the strength of a lamina in the direction of the fibers. A detailed discussion with empirical data for fiber breakage in a laminate due to large deflections is given in reference 43. This study showed that the onset of fiber breakage was in laminae near the bottom of the plate.

2.3.2 Stacking Sequence

Stacking sequence of the laminate is very important in determining the mode and size of damage due to foreign object impact; thus, the residual performance of the structure. For structures which experience high contact stresses, it has been shown⁴⁴ that placing nonload-bearing fibers on the outer plies of the laminate to protect the load-bearing 0° plies is advisable. However, as Cantwell et al.⁴⁵ suggested outer 0° plies would increase the elastic energy absorption capacity by increasing the flexural stiffness. When examined from a damage-tolerance point of view, Cantwell et al.⁴⁵ showed that the residual compressive strength of a composite with the load-bearing 0° fibers away from the surfaces and not next to the outermost delamination was larger than specimens that had outer 0° fibers that delaminated from the angled ply next to them. The delaminated 0° outer plies could easily buckle away from the rest of the laminate and the strength effect of these fibers would then be lost.

From a damage-resistance point of view, Kwon and Sankar²⁷ examined $0/90$ bidirectional and $\pi/4$ and $\pi/8$ quasi-isotropic stacking sequences. Results showed that initial damage due to transverse loading occurred relatively early in the $\pi/8$ laminates but this damage did not cause as drastic a load drop (as measured by instrumented impact) as the other two layups. This is because transverse cracks between plies of different orientation have a smaller angle between them in the $\pi/8$ laminates and the resulting delaminations that form between these cracks between plies (see section 2.3.1) sweeps out a smaller area which requires less energy. The bidirectional laminates have a full 90° between ply orientations and the delaminations between cracks in adjacent plies in these laminates must sweep out the largest area of any stacking sequence, therefore, the large load drop due to the formation of these large delaminations. In this study,²⁷ cross-sectional examination of the damaged laminates revealed that the bidirectional laminates contained the most massive and numerous delaminations followed by the $\pi/4$ and then the $\pi/8$ laminates.

By stacking a laminate such that the number of grouped plies of equal orientation is at a minimum, increases the interfaces at which a delamination can occur (delaminations do not form between plies of equal orientation). This was shown to reduce the overall damage area in references 46 and 38 since the laminates with less ply interfaces at which delamination could occur produced larger delaminations between the plies that could delaminate in order to dissipate the same amount of energy. For bidirectional laminates it has been shown⁴⁷ that dispersing the plies of different orientation significantly increases a laminate's impact resistance (as measured by impact energy to produce initial damage) and that increasing the number of 0° plies on the outer surfaces increases a laminate's compressive damage tolerance by increasing the buckling resistance of the sublaminate on the critical outer plies.⁴⁸

For honeycomb sandwich panels,⁴⁹ it was found that the facings would experience less delamination than equivalent laminates and that contact forces dominate since bending is restricted on the facings of sandwich panels due to the existence of the core. This was supported by data which showed that at low impact, energies that did not cause large laminate deflections (and were thus contact stress-dominated), facings and equivalent laminates had approximately the same total delamination areas, but as the impact level increased to cause large deflections of the laminates, the facings would experience a smaller, total delamination area since the large bending stresses in the laminate caused larger delaminations than those caused by contact stresses. It was also found in this study that layups with large angular orientations between plies (e.g., 90°) tended to cause a larger total delamination area *across all of the ply interfaces* (through-thickness) compared to layups that had 45° as the largest angular orientation between plies.

2.3.3 Residual Tensile Strength

In this and the following section, the effects of incurred impact damage on composite laminates is assessed by examining residual strength (tension or compression), a measurement of the composite's damage tolerance. While some papers will present results as plots of residual strength versus damage area (thus isolating the damage tolerance response), many others show results on residual strength versus impact energy plots which actually serves to effectively combine the impact resistance and damage tolerance portions of the impact event.

Once damage has been introduced into a composite laminate, the critical question is how the damage will affect the desired properties of the material. Measurements and predictions of residual strength have seen extensive research, especially since the early 1980's. Much of this work has concentrated on compression-after-impact (CAI) strength since impact events cause delaminations which can lead to a lower compressive strength due to the localized instability caused by the delaminations (this will be discussed in the next section). However, many load-bearing composite structures will be dominated by tensile forces (such as pressure vessels), so this aspect of the impact problem also needs to be examined.

Husman et al.¹² were among the first to investigate and attempt prediction of the residual tensile strength of impacted coupons. The residual strength prediction was based on an analogy with an inserted flaw of known dimensions and a stress intensity factor for an isotropic material. As a result it was predicted that the residual strength would drop off in proportion to the square root of the impact energy of the projectile. It was noted that departure from this analysis will occur as the specimen experiences complete penetration. Graphically, the residual tensile strength versus impact energy curve as predicted by Husman et al. is given in figure 6. Limited data were given to support this analysis and since ballistic-type impacts were used, the fibers on the impacted surface (which were 0° plies) may have broken at low impact energies (but still high velocities), yielding a drop in residual at the lowest impact energies used in this investigation.

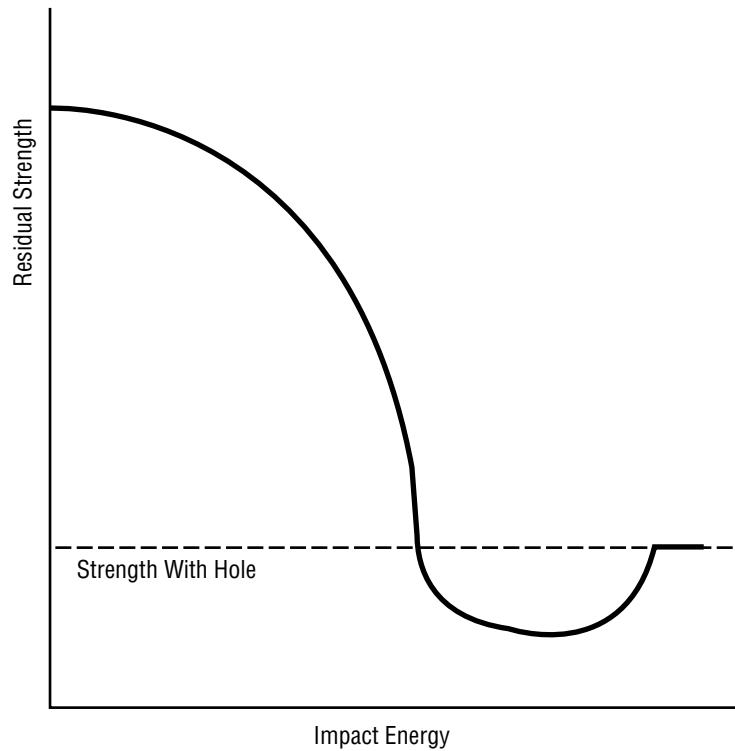


Figure 6. Residual strength versus impact energy curve as predicted by Husman et al.¹²

This study also suggested that the width of the specimen be at least six times the diameter of the projectile in order to minimize damage zone/edge interaction. This is an important factor to consider when evaluating residual strength on laboratory specimens. For example, one researcher may impact 2.54-cm-wide (1-in-wide) specimens while another performs identical impact tests on 15.24-cm- (6-in-) wide specimens. If the damage zone is 2.54 cm (1 in) in both specimens, then the narrower specimens will register a much lower residual strength (possibly zero; i.e., catastrophic failure) than the wider specimens which possess undamaged material around the damage zone to help carry the load. Thus, if a structure is larger than the coupons used to perform the impact damage characterization on it, then the coupons need to be of sufficient width so that free-edge stress/damage zone interactions do not occur. In addition, if the damage zone is a sizable percentage of the specimen width, then the cross-sectional area rendered ineffective due to damage must be removed from the residual stress calculations. This is an argument for measuring residual strain which eliminates needing to know the cross-sectional area rendered ineffective to carry load.

Data by Rhodes,⁵⁰ also generated by ballistic-type impacts, seems to support the notion that both residual tensile and compressive strengths drop rapidly from the undamaged strength even at the lowest impact energies tested (fig. 7). It is worth noting that these data were from honeycomb sandwich panels whose composite facesheets undergo smaller deflections (due to the backing rigidity of the core), resulting in a more localized damage which includes more fiber breakage.

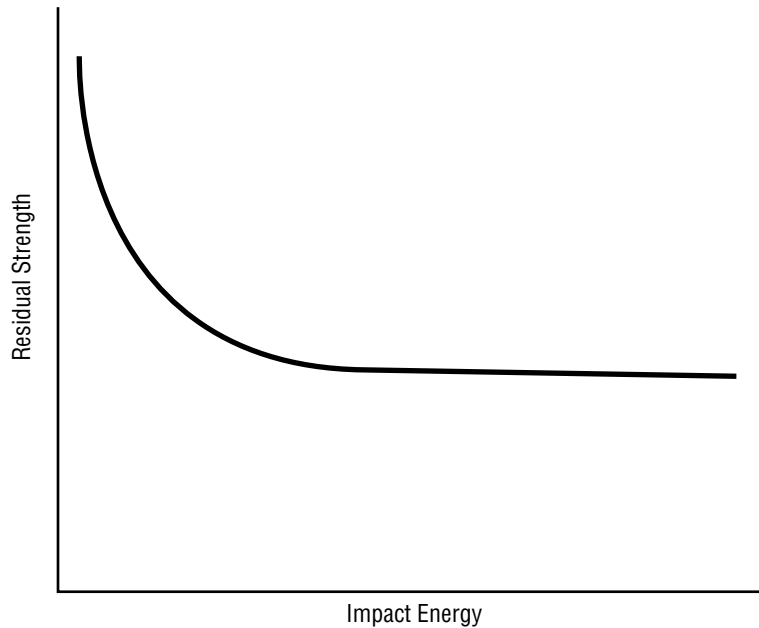


Figure 7. Rapid reduction in residual strength as measured by Rhodes.⁵⁰

Other studies have shown that for high-velocity impacts, the residual tensile strength does indeed begin to drop quite rapidly at the lowest impact energy levels tested.^{51–54} A study by Cantwell and Morton²⁶ contained residual tensile strength data for eight-ply specimens in which the tensile strength did not begin to drop off until a critical impactor kinetic energy was obtained. Cairns⁵⁵ also found that there existed a plateau region of residual strength before degradation for 12-ply carbon/epoxy specimens. This study also showed that for equivalent energy, higher velocity (smaller mass) projectiles, the residual strength began dropping off much more rapidly, indicating that the plate's inertial effects become more important at higher velocities, as pointed out in section 2.1.3.

Lower velocity impacts, such as drop-weight tests, generate a different material response than high-velocity impacts, as mentioned in sections 2.1.3 and 2.1.4. Therefore, it may be expected that the residual tensile strength response may differ. Comparisons of equal energy high- and low-velocity impacts have been conducted by Adsit and Waszczak⁵⁶ and Dorey.^{44,57} In reference 56, carbon/epoxy facesheet honeycomb panels were impacted at low velocities with drop weights and at high velocities utilizing a compressed air gun to project small granite stones. A plot of residual tensile strength versus impactor kinetic energy shows that the strength reduction begins at a lower level of impact energy for the high-velocity stones and also drops off at a faster rate with increasing impactor kinetic energy for the higher velocity tests. In reference 44, the residual strength is seen to drop at a smaller impact energy for ballgun impacted specimens, but once a decrease in strength is seen, it is more rapid for drop-weight tests. This trend is shown schematically in figure 8. This effect is much more pronounced for residual flexural testing as seen in reference 56. The type of resin used can have an effect on these results, as discussed in section 2.3.5.

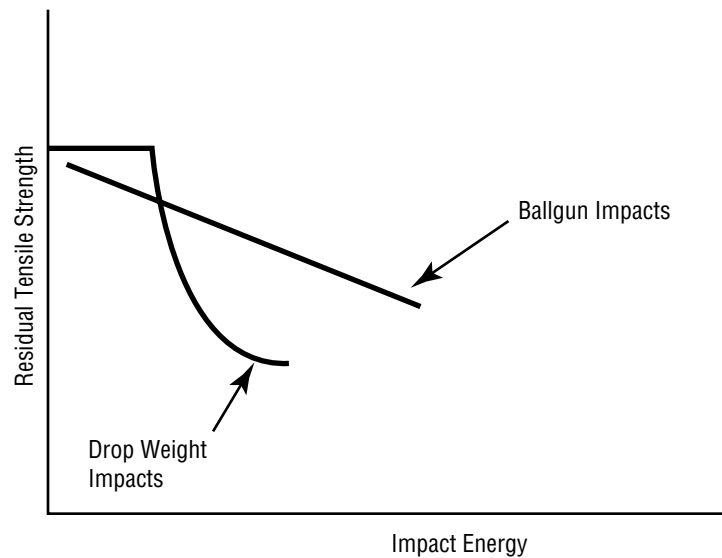


Figure 8. Schematic of residual tensile strength versus impact energy for high- and low-velocity impacts.

Low-velocity impact tests with resulting residual tensile strength tests show that, for most cases, a region of impact energies where strength degradation does not occur is readily apparent. This phenomena is seen in data by Cantwell et al.,^{45,58} Dorey et al.,⁵⁹ Morton and Godwin,⁶⁰ Caprino,⁶¹ Nettles,⁶² Bishop,⁶³ Lal,⁶⁴ and Poe.⁶⁵

However, once strength degradation does occur, the residual strength usually decreases rapidly with increasing impactor kinetic energy, depending upon the material and geometry of the impact event. For example, specimens supported as short beams^{60–61} or as small diaphragms⁶² experience a high level of contact stresses immediately below the impactor, thus breaking fibers and causing a rapid reduction in residual tensile strength. Specimens supported over larger areas, such as in references 59 and 64, demonstrate a more gradual decrease in residual tensile strength with increasing kinetic energy since the large elastic deformations can absorb much of the incident impactor kinetic energy and local contact forces under the impactor are less severe. The effects of boundary conditions will be examined further in section 2.3.6.

2.3.4 Residual Compressive Strength

Residual compression strength after impact has drawn much more interest than residual tensile strength since laminates have been shown to be much more susceptible to this type of loading. The impact event can cause delaminations within the material which cannot be seen from the surface, yet can severely reduce the CAI strength of the composite structure. While the tensile strength of a composite laminate is fairly dependent on the test sample's geometry, compression testing of laminates is virtually a complete structural test as opposed to a true material test. Thus extreme caution must be used when examining data from CAI tests and direct comparisons between studies is virtually impossible. Therefore, only general observations will be made based on the results of some of the findings of past research on this topic.

In low-velocity impact studies where both residual tensile and compressive strengths were tested, the residual compressive strength always fell at a faster rate than the residual tensile strength.^{44, 45, 57, 60, 63, 66} Rhodes⁵⁰ presented data for projectile-type impacts that showed the residual tensile strength decreasing at a slightly faster rate than the residual compressive strength. These results are because a specimen will lose tensile strength only when load-bearing fibers are broken, but compressive strength can drop due to delaminations. In most test programs the specimens are supported such that matrix cracking and delamination will occur before any fibers are broken. Broken fibers without delaminations only occur in thick specimens, or in ballistic-type impacts, in which the specimen does not have time to deform and create the high interlaminar shear stresses that cause delamination.

For low-velocity impacts (drop weight), the characteristic shape of the CAI versus impact energy curve is heavily dependent upon the specimen material and geometry. In a study by Prichard and Hogg,⁶⁷ carbon/epoxy and carbon/polyetheretherketone (PEEK) specimens were supported over a relatively small, clamped annular opening to induce delamination-type damage. The resulting CAI versus impact energy curves show that the compression strength of the carbon/epoxy dropped off extremely rapidly whereas the curve for carbon/PEEK gradually dropped off with increasing impactor kinetic energy, almost in a linear fashion. The same results were found in references 60 and 68 for specimens clamped with a larger annular diameter support, although the carbon/epoxy CAI strength did not drop off quite as rapidly. In general, it has been shown that for a wide range of carbon/epoxy specimen geometry and CAI test methods, the CAI strength falls rapidly for increasing impactor kinetic energies at the lower level of impact energies until a plateau or modest linear decrease zone is reached.^{44, 45, 61, 63, 66, 69–75}

For high-velocity- (projectile-) type impacts the CAI strength versus impact kinetic energy curve does not possess as drastic a drop in CAI strength with increasing impactor kinetic energy as shown in references 50, 52, 76, and 77. This is mainly because the much more localized response of the high-velocity impacted specimens in which delamination tends to be extensive through the thickness, but not as widespread in areas such as lower velocity-impacted specimens. Thus, the lower velocity-impacted specimens contain a larger delamination area, causing a larger reduction in structural stability of the test coupon than the smaller delaminations formed by higher velocity impacts. This notion is supported by data in reference 78 in which the CAI strength of specimens impacted with high- and low-velocity impactors did not vary a great deal when plotted versus damage width, but were different when plotted versus impact energy.

From drop-weight impact data, Prichard and Hogg⁶⁷ showed that when plotted as a function of damage width, the residual compression strength of two very different laminated composite materials (epoxy and PEEK matrices) were the same. Similar results were obtained by Teh and Morton⁶⁸ and Dempsey and Horton.⁷³ However, other studies⁷⁹ have shown that a specimen of one type of material may have a much larger damage zone than another type of material impacted under identical conditions, yet have a higher retention of initial compressive strength. Indeed, if the residual strength versus damage size plots were similar for all materials, then this would imply that there is no difference in the damage tolerance of laminated composites, only a difference in damage resistance.

Of practical importance for composite structures that see multiple impacts at nearby sites (such as during a hailstorm), Jones⁸⁰ showed that the CAI strength was unaffected by the multiple impacts as long as they were approximately one damage zone diameter apart (i.e., the impact sites do not interact when spaced apart by at least one diameter of damage zone).

2.3.5 Fiber/Resin Systems

Of the most interest to designers and end users of composite structures are which fiber/resin systems are the most damage resistant, or more importantly, damage tolerant. Since the chosen fiber/resin system is a variable that can be controlled from the onset of design, this information is vital to any program utilizing laminated composites. In the past decade, a concentrated effort has taken place within the industry to produce fibers with higher strain to failures and matrix resins that better resist cracking and delaminations. More exotic techniques such as stitching or using three-dimensional preforms,^{81–85} interleaving,^{86–88} and using hybrids (more than one fiber type)^{36, 89–95} have been investigated, although they have not yet seen widespread usage.

The toughness of the matrix resin can severely affect the damage resistance/tolerance of laminated structures. A direct comparison of thermoplastic and thermoset resins usually shows that the thermoplastic matrix material is more damage resistant. The most promising high-performance thermoplastic resin is PEEK which has been studied extensively in damage-tolerance programs. A comparison of PEEK with epoxy resin composites was made by Dorey et al.⁵⁹ and Demuts and Sharpe⁹⁶ and showed that the PEEK laminate was much more damage resistant (as measured by C-scanned damage area), resulting in greater retention of CAI strength. In reference 59, for the highest impact energies used (8 J), the carbon PEEK had about one-fourth of the damage area as the carbon/epoxy tested. When compared to another thermoplastic such as polyphenylene sulfide (PPS),⁹⁷ PEEK was still more damage resistant with about a 50-percent smaller delamination size for the highest impact energies tested.

By plotting CAI strength versus damage size for carbon/epoxy and carbon/PEEK laminates and obtaining similar results,⁶⁷ it follows that the superior CAI resistance of the PEEK laminates is due mainly to the smaller delamination area formed for a given impact energy level. This is further supported by work performed on a number of toughened epoxies and bismaleimide (BMI) resins in which the CAI strength was found to correlate strongly with mode II interlaminar fracture toughness.⁹⁸ Mode II fracture resistance controls the amount of delamination that forms during an impact event whereas the CAI strength is strongly controlled by mode I peeling as the delamination grows.

Although thermoplastics such as PEEK have distinct advantages over thermoset resins, these materials require a high temperature and pressure to cure the plies into a laminate. Furthermore, lack of any tack and little drape make further processing complicated. Until more advanced processing methods are found, thermosets will continue to dominate the resins in use on composite structures; thus, mechanisms for making existing thermosets tougher has seen much activity. The two principle methods of toughening thermosets is by modifying these resins either with elastomeric particulates or by blending in a controlled amount of thermoplastic resin. Both methods can substantially increase a laminate's toughness and modified resins of both type are commercially available and in wide use. Damage resistance/tolerance comparisons of some of these resins have been made in a number of studies.^{53, 75, 79, 99}

2.3.6 Boundary Conditions

Another critical factor that determines the amount of damage that a composite laminate will experience due to a foreign object impact event is the laminate's geometry and boundary conditions. For high-velocity impacts, the boundary conditions of the target are less important than the areal mass of the target in determining the impact response¹⁰⁰ (unless stress waves account for damage). The impactor has already rebounded from, or penetrated the target by the time the stress response reaches the edges of the target specimen; thus, boundary conditions are much more critical for lower velocity impacts. Cantwell and Morton¹⁰¹ showed that for a given target thickness, the increase in energy required to cause initial damage and to cause perforation for impacted beams, was roughly proportional to the increase in beam length. It was also shown in this study, that for a given impact energy, lengthening the beam caused the beam to experience larger deflections, thus storing more of the energy as elastic energy and reducing the size of the damage zones. Kwon and Sankar²⁷ demonstrated that if the delamination size is plotted as a function of maximum load of impact, then the specimen support size effect is eliminated, since larger supports allow larger deflections and thus lower impact forces. In a study by Verpoest et al.,¹⁰² the size of the support was shown to be more important than the shape. Another aspect of the varying response of the target, due to support geometry, is where the majority of damage is most likely to form. For specimens supported in a smaller geometry, the top surface will experience higher contact stresses and thus more damage will form at this location than on a similar target, only with larger geometrical boundaries, which will experience bottom surface splitting/fiber breakage due to the larger bending stresses that are present.¹⁰³

Also of importance is how the specimen is supported at its boundaries (i.e., clamped, simply supported, etc.). The same general rule of thumb applies here also. If the boundary conditions restrict the specimen from deforming, then the damaging stresses will migrate more from bending type to contact type. This was shown analytically by Shivakumar et al.¹⁰⁴

Another critical aspect of the impact event, the shape of the impactor, has seen relatively little attention. Various sizes of hemispherically ended impactors have been used, but other geometries of impactor were studied by Poe.¹⁰⁵ This study was conducted on thick sections of graphite epoxy that simulated a section of a rocket motor case. Impactors of two different hemispherically ended radii—a sharp, bolt-like rod—were used. The corner-type impactor caused very high localized Hertzian contact pressures, producing visible damage earlier than the hemispherical indentors. The cylindrical bolt-type indenter acted like a punch, slicing through the upper layers of the laminate. The shape of the impactor will have a much greater effect on laminates which are relatively stiff, since the Hertzian contact pressures are more important for this type of impact event.

2.3.7 Scaling of Impact Damage

The ultimate goal of the vast amount of research that has been conducted on impact-to-laminated advanced composites is to be able to predict the effects of a foreign object impact event to a full-scale composite structure. Since this can turn into a very expensive program, laboratory-size specimens must be used and the results scaled to those of larger structures. The problem of scaling impact damage to composites has been investigated by Morton.¹⁰⁶ Morton used the principles of similitude and pointed out, that for most practical cases, complete similarity between “model” (coupon) and “prototype” (full scale) is rarely possible when rate- or notch-sensitive materials are involved. For composite laminates,

the problem is further complicated since the fiber diameter and lamina thickness should ideally be variable to accommodate scaling. In practical applications, this is virtually impossible. Test results on impact of composite beams showed that classical scaling laws apply for elastic behavior of the beams (i.e., before damage is induced) but significant deviation was observed as damage was induced into the specimen with the smaller specimens always stronger than the scaled-up ones. Swanson¹⁰⁷ has also examined the scaling effects of impact damage to composite laminates and found that delamination damage was dependent upon the absolute specimen size, whereas, fiber breakage was not. Thus, the effects of scaling must be different for different failure modes.

For delamination damage, Bucinell et al.¹⁰⁸ tested laminated plates of scaling factors 1, 2, and 4 and showed that the response followed an inverse square root of the scaling factor. The response measured was the percentage of laminate area delaminated as detected by ultrasonic C-scans. The impact parameters and responses were scaled according to the development of Morton.¹⁰⁶ It was also demonstrated in this study that quasi-static and dynamic impact events of equal energy scale similarly.

Through finite element analysis, Chen et al.¹⁰⁹ showed that the stress concentration due to a damage zone is concentrated around that zone and local stress distributions between test coupons and stringer-stiffened panels were similar. Thus, the measured differences in CAI strength in which the larger panels retained more strength¹¹⁰ is due to the larger panels experiencing less damage for a given impact energy per unit thickness.

2.4 The Effects of In-Plane Loading, N_x

A limited amount of research into the effects of tensile or compressive preloads on the impact response of composites has been performed. Olster and Roy¹¹¹ performed ballistic penetration tests on tensile preloaded graphite/epoxy plates and found that the combination of impact and preload could cause a 45-percent reduction in ultimate tensile strength whereas penetrated plates without a preload would fail at an approximately 38-percent reduction in ultimate tensile strength. This suggests an interaction between the preload stresses and the stresses set up by the impact event. Since all specimens were completely penetrated by the projectiles, the residual tensile strength was found to be independent of the preload.

For nonpenetrating impacts on preloaded specimens, Avva (formerly Sharma)^{112–115} has produced the most experimental data on this topic. Typically, a “failure threshold curve” is obtained by plotting specimen preload (tension or compression) versus impactor kinetic energy and drawing a faired curve between the data in which the specimens broke upon impact (a “catastrophic” break) and those which survive the impact. A sample curve (not from actual data) is presented in figure 9 for clarity on this subject. As will subsequently be seen, a well-defined area between the two zones exists in most actual experimental data.

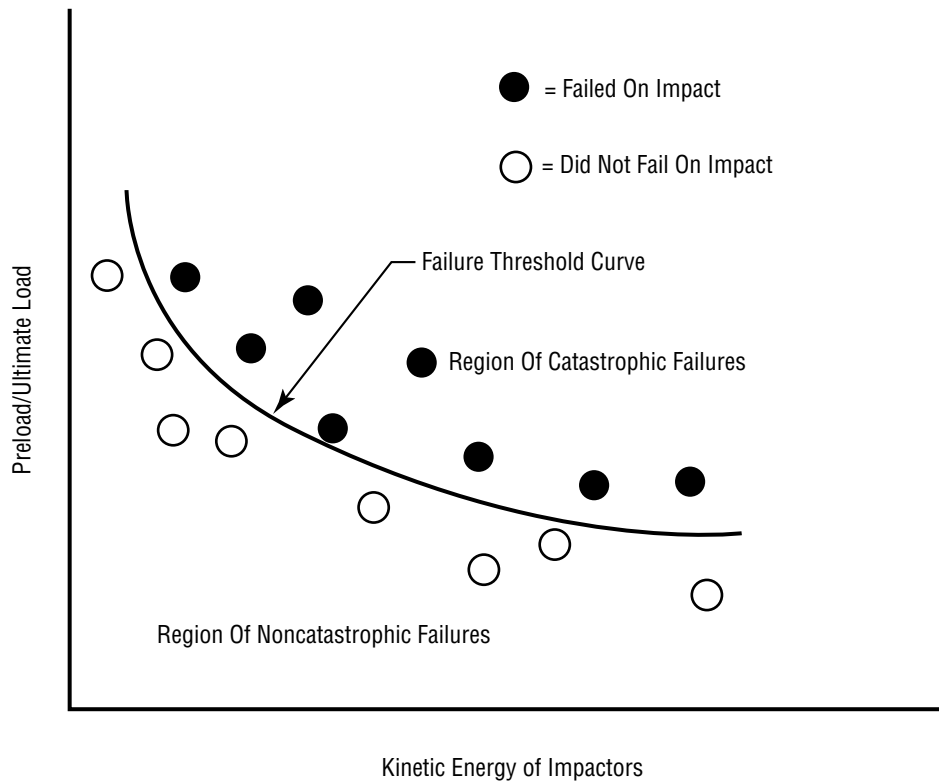


Figure 9. Example plot of preload versus impact energy curve to demonstrate concept of a failure threshold curve.

In a study on honeycomb sandwich panels impacted by projectiles from a light gas gun¹¹² it was found that tensile preloads on the facings of sandwich panels could cause catastrophic failure at stress ratios (ratio of preload stress to ultimate breaking stress) below 40 percent for 1 J (0.7 ft-lb) of impactor kinetic energy. This was for facings of T300/5208 carbon/epoxy in a stacking sequence of $[90, +45, -45, 0]_s$ bonded to a 130 kg/m^3 (8.1 lbm/ft^3) aluminum honeycomb core. For stacking sequences of $[+45, -45, 0]_s$ and $[+45, -45, 90, 0]_s$, higher prestresses needed to be applied to cause catastrophic failure for a given impact energy. This is understandable for the $[+45, -45, 0]_s$ layup since it is thicker and contains more 0° plies. Limited data were supplied for the $[+45, -45, 0]_s$ and $[+45, -45, 90, 0]_s$ specimens, so conclusions on why this may be are difficult to draw. Contact stresses surely dominated in this study since the facesheets were backed by a relatively hefty honeycomb of 130 kg/m^3 (8.1 lbm/ft^3) density. For specimens that did not catastrophically break upon impact, the residual strength was obtained. Although this aspect of the study was not highlighted in the paper, it is observed that the tensile residual strength is not much higher than the failure threshold curve for the limited data presented. For compression, the residual strength could be much more above the failure threshold curve. This is probably due to the stiff honeycomb backing preventing large deflections; thus, the large delamination areas associated with them.

In a study that contained much more data,¹¹³ the effects of a preload on the residual strength of specimens were noted. The specimens were made of T300/5208 carbon/epoxy with a stacking sequence of $[45_2, -45_2, 0_2, 90_2]_s$. The support conditions were clamped/clamped (perpendicular to the 0° -direction)-free/free with a width of 7.62 cm (3 in) and length (0° -direction) of 15.24 cm

(6 in) for tension loaded specimens and 6.35 cm (2.5 in) for compression-loaded specimens. An aluminum sphere of 1.27 cm (0.5 in) diameter was propelled at velocities between 18.6 m/sec (61 ft/sec) and 106.7 m/sec (350 ft/sec) and struck the specimens at their geometrical midpoints. This testing geometry will induce relatively large, local contact stresses while not causing much global deflection as would be present in a high-mass/low-velocity impact event, thus minimizing the increased stiffness response due to the tensile preloads (or decreased stiffness response due to compressive preloads).

For the data presented on tensile loading, a faired curve could easily be drawn between regions of catastrophic and noncatastrophic failures. For the specimens that did not experience catastrophic failures, the residual tensile strengths were much above the catastrophic failure curve. Specimens which were impacted while under no preload demonstrated a residual strength versus impact energy curve higher than the catastrophic failure curve. The residual strength data from the preloaded specimens that did not catastrophically fail fall close to the no preload residual strength curve. An additional set of tests were conducted using the catastrophic failure curve as a guide for setting preloads at three different impact energies. All of these specimens were preloaded in the region of the catastrophic failure curve. As expected, most of the specimens failed catastrophically upon impact, and those that did not had very little residual strength remaining.

Similar experiments were conducted for specimens under a compressive preload. For the specimens that did not fail catastrophically upon impact, the residual compression strength was seen not to rise much above the catastrophic failure curve. In addition, the catastrophic failure curve was close to the residual strength versus impact energy curve of specimens impacted with no preload whereas for the tensile specimens, the catastrophic curve was approximately 30-percent lower than the residual strength versus impact energy curve for unloaded specimens. These results are sketched out graphically in figure 10 for clarity and comparison. Only pertinent data points are included to reduce clutter in the plots. Thus, from this study it appears that a tensile preload can reduce the residual strength-carrying capability of the impacted laminate, but only when preloaded near the “catastrophic failure” curve.

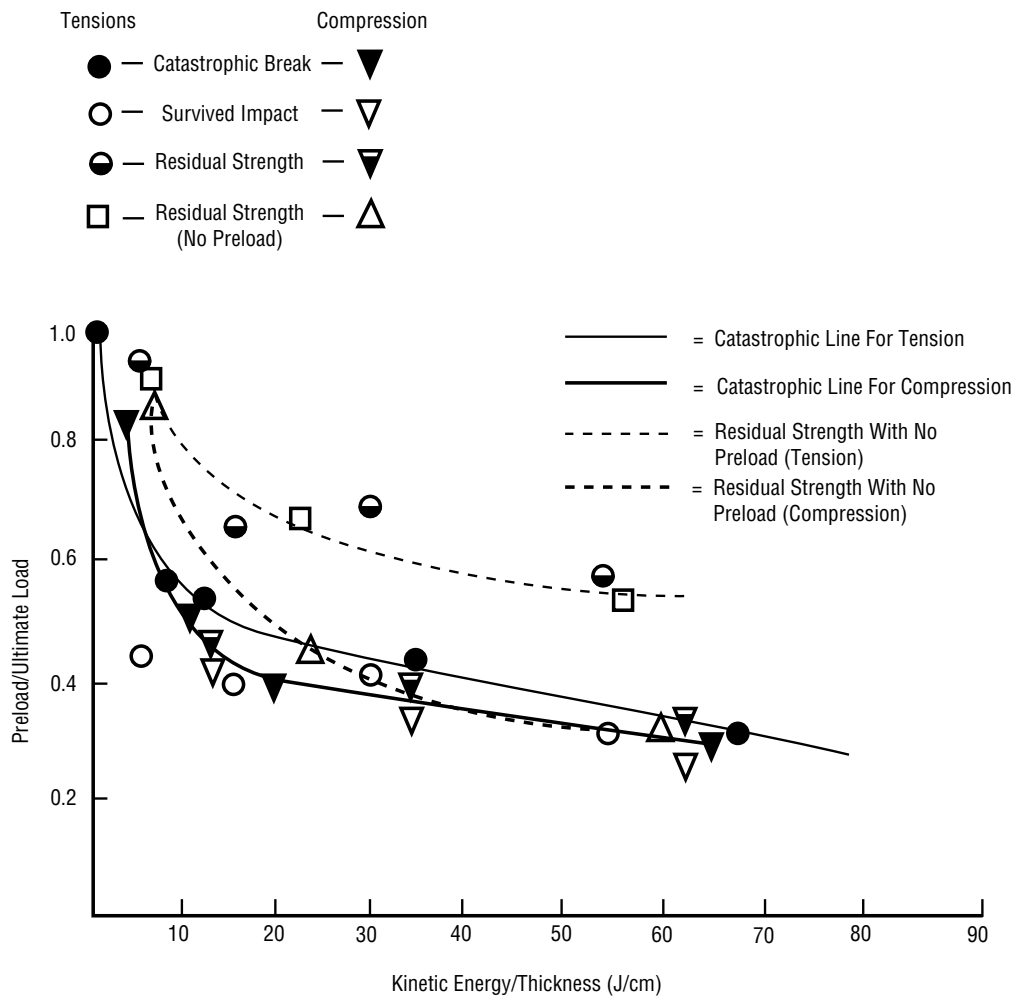


Figure 10. Representative data from Avva.¹¹³

In a very similar study,¹¹⁴ specimens of T300/934 carbon/epoxy with a stacking sequence of $[+45, -45, 0, 90]_{2s}$ were impacted by an aluminum sphere of 1.27 cm (0.5 in) diameter while under a tensile preload. The catastrophic failure curve for this study is very similar to that shown in figure 10. The only noticeable difference between these two studies is that the residual strength of the preloaded specimens that did not fail catastrophically fell closer to the catastrophic failure curve in this study as compared to the study in reference 113. A summary of this study can be found in reference 115. In an impact damage study by Starnes et al.⁷⁶ the residual compressive strengths of 48-ply laminates loaded with a compressive preload were evaluated. This represents an extremely thick test coupon and global deflections should be negligible due to the laminates high bending stiffness. The projectile used was a 1.27 cm (0.5 in) aluminum sphere propelled between velocities of 52 to 101 m/sec (171 to 331 ft/sec). The material used was T300/5208 carbon/epoxy with a stacking sequence of $[+45, -45, 0_2, +45, -45, 0_2, +45, -45, 0, 90]_{2s}$ cut into specimens 11.4 cm (4.5 in) wide by 24.8 cm (9.75 in) long. Catastrophic failure threshold curves were determined from the data and the two zones between specimens that survived the impact and those that failed on impact were very distinguishable. For those specimens that did survive impact the residual strengths were determined. Below 5 J (3.7 ft-lb)

of impact energy, the residual strength values were within the scatter band of specimens that had not been impact damaged. For impact energy values that did cause a reduction in residual compression strength, the preload appears to decrease the residual compressive strength to a small degree, although only six data points are used for this conclusion. In a continuation of this study,¹¹⁶ additional data on 40-ply laminates of stacking sequence $[+45, -45, 0_4, -45, +45, +45, -45, 0_4, -45, +45, +45, -45, 0_2]_S$ demonstrated that specimens impacted while under a compressive preload experienced slightly larger areas of damage, as detected by brittle lacquer spallation on the nonimpacted side of the test coupon. Specimens of a quasi-isotropic layup, $[+45, -45, 0, 90, -45, +45, 0, 90]_{3S}$ were also tested, with and without compressive preloads, with no real discernible drop in CAI strength due to the compressive preloads. These results are also presented in reference 117.

Low-velocity drop-weight tests on tensile prestressed thinner specimens were performed in a study by Park.¹¹⁸ T300/914C carbon/epoxy with four- and eight-ply bidirectional layups were impacted by a 1.5-kg (3.3-lbm) mass impactor with a 6-mm (0.24-in) diameter tup. The 2.5-cm- (1-in-) wide specimens were supported as clamped-clamped/free-free with a span of 5 cm (2 in). Catastrophic threshold curves were generated (termed “impact maps” in this study) and showed that ballistic impacts had a higher threshold curve than drop-weight impacts since the ballistic tests caused localized penetration and the drop-weight tests caused damage across the entire specimen area. A limited number of tests on the residual tensile strength of preloaded coupons, impacted ballistically, showed that the residual strength dropped sharply as the preload neared the ultimate tensile strength of the test coupon.

A C-scan analysis of impacted beams under a tensile preload was conducted by Sankar and Sun.¹¹⁹ Although only one initial preload value was used (about one-third of ultimate load) the results did show differences in those beams impacted with an initial tensile stress and those impacted with no initial stress. The beams were 20-ply graphite/epoxy with a stacking sequence of $[0_2, 90_2, 0_2, 90_2, 0_2]_S$ supported as clamped-clamped/free-free. A 1.27-cm- (0.5-in-) diameter steel ball was used as a projectile at speeds of 10–40 m/sec (33–131 ft/sec). The span of the impacted beams was set at 18 cm (7 in) and were 3.8 cm (1.5 in) wide. Although ballistic projectiles were used, the relatively high aspect ratio for these plates could possibly allow more global deflection than the specimens impacted in the previously cited studies in this section. Results to note are that larger zones of delamination were found to exist for those specimens impacted while preloaded. The only exception to this trend was a reduction in the delamination area near the back plies on preloaded samples for larger energy impacts. Residual tensile strength was also determined for these specimens. It is evident that the tensile preload causes a reduction in residual tensile strength by approximately 10 percent for the impact velocities used in this study.

Data for thinner plates impacted at low-velocity (drop-weight) impacts have been presented by Nettles and Lance.¹²⁰ Compressive preloads were applied to 16-ply test coupons of T300/934 and IM7/8551–7 carbon/epoxy with a quasi-isotropic stacking sequence of $[0, 45, 90, -45]_{S2}$. Coupon dimensions were 7.6 cm (3 in) wide by 10.2 cm (4 in) gauge length. The preloaded specimens were supported over a 6.4-cm- (2.5-in-) diameter circular opening and clamped around its periphery. A design of experiments approach was undertaken to try to identify significant variables without testing numerous specimens. A total of 18 specimens (two replicates of 9) of each material type were tested. Preloads ranged from 890 to 44,500 N (200 to 10,000 lb) and impact energies varied between 1 and 16 J (0.7 and 11.8 ft-lb). In general, it was found that the compressive preloads tended to cause a decrease in residual compression strength after impact as the preload was increased, although quantitative values

are suspect due to the small number of specimens tested and the variables not being allowed to go to their extremes.

A recent study¹²¹ examined the effect of impact response on biaxially loaded specimens of chopped E-glass in a polyester resin matrix. The preloads could be introduced in any combination of tension and compression in the two principal axes of the plate. Impacts were performed by a drop-weight apparatus at an energy of 21.5 J (15.9 ft-lb) for all specimens. Results measured were indentation depth, absorbed impact energy, maximum force of impact, and damage area. The largest level of damage was observed to occur for specimens loaded in equal tension-compression (i.e., pure shear). The maximum force of impact was largest for the highest values of tension-tension preloading and lowest for the largest values of tension-compression (pure shear). A state of biaxial compression produced maximum loads of impact between these two extremes. Very little energy was absorbed for specimens loaded in tension-tension but as compressive preloads were introduced, the absorbed energy dramatically increases. Care must be taken when interpreting these results to continuous fiber-reinforced, layered laminates since the damage modes are so very different.

Analytical treatments of this problem have been undertaken in a few studies.^{122–125} In all of these studies it was shown that a tensile prestress will decrease the maximum deflection due to impact and will raise the maximum load of impact. Compressive preloads will do the opposite.

3. ANALYTICAL

In this chapter, finite element solutions to the problem of transverse impact of a prestressed plate are made. None of these solutions are detailed to the extent that heavy experimental testing need not be performed. In keeping with the empirical nature of this work, the analyses presented will be simple and produced more to explain observed physical phenomena rather than to predict extent of damage as a function of impactor kinetic energy and applied preload. First, an approximate energy method model of the problem is presented. A solution of this problem can only be performed numerically and many assumptions have to be made, making the finite element technique much more informative and accurate. However, some basic physical phenomena can be qualified from the energy method problem before it is completely solved. These results can help explain some of the results from the finite element analysis.

3.1 Energy Method

The energy involved in the system is assumed to consist of the elastic potential energy stored in the deflected laminate and the energy due to the external transverse load. The energy stored in a laminate due to bending is given by

$$E_{bend.} = \frac{1}{2} \int_{y=0}^{y=b} \int_{x=0}^{x=L} \left[D_{11} \left(\frac{\partial^2 w}{\partial x^2} \right)^2 + 2 D_{12} \frac{\partial^2 w}{\partial x^2} \frac{\partial^2 w}{\partial y^2} + D_{22} \left(\frac{\partial^2 w}{\partial y^2} \right)^2 + 4 \left(D_{16} \frac{\partial^2 w}{\partial x^2} + D_{26} \frac{\partial^2 w}{\partial y^2} \right) \frac{\partial^2 w}{\partial x \partial y} + 4 D_{66} \left(\frac{\partial^2 w}{\partial x \partial y} \right)^2 \right] dx dy , \quad (1)$$

where b is the width of the laminate, L is the length of the laminate, and w is the transverse displacement of the laminate. The D_{ij} are the components of the bending stiffness matrix, x is the coordinate along the length of the plate, and y is the coordinate along the width of the plate.

The energy stored by midplane (membrane) stretching is given by

$$E_{mem} = \frac{1}{2} \int_{y=0}^{y=b} \int_{x=0}^{x=L} \left[\frac{A_{11}}{2} \left(\frac{\partial w}{\partial x} \right)^4 + (A_{12} + 2 A_{66}) \left(\frac{\partial w}{\partial x} \frac{\partial w}{\partial y} \right)^2 + \frac{A_{22}}{2} \left(\frac{\partial w}{\partial y} \right)^4 \right] dx dy , \quad (2)$$

where the A_{ij} are components of the extensional stiffness matrix.

The energy stored due to the externally applied preload, N_x , is given by

$$E_{N_x} = \frac{1}{2} \int_{y=0}^{y=b} \int_{x=0}^{x=L} \left[N_x \left(\frac{\partial w}{\partial x} \right)^2 \right] dx dy \quad , \quad (3)$$

where N_x is the x -direction stress resultant.

The energy put into the system by the transverse load, P , is given by

$$E_P = - \int_{y=0}^{y=b} \int_{x=0}^{x=L} \frac{4P}{Lb} w dx dy \quad . \quad (4)$$

The total energy of the system is given by

$$E_{tot} = E_{bend} + E_{mem} + E_{N_x} + E_P \quad . \quad (5)$$

Assume the deflected surface to be of the form

$$w(x, y) = C_0 (x^2 - Lx)^4 \sin\left(\frac{\pi y}{b}\right) \quad , \quad (6)$$

where C_0 is a constant, satisfies the boundary conditions at $x=0$ and $x=L$. The boundary conditions at $y=0$ and $y=b$ restrict the plate from deflecting along these edges when in actuality they are free to move. (However, from experimental data to be given later, these edges deflect very little so this approximation will suffice for qualitative purposes.)

Assume the typical values for carbon/epoxy as:

$$A = \begin{bmatrix} 410,000 & 124,000 & 0 \\ 124,000 & 410,000 & 0 \\ 0 & 0 & 143,000 \end{bmatrix} \text{ and } D = \begin{bmatrix} 67 & 22 & 14 \\ 22 & 32 & 14 \\ 14 & 14 & 24 \end{bmatrix} \quad (\text{units in pounds and inches})$$

and putting equation (6) into equations (1), (2), (3), and (4) and performing the integrations (some numerically) with $L=16$ cm (6.3 in) and $y=9.5$ cm (3.75 in), then using equation (5) gives

$$7.10 \times 10^{20} C_0^4 + (8.3 \times 10^7 N_x + 4.66 \times 10^{10}) C_0^2 - 1.02 \times 10^5 P C_0 = E_{tot} \quad , \quad (7)$$

with units in pounds and inches.

From the principle of virtual work,

$$\frac{\partial E_{tot}}{\partial C_0} = 0 \quad . \quad (8)$$

Applying this operation to equation (7) gives:

$$2.84 \times 10^{21} C_0^3 + (1.66 \times 10^8 N_x + 9.32 \times 10^{10}) C_0 = 1.02 \times 10^5 P \quad . \quad (9)$$

At the center of the plate, $w=w_{\max}$, $x=L/2$ and $y=b/2$. Therefore,

$$C_0 = 1.032 \times 10^{-4} w_{\max} \quad , \quad (10)$$

and equation (9) becomes

$$P = 30,600 w_{\max}^3 + (0.168 N_x + 94.3) w_{\max} \quad . \quad (11)$$

The cubic equation (9) can also be solved for C_0 and then these values placed in equation (6) to determine the deflection at any point on the plate. Table 1 gives load (P)-preload (N_x) combinations with the associated transverse displacement at the center of the plate (W_{\max}). The same values are obtained using equation (11). These values are plotted in figure 11 for constant values of P with varying N_x and in figure 12 with constant N_x and varying P .

From equation (7), if E_{tot} represents the total impactor kinetic energy put into the system, then if N_x increases, P increases and C_0 decreases in order to maintain the energy balance of the system. Thus, from an energy balance formulation of the problem of a transverse load acting on a prestressed plate, the higher the prestress, the larger the maximum transverse load and the lower the maximum transverse deflection for a given amount of energy put into the system.

Table 1. Calculated data from equation (9).

Transverse Load, P N (lb)	Preload N/cm (lb/in)	Prestrain me	Deflection, W_{\max} mm (in)
223 (50)	0 (0)	0	2.82 (0.111)
223 (50)	1,229 (702)	2,000	2.53 (0.0998)
223 (50)	2,459 (1,405)	4,000	2.27 (0.0892)
223 (50)	3,687 (2,107)	6,000	2.01 (0.0793)
445 (100)	0 (0)	0	3.66 (0.144)
445 (100)	1,229 (702)	2,000	3.43 (0.135)
445 (100)	2,459 (1,405)	4,000	3.2 (0.126)
445 (100)	3,687 (2,107)	6,000	3.00 (0.118)
668 (150)	0 (0)	0	4.24 (0.167)
668 (150)	1,229 (702)	2,000	4.04 (0.159)
668 (150)	2,459 (1,405)	4,000	3.84 (0.151)
668 (150)	3,687 (2,107)	6,000	3.66 (0.144)
890 (200)	0 (0)	0	4.70 (0.185)
890 (200)	1,229 (702)	2,000	4.52 (0.178)
890 (200)	2,459 (1,405)	4,000	4.34 (0.171)
890 (200)	3,687 (2,107)	6,000	4.17 (0.164)
1,113 (250)	0 (0)	0	5.08 (0.200)
1,113 (250)	1,229 (702)	2,000	4.90 (0.193)
1,113 (250)	2,459 (1,405)	4,000	4.75 (0.187)
1,113 (250)	3,687 (2,107)	6,000	4.57 (0.180)
1,335 (300)	0 (0)	0	5.38 (0.212)
1,335 (300)	1,229 (702)	2,000	5.23 (0.206)
1,335 (300)	2,459 (1,405)	4,000	5.08 (0.200)
1,335 (300)	3,687 (2,107)	6,000	4.93 (0.194)
1,558 (350)	0 (0)	0	5.69 (0.224)
1,558 (350)	1,229 (702)	2,000	5.54 (0.218)
1,558 (350)	2,459 (1,405)	4,000	5.38 (0.212)
1,558 (350)	3,687 (2,107)	6,000	5.23 (0.206)
1,780 (400)	0 (0)	0	5.94 (0.234)
1,780 (400)	1,229 (702)	2,000	5.82 (0.229)
1,780 (400)	2,459 (1,405)	4,000	5.66 (0.223)
1,780 (400)	3,687 (2,107)	6,000	5.54 (0.218)
2,003 (450)	0 (0)	0	6.20 (0.244)
2,003 (450)	1,229 (702)	2,000	6.07 (0.239)
2,003 (450)	2,459 (1,405)	4,000	5.92 (0.233)
2,003 (450)	3,687 (2,107)	6,000	5.79 (0.228)

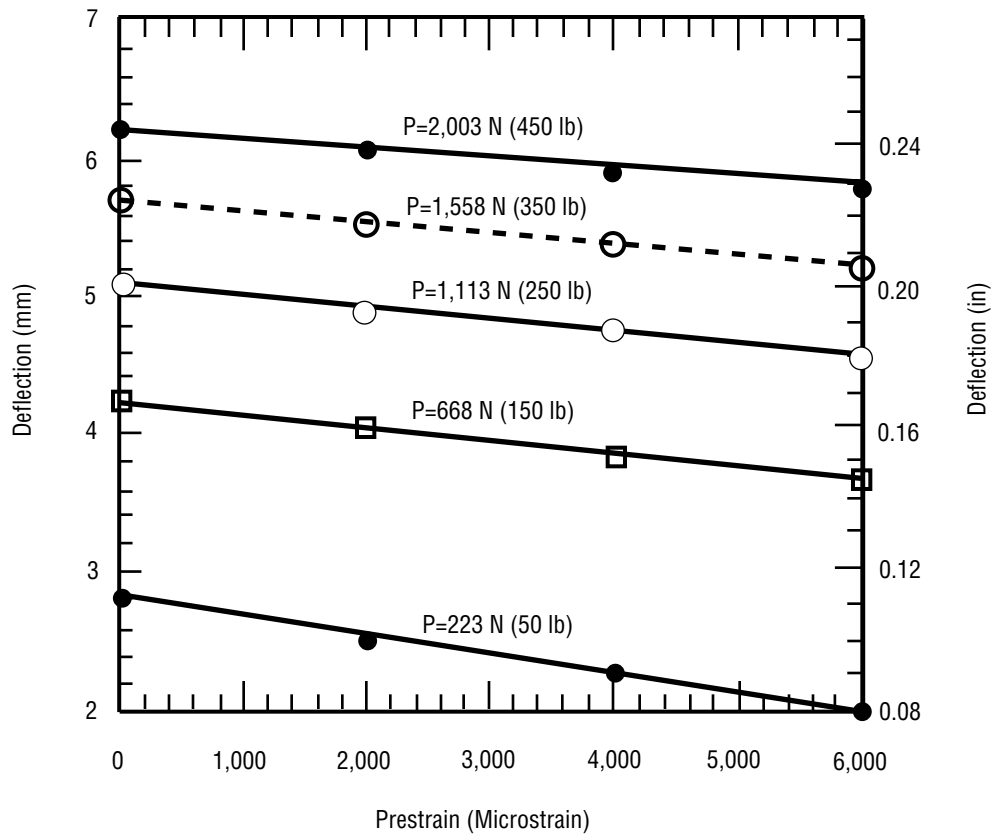


Figure 11. Deflection, w_{\max} , versus preload for constant values of transverse load, P from equation (9).

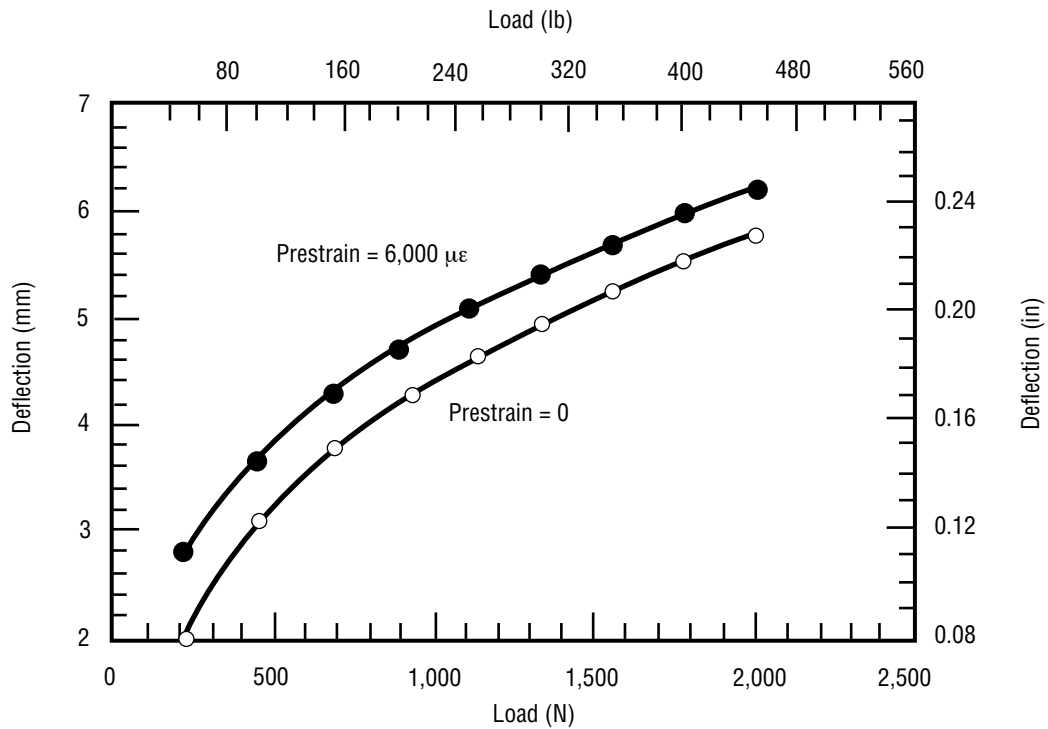


Figure 12. Load versus displacement for constant values of prestrain from equation (9).

3.1.1 Formation of Damage

The above analysis does not take into account any damage that forms in the laminate. From equation (5), the energy due to formation of this damage must be included in the total energy. Since this energy is lost to the system, it will have a negative value and would tend to decrease the terms in equation (11), implying larger deflections will occur for a given transverse load if damage is present, thus the “softening” effect.

3.2 Finite Element Technique

For this study, a commercially available finite element program called COSMOS/M was utilized. The plate was modeled as being statically loaded with a transverse load at the geometric midpoint of the plate. Two edges were clamped while the other two were free. Figure 13 shows the plate geometry used for the finite element analysis. Large displacement formulation was used where the structural stiffness matrix was recalculated after each incremental loading of 44.5 N (10 lb). This was necessary to account for the changing geometry of the problem since the midplane strains could no longer be ignored; i.e., the strain within the laminate midplane is given by:

$$\begin{aligned}\varepsilon_x &= \frac{\partial u}{\partial x} + \frac{1}{2} \left(\frac{\partial w}{\partial x} \right)^2 \\ \varepsilon_y &= \frac{\partial v}{\partial y} + \frac{1}{2} \left(\frac{\partial w}{\partial y} \right)^2 \\ \varepsilon_{xy} &= \frac{\partial v}{\partial x} + \frac{\partial u}{\partial y} + \left(\frac{\partial w}{\partial x} \frac{\partial w}{\partial y} \right)\end{aligned}\tag{12}$$

where u is displacement in the x -direction and v is displacement in the y -direction. For small displacements the final terms in equation (12) can be dropped. However, for displacements greater than approximately one-half the plate thickness, these terms can become significant. The finite element large displacement formulation performs calculations retaining these terms and recalculating them at each step in the loading process.

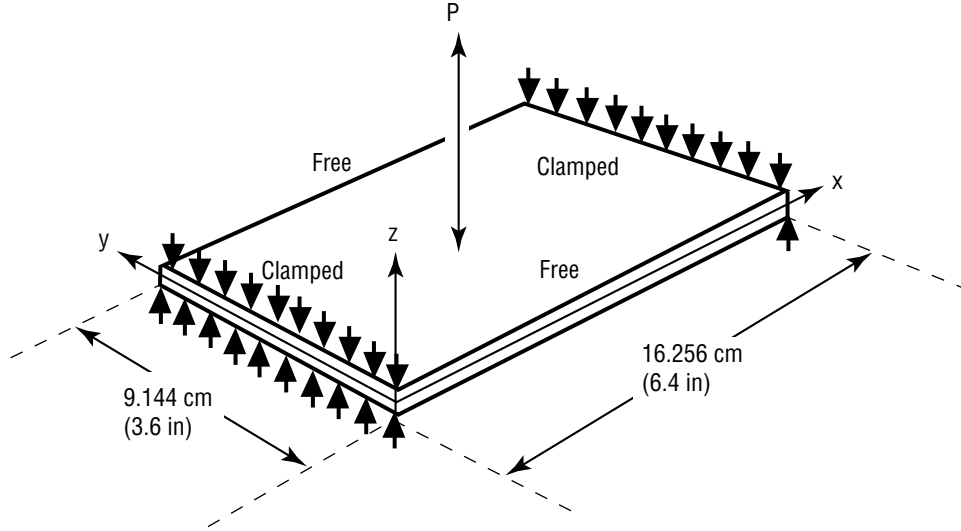


Figure 13. Plate geometry for finite element model.

The plate was meshed with rectangular composite shell elements 1.016 cm (0.4 in) by 0.914 cm (0.36 in) for a total of 160 elements. Each element contained eight layers of orthotropic material with properties and directions $[+45, 0, -45, 90]_s$ similar to those of the actual specimens to be used. This mesh provided adequate aspect ratios for the elements and also produced a grid that was not too coarse, yet not so fine as to extend computational runtime and memory. The transverse load was modeled as a point load at the top, centermost node in the mesh. The clamped boundary conditions were achieved by restricting all displacements and rotations at all nodes along the sides that were to be clamped.

Preload was introduced into the laminate by initially displacing one of the clamped ends a certain amount in the x -direction.

After each run, the desired output response (z -direction displacement, stress in the principal material direction of any ply, etc.) could be loaded and plotted.

3.3 Finite Element Results

3.3.1 Transverse Displacement

The most easily compared result between the finite element (FE) analysis and experimental results is the transverse load/displacement relationship. The FE runs were performed for transverse loads of 223; 445; 668; 890; 1,113; 1,335; 1,558; 1,760; and 2,003 N (50, 100, 150, 200, 250, 300, 350, 400 and 450 lb) with four prestrains of 0; 2,000; 4,000; and 6,000 $\mu\epsilon$ at each transverse load value for a total of 36 runs.

The output from each analysis was presented as a contour plot and the maximum transverse displacement (the node under the transverse load) value was recorded. The results from the runs are presented in table 2. Figure 14 shows results for a constant transverse load P with varying preload and figure 15 for a constant preload N_x with a varying transverse load.

From the results it can be seen that the maximum deflection decreases with increasing prestrain in a nonlinear fashion. The results from the energy balance formulation showed a linear relationship that had a much smaller effect (fig. 11). Initially, the added prestrain causes a rapid drop in maximum deflection and as the prestrain is increases, this drop becomes less pronounced. As the transverse load increases, the absolute drop in maximum deflection is decreased by a very small amount. That is at a transverse load of 1,335 N (300 lb), the maximum deflection decreases a total of 2.642 mm (0.104 in) as the prestrain increases from 0 to 6,000 $\mu\epsilon$. For the same increase in prestrain at a transverse load of 2,003 N (450 lb), the maximum deflection decreases a total of 2.591 mm (0.102 in).

The load-displacement plots for given prestrain values show that as the prestrain increases, the maximum load needed to achieve a given deflection increases by a substantial amount. As the prestrains increase, the load-displacement plots become more linear. This was not the case for the energy balance results as plotted in figure 2.

The finite element method predicts a larger influence of the preload on the impact response of the laminate than does the energy balance method. Comparisons with experimental results will be made in chapter 6.

Table 2. Results from the finite element analysis.

Transverse Load, P N (lb)	Preload N/cm (lb/in)	Prestrain me	Deflection, w_{max} mm (in)
223 (50)	0 (0)	0	2.82 (0.111)
223 (50)	1,229 (702)	2,000	1.25 (0.0493)
223 (50)	2,459 (1,405)	4,000	0.833 (0.0328)
223 (50)	3,687 (2,107)	6,000	0.638 (0.0251)
445 (100)	0 (0)	0	3.78 (0.149)
445 (100)	1,229 (702)	2,000	2.21 (0.0870)
445 (100)	2,459 (1,405)	4,000	1.57 (0.0618)
445 (100)	3,687 (2,107)	6,000	1.23 (0.0486)
668 (150)	0 (0)	0	4.47 (0.176)
668 (150)	1,229 (702)	2,000	2.95 (0.116)
668 (150)	2,459 (1,405)	4,000	2.20 (0.0866)
668 (150)	3,687 (2,107)	6,000	1.77 (0.0698)
890 (200)	0 (0)	0	5.00 (0.197)
890 (200)	1,229 (702)	2,000	3.56 (0.140)
890 (200)	2,459 (1,405)	4,000	2.74 (0.108)
890 (200)	3,687 (2,107)	6,000	2.26 (0.0888)
1,113 (250)	0 (0)	0	5.46 (0.215)
1,113 (250)	1,229 (702)	2,000	4.09 (0.161)
1,113 (250)	2,459 (1,405)	4,000	3.23 (0.127)
1,113 (250)	3,687 (2,107)	6,000	2.69 (0.106)
1,335 (300)	0 (0)	0	5.87 (0.231)
1,335 (300)	1,229 (702)	2,000	4.55 (0.179)
1,335 (300)	2,459 (1,405)	4,000	3.66 (0.144)
1,335 (300)	3,687 (2,107)	6,000	3.23 (0.127)
1,558 (350)	0 (0)	0	6.22 (0.245)
1,558 (350)	1,229 (702)	2,000	4.95 (0.195)
1,558 (350)	2,459 (1,405)	4,000	4.04 (0.159)
1,558 (350)	3,687 (2,107)	6,000	3.61 (0.142)
1,760 (400)	0 (0)	0	6.55 (0.258)
1,760 (400)	1,229 (702)	2,000	5.31 (0.209)
1,760 (400)	2,459 (1,405)	4,000	4.42 (0.174)
1,760 (400)	3,687 (2,107)	6,000	3.94 (0.155)
2,003 (450)	0 (0)	0	6.86 (0.270)
2,003 (450)	1,229 (702)	2,000	5.64 (0.222)
2,003 (450)	2,459 (1,405)	4,000	4.75 (0.187)
2,003 (450)	3,687 (2,107)	6,000	4.27 (0.168)

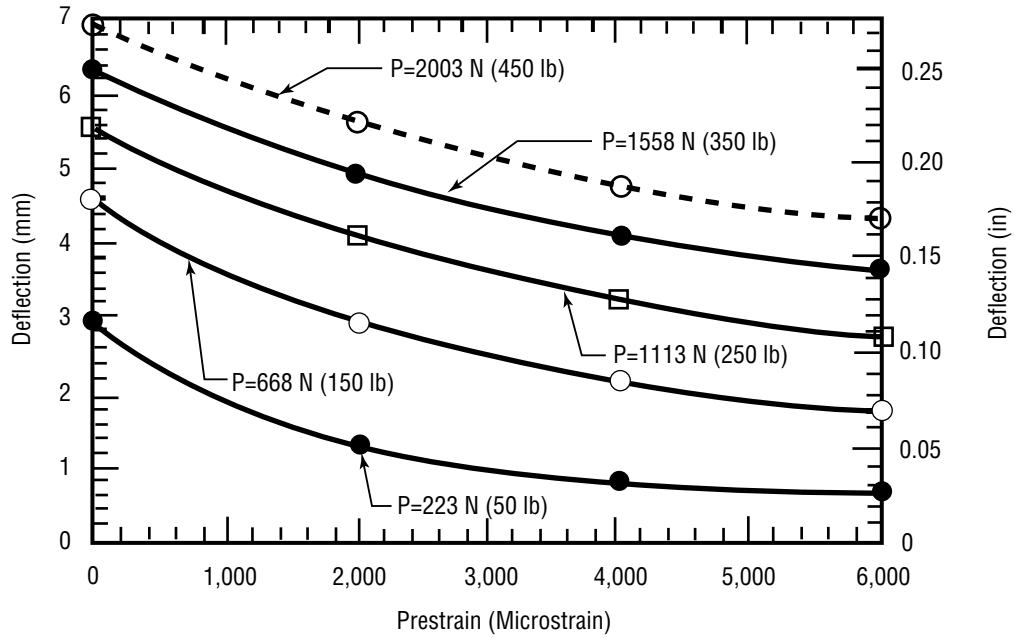


Figure 14. Finite element results for prestrain versus deflection at constant transverse load.

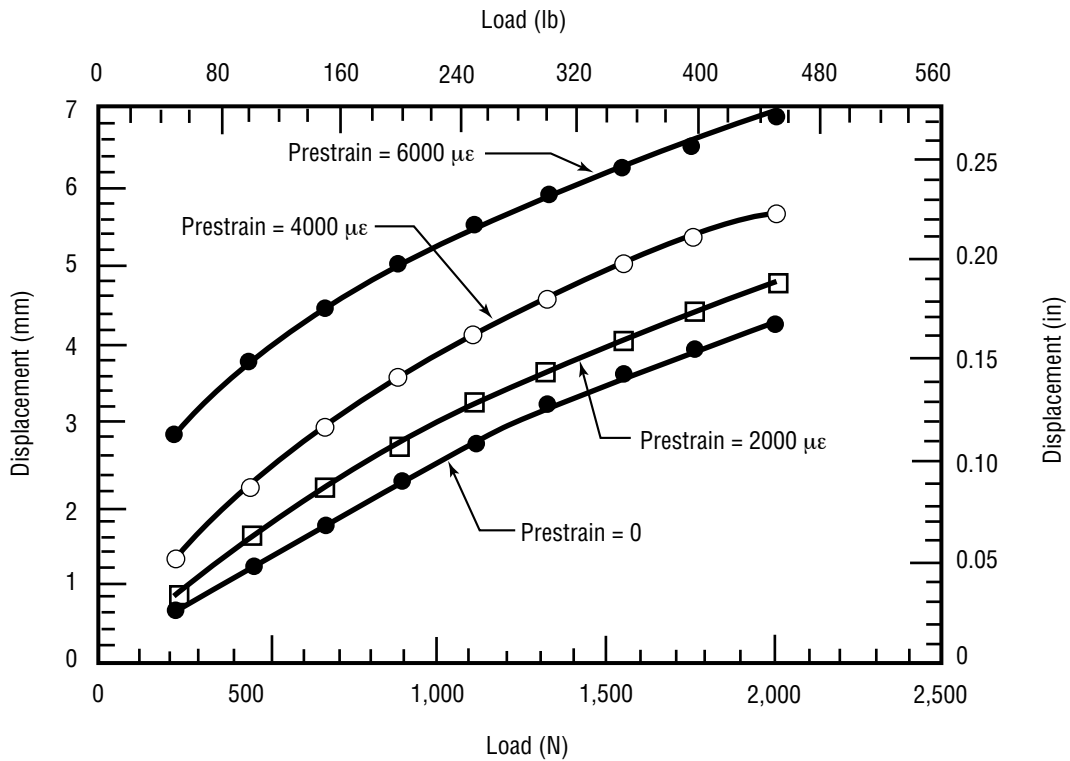


Figure 15. Finite element results for displacement versus load for constant values of prestrain.

3.3.2 Shape of Deflected Surface

From the contour plots of transverse displacements output by the FE program, the shape of the deflected surface could be predicted. The surface tended to form a “bowl” shape around the loading point rather than deflect as a cylindrical surface (as would be expected for long spans). This precluded any closed form analysis of the problem as one of cylindrical bending which would have greatly simplified the problem.

Contour plots for four combinations of transverse load-prestrain values are given in figures 16–19. These values represent both no prestrains and high prestrains at a low transverse load and a high transverse load.

As the prestrain increased, the edges along the free sides of the laminate deflected less and even began to deflect upward at the highest prestrain, as demonstrated in figures 7 and 9. With no preload, the specimen’s free edge did deflect, but at a relatively small amount compared to the maximum deflection, as shown in figures 6 and 8.

3.3.3 Maximum Stresses Within Plies

The maximum stresses within each ply were also calculated by the finite element method. Table 3 gives results (in principal material directions) for the four highest transverse loads for which the maximum stresses were calculated. These values are presented to demonstrate general trends in the maximum ply stresses with increasing transverse load and prestrain. The maximum stresses presented are those at the center of the respective ply. This value was used since most of the stress arises from membrane stretching and the values are only an approximation to begin with.

For the lower plies, the maximum stress increases with both increasing transverse load and increasing prestrain, an expected result. However, this trend also holds for the upper plies as well. This is to be expected with increasing prestrain but with increasing transverse loads, one might expect the upper plies to go more into compression due to the higher bending involved. This demonstrates the significance of the large deflection theory as the higher transverse loads add more to the overall membrane-type stresses than to the bending stresses. The maximum stresses in the plies in both principal material directions decrease from the bottom to the upper plies. Note that only the top two plies ever go into compression in the data presented, with these values being very small. Thus, compressive-type failures are not expected unless they are due to some mechanism not accounted for in the finite element analysis such as contact stresses or dynamic effects.

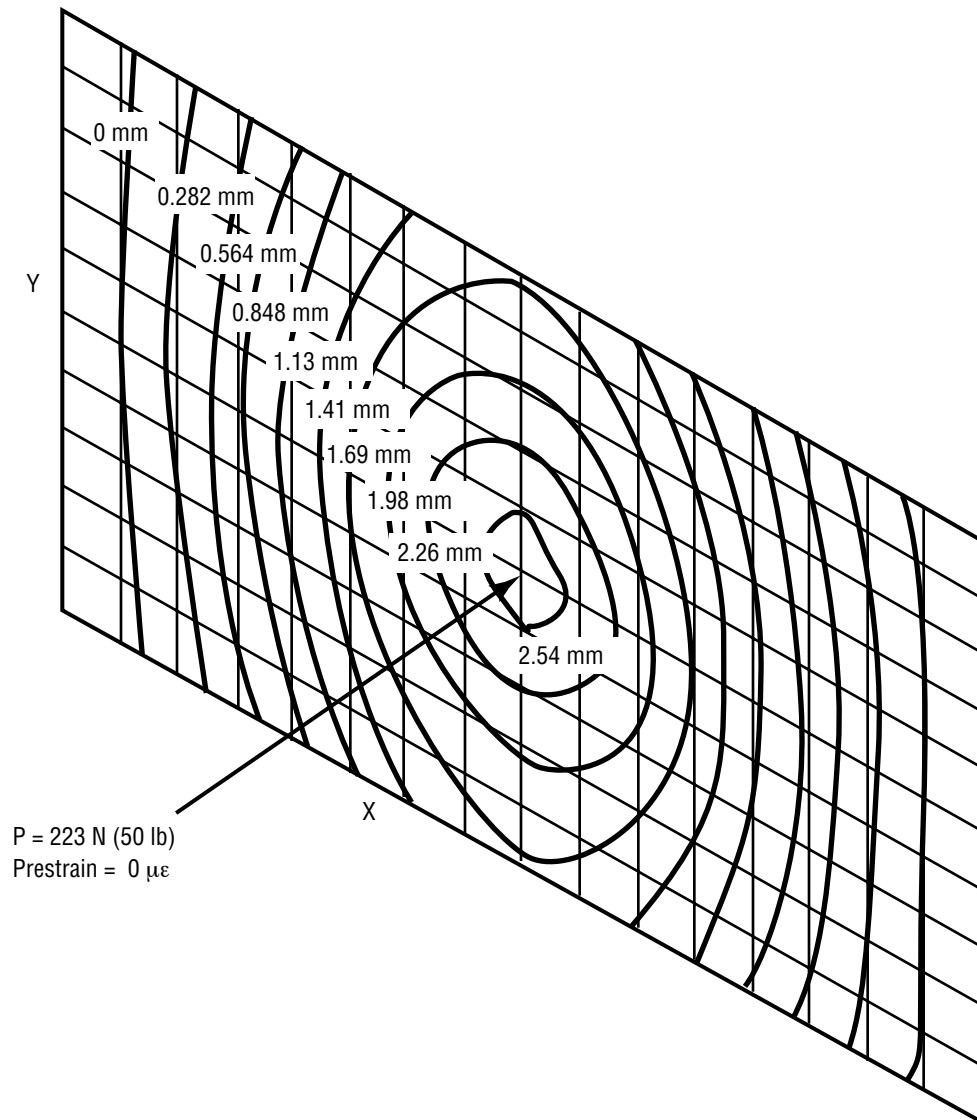


Figure 16. Contour plot of transverse deflection for a transverse load of 223 N (50 lb) and no prestrain.

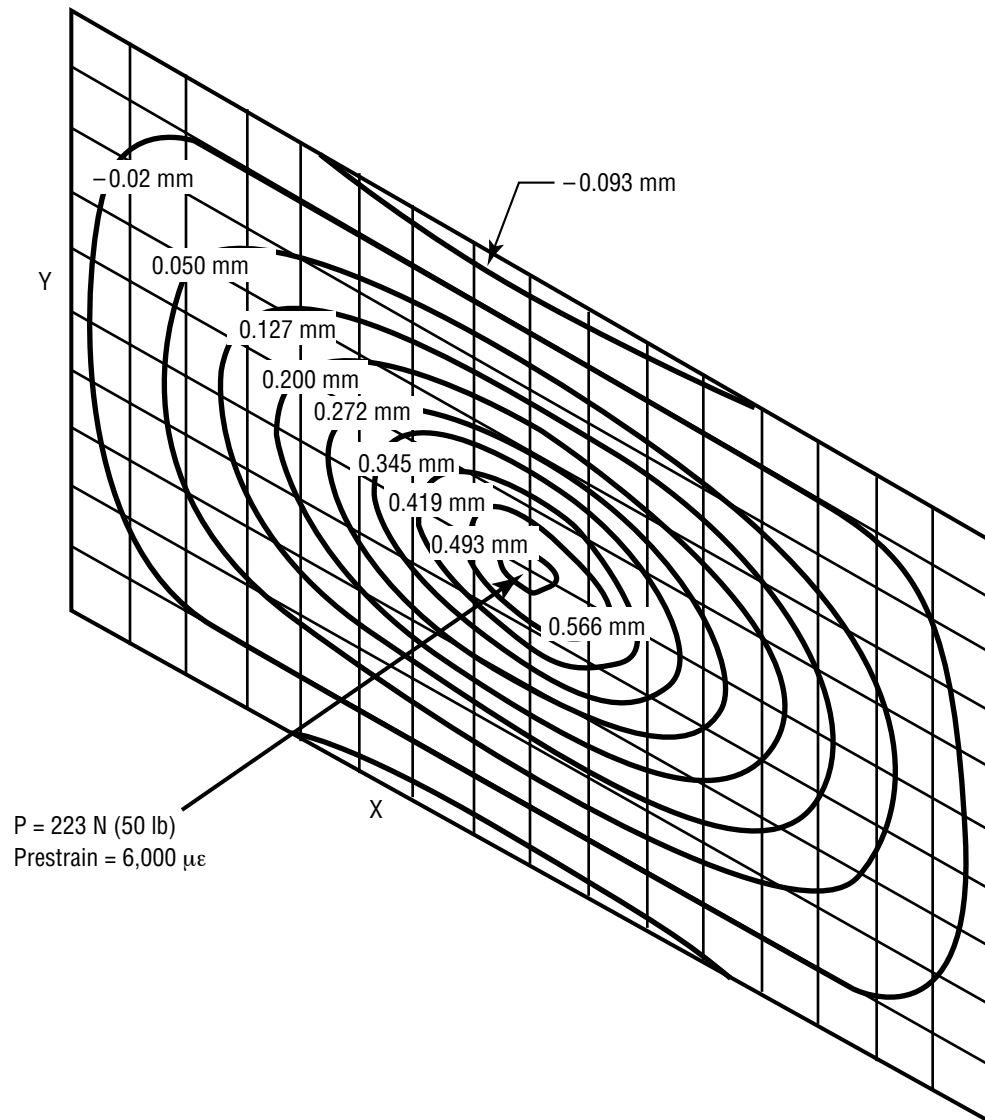
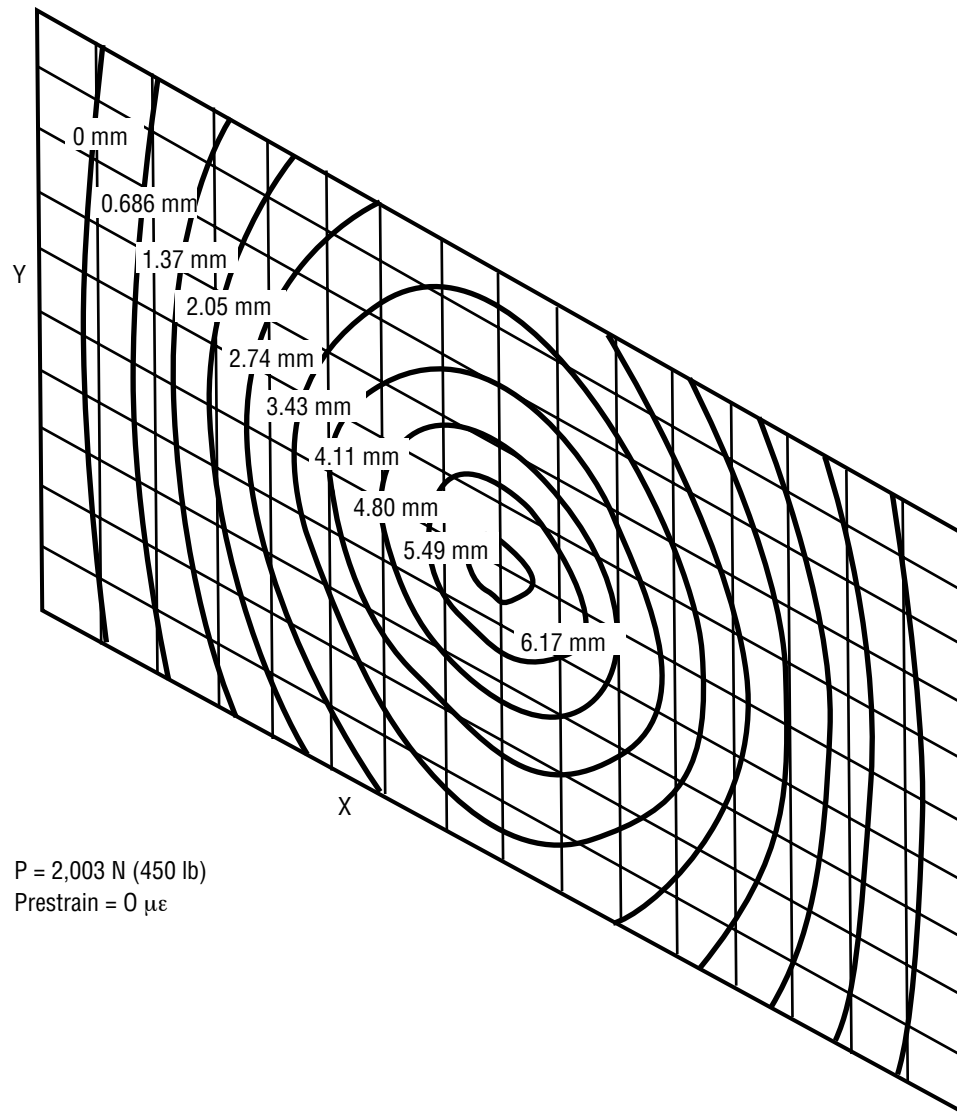


Figure 17. Contour plot of transverse deflection for a transverse load of 223 N (50 lb) and a prestrain of 6,000 $\mu\epsilon$.



$P = 2,003 \text{ N (450 lb)}$
 $\text{Prestrain} = 0 \text{ } \mu\epsilon$

Figure 18. Contour plot of transverse deflection for a transverse load of 2,003 N (450 lb) with no prestrain.

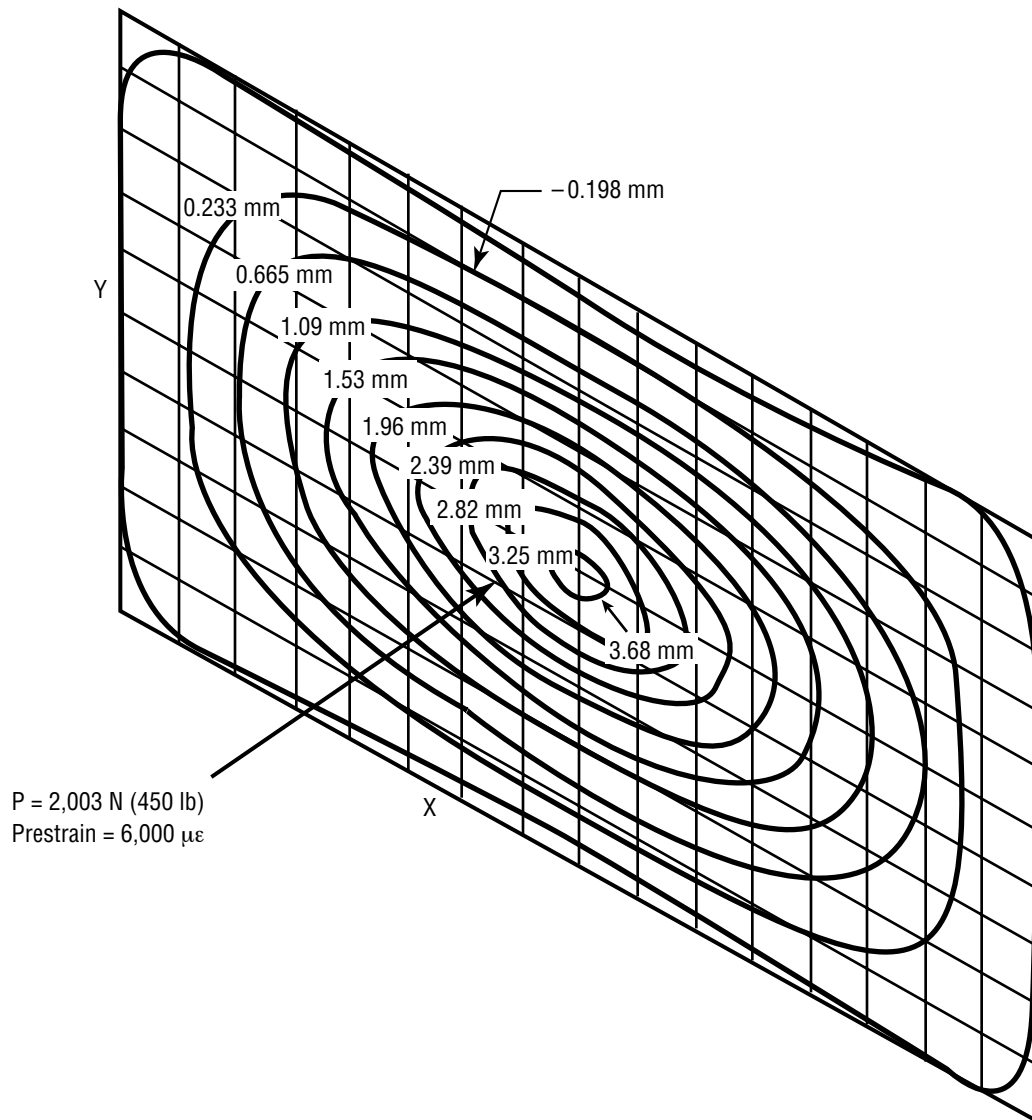


Figure 19. Contour plot of transverse deflection for a transverse load of 2,003 N (450 lb) and a prestrain of 6,000 $\mu\epsilon$.

Table 3. Finite element results for stresses within plies.

		P=1,335 N (300 lb)										(Values in MPa)					
		Ply 8		Ply 7		Ply 6		Ply 5		Ply 4		Ply 3		Ply 2		Ply 1	
Prestrain		σ_1	σ_2	σ_1	σ_2	σ_1	σ_2	σ_1	σ_2	σ_1	σ_2	σ_1	σ_2	σ_1	σ_2	σ_1	σ_2
0		758	72	641	59	544	45	365	34	227	20	143	10	49	-1.6	37	-11.0
2,000		799	76	675	62	577	48	402	37	258	24	183	13	58	5.2	42	-7.3
4,000		847	80	717	66	624	53	449	41	323	28	240	19	114	7.0	54	-1.3
6,000		882	83	737	69	664	57	493	44	411	35	300	22	156	12.0	66	4.2

		P=1,558 N (350 lb)										(Values in MPa)					
		Ply 8		Ply 7		Ply 6		Ply 5		Ply 4		Ply 3		Ply 2		Ply 1	
Prestrain		σ_1	σ_2	σ_1	σ_2	σ_1	σ_2	σ_1	σ_2	σ_1	σ_2	σ_1	σ_2	σ_1	σ_2	σ_1	σ_2
0		841	80	717	65	612	50	411	38	251	23	201	8.9	54	-8	41	-10.0
2,000		875	83	751	69	644	53	448	41	320	27	217	14	66	3.1	45	-6.5
4,000		923	88	785	72	689	58	665	45	404	31	283	21	123	7.5	57	-1.1
6,000		965	91	834	75	730	62	677	48	420	36	318	24	161	13	68	4.0

		P=1,780 N (400 lb)										(Values in MPa)					
		Ply 8		Ply 7		Ply 6		Ply 5		Ply 4		Ply 3		Ply 2		Ply 1	
Prestrain		σ_1	σ_2	σ_1	σ_2	σ_1	σ_2	σ_1	σ_2	σ_1	σ_2	σ_1	σ_2	σ_1	σ_2	σ_1	σ_2
0		909	88	779	72	677	54	456	42	314	26	226	12	59	2.4	45	-8.9
2,000		951	91	813	75	710	58	492	45	336	30	259	17	76	3.5	49	-5.6
4,000		992	95	854	79	751	62	544	49	379	34	312	23	134	7.9	60	-0.6
6,000		1,034	99	889	81	792	66	601	52	430	38	341	26	165	13	70	4.2

		P=2,003 N (450 lb)										(Values in MPa)					
		Ply 8		Ply 7		Ply 6		Ply 5		Ply 4		Ply 3		Ply 2		Ply 1	
Prestrain		σ_1	σ_2	σ_1	σ_2	σ_1	σ_2	σ_1	σ_2	σ_1	σ_2	σ_1	σ_2	σ_1	σ_2	σ_1	σ_2
0		978	94	847	77	737	59	500	46	340	29	263	16	63	6.1	48	-7.6
2,000		1,013	98	882	81	772	62	535	49	350	33	294	17	84	7.0	52	-4.5
4,000		1,061	102	916	85	813	67	557	53	431	37	347	21	143	8.3	62	0.2
6,000		1,102	105	951	87	847	70	613	56	440	40	368	26	169	14.0	72	4.7

The strength value in the second principal material direction (≈ 35 Mpa (5,100 psi) as determined by 90° tension tests) in the bottom four plies is always exceeded. However, synergistic effects with neighboring plies can help keep the ply from failing in this direction at the values obtained by the 90° tension tests. It is still expected that much matrix cracking parallel to the fibers in these plies should occur, especially in the bottom ply which has the highest stresses and also has only one neighboring ply to help “hold together” this ply.

The breaking stress ($\approx 2,700$ Mpa (400,000 psi)) in the first principal material direction (along the fibers) is never exceeded in any of the plies, thus fiber breakage is not expected to occur for the load-prestrain values presented. In fact the stresses calculated are never even one-half that of the breaking stress of a ply in the fiber direction. Thus, if fiber breakage is found, it must be due to another mechanism other than the stresses set up solely by the transverse load-prestrain combination.

4. EXPERIMENTAL

Before the specifics of this particular research program are given, a few general comments about the empirical study of impact to composites are in order; however, direct comparisons between studies are very difficult due to a lack of standardization, allowing whatever convenient specimen geometry or support system best suits the researcher. However, a hasty rush for a standard can, and would, do more harm than good at this point in the evolution of composites, since much remains to be understood about the many variables involved in impact testing. Even a standard meant to compare composite materials for damage resistance and damage tolerance (such as the Boeing 48-ply CAI standard) can be very misleading. For example, in this standard, a 48-ply specimen of a quasi-isotropic stacking sequence, 8 inches by 10 inches in size is impacted with 1,500 in-lb of energy per inch of specimen thickness. Assuming all impact events are conducted with the same boundary conditions, impactor size, shape, and velocity (which they are not), the only response measured is damage tolerance in a structurally compressive test, which is inconclusive for assessing a fiber/resin system for impact damage tolerance. It should be noted that compression testing a panel of this size is a structural, not material, property test. The most important parameter—velocity of the impactor—is not specified, thus high-velocity/low-mass impacts could be used to obtain the required energy level, resulting in very localized damage and a smaller reduction in CAI strength than would have been found from a high-mass/low-velocity test. In addition, 48 plies is a relatively thick laminate and would not be encountered in many engineering applications, thus bringing the issue of scaling into the problem. The thick laminate is called for to minimize the global buckling of the plate during compression testing but during the impact event, the flexural stiffness is so high that the large interlaminar shear stresses that normally develop in an impact event are minimized. Thus, a material with a higher mode II shear strength would not register as being more damage resistant than a material with a lower mode II shear strength, although it would for thinner test panels.

Any standard developed is going to have to examine a range of impact energies. The 1,500 in-lb/in called for on the Boeing CAI tests represents just one datum. A material may perforate at this level, giving a CAI strength equal to the compression strength of a panel with a hole the size of the impactor drilled through it. Another, more damage-resistant/tolerant material may develop a large area of fiber breakage (not penetration) associated with delaminations that could produce a much lower CAI strength than the less damage-resistant material. At lower impact energies this would have been detected, since perforation would not have occurred in the less damage-resistant material and a much larger area of damage would have developed whereas the tougher material would probably show a smaller region of damage and a higher CAI strength. In other words, it is entirely possible to have material *A* be more damage-resistant/tolerant at one impact energy level than material *B*, but at a different impact energy level, material *B* can be more damage-resistant/tolerant than material *A*.

4.1 Material

The fiber/resin system chosen for study was IM7 fiber in 977-2 toughened epoxy. This material was readily available and represents a very common type of system (high-strength carbon fibers in a toughened epoxy) being used on many programs for NASA. The layup configuration chosen for the

impact tests was a quasi-isotropic one of $[+45,0,-45,90]_s$. This configuration is typical of the basic layup unit being used for many primary structures on air and spacecraft. The material was processed from unidirectional prepreg tape as flat panels, using a hot press. The cure cycle consisted of vacuum bagging, then heating the panel at $1.7\text{ }^{\circ}\text{C}$ ($3\text{ }^{\circ}\text{F}$) per minute up to $177\text{ }^{\circ}\text{C}$ ($350\text{ }^{\circ}\text{F}$) and holding for 2 hr. Cooling was then ramped back down to room temperature at a rate of $2.8\text{ }^{\circ}\text{C}$ ($5\text{ }^{\circ}\text{F}$) per minute. A constant pressure of 550 kPa (80 psi) was applied during the entire cycle. The resulting panels had nominal ply thicknesses of approximately 0.12 mm (0.0047 in).

A select series of tests were performed on specimens to determine some key material property values. These specimens were manufactured from the same prepreg roll as the impact specimens. The cure cycle also remained the same for these specimens.

4.1.1 0° and 90° Tensile Testing

Unidirectional laminates of IM7/977-2 were tested to obtain load/strain data so the modulus and Poisson's ratio of the laminae in the fiber direction and perpendicular to the fiber direction could be determined. Strain-gauge rosettes were attached to five different specimens of each orientation and readings were taken at 445-N (100-lb) increments for the 0° specimens and at 4.45-N (10-lb) increments for the 90° specimens. These data were then plotted and a least-squares regression line fit determined the measured modulus of elasticity and Poisson's ratio in the respective direction. The averages were $E_{11}=1,867\text{ Gpa}$ (27.1 msi), $\nu_{12}=0.37$, $E_{22}=9.85\text{ Gpa}$ (1.43 msi), and $\nu_{21}=0.0187$.

4.1.2 $\pm 45^{\circ}$ Tensile Testing

Tensile testing was performed on $\pm 45^{\circ}$ specimens to determine the shear modulus of the laminae. Twenty-two-ply specimens were tested with strain-gauge rosettes with readings being taken at 223-N (50-lb) increments. The stress divided by two versus $|e_1| + |e_2|$ was plotted and a least-squares regression fit on the linear portion of the plot gave an average G_{12} of approximately 7.03 Gpa (1.02 msi).

4.1.3 Laminate Testing

Tensile specimens of the eight-ply $[+45,0,-45,90]_s$ laminates were also tested with strain-gauge rosettes. Readings were taken at 445-N (100-lb) increments and the data were plotted and a least-squares fit used to determine the tensile modulus and Poisson's ratio. The average values were $E_x=E_y=60.5\text{ Gpa}$ (8.78 msi) and $\nu_{12}=0.32$.

Strength measurements were also taken on these laminates. It should be noted that edge delamination occurred before ultimate fracture. This result is expected as high tensile normal stresses can be set up in the region of a free edge on a tensile specimen as outlined by Pipes and Pagano.¹²⁶ The ultimate average failure strain was $12,875\text{ }\mu\epsilon$ which corresponds to an average stress of 779 Mpa (113 ksi). The edges began to noticeably delaminate at approximately 689 Mpa (100 ksi). The delamination extended far into the specimen width before fracture of the 0° plies. A full analysis and discussion of this phenomenon is beyond the scope of this text and the interested reader is referred to other references for a more detailed treatment of the subject.^{127,128}

4.2 Impact Specimens

The specimens manufactured for impact testing consisted of eight-ply quasi-isotropic samples with a stacking sequence of $[+45,0,-45,90]_S$, cut into coupons 9.5 cm (3.75 in) wide and 29.8 cm (11.75 in) long. The coupons were cut from the cured panel with a diamond-wheel table saw. Fiberglass end tabs 11.4 cm (4.5 in) wide were bonded onto the ends of the specimen with epoxy adhesive to facilitate loading into the pretensioning device. The specimen dimensions are given in figure 20.

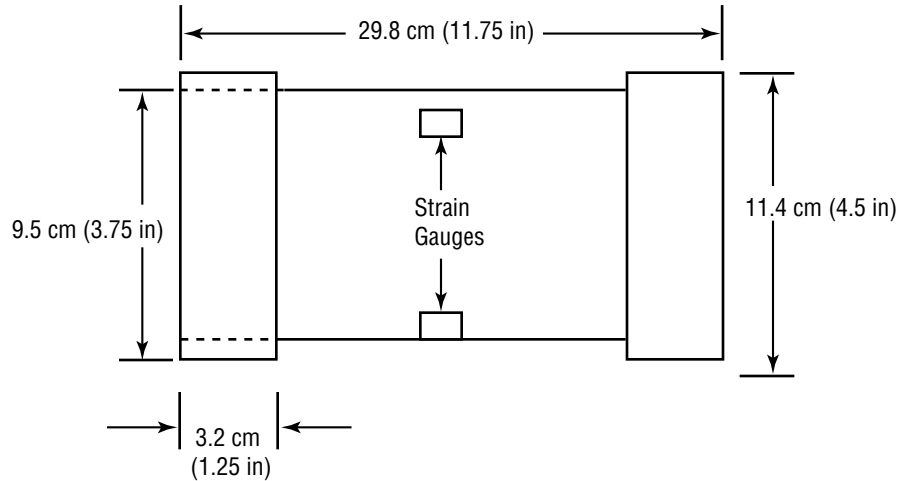


Figure 20. Specimens used for impact testing.

4.2.1 Specimen Strain-Gauging

Each specimen had two strain gauges bonded to it so that a uniform prestrain was ensured. The gauges were 1.3 cm (0.5 in) from the specimen's edges to detect strain gradients across the width (see fig. 20). This instrumentation was determined from a series of preliminary tests on samples that contained numerous strain gauges on the surfaces of the specimen. From these tests it was found that bending was never introduced into the specimen so gauges need only be placed on the same surface. In addition, it was found that the strain remained constant along the longitudinal axis of the specimen and the only variations in strain were across the width of the specimen. As long as the outermost gauges (1.3 cm (0.5 in) in from each edge) had the same strain, the ones between them also had this same strain, thus it was determined that only the two gauges nearest the edges and on the same side need be measured to ensure a uniform strain field was being set up in the specimen.

4.3 Pretensioning Device

The device to apply tensile preloads to the specimens basically consisted of two wedge grips connected to a load cell and a hydraulic piston. As the piston was pumped with hydraulic fluid it would cause the grips to move apart, putting the composite specimen in a state of tension. A sketch of the apparatus with the various parts is given in figure 21.

The wedge adjustment blocks were first tightened together to lodge the specimen in the grips. These blocks also prevented the wedges from moving apart (and stop gripping) during the application of the preload. As the preload was applied and the strain gauges were monitored, when one gauge deviated from the other, that side reading the lower strain could have its adjustment blocks loosened, allowing the specimen to expand slightly along that side, causing the strain to rise on that side. These adjustments were made until the final level of strain was reached and the adjustment blocks could be fine-tuned to give a nearly uniform prestrain across the width of the specimen.

4.3.1 Boundary Conditions

The boundary conditions chosen for this study were clamped-clamped/free-free with the clamped edges perpendicular to the applied preload. This geometry was chosen since it was demonstrated in a previous program¹²⁹ that this condition most closely represented a pressure vessel being impacted. Pressure vessels are of vital interest to this study since they are tension-carrying structural members.

Once the level of prestrain was achieved, the top clamp plates were tightened down with the 12 bolts, each at a torque of 28 N-m (250 in-lb), to obtain the desired boundary condition. A true clamped boundary condition would mean that the hydraulic piston could be released and the specimen would continue to carry the prestrain between the region of the clamps. However, in practice this was not the case and was never achieved despite trying a number of techniques. The methods that came closest to achieving this tended to crush the specimen in the region of clamping; therefore, it was determined that the hydraulic piston would be held in place during the impact event. Measurements of the strain before and after impact indicated that the specimen did not move significantly in the clamps. The high torque on the clamp-down bolts ensured that no bending moments could occur under the clamps.

4.4 Impact Testing

Once the desired level of prestrain was achieved, the preloading device with the specimen was positioned under a Dynatup 8200 drop tower as shown in figure 22. The height of the crosshead was adjusted to give the desired impact energy. In this study, the mass of the crosshead with tup was 2.4 kg (5.22 lb). Since the crosshead/guideposts interface does not contain linear bearings or another such friction-reducing device, an exact prediction of impact energy from the drop height was impossible. Although this friction is present, the measured impact energy is quite precise since the velocity of the falling crosshead is measured just prior to impact. Once a desired drop height was decided upon, all impact tests at that corresponding impact energy level were conducted before the cross head was moved again. This ensured uniformity in the impact energy levels used. A total of three impact energies were used in this study: 3.4, 4.5, and 6.0 J (2.5, 3.3, and 4.4 ft-lb). These levels induced damage from visible to nonvisible.

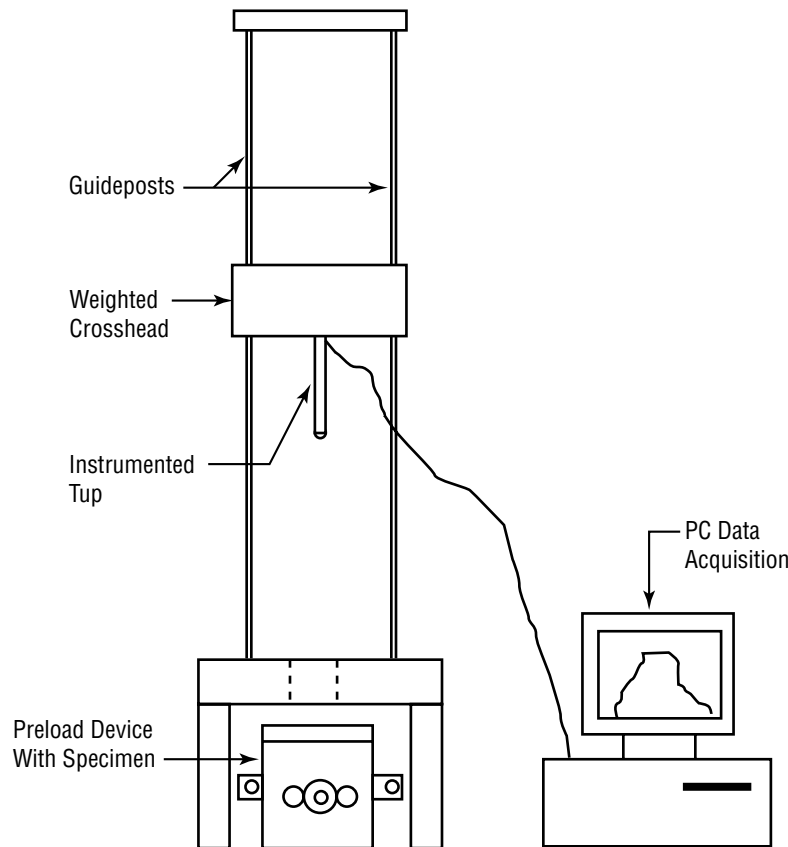


Figure 22. Preload and impact apparatus.

4.5 Postimpact Testing

In order to assess the effects of tensile preloads on the damage resistance of the specimens tested, three forms of postimpact inspection were used. The first type of inspection was a visual one to see if any damage could be detected from either surface of the plate. This was followed by a nondestructive x-ray inspection and then a destructive cross-sectional examination of the specimen through the damage zone.

4.5.1 Visual Inspection

After each specimen was impacted, it was carefully removed from the preload device and inspected for visual damage. No magnifying devices were used; however, if damage could be felt and not seen, this was recorded as “visual” damage since no special tools were needed to identify this damage. The extent and type of visual damage was recorded for each impacted specimen. The type of damage that could be detected consisted of back face (nonimpacted side) matrix splitting, front face (impacted side) indentation damage, and small matrix splits being felt on the back surface.

4.5.2 X-ray Inspection

For specimens that did contain observable damage on one of the two faces, a small circular dam of plumber’s putty was placed around the damage on one of the faces to hold in a zinc iodide (ZnI) dye

penetrant solution as shown in figure 23. The dye penetrant is opaque to x rays and was allowed to soak on the specimen (at a damage site) for at least 24 hr. The solution consisted of 100 g of ZnI powder in 100 ml of water and 100 ml of Kodak Photoflow™ which breaks the surface tension of the solution to allow full penetration into all cracks and delaminations.

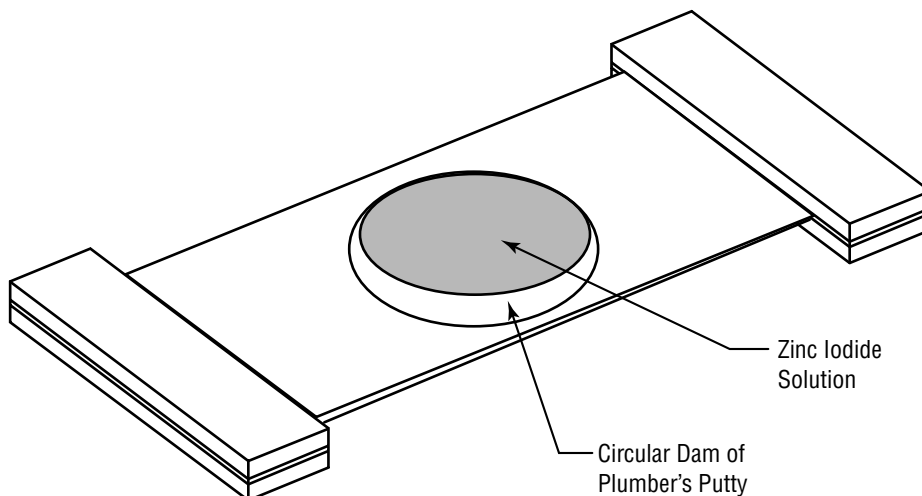


Figure 23. Dam of plumber's putty to hold zinc iodide solution over damage area.

For specimens that did not contain damage on one of the two faces, a small hole of ~0.5 mm (0.02 in) was drilled through the specimen at the impact site to allow the dye penetrant to be exposed to any through-the-thickness damage that may have occurred within the laminate.

The specimens were wiped clean of the plumber's putty and excess penetrant after at least a 24-hr soak and exposed to x rays with a Torrex 150D x-ray inspection system manufactured by EG&G Astrophysics Research. Polaroid type 55 film was placed directly under the specimen to obtain a permanent copy of the x-ray signature of each specimen. The dye penetrant was seen to seep into all matrix delaminations and cracks and was easily detectable on the developed film.

4.5.3 Cross-Sectional Examination

Some of the specimens were sectioned through a part of the damage zone in an attempt to gather more detailed information about the induced damage. This was particularly helpful in identifying areas where fibers were broken, and in identifying the interface of a delamination.

A technique was developed during this study whereby the location of the cross-sectional cut relative to the damage as seen by the x rays could be determined. The x rays, which corresponded to the specimens at a 1:1 ratio, were photocopied onto film transparency. The clear film now had the image of the x ray at a 1:1 ratio with the specimen. Strain gauges that would register on the x rays provided accurate guides as to the location that the film needed to be placed to be a surface marker of the internal damage. The area of impact on the specimen was painted white to enhance the visibility of the x ray on the clear film transparency which was matched to the specimen and applied with double-sided tape. The damage zone was then cut from the specimen and two clear acrylic plates were used to sandwich

the cut specimen with the x-ray pattern on the surface. These clear plastic plates were bonded to the specimen with cyanoacrylate ester glue. The x-ray pattern could be seen clearly through the acrylic plate. Any cuts made on the sandwiched specimen could now be associated with the damage, as seen by the x-ray inspection technique.

A microscope equipped with a Polaroid camera was used to examine the cross-sectioned specimens. Magnifications between $\times 7.25$ and $\times 160$ were possible.

4.6 Static Indentation Testing

In order to better understand the load/deflection and in-plane strain response of the transversely loaded specimens, a series of static indentation tests were performed using a dial indicator to measure transverse displacement and various strain gauges to measure the surface strains at given locations. The pretensioning device was placed in an Instron 1125 load frame and the indenter was attached to the upper crosshead/load cell. After applying the desired amount of prestrain, the specimen was incrementally loaded with the indenter at the center of the specimen (as in the impacts) and transverse displacement and strain-gauge readings were taken. This step process was continued until a cracking noise was heard, indicating specimen damage.

The specimens were unloaded in the same incremental fashion to obtain a complete load-displacement history of the entire process. This could provide valuable information on how much energy is being lost during the process.

In addition, two static indentation tests were performed in which the specimen was loaded to failure. Surface strains were not monitored but load-displacement data were. These two tests were performed to gain insight on the load-deflection behavior of specimens with a medium level of prestrain, as well as gather information on the static behavior once damage becomes severe in the specimen.

4.6.1 Static Indentation Strain Gauging

Strain gauges were placed on the specimens so that information could be obtained about the surface strains at areas of interest. For practical reasons, strain gauges could not be placed at the center of the specimen since the indenter would interfere with it from the top and the dial indicator from the bottom. A number of strain-gauge setups were used on the 10 samples tested. Table 4 lists the strain-gauge placement on each sample along with the rationale behind choosing these locations.

4.6.2 Loading/Unloading Curves

As mentioned previously, the transverse load was applied incrementally. After initial readings were taken at zero-applied load, the specimen was loaded with 44.5 N (10 lb) and a second reading taken. The third reading was taken at 111.25 N (25 lb) and then readings were taken at 111.25-N (25-lb) increments thereafter until a popping or cracking noise was heard, at which point the specimen was then unloaded in 222.5-N (50-lb) increments. The transverse load was applied at a rate of 1.27 mm/min (0.05 in/min) between stops.

Table 4. Specimens for static indentation tests.

Specimen	Strain Gauge Placement			Objective	
1		Gauge	x ¹	y ¹	To test setup and obtain load/deflection data.
		1	67	13	
		2	67	82	
		I ²	79	47	
2		Gauge	x	y	To examine across-the-width strain field and strain near center ends on top surface of a low prestrained (500 $\mu\epsilon$) specimen.
		1	79	13	
		2	79	38	
		3	79	58	
		4	79	83	
		5	140	48	
		6	13	48	
		I	79	48	
3		Gauge	x	y	To examine across-the-width strain field on top and bottom sides of specimen of a low prestrained (500 $\mu\epsilon$) specimen.
		1	79	13	
		2	79	38	
		3	79	57	
		4	79	82	
		(5) ³	79	82	
		(6)	79	57	
		(7)	79	38	
		(8)	79	13	
		9	10	47	
		(10)	19	47	
4		Gauge	x	y	To examine top and bottom strains near edges and ends at a moderate (4,500 $\mu\epsilon$). Note: Specimen not clamped.
		1	73	82	
		2	73	13	
		3	146	47	
		4	73	82	
		5	73	13	
		6	146	47	
		I	79	47	

1. Dimensions in mm.

2. I denotes indenter location.

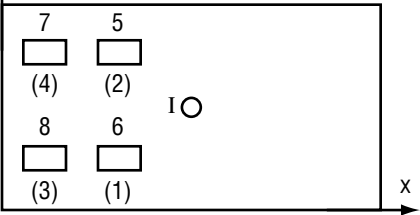
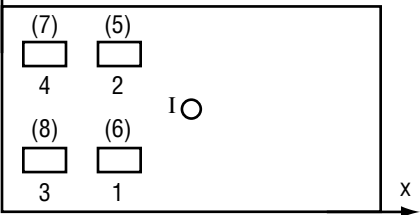
3. Numbers in parenthesis indicate strain gauge on opposite side of specimen.

Table 4. Specimens for static indentation tests (continued).

Specimen	Strain Gauge Placement	Objective																														
5	<table border="1"> <thead> <tr> <th>Gauge</th><th>x</th><th>y</th></tr> </thead> <tbody> <tr><td>1</td><td>86</td><td>13</td></tr> <tr><td>2</td><td>86</td><td>78</td></tr> <tr><td>3</td><td>137</td><td>45</td></tr> <tr><td>4</td><td>86</td><td>78</td></tr> <tr><td>5</td><td>86</td><td>13</td></tr> <tr><td>6</td><td>137</td><td>45</td></tr> <tr><td>7</td><td>79</td><td>45</td></tr> </tbody> </table>	Gauge	x	y	1	86	13	2	86	78	3	137	45	4	86	78	5	86	13	6	137	45	7	79	45	To replicate specimen #4 with plates clamped.						
Gauge	x	y																														
1	86	13																														
2	86	78																														
3	137	45																														
4	86	78																														
5	86	13																														
6	137	45																														
7	79	45																														
6	<table border="1"> <thead> <tr> <th>Gauge</th><th>x</th><th>y</th></tr> </thead> <tbody> <tr><td>1</td><td>79</td><td>13</td></tr> <tr><td>2</td><td>79</td><td>78</td></tr> <tr><td>3</td><td>79</td><td>13</td></tr> <tr><td>4</td><td>79</td><td>78</td></tr> <tr><td>5</td><td>17</td><td>45</td></tr> <tr><td>6</td><td>17</td><td>45</td></tr> <tr><td>7</td><td>79</td><td>45</td></tr> </tbody> </table>	Gauge	x	y	1	79	13	2	79	78	3	79	13	4	79	78	5	17	45	6	17	45	7	79	45	To replicate #5 with a low prestrain ($300 \mu\epsilon$).						
Gauge	x	y																														
1	79	13																														
2	79	78																														
3	79	13																														
4	79	78																														
5	17	45																														
6	17	45																														
7	79	45																														
7	<table border="1"> <thead> <tr> <th>Gauge</th><th>x</th><th>y</th></tr> </thead> <tbody> <tr><td>1</td><td>92</td><td>13</td></tr> <tr><td>2</td><td>92</td><td>82</td></tr> <tr><td>3</td><td>57</td><td>47</td></tr> <tr><td>4</td><td>13</td><td>47</td></tr> <tr><td>5</td><td>92</td><td>13</td></tr> <tr><td>6</td><td>92</td><td>82</td></tr> <tr><td>7</td><td>57</td><td>47</td></tr> <tr><td>8</td><td>13</td><td>47</td></tr> <tr><td>9</td><td>79</td><td>47</td></tr> </tbody> </table>	Gauge	x	y	1	92	13	2	92	82	3	57	47	4	13	47	5	92	13	6	92	82	7	57	47	8	13	47	9	79	47	To examine the change in strain from near an end toward the indenter location at a small prestrain ($300 \mu\epsilon$).
Gauge	x	y																														
1	92	13																														
2	92	82																														
3	57	47																														
4	13	47																														
5	92	13																														
6	92	82																														
7	57	47																														
8	13	47																														
9	79	47																														
8	<table border="1"> <thead> <tr> <th>Gauge</th><th>x</th><th>y</th></tr> </thead> <tbody> <tr><td>1</td><td>79</td><td>13</td></tr> <tr><td>2</td><td>79</td><td>83</td></tr> <tr><td>3</td><td>57</td><td>48</td></tr> <tr><td>4</td><td>13</td><td>48</td></tr> <tr><td>5</td><td>79</td><td>13</td></tr> <tr><td>6</td><td>79</td><td>83</td></tr> <tr><td>7</td><td>57</td><td>48</td></tr> <tr><td>8</td><td>13</td><td>48</td></tr> <tr><td>9</td><td>79</td><td>48</td></tr> </tbody> </table>	Gauge	x	y	1	79	13	2	79	83	3	57	48	4	13	48	5	79	13	6	79	83	7	57	48	8	13	48	9	79	48	To replicate #7 at a higher prestrain ($4,100 \mu\epsilon$).
Gauge	x	y																														
1	79	13																														
2	79	83																														
3	57	48																														
4	13	48																														
5	79	13																														
6	79	83																														
7	57	48																														
8	13	48																														
9	79	48																														

1. Dimensions in mm.
2. I denotes indenter location.
3. Numbers in parenthesis indicate strain gauge on opposite side of specimen.

Table 4. Specimens for static indentation tests (continued).

Specimen	Strain Gauge Placement			Objective	
9		Gauge	x	y	Examine strain near center end of specimen.
		1	51	13	
		2	51	78	
		3	13	13	
		4	13	78	
		(5)	51	78	
		(6)	51	13	
		(7)	13	78	
		(8)	13	13	
		I	79	46	
10		Gauge	x	y	To replicate #9 at a low prestrain ($400 \mu\epsilon$).
		1	44	13	
		2	44	82	
		3	6	13	
		4	6	82	
		(5)	44	82	
		(6)	44	13	
		(7)	6	82	
		(8)	6	13	
		I	79	47	

1. Dimensions in mm.
2. I denotes indenter location.
3. Numbers in parenthesis indicate strain gauge on opposite side of specimen.

5. RESULTS

This chapter presents the results of the experimental portion of the work. Since this study is empirically based, the material presented is quite detailed, and most of the raw data are presented in the appendices. Every effort has been made to make this chapter as complete and thorough as possible. Discussion of the particulars of the results and noteworthy comparisons are not made in this chapter but rather will be made in chapter 6 which is devoted entirely to a discussion of the results.

5.1 Instrumented Impact Testing

The amount of tensile preload on the impacted specimens had a measurable effect on the maximum load of impact, duration of impact, maximum deflection, and absorbed energy of the specimen. The following sections will present the results from these data.

5.1.1 Maximum Load of Impact

As calculated in chapter 3, the higher the tensile prestrain, the higher the impact force should be for given impact conditions. This was clearly the case for the specimens examined in this study. The results for each of the three impact levels used are shown in figures 24–26. As damage forms in the specimen (not accounted for in the analysis in chapter 3), the maximum load of impact tends to level off, and even drop some with increasing prestrain (which tends to increase the damage).

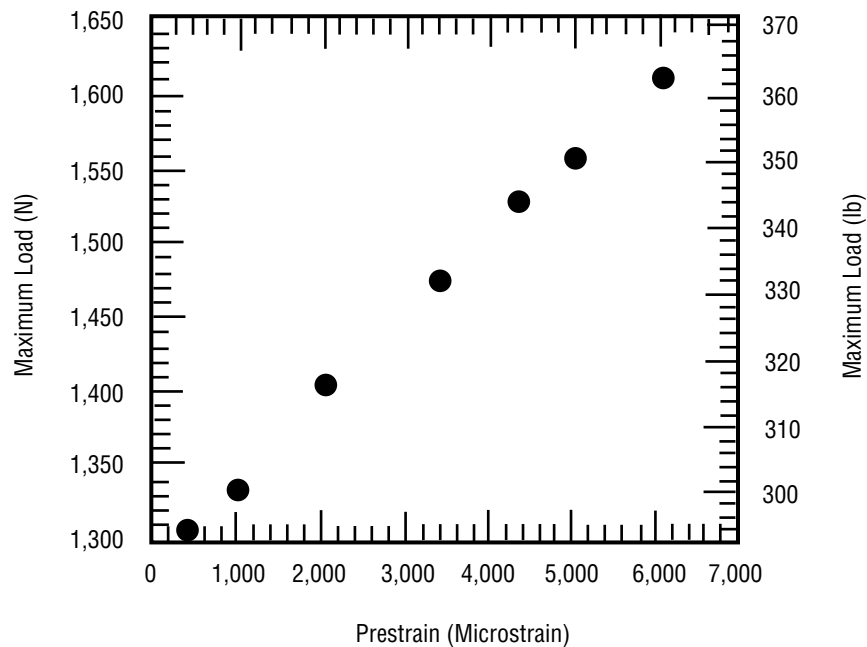


Figure 24. Maximum load of impact versus applied prestrain for 3.4 J (2.5 ft-lb) impacts.

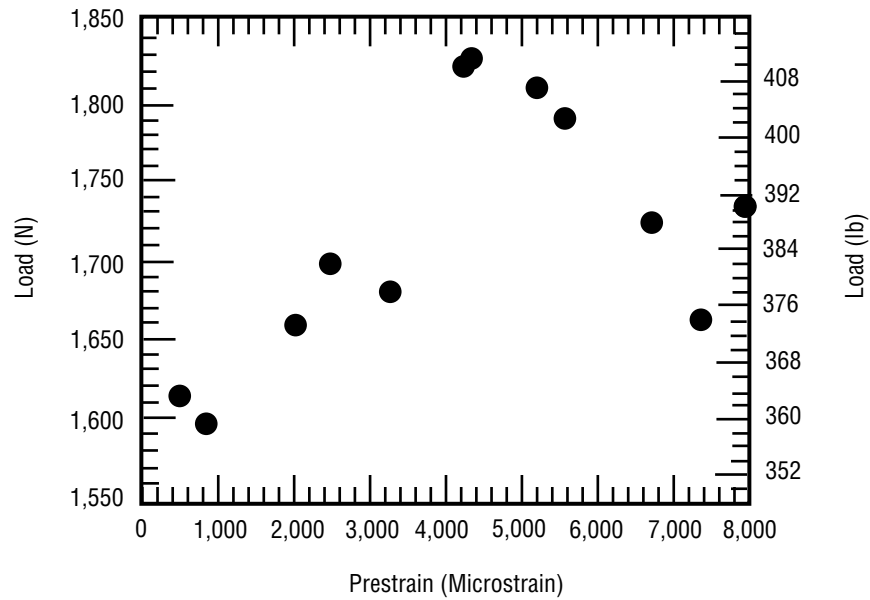


Figure 25. Maximum load of impact versus applied prestrain for 4.5 J (3.3 ft-lb) impacts.

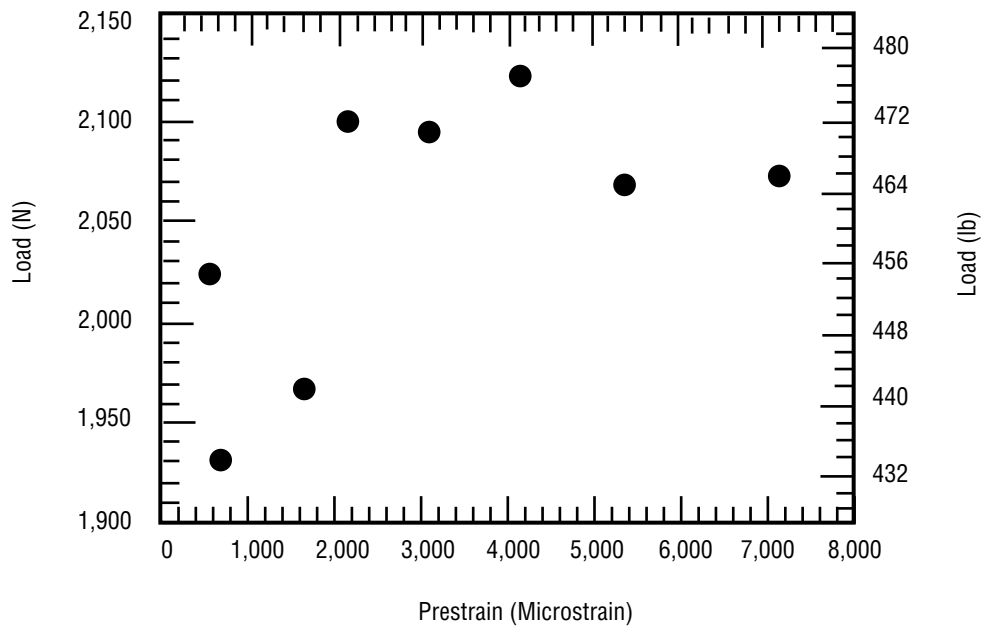


Figure 26. Maximum load of impact versus applied prestrain for 6.0 J (4.4 ft-lb) impacts.

5.1.2 Duration of Impact

Figures 27–29 show that as the tensile prestrain increased, the duration of the impact event decreased. This variable was not examined in the analysis, but as the maximum deflection decreases

with increasing prestrain (as will be seen in the next section), it is expected that the duration of impact should follow the same trend. Note the nonlinearity in this relationship.

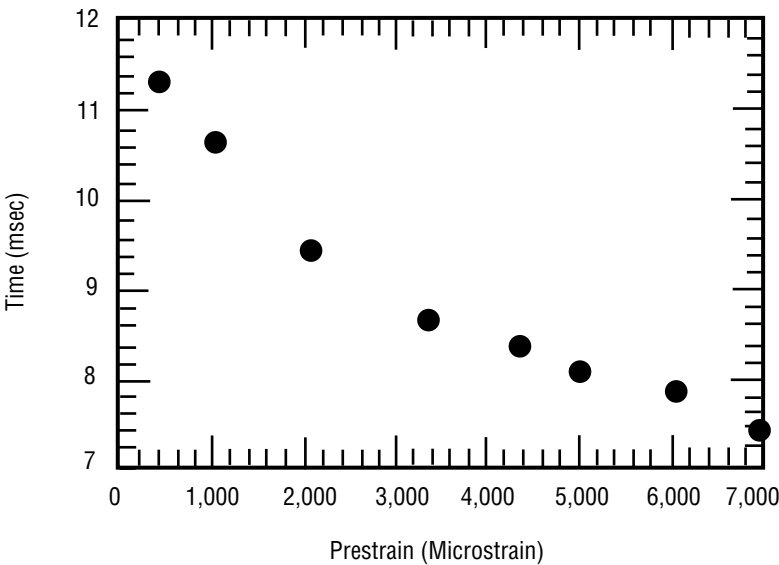


Figure 27. Total time of impact versus prestrain for 3.4 J (2.5 ft-lb) impacts.

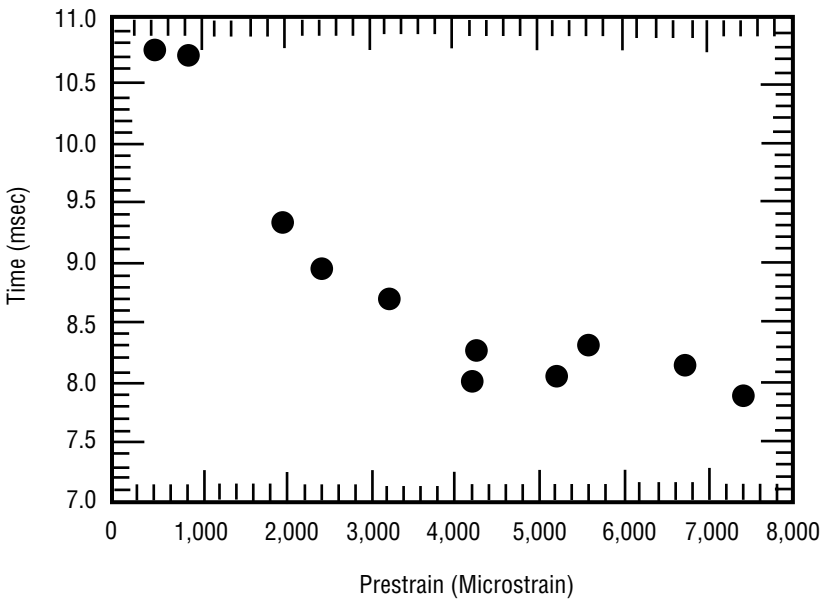


Figure 28. Total time of impact versus prestrain for 4.5 J (3.3 ft-lb) impacts.

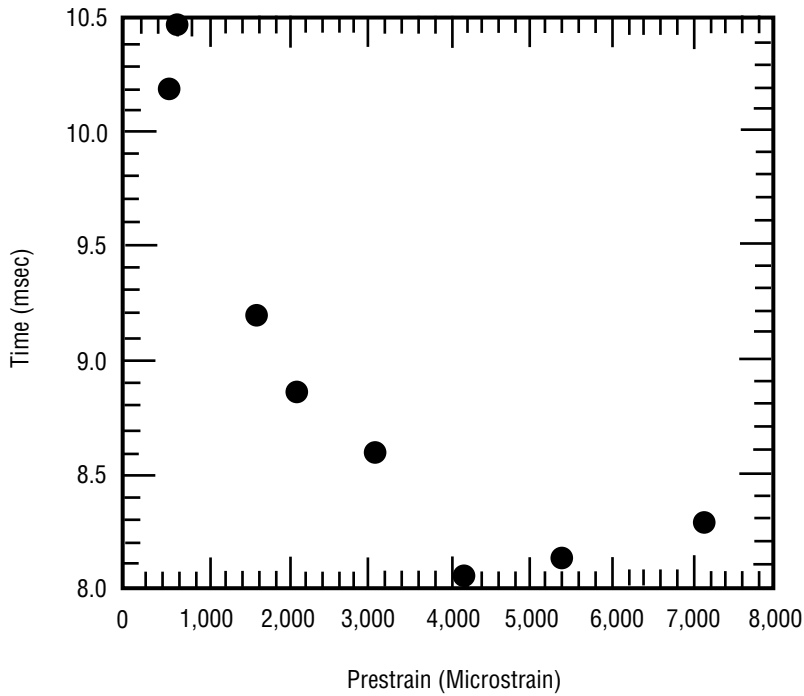


Figure 29. Total time of impact versus prestrain for 6.0 J (4.4 ft-lb) impacts.

5.1.3 Maximum Deflection

The maximum deflection of impact was predicted to decrease with increasing tensile prestrain as determined in chapter 3. Plots of the measured data are shown in figures 30–32. These plots are nonlinear in a similar fashion to those from the previous section. The maximum deflection data begins to drop rather rapidly with increasing prestrain, then level off at the higher end of prestrains.

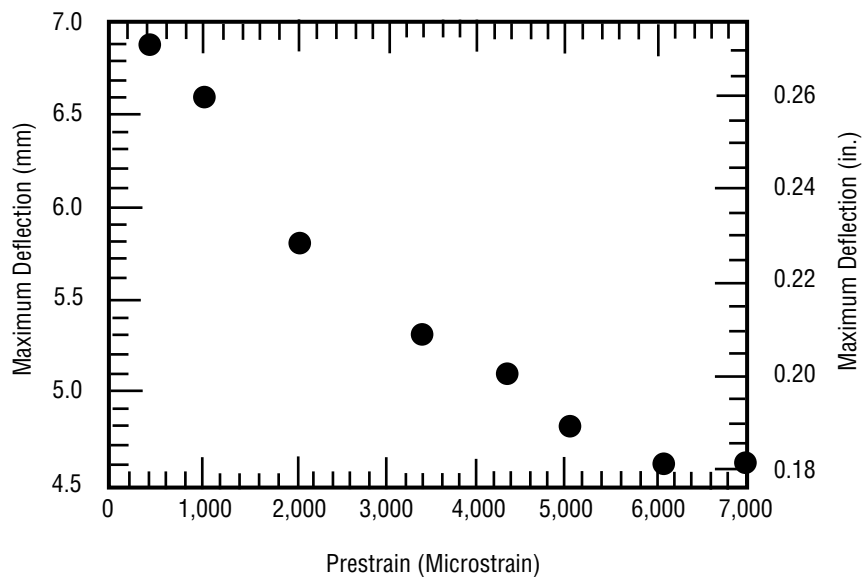


Figure 30. Maximum center deflection versus prestrain for 3.4 J (2.5 ft-lb) impacts.

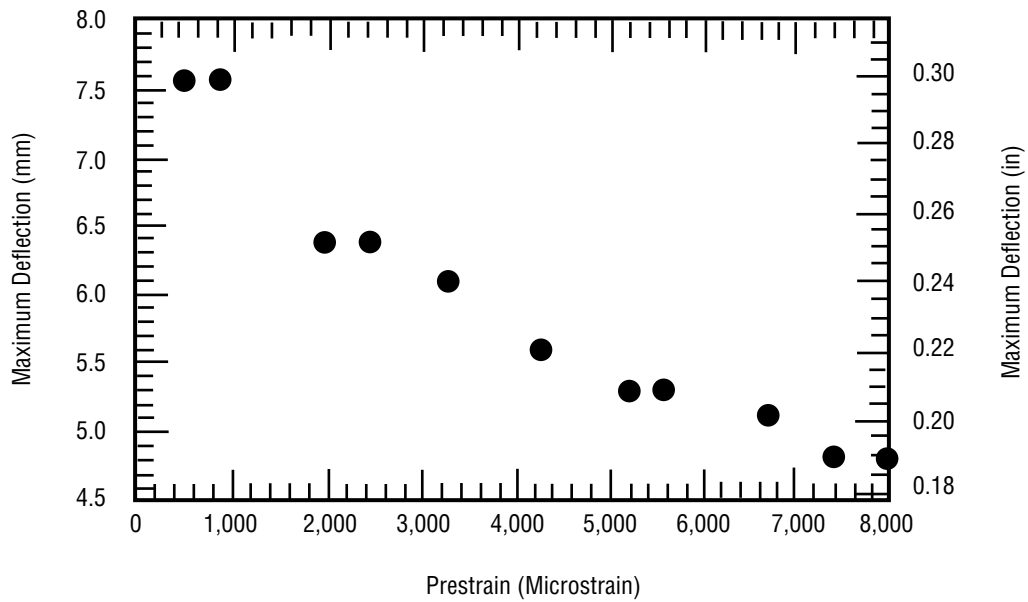


Figure 31. Maximum center deflection versus prestrain for 4.5 J (3.3 ft-lb) impacts.

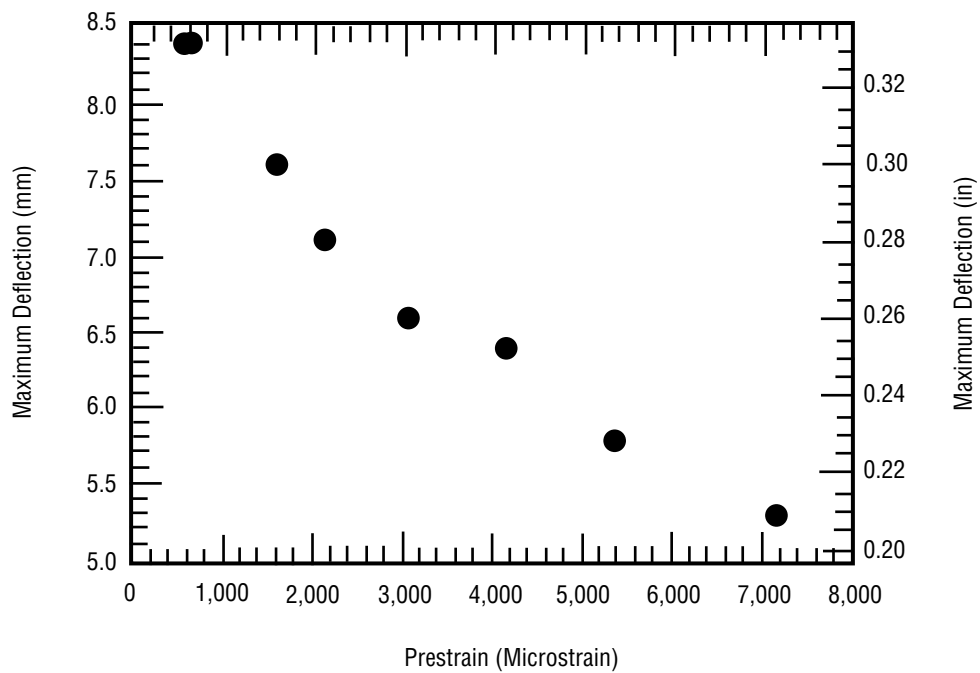


Figure 32. Maximum center deflection versus prestrain for 6.0 J (4.4 ft-lb) impacts.

5.1.4 Absorbed Energy of Impact

The amount of energy lost during the impact event is termed “absorbed energy.” The absorbed energy versus prestrain plots are given in figures 33–35. For low prestrains the absorbed energy is seen to decrease with increasing prestrain up to a critical level, at which point it begins to rise. The smaller the

impact energy the larger the initial drop in absorbed energy with increasing prestrain. This is thought to be a result of compliance in the preloading device. Since a true clamped condition was not practical, at low prestrains the specimen could displace a given amount in the fixture, thus losing a given amount of energy. As the impact energies increased, this amount of energy became a lower percentage and was less noticed. As the prestrain increased, the grips tended to help hold the specimen in a true clamped configuration and there was less displacement of the specimen, thus less energy lost due to this movement of the laminate being tested.

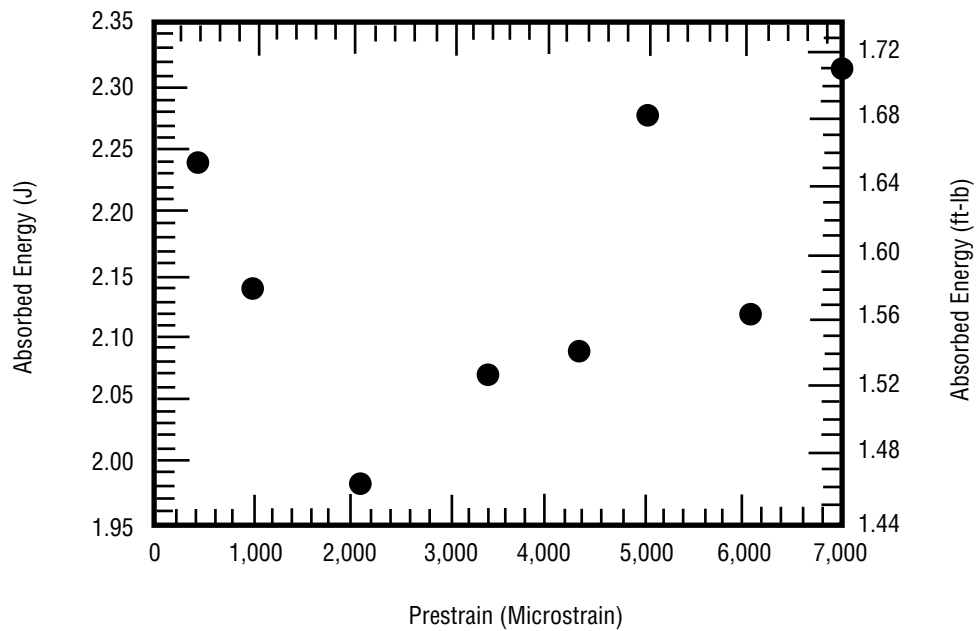


Figure 33. Absorbed energy during impact versus prestrain for 3.4 J (2.5 ft-lb) impacts.

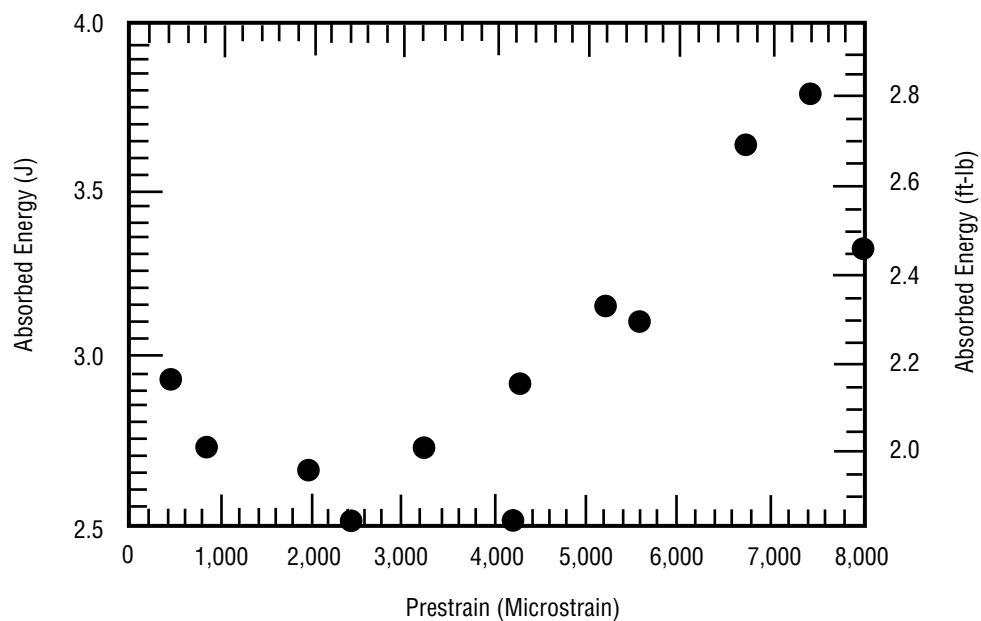


Figure 34. Absorbed energy during impact versus prestrain for 4.5 J (3.3 ft-lb) impacts.

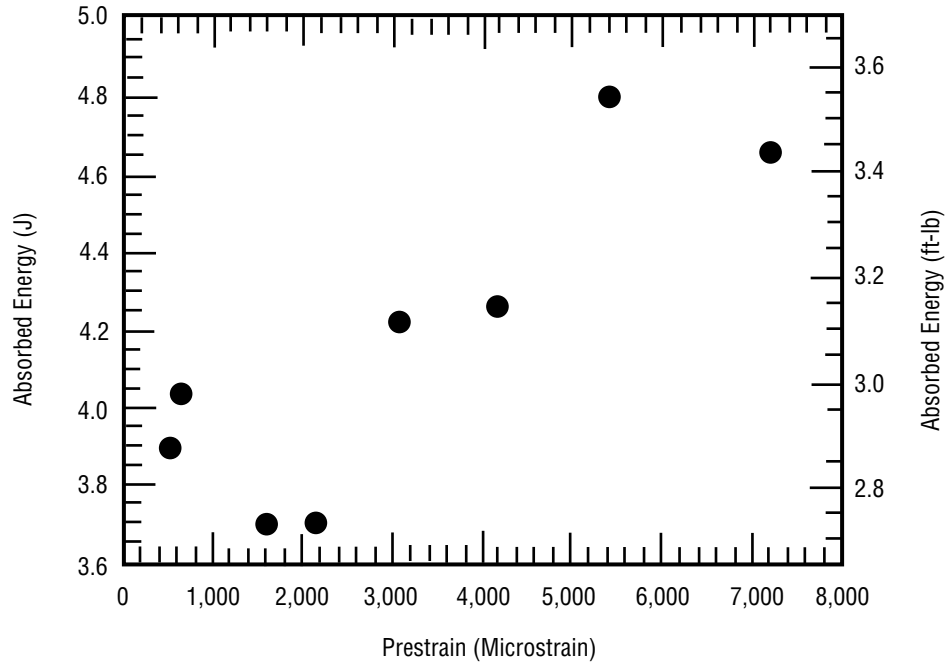


Figure 35. Absorbed energy during impact versus prestrain for 6.0 J (4.4 ft-lb) impacts.

5.1.5 Load-Deflection Curves

For all of the specimens tested, the load-deflection plots show that a significant amount of energy is lost during the impact event, even at the lowest impact energy level used. A typical load/deflection curve is shown in figure 36 for the lowest level impact at the smallest prestrain and in figure 37 for the highest level impact at the highest prestrain. These two plots represent the two extreme cases of impact tested in this study. All of the load/deflection curves are given in appendix A.

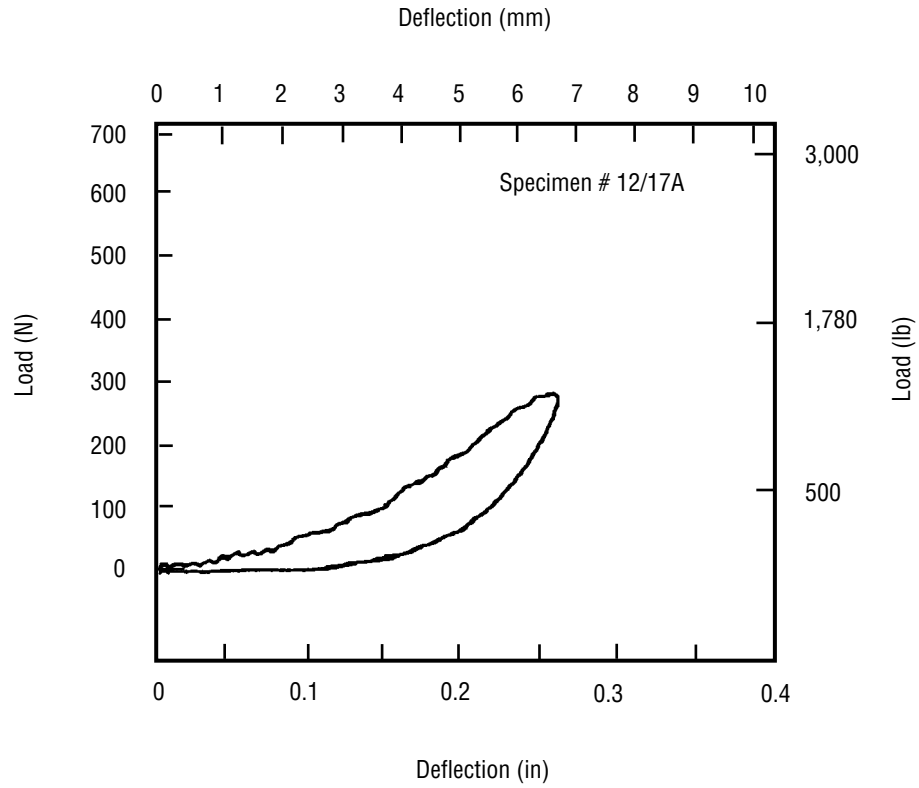


Figure 36. Load/displacement curve for lowest level impact at lowest prestrain.

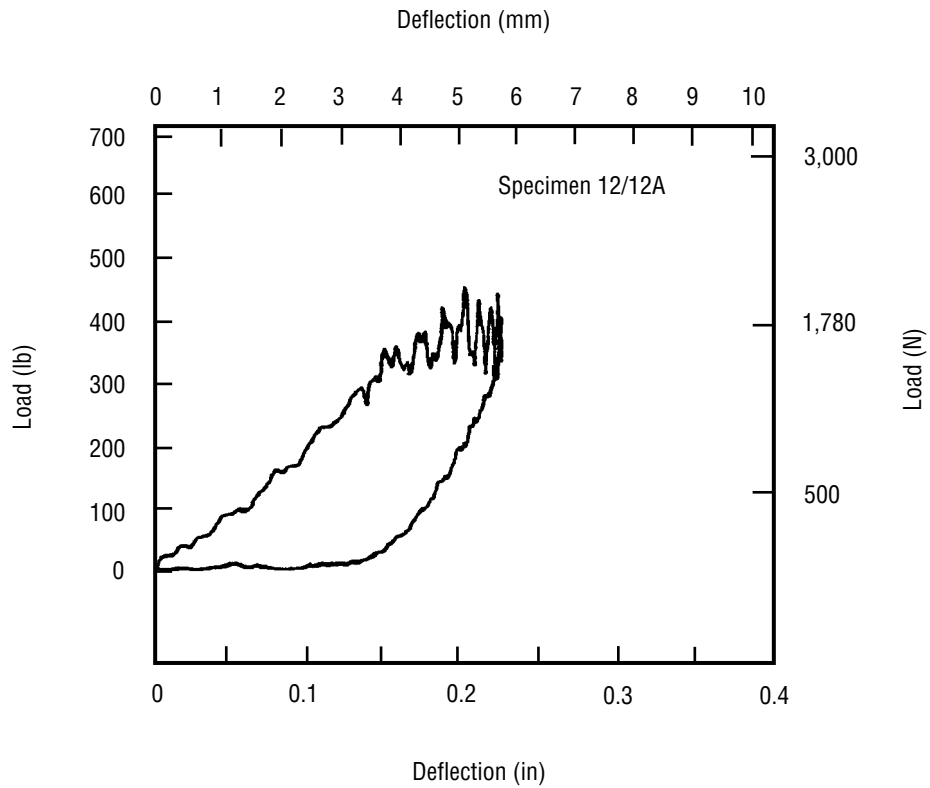


Figure 37. Load/displacement curve for highest level impact at highest prestrain.

5.2 Visual Examination

In general, as the preload increased, the amount of visual damage also increased. This corresponds to the higher impact force induced into the specimen. The first sign of visible damage was always splitting of the matrix between fibers on the back 45° face. Contact stresses produced visible damage at the impact site in some of the specimens. Table 5 gives values for all of the specimens tested, along with a description of the visual damage.

Table 5. Specimens tested with associated parameters and results.

Specimen No.	Impact Energy (J)	Prestrain (me)	Maximum Load (N)	Maximum Deflection (mm)	Total Time (msec)	Absorbed Energy (J)	Visual Damage
L1	4.5	5,182	1,811	5.3	8.06	3.16	22-mm split on back face
L2	4.5	3,229	1,682	6.1	8.70	2.73	None
L3	4.5	452	1,615	7.6	10.79	2.93	18-mm split on back face
L4	4.5	833	1,598	7.6	10.73	2.73	17-mm split on back face
L5	4.5	7,399	1,664	4.8	7.88	3.81	116-mm split on back face Dent w/short split, front
L6	4.5	5,564	1,793	5.3	8.31	3.11	47-mm split on back face
11/13A	4.5	2,430	1,700	6.4	8.95	2.52	17-mm split on back face
11/13B	4.5	1,960	1,660	6.4	9.31	2.66	18-mm split on back face
11/14A	4.5	7,970	1,736	4.8	7.36	3.35	65-mm split on back face Dent w/small split, front
11/14B	4.5	4,205	1,825	5.6	8.01	2.51	None
11/25A	4.5	4,268	1,829	5.6	8.25	2.92	30-mm split on back face
11/27A	4.5	6,698	1,727	5.1	8.14	3.65	60-mm split on back face Dent w/small split, front
11/28A	6.0	5,384	2,069	5.8	8.13	4.80	Split across width Dent with short split on front
11/28B	6.0	498	2,025	8.4	10.21	3.89	21-mm split on back face
12/12A	6.0	7,173	2,074	5.3	8.29	4.66	Split across width Dent with splits on front
12/12B	6.0	2,132	2,100	7.1	8.86	3.70	18-mm split on back face
12/12C	6.0	4,156	2,123	6.4	8.06	4.26	45-mm split on back face Dent w/small split, front
12/12D	6.0	3,053	2,096	6.6	8.59	4.22	53-mm split on back face. Dent on front
12/13A	6.0	1,594	1,967	7.6	9.20	3.70	20-mm split on back face
12/13B	6.0	634	1,931	8.4	10.49	4.04	19-mm split on back face
12/14B	3.4	6,972	1,633	4.6	7.44	2.32	27-mm split on back face
12/14C	3.4	987	1,335	6.6	10.66	2.14	None
12/14D	3.4	3,387	1,477	5.3	8.69	2.07	None
12/14E	3.4	5,012	1,562	4.8	8.09	2.28	26-mm split on back face
12/17A	3.4	400	1,308	6.9	11.34	2.24	None
12/17B	3.4	4,334	1,531	5.1	8.38	2.09	19-mm split on back face
12/17C	3.4	6,060	1,615	4.6	7.85	2.12	24-mm split on back face
12/17D	3.4	2,045	1,406	5.8	9.50	1.98	None

5.3 X-ray Inspection

As expected, the specimens that contained more visible damage also contained more internal damage, mostly in the form of matrix splitting and delaminations. The specimens that had no externally visible damage demonstrated that some delaminating occurred (the small drilled hole allowed the penetrant to reach these areas). These delamination zones were relatively small compared to the specimens that had visual damage associated with them. A typical x ray of this type is shown in figure 38. Note that matrix cracking is associated with the delaminations, a feature seen in all of the specimens.

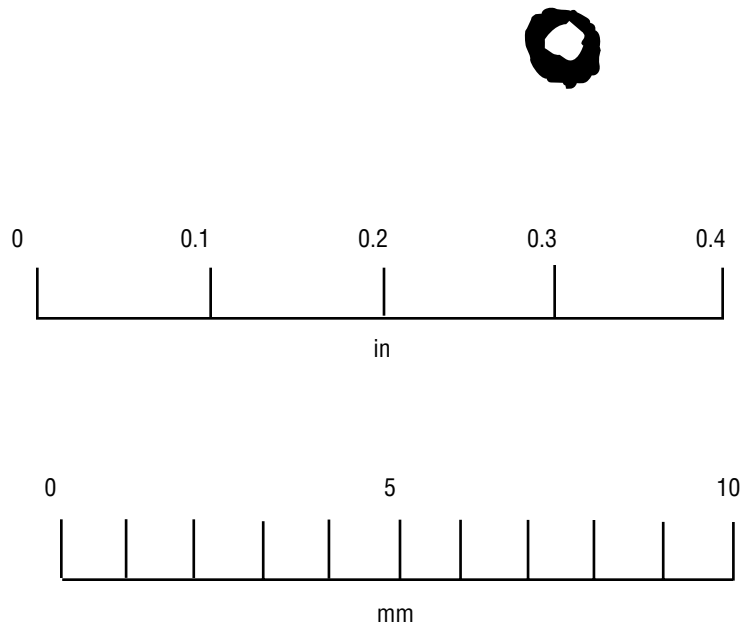


Figure 38. Typical x-ray signature for a specimen that exhibits no visible damage.

For the specimens that did contain externally visible damage, the matrix crack on the back 45° face was clearly visible and always had delaminations emanating from the crack. These delaminations tended to form a lobe shape and end at a crack in the ply above the 45° ply (the 0° ply). A typical x ray with this form of damage is shown in figure 39.

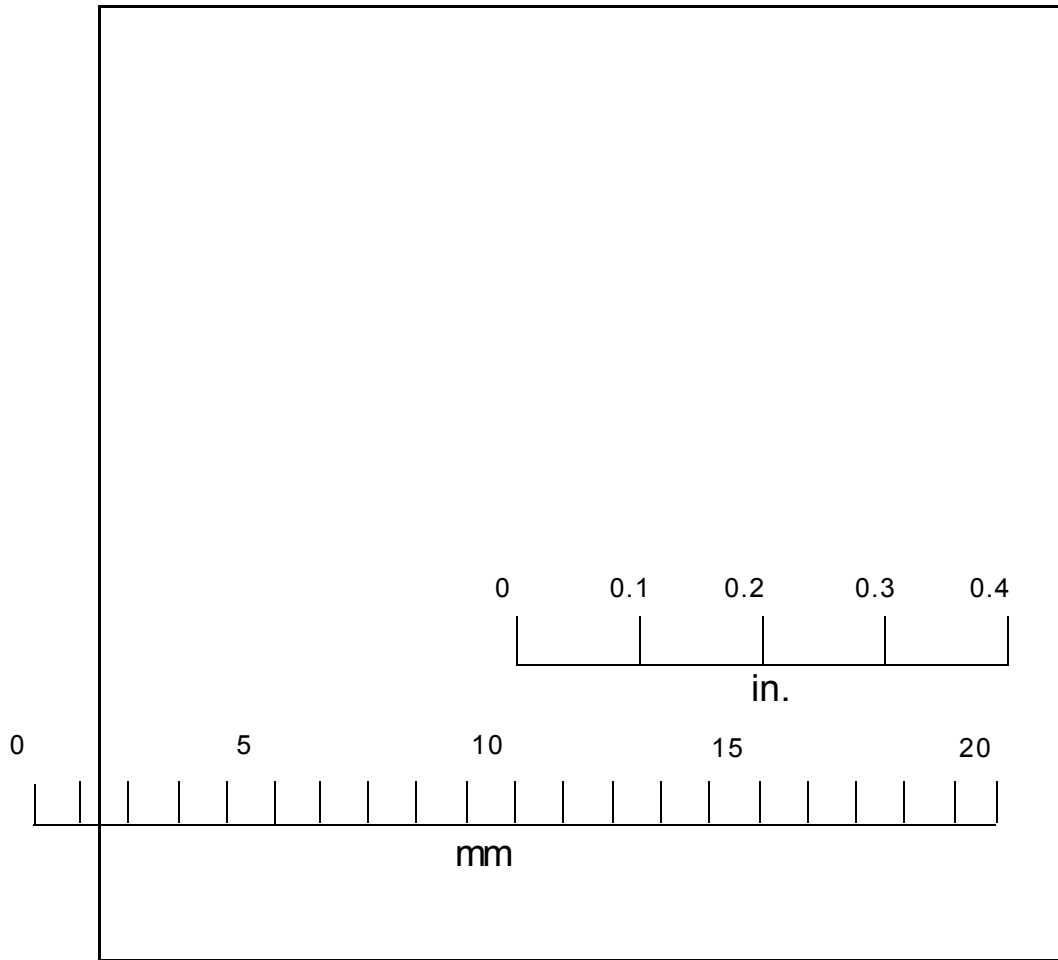


Figure 39. Typical x-ray signature for a specimen that contains back face matrix splitting.

As the damage in the specimen became more severe due to higher preloads, damage on the impacted side of the specimen would begin to form. For these specimens, the dye penetrant would tend to “pool up” and form very dark areas on the x-ray signatures as shown in figure 40. This made detection of broken fibers difficult since these breaks are hidden by the large amount of dye penetrant. Cross-sectional examination was the method used in this study to detect broken fibers. All of the x-ray signatures of damage are shown in appendix B. The static indentation test samples are also included.

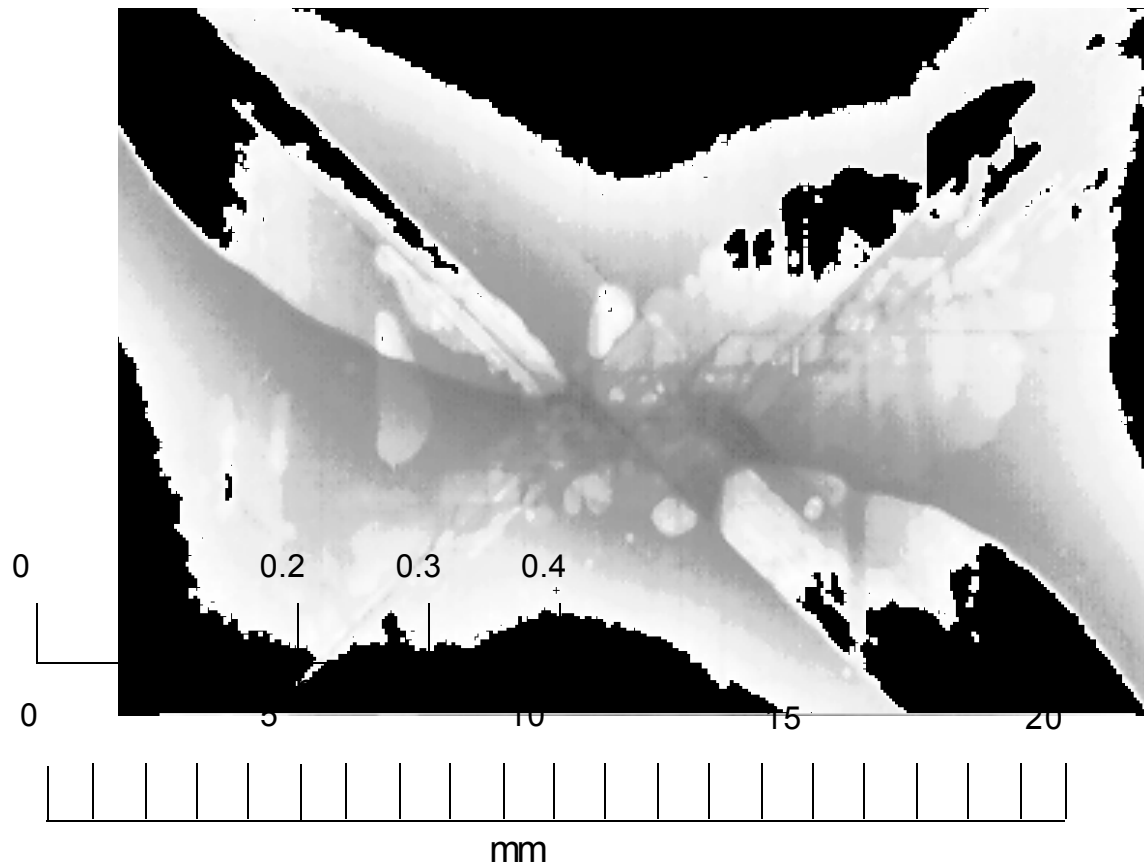


Figure 40. Typical x-ray signature for a specimen that exhibits visible damage on the impacted side.

5.4 Cross-Sectional Examination

For specimens in which the x rays did not provide sufficient enough detail (usually associated with fiber breakage), cross-sectional examinations proved useful. The x rays gave an accurate description of the damage formed due to the impact event, but fiber breakage was difficult to detect. When specimens were cross-sectioned through the dark areas of the x ray, fiber breakage could sometimes be seen. Cross-sectional photographs of selected specimens, along with their x rays showing where the cuts were made, are shown in figures 41–49. Note that the 0° fiber breakage areas are always in very close proximity to the matrix cracks both above and below this area because these areas are subject to the highest stresses, and also, as a matrix crack forms, the component of stress perpendicular to the fibers in that layer is now transferred to the layer next to it, in the vicinity of the crack.

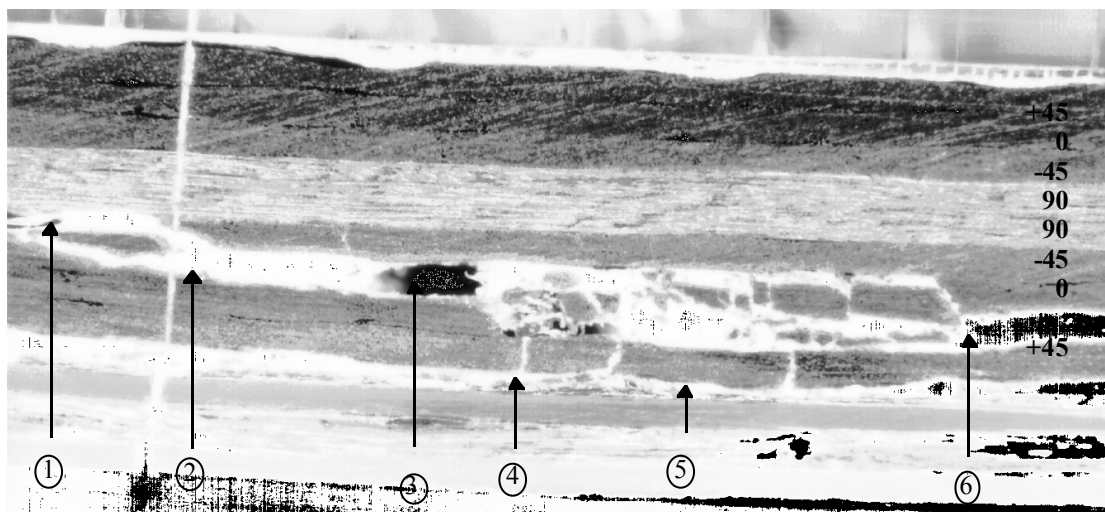
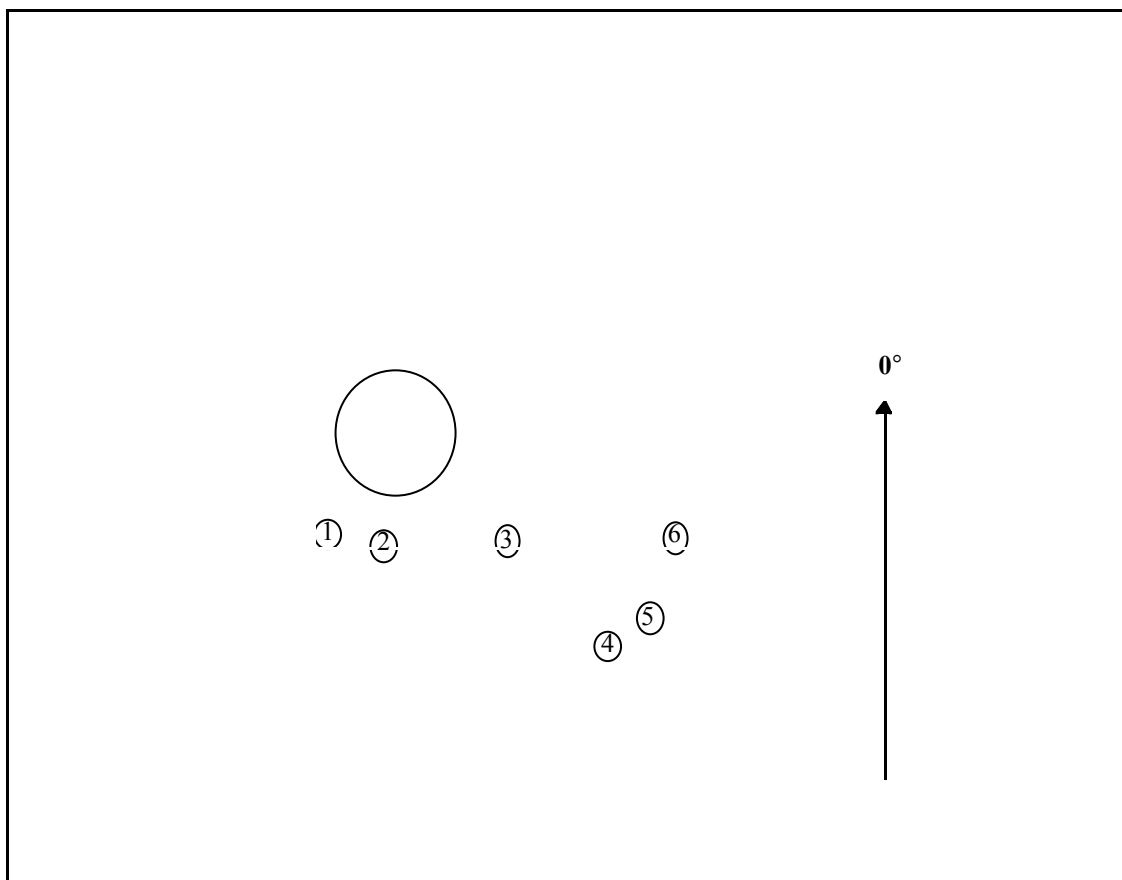


Figure 41. Cross-section of specimen # Static # 5.

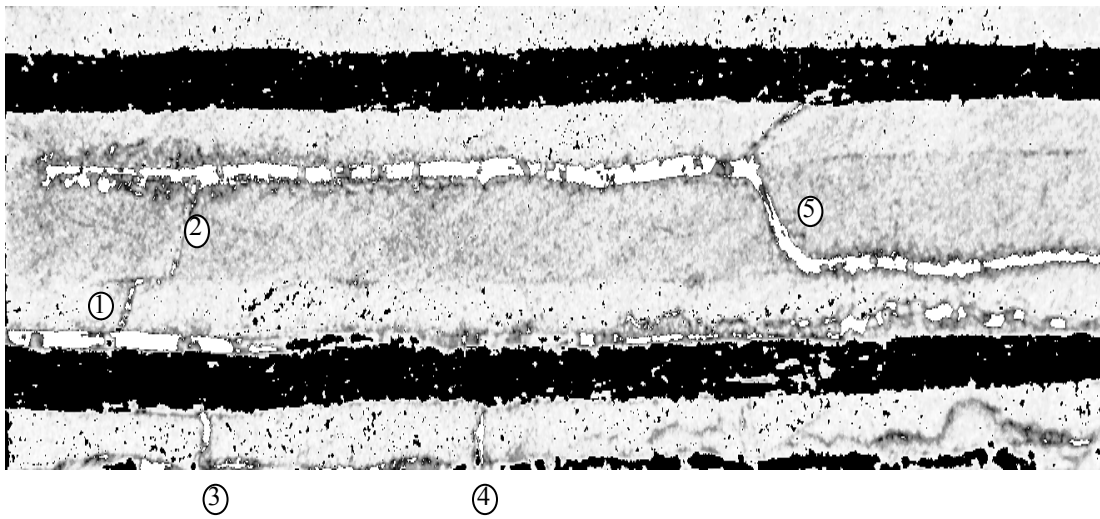
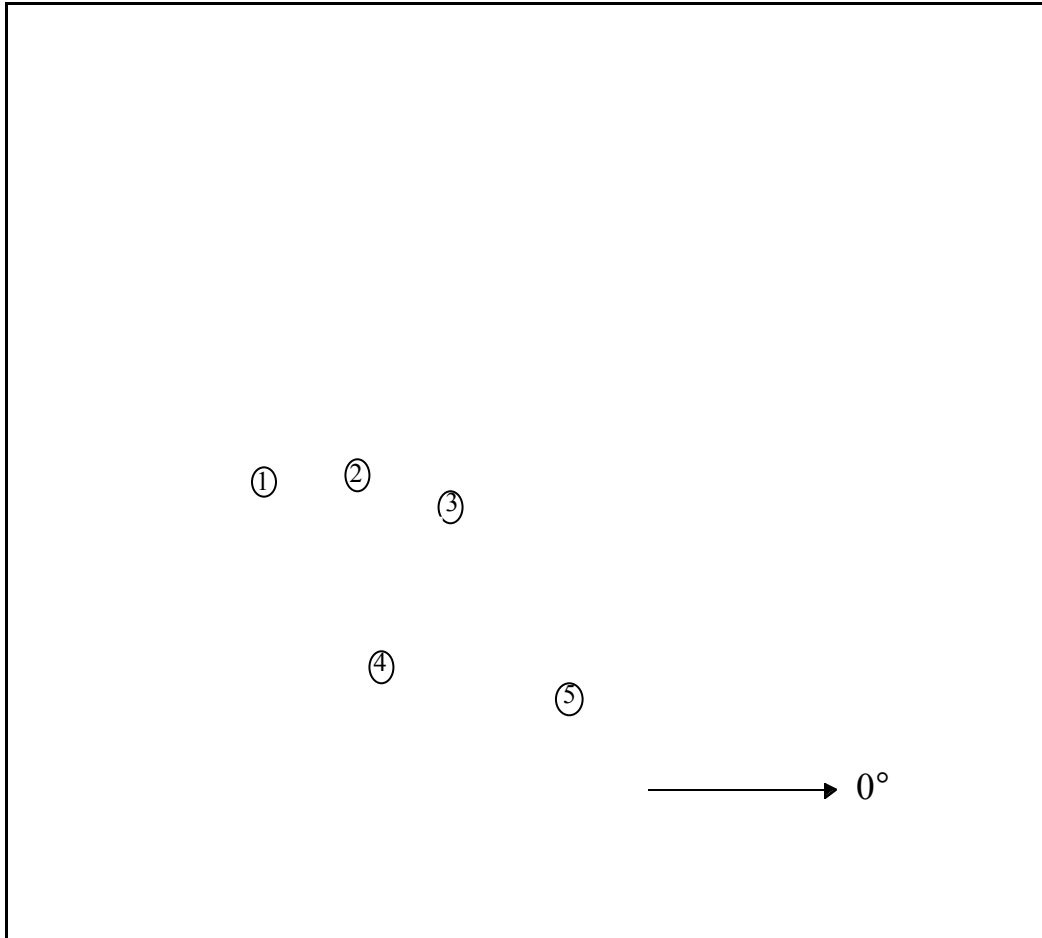


Figure 42. Cross-section of specimen # 12/13B.

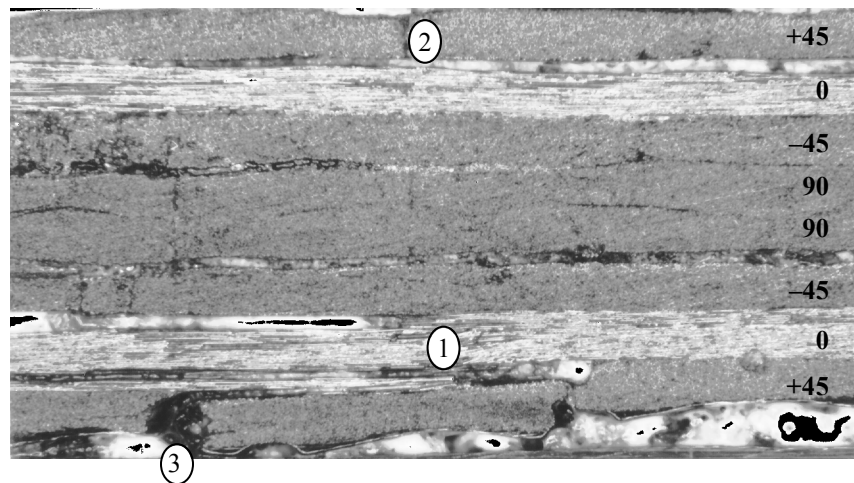
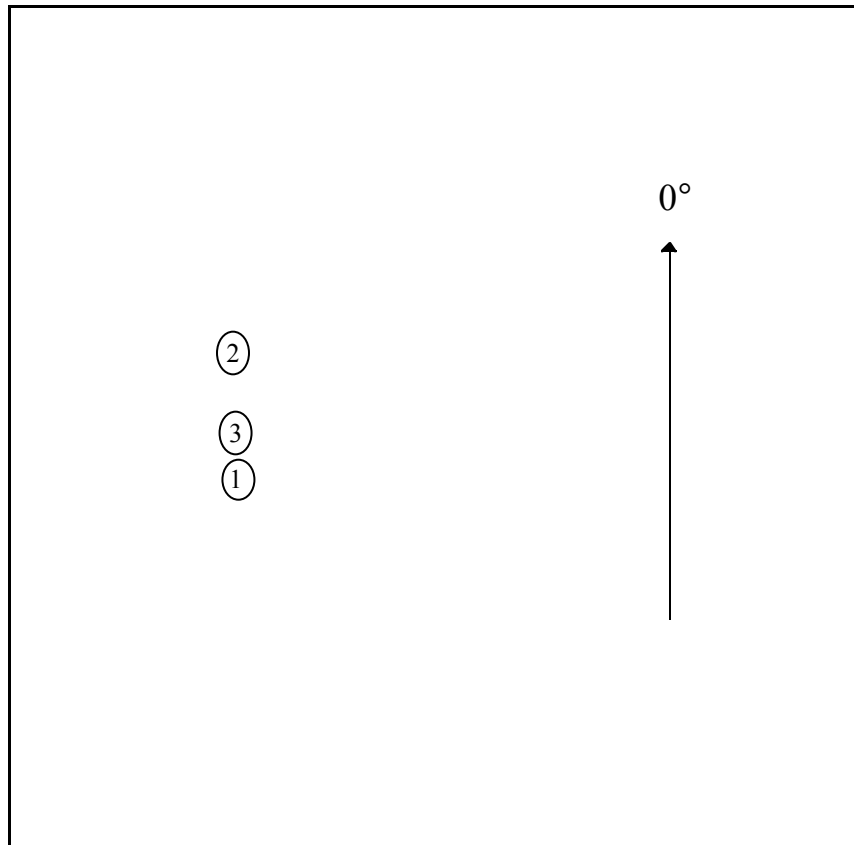


Figure 43. Cross-section of specimen # 12/12A, cut 1.

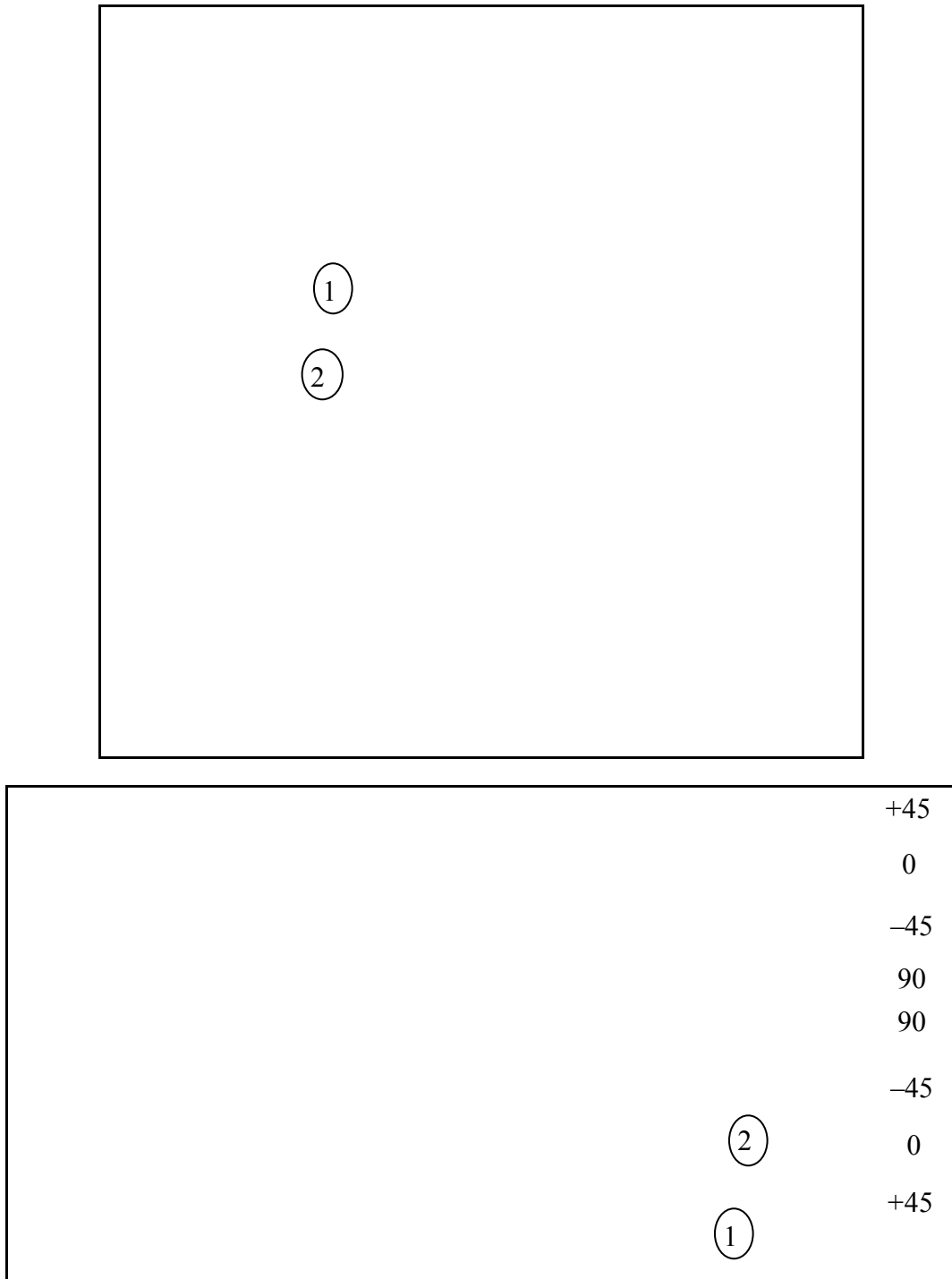


Figure 44. Cross-section of specimen # 12/12A, cut 2.

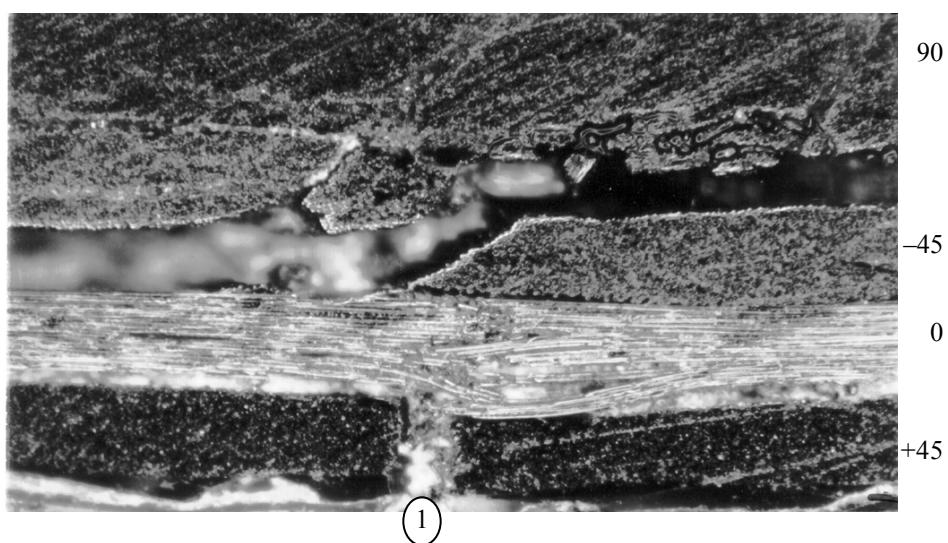
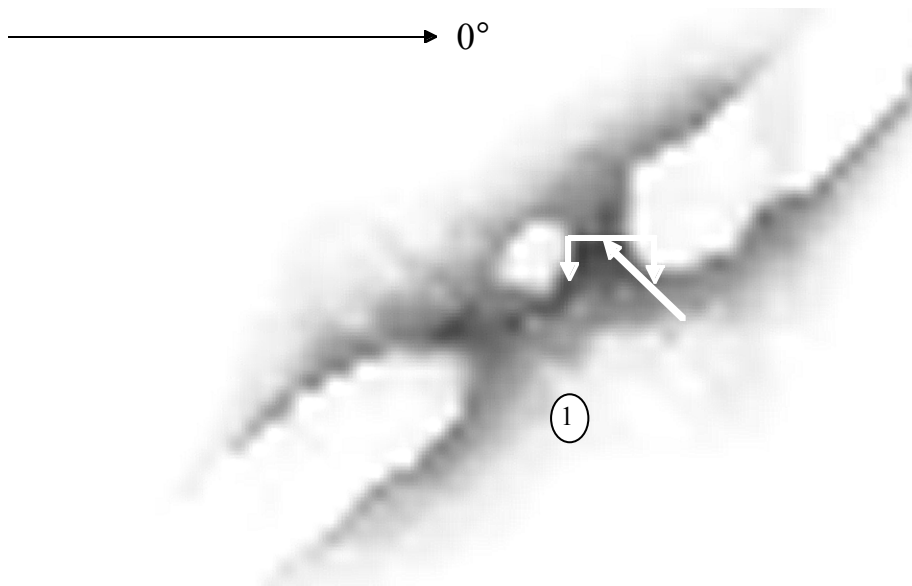


Figure 45. Cross-section of specimen # L6, cut 1.

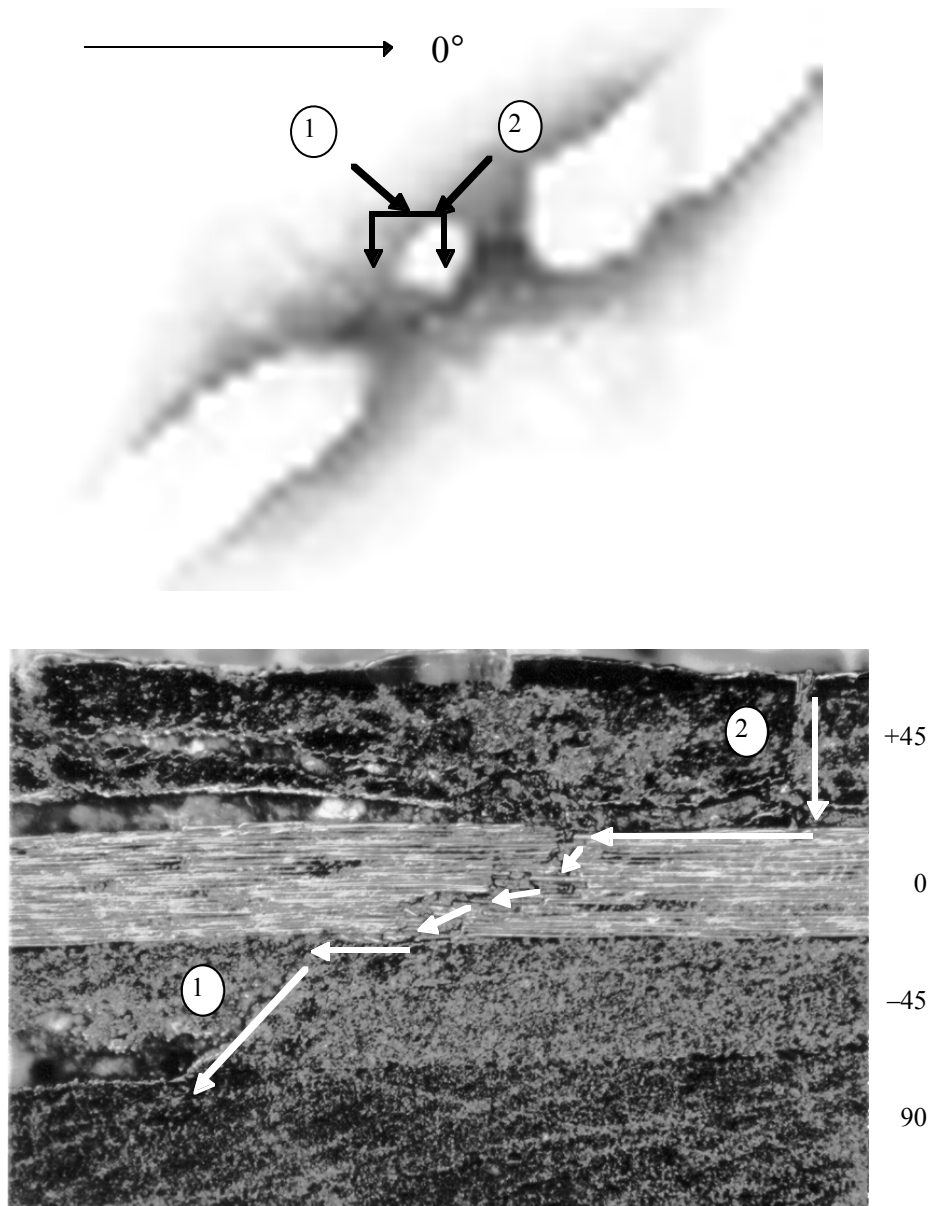


Figure 46. Cross-section of specimen # L6, cut 2.

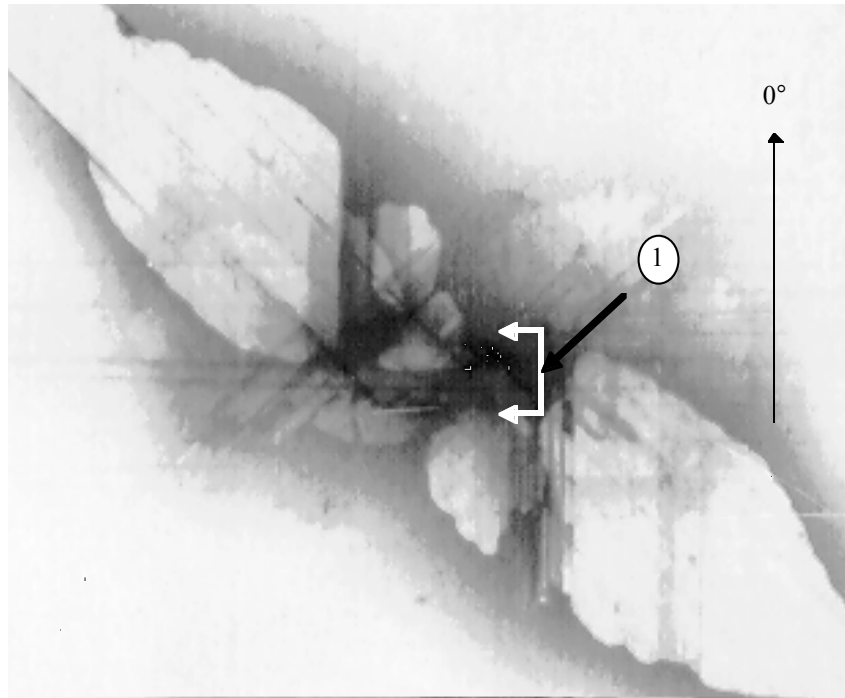


Figure 47. Cross-section of specimen # 12/12C, cut 1.

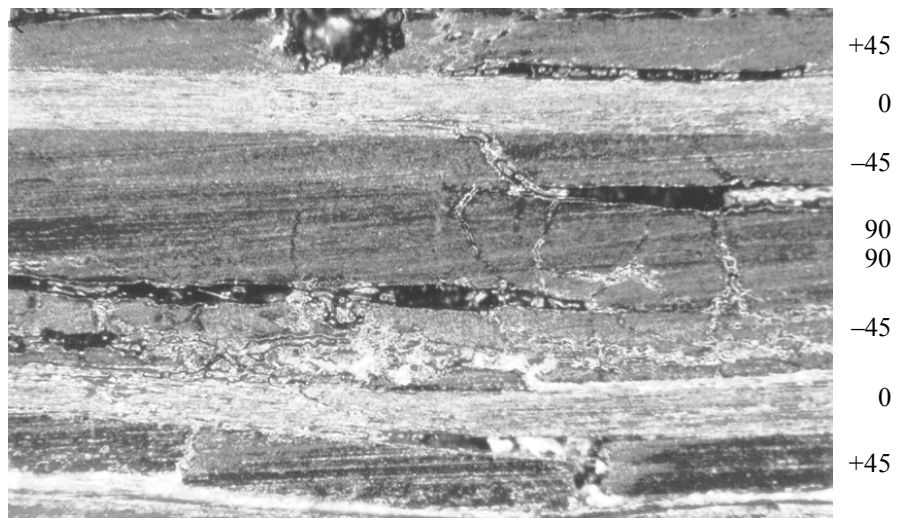
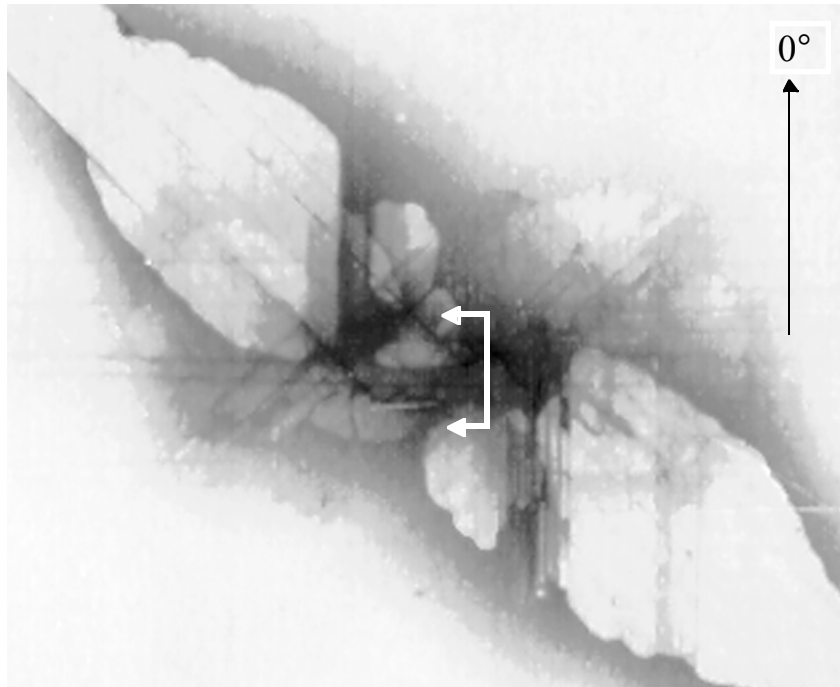


Figure 48. Cross-section of specimen # 12/12C, cut 3.

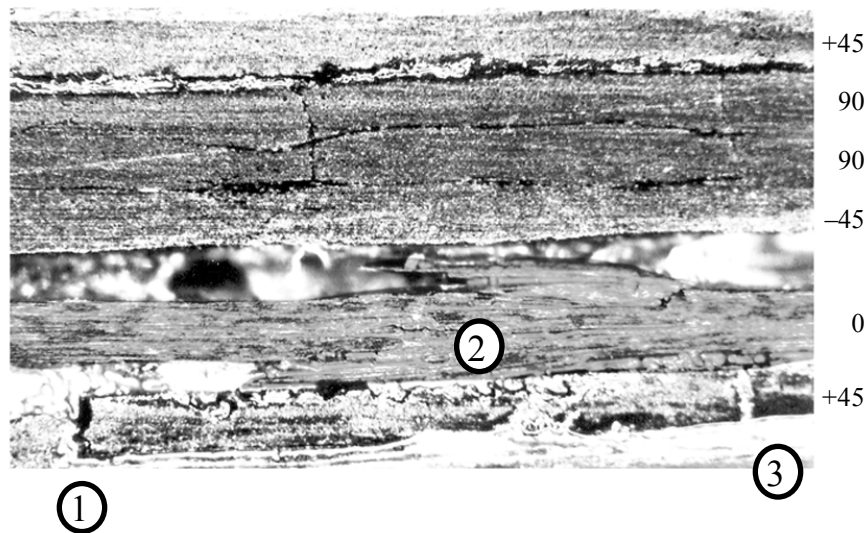
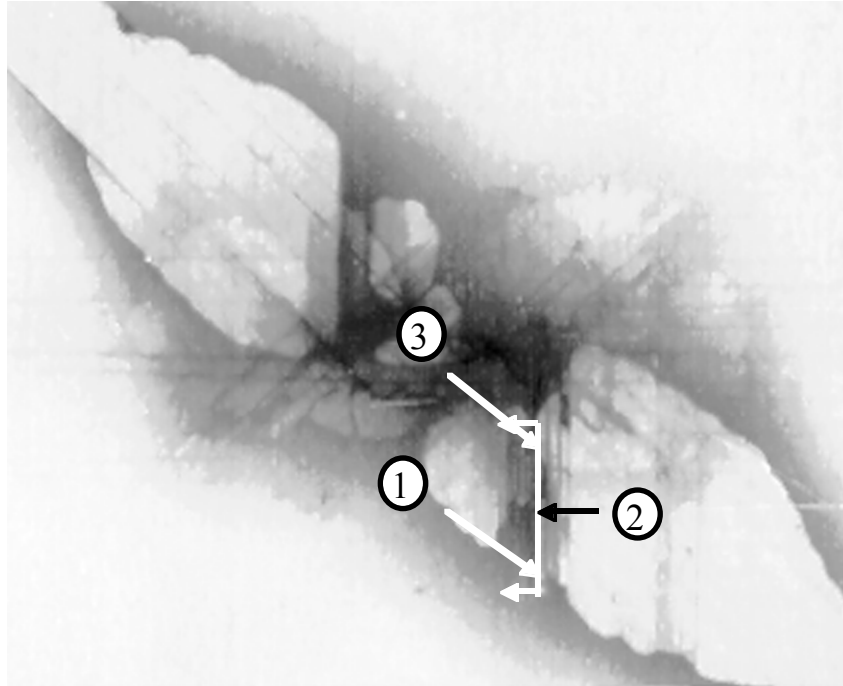


Figure 49. Cross-section of specimen #12/12C, cut 2.

Figure 41 is a cross-sectional view of a statically loaded specimen that experienced a maximum load of 1,780 N (400 lb). The cut on this specimen was made perpendicular to the 0° fibers in order to demonstrate that the long dark areas running in the 0° direction consists of heavy matrix cracking in the 0° ply. Note that between delamination zone #3 and matrix cracks #4 and #5, there is much matrix damage in the lower 0° ply, which shows up as a dark stripe in the 0° direction on the x-ray signature.

For the remainder of the cross-sectioned specimens presented, the cross-sectional cut was made parallel to the 0° fibers in order to check for fiber breakage in the critical 0° plies. Figure 42 demonstrates

that much matrix cracking can exist with no fiber breakage. When fiber breakage is seen, as in figure 43, a matrix crack in one of the two adjacent plies is accompanying the 0° fiber breaks. The 0° fiber breaks (crack #1) are also seen to be in relatively close proximity to the bottom $+45^\circ$ split (crack #3), that is the first and most visible form of damage noted. When the same specimen is sectioned at a point where the main $+45^\circ$ and -45° cracks intersect, as shown in figure 44, the bottom 0° fiber breakage is closer to the bottom $+45^\circ$ split. For more heavily damaged specimens, fiber breakage in the lower 0° ply is directly above the $+45^\circ$ ply split as shown in figure 45.

Broken 0° fibers in the upper part of the laminate are always seen to be a part of a crack running either from the ply above it (the top $+45^\circ$ ply) or below it (the first -45° ply) or both as shown in figure 46. The crack in the upper $+45^\circ$ ply (crack #2) and the first 45° crack (crack #1) are joined by broken fibers in the 0° ply between them. Figure 47 shows a feature that was seen in many of the sectioned specimens. A crack will form from a ply adjacent to the upper 0° ply and transverse part of the ply until the crack begins to grow parallel to the fibers, causing the 0° ply to be only partly fractured. This crack

is highlighted by white arrows in the figure. Figure 49 shows a -45° ply crack that starts into the 0° ply above it but only breaks fibers a short distance into the 0° ply when the crack is deflected parallel to the 0° fibers. Note the severe damage in all plies in this cross-sectional view.

Figure 49 demonstrated the difficulty in trying to identify broken fibers from the x-ray signatures. From the cross-sectional view, bottom 0° fibers are clearly broken, yet between cracks #1 and #3 on the x-ray signature, there is nothing obvious to indicate that fibers are broken (area #2). This was the case for the vast majority of specimens.

5.5 Static Indentation Tests

Data from the static indentation tests aided in indicating the shape of the deflected surface as well as showing the different strain fields associated with a low versus a high prestrain. The lower preloaded specimen demonstrated more nonlinearity at the lower end of loading than the heavily preloaded specimen as shown in figures 50 and 51. This is to be expected from the analysis in chapter 3. From the unloading data it is seen that a hysteresis is associated with all of the specimens tested at the lower prestrain levels. This indicates that there is either more damage being formed in these specimens or more compliance in the preloading device at the lower prestrains. Results from the x-ray analysis indicates that more damage was not formed, indicating compliance in the fixture at low levels of preload. Complete data from the 10 specimens tested are given in appendix C (specimen #2 is not included since the dial indicator was not set up properly).

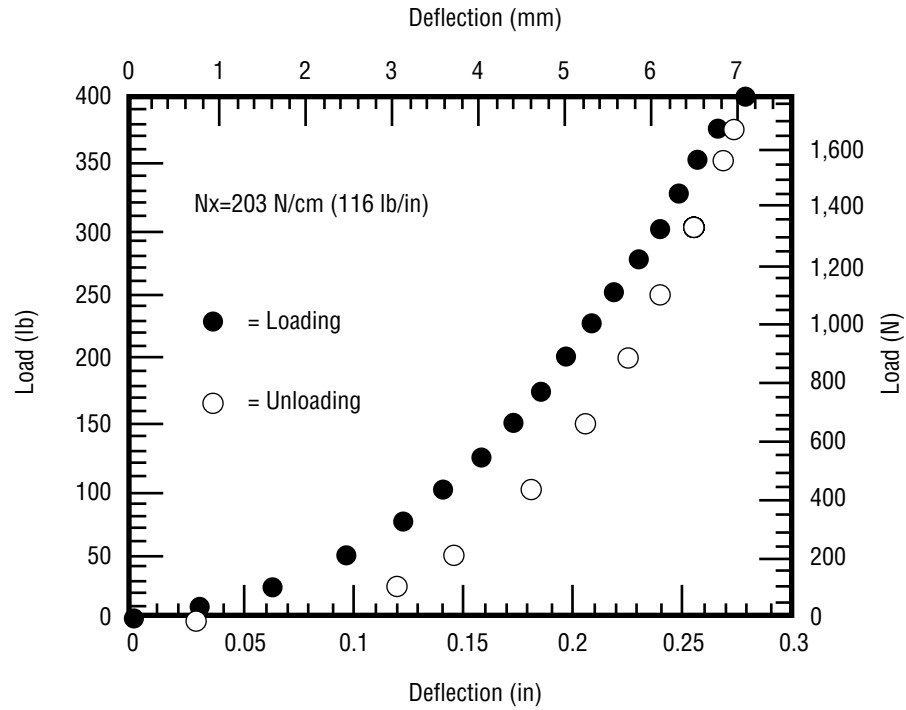


Figure 50. Load displacement from a statically loaded specimen at a low prestrain.

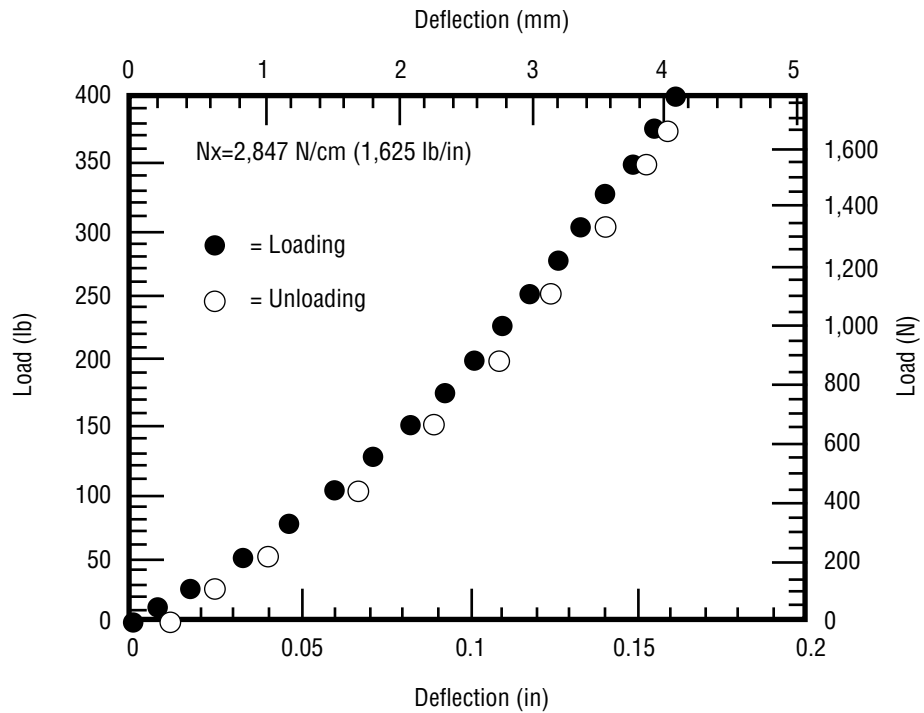


Figure 51. Load displacement from a statically loaded specimen at a high prestrain.

From the in-plane strain measurements as determined from the gauges placed on the specimens, as shown in table 4, it was clear that little strain was set up along the edges of the specimen due to transverse loading, especially on the highly pretrained specimens. Compressive strains due to transverse loading were always found in the vicinity of the applied load on the top surface and the strains on the opposite side (back face) would be tensile unless the preload was high, in which case they became negative. Plots of strain versus applied transverse load for the 10 specimens tested are given in appendix D. Note that at regions near the clamped edges (up to 57 mm from a clamped edge for specimens #7 and #8), both the top and bottom surface are put into tension due to the transverse load. At high preloads, the bottom surface sometimes went into compression from the transverse load (static #5), but this appears to be an isolated case.

5.5.1 Static Indentation Tests to Failure

Two specimens were pretrained and statically loaded until they could no longer hold a load. Only load-deflection data were generated from these tests. The results are shown in figures 52 and 53.

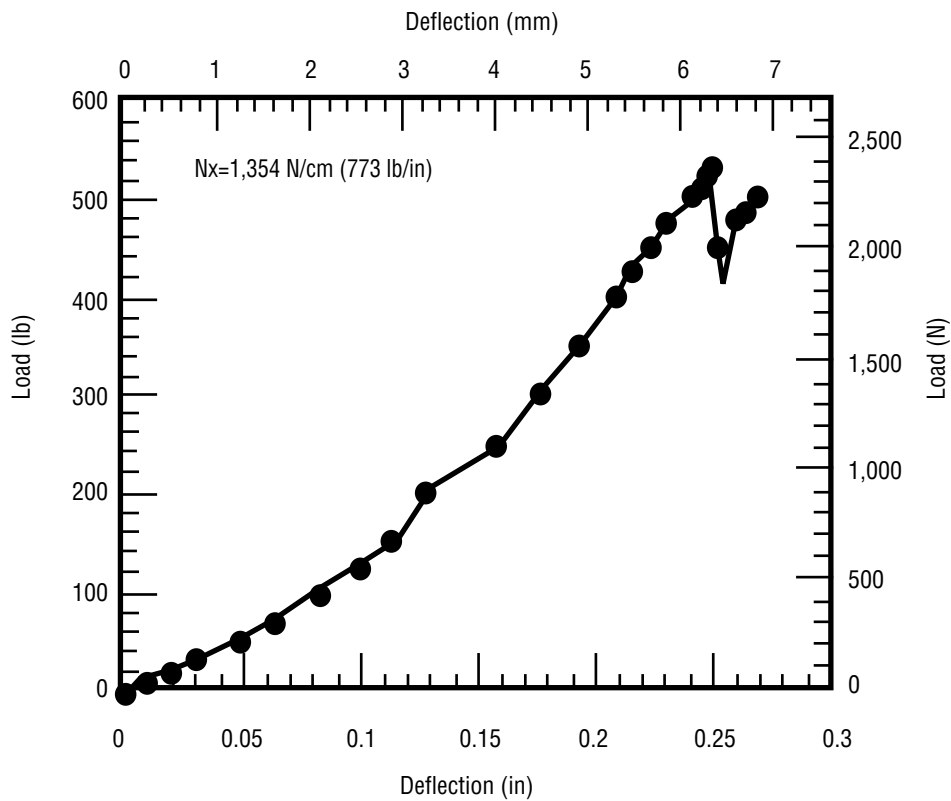


Figure 52. Load displacement from a statically loaded specimen (loaded until failure).

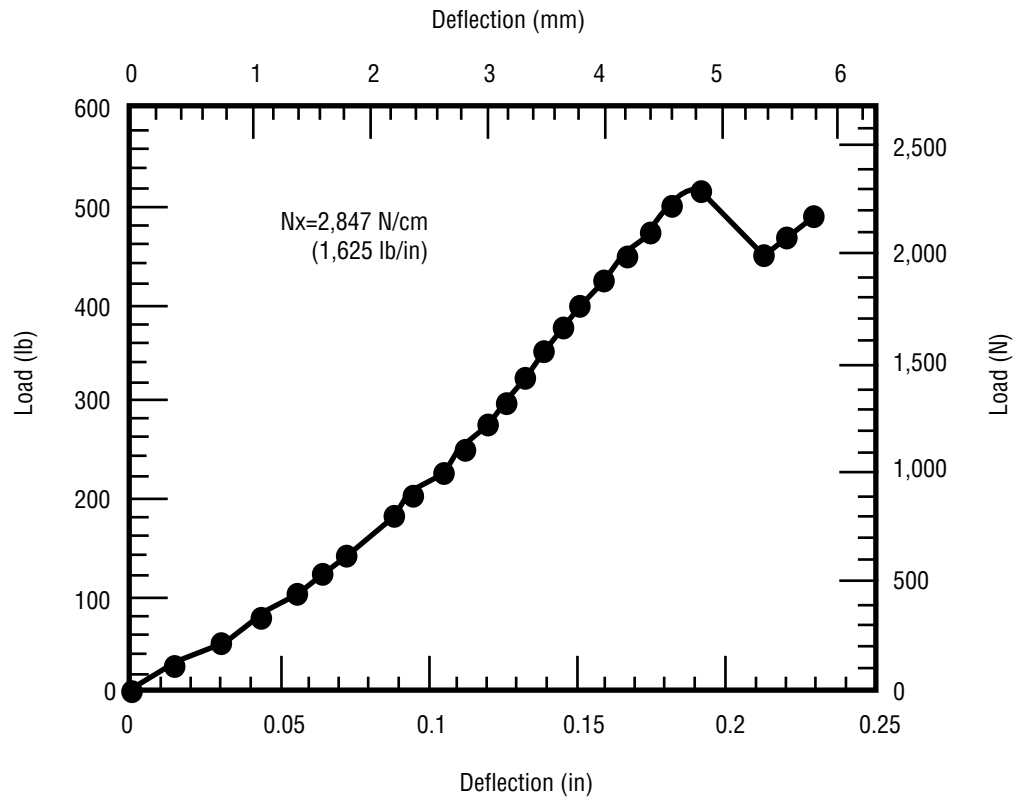


Figure 53. Load displacement from a statically loaded specimen (loaded until failure).

6. DISCUSSION OF RESULTS

This chapter is a discussion of the experimental results obtained in the previous chapter, along with results from the analytical analysis performed in chapter 3.

6.1 Instrumented Impact Testing

6.1.1 Maximum Load of Impact

For impact conditions in which the specimen did not sustain heavy damage, the maximum load of impact increases linearly with increasing preload. This can be seen for all of the data at the 3.4 J (2.5 ft-lb) impact energy level, data up to $\approx 5,000 \mu\epsilon$ prestrain for the 4.5 J (3.3 ft-lb) impact energy level and up to $\approx 4,000 \mu\epsilon$ for the 6.0 J (4.4 ft-lb) impact energy level. More scatter exists for the higher two impact energy levels due to the development of more severe damage. From equation (7) in chapter 3, it was predicted that the maximum load of impact was expected to increase at a linear rate with increasing prestrain for a given amount of impact energy.

6.1.2 Duration of Impact

The total time of impact is seen to decrease in a nonlinear fashion with increasing tensile prestrain. As damage is formed in the specimen, the duration tends to be a little longer due to local “softening” of the specimen. Thus, the nonlinearity is due mostly to damage. Note that the total duration of impact seems independent of impact energy. This should be the case if the transverse load is approximately proportional to the transverse deflection. For a spring-mass system (which can approximate the impact problem), the total time of impact (contact of mass on spring) is given by:

$$t = \sqrt{\frac{2mx}{F}} \quad (13)$$

where F is the force exerted by the laminate (spring), x is the displacement, and m is the impactor mass. Assuming $F \propto x$ (or $F=kx$, k =“spring constant”), then equation (1) can be written as:

$$t = \sqrt{\frac{2m}{k}} \quad (14)$$

which is independent of deflection and therefore independent of impact energy since m and k are fixed constants.

6.1.3 Maximum Deflection

The maximum deflection of impact decreases in an almost linear fashion with increasing prestrain for a given impact level. This linear relationship is not obvious from equation (7). This tends to hold true of samples in which incurred damage caused departure from linearity in maximum load and duration data. This is due to the “softening” which caused departure from linearity in the maximum load and duration data, increasing the deflection, yet the load drops which cancels it out.

6.1.4 Maximum Absorbed Energy

These data are seen to decrease with increasing prestrain for the lower values of prestrain, then rise with increasing prestrain for the rest of the data. It is predicted that as the preload increases, more energy would be lost due to the impact event since higher prestrains tended to cause more damage in the specimen. An explanation for this can be gained from the results of the static indentation tests in which more hysteresis were formed at the lower prestrains, due to fixture compliance.

Thus at the low preloads, fixture compliance attributes to energy lost in the system, but as the preload increases, this compliance tends to become less severe. At higher prestrain levels, damage begins to form in the specimens and the energy lost in the system begins to rise again.

6.1.5 Load-Deflection Curves

For higher preloads, the load-displacement plots become more linear up until the point of damage. At this point on the curve, the load begins to fluctuate at a high frequency as matrix cracks, delaminations, and possibly fiber breakage occurs.

A large amount of hysteresis is observed for all of the impacted specimens regardless of transverse load-preload combinations. For specimens that contain significant damage, this result is expected, but for specimens with little or no damage, little hysteresis would be expected. This implies that energy is being lost to the system in modes other than specimen damage. The particular impact tester used in this study does not have linear bearings or other such friction-reducing devices between the falling weight crosshead and the guideposts. This has always been suspected of causing the system to lose a fair amount of energy in the reaction between the falling crosshead and the guideposts during the impact event. This suspicion has never formally been confirmed and documented.

6.2 Visual Examination

The first form of noticeable damage that formed was splitting of the matrix along the fibers in the bottom +45° ply. This is to be expected from the finite element results, presented in table 3, which show these plies develop the highest stresses in the second principal material direction, which are almost twice as high as the breaking stress for a lamina.

The next sign of visual damage was usually associated with contact stresses on the impacted face of the specimen. A small dent would become noticeable and as either the prestrain or the transverse impact load increased, matrix cracking and fiber breakage was noticed inside the indentation.

At relatively high impact levels, broken fibers would begin to protrude from the back face of the impacted specimen along a crack in the bottom +45° ply.

This type of damage progression is typical of fibrous laminates that are allowed to undergo large deflections during impact, thus setting up high tensile strains on the back surface of the impacted laminate.

6.3 X-ray Inspection

The most notable feature of the x-ray signatures for both the statically loaded and impacted specimens is that the damage tended to form along the direction of the bottom +45° ply. Delaminations, emanating from a matrix crack in this ply, were always noted on the x-ray results (unless no damage at all formed). This feature is shown schematically in figure 54. The mechanics thought to be behind these delaminations are given in the next section.

6.3.1 Initial Damage Formed

The initial damage consisted of a matrix crack in the bottom +45° ply with delaminations forming as shown in figure 54. On either side of the impact site, the delaminations consisted of two zones, one usually smaller than the other. As a matrix crack develops in the bottom +45° ply, a free edge is created and the stresses must redistribute themselves so that equilibrium is maintained. This “free edge effect” is the same mechanism outlined by Pipes and Pagano.¹²⁶ Figure 55 shows schematically how the geometry of the problem influences the delamination growth, mainly due to the transverse interlaminar stress, σ_z , that is set up because of the free edge (called face 1 in the figure).

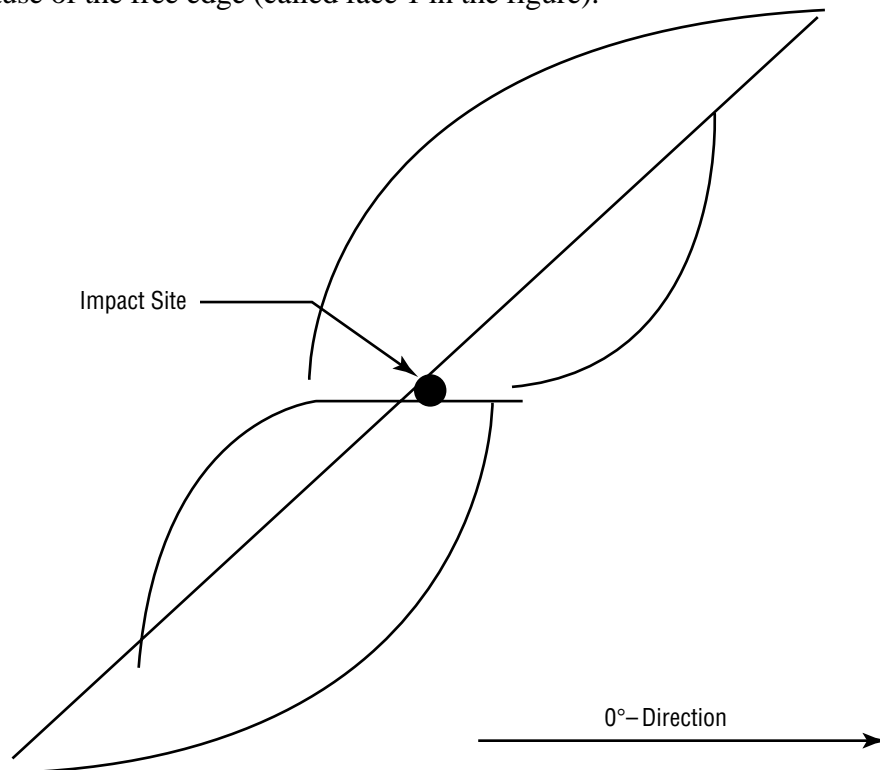


Figure 54. Schematic of bottom ply splitting and associated delaminations.

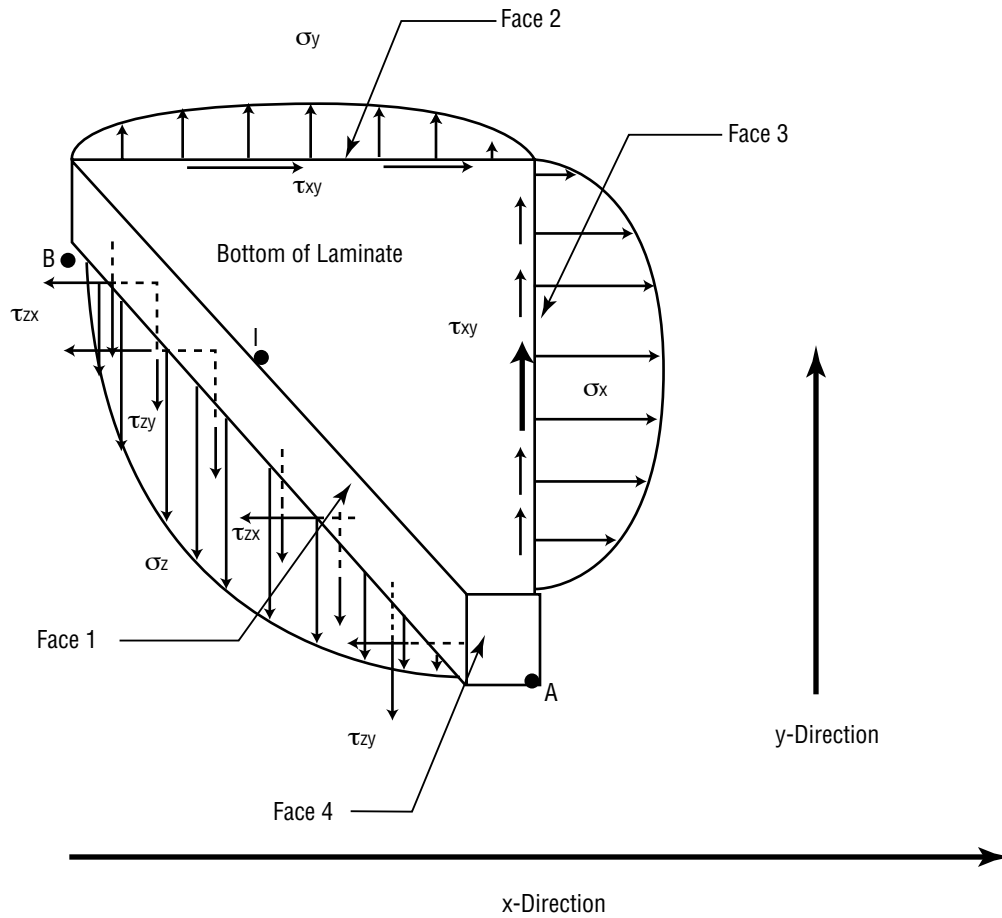


Figure 55. Stresses associated with back face matrix crack.

Face 3 of the ply is carrying the x -direction stresses, just as it was before the crack was formed. The stress distribution is such that the closer a point on the face is to the impact point (I), the higher the x -direction and y -direction (face 2) stresses are. This is known from the finite element results. The moment about a line through point A running in the y -direction must be zero for equilibrium conditions to be satisfied. The face 3 stress, σ_x , creates a moment about this line. To balance this moment, stresses in the z -direction, σ_z , are set up along the crack boundary. Since σ_x is largest at the point closest to the impact point, I, σ_z is also largest at this point. As the crack moves farther away from the line through A (i.e., as y increases), the z -direction stress rapidly decays since σ_x gets smaller in this direction and also the “moment arm” is getting longer, so to maintain a given moment, the z -direction force gets smaller. The opposite should hold true as the crack gets closer to face 3. The “moment arm” becomes smaller, so the stresses need to be larger to maintain a constant moment. However, σ_x gets smaller, so the moment needed for equilibrium also gets smaller at points further away from the impact point I.

The above also holds true for σ_y which also creates a moment about a line through point B running along the x -direction. This will tend to cause symmetry of σ_z along the crack for equal values of σ_x and σ_y . However, since σ_y is generally smaller than σ_x , especially for heavily preloaded specimens, the overall effect is to have slightly larger σ_z values near the face 4 end of the crack than at the face 2 end.

When face 1 is created, the shear stresses also redistribute themselves to maintain equilibrium. The shear stresses on faces 2 and 3, τ_{xy} , are no longer balanced by shear stresses on face 1, since it is free, or on face 4, since it can be considered infinitely small. New interlaminar shear stresses τ_{zy} and τ_{zx} are created to balance the moments due to the shear stresses. Since τ_{xy} is largest nearest the point of impact (as it was for σ_x and σ_y), τ_{zx} and τ_{zy} will also be largest nearest the impact point, I.

6.4 Cross-Sectional Examination

Large matrix cracks and delaminations could easily be detected by x-ray analysis but fiber breakage was difficult to detect except by cross-sectional examination. Cross-sectional examination showed that fiber breakage could occur in a laminate at a point that was not obvious from the x-ray signature. A large amount of matrix damage was always associated with neighboring plies of a ply with broken fibers. These areas of high crack density tended to cause the dye penetrant to “pool-up” and create dark areas on the x-ray signatures which would obscure the broken fiber damage.

The cross-sectional analysis also revealed that fiber breakage in the bottom 0° ply differed from that in the upper 0° ply. The fiber breakage in the bottom 0° ply always ran completely through the ply but fiber breakage in the upper 0° ply did not. In many instances the fiber fracture would only travel one-half or one-third the thickness of the lamina and then deflect parallel to the fibers, running through the matrix in the upper 0° ply. The bottom 0° ply fiber breakage was always associated with large delaminations between this ply and the bottom $+45^\circ$ ply. The fiber breakage in the upper 0° ply was characterized by the propagation of the crack containing the fiber breakage into one, or if the ply was completely fractured, both adjacent plies through the matrix material in these adjacent plies. Delamination was sometimes, but not necessarily, associated with these cracks.

The failure modes of the two 0° plies can be expected to differ, based on the maximum ply stress values given in table 3. The upper 0° plies are subjected to small stress values that are not even within an order of magnitude of the fiber-breaking stress for these plies. Thus, the fiber breakage must come from another stress mechanism setup, other than that by preload or membrane and bending stresses arising from the transverse load. Since dents were observed on the impacted surface of many of these laminates, it is assumed that contact stresses are responsible for fiber breakage in the upper 0° ply. The stresses predicted for the lower 0° plies are much larger (although they never exceed one-half the breaking stress) and with added stress from cracked plies transferring stress to the main load-bearing 0° fibers, it is likely that these fibers simply break in tension (causing the complete fracture of the ply).

6.5 Static Indentation Tests

The static indentation tests showed that a tensile preload increases the flexural stiffness of the laminate, especially at lower levels of transverse load, at which point the induced membrane stresses due to large deflection are not as large.

6.5.1 Comparison With Energy Balance and Finite Element Models

Figure 56 shows load-deflection curves for specimens prestrained at $4,000 \mu\epsilon$ as predicted by equation (9) and the finite element analysis. Data from a static indentation test are included for comparison. It is clear that the finite element method comes closer to predicting the actual load-displacement behavior of the laminate.

Figure 57 shows prestrain-deflection data as calculated by the two models, along with data from the static indentation tests at a constant transverse load of 223 N (50 lb). The finite element method matches up extremely well with the experimental data. The curve as predicted by the energy balance model (equation (9)), greatly underestimates the effect of prestrain on deflection and also predicts a linear relationship which does not agree with experimental data.

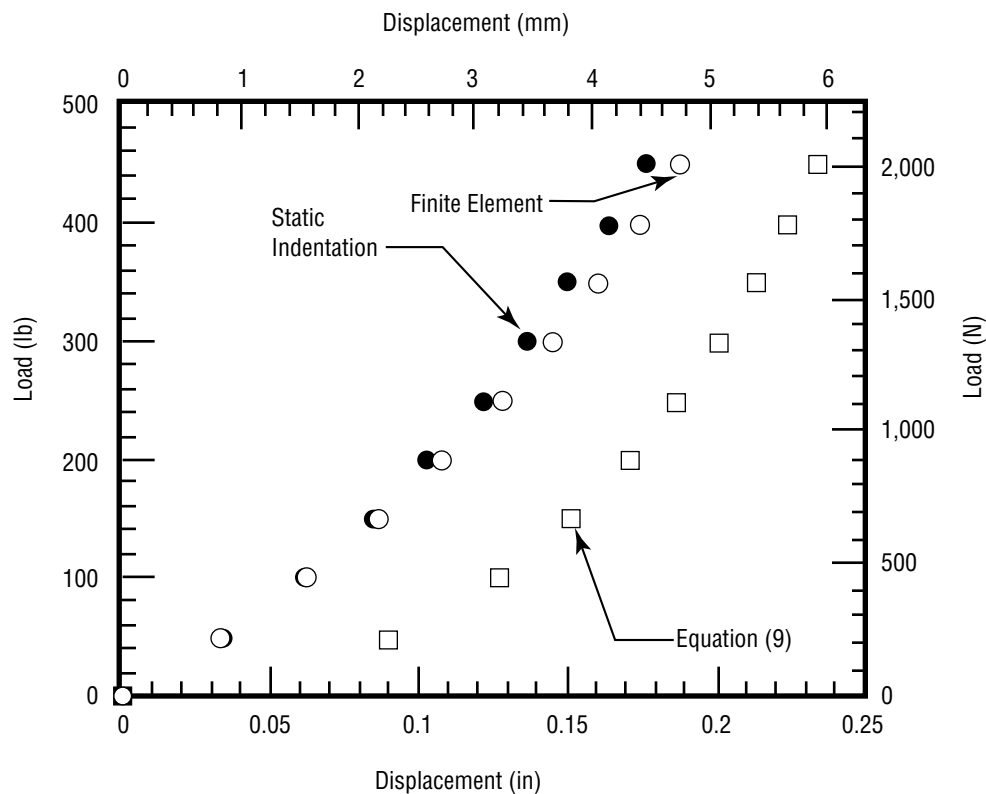


Figure 56. Load-deflection data comparison between equation (9), the finite element method, and static indentation data for a prestrain of $4,000 \mu\epsilon$.

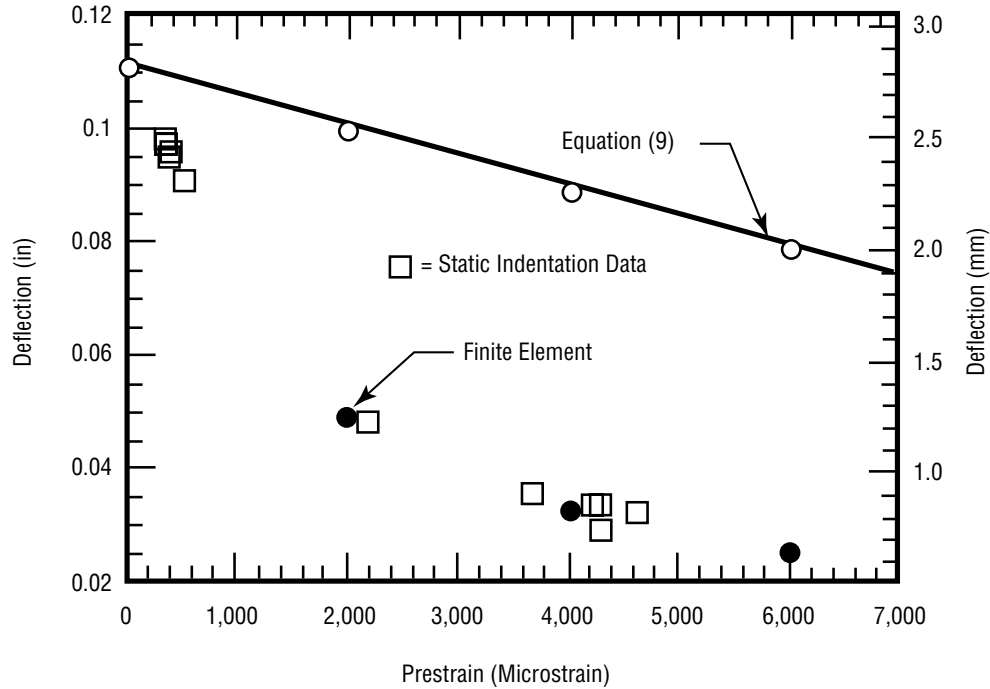


Figure 57. Prestrain-deflection data for a constant transverse load of 223 N (50 lb).

The data from the in-plane strain measurements agreed qualitatively with the finite element results and showed that at high preloads, little deflection or strain is induced into the laminate near the free edges due to the transverse load.

A result that was found experimentally that was not predicted was the compressive strains that appeared on the top surface of the laminates due to the transverse load during the static indentation tests. From table 3 it was predicted that as the transverse load increased, the stress (or strain) on the top surface would become more positive due to the large membrane stresses set up in the laminate. One cause for this could be the previously mentioned contact stresses which are not accounted for in the model.

6.5.2 Comparisons of Impact and Static Indentation Curves

From all accounts, the impacts in this study were of a quasi-static nature with no contributions from material inertia or material vibrations. The conditions for a quasi-static impact event, low target mass, and a large impactor mass were certainly met in this study. Thus, it is expected that the static indentation data should be very similar to the impact data.

Figures 58–60 show load-deflection data for three different levels of preload for both the static indentation and impact tests. These data are seen to match fairly well, especially at the lower end of transverse deflection and at lower preloads. The static indentation data show a larger load for a given deflection at the higher end of deflection. Note that the data from the impact tests show a small drop in stiffness along the load-deflection curve whereas this drop is not seen in the data from the static indentation tests. In addition, figure 59, which has static indentation data for a specimen with heavy damage, shows that the static indentation specimens can sustain a slightly higher load before the first sudden drop in load is observed. In figure 60, no damage has occurred on the static indentation specimen at 1,780 N (400 lb), but obvious damage has occurred in the impacted specimen.

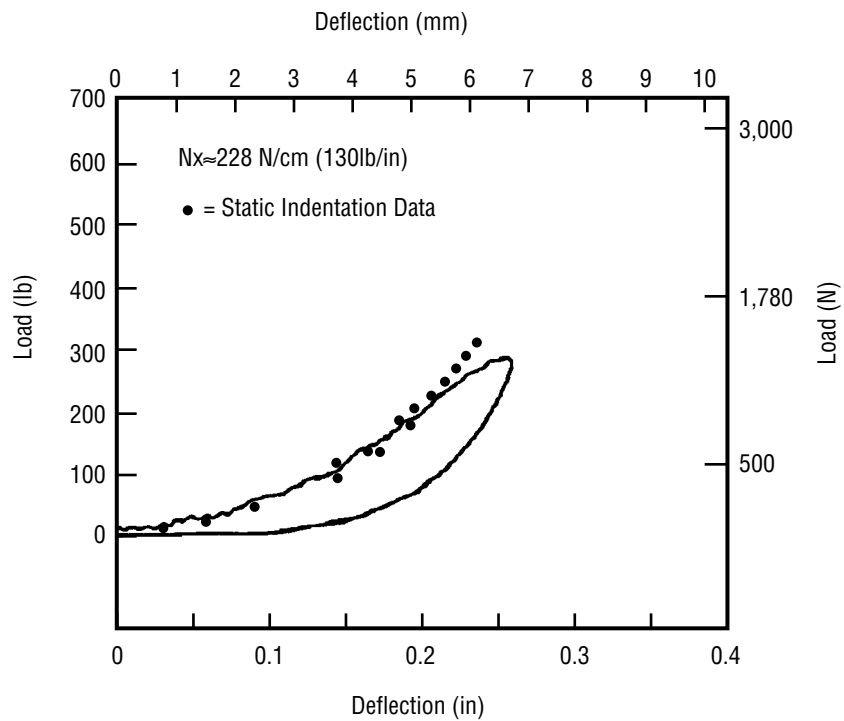


Figure 58. Comparison of load-deflection curves for a static indentation specimen and an impact specimen both preloaded at $\approx 228 \text{ N/cm (130 lb/in)}$.

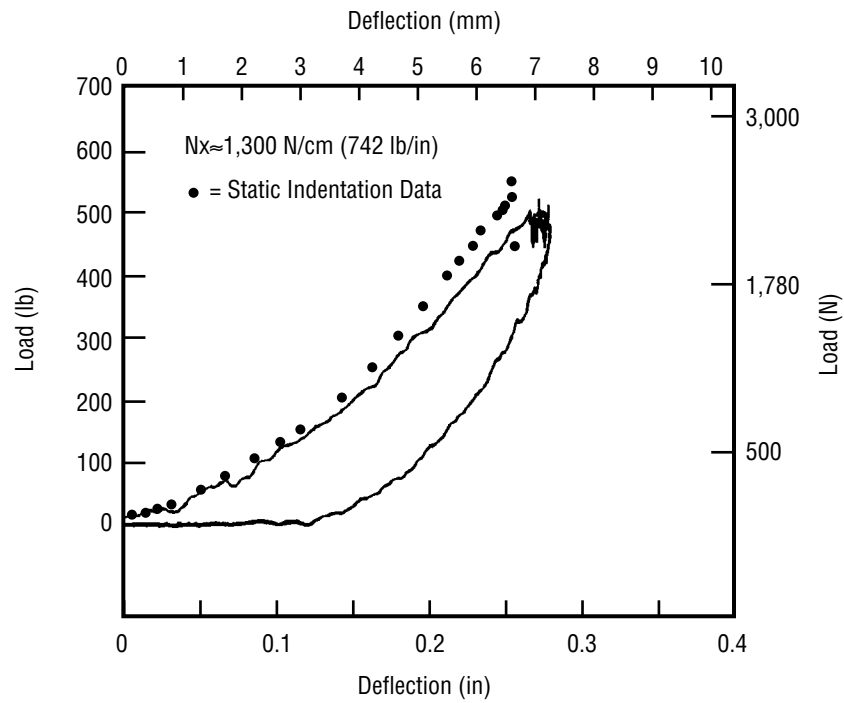


Figure 59. Comparison of load-deflection curves for a static indentation specimen and an impact specimen both preloaded at $\approx 1,300 \text{ N/cm (742 lb/in)}$.

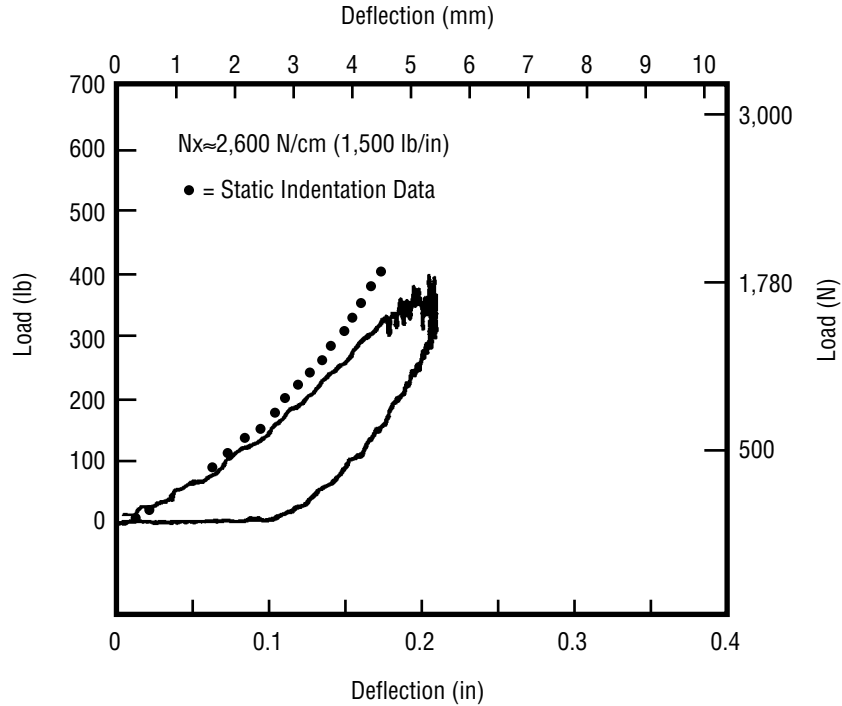


Figure 60. Comparison of load-deflection curves for a static indentation specimen and an impact specimen both preloaded at $\approx 2,600 \text{ N/cm}$ ($1,500 \text{ lb/in}$).

It was noticed during the static indentation tests that when a specimen was at a load that could cause damage formation, damage did not always immediately occur in the specimen. As the load was held constant and a displacement reading was being taken, the specimen would sometimes produce a loud pop which indicated the formation of damage after a time interval at a given load.

From x-ray results on specimens that experienced similar maximum transverse load-preload combinations, some impacted specimens showed more damage than the specimens that were statically loaded, although the differences were not great. Most of these specimens contained very similar x-ray signatures.

Thus some subtle differences can be noted for impacted and statically loaded specimens in this study.

7. CONCLUSIONS AND RECOMMENDATIONS

7.1 Overview

This chapter contains conclusions that can be drawn from this study and recommendations for future studies of relevance.

7.2 Conclusions

The following are the major conclusions of this study:

- For all other impact parameters which are the same, a tensile prestress tends to increase the maximum force of impact and the amount of damage formed. A decrease is seen in the duration of impact and in the maximum transverse deflection due to impact.
- The types of damage formed are matrix cracking (splitting), delaminations, and fiber breakage. The first sign of damage is matrix splitting in the bottom $+45^\circ$ ply. Large delaminations emanate from the matrix split and tend to run between this split to a split in a neighboring ply. Smaller delaminations form directly under the impact zone due to the high contact stresses set up in this area.
- Large deflection plate theory must be taken into account for analysis in which the plate deflects more than one-half its thickness. The induced midplane stretching from the large deflections rapidly dominate the load/displacement response of the plate.
- Finite element techniques do a good job of predicting the elastic response of a transversely loaded plate, but the introduction of damage greatly complicates the problem.
- X-ray inspection can easily detect matrix cracks and delaminations; however, fiber breakage is difficult to detect.
- Cross-sectional examination revealed that fiber breakage did occur, even though the finite element analysis predicted that the maximum stresses along the fibers in a ply would not even be one-half the breaking strength of the ply.
- Fiber breakage in the lower 0° ply was dominated by tensile stresses whereas fiber breakage in the upper 0° ply was dominated by contact stresses and showed a complex failure mode.
- Statically loaded specimens and impact loaded specimens show the same general behavior if the target mass is small and the impactor mass high, but subtle differences do exist, especially at high tensile prestrain values.

7.3 Recommendations

The following recommendations are for related programs that may be conducted in the future concerning impact damage of composite laminates:

- The gray area between “quasi-static” and dynamic cases must be accounted for since many impacts may fall into this regime.
- Finite element analysis must be handled with care once damage is incorporated into the model.
- The inclusion of the x -displacement values, u , in the energy balance solution should be incorporated for more accuracy involving the influence of the preload.
- The effects of compressive preloads should be studied, since by the arguments given in section 6.3.1, if a crack forms, σ_z should be compressive and help to suppress delamination growth.
- Nondestructive evaluation (NDE) techniques need to be examined extensively since, in the field, this will ultimately be the tool that determines the amount of damage present due to an impact event.

8. SUMMARY

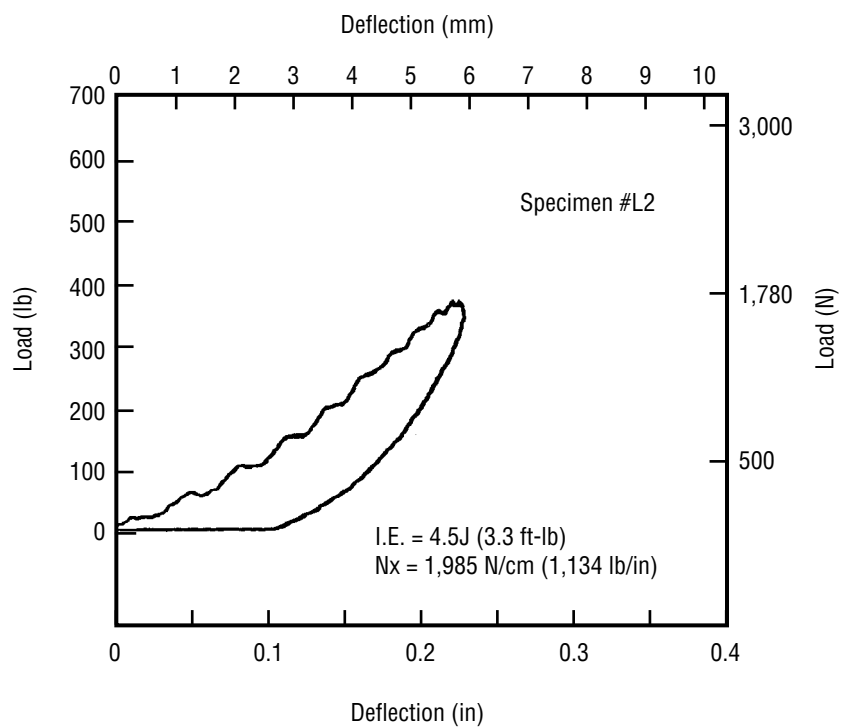
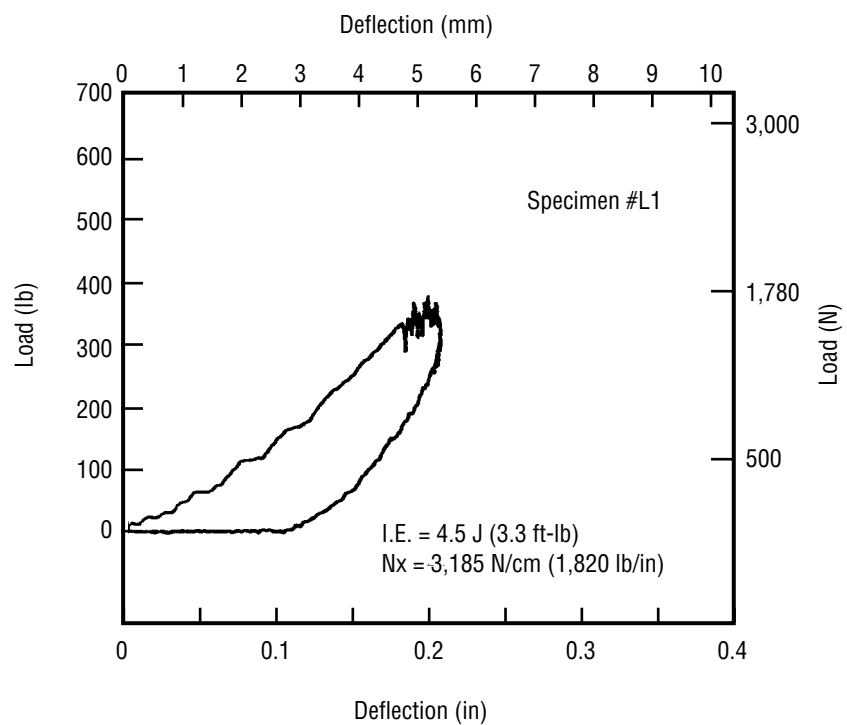
Tensile preloads tend to increase the maximum force of impact and decrease the duration of the impact event and the maximum transverse deflection for low-velocity impacts. Higher tensile preloads also tend to cause more damage to form in the specimen due to the higher impact forces and normal tensile stresses, σ_z , that are set up along a back face split that helps to form a delamination.

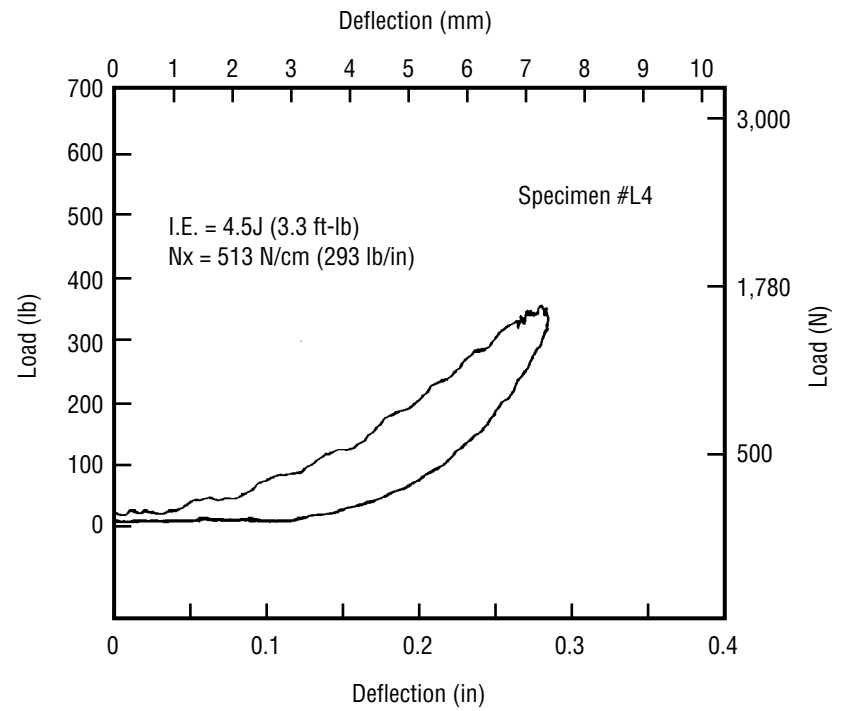
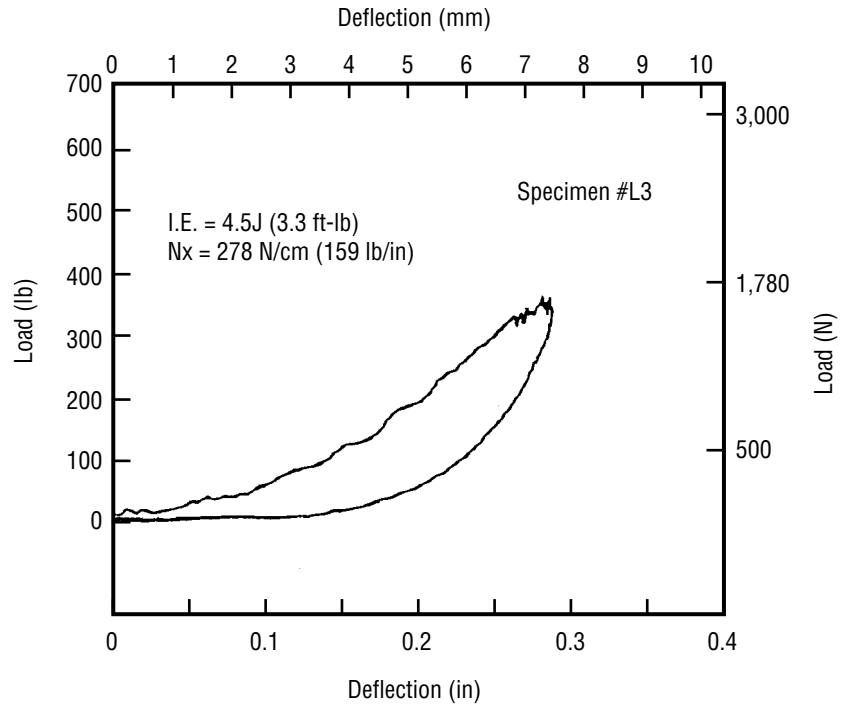
Finite element analysis can predict the material response well but once damage is induced into the specimen, the problem becomes much more complex.

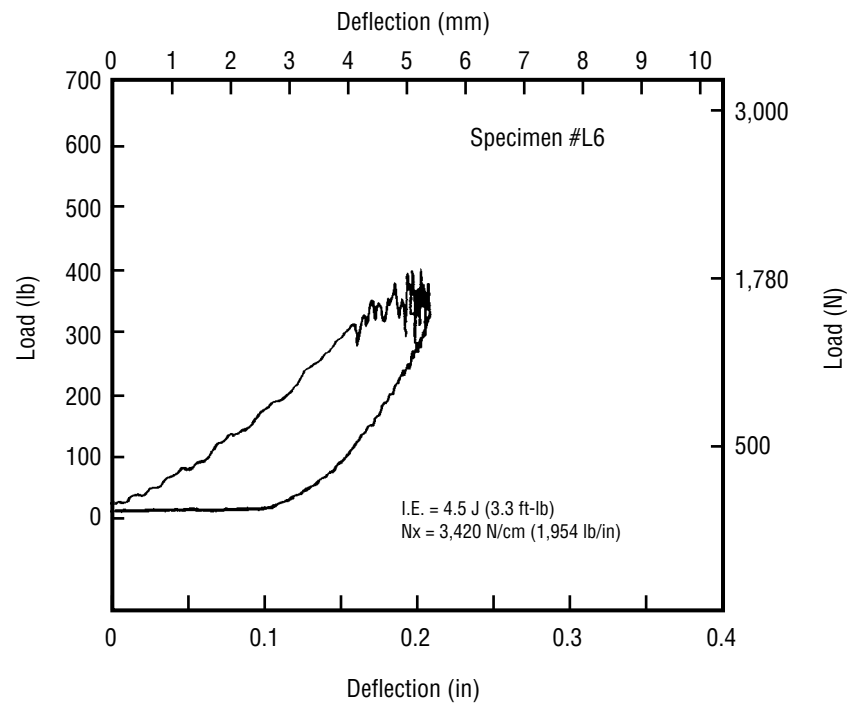
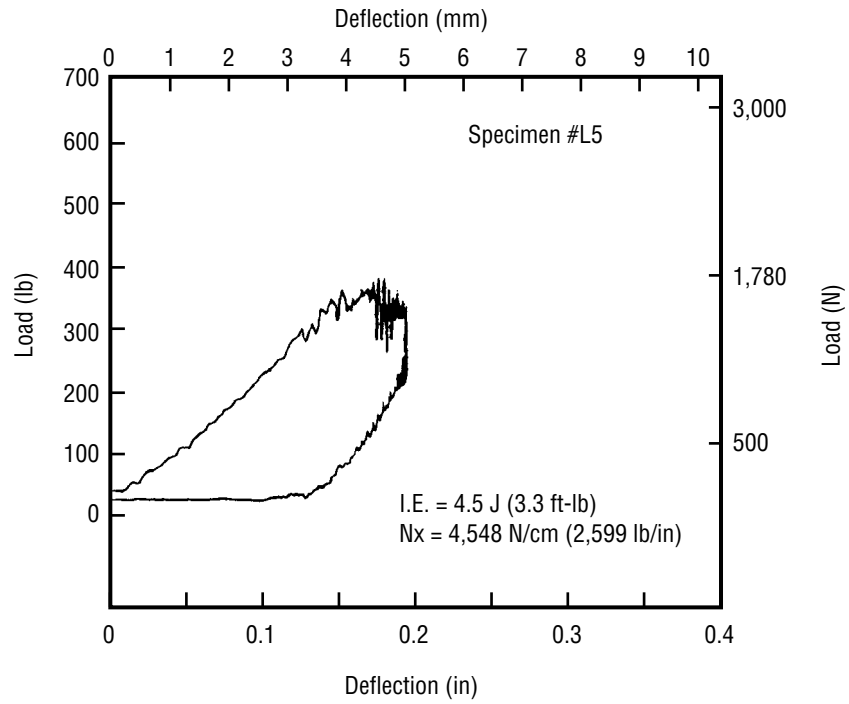
Fiber breakage is difficult to detect from x-ray signatures of the damage zone due to the high matrix crack density associated with such a specimen, causing the dye penetrant to “pool-up” and hide the fiber breaks.

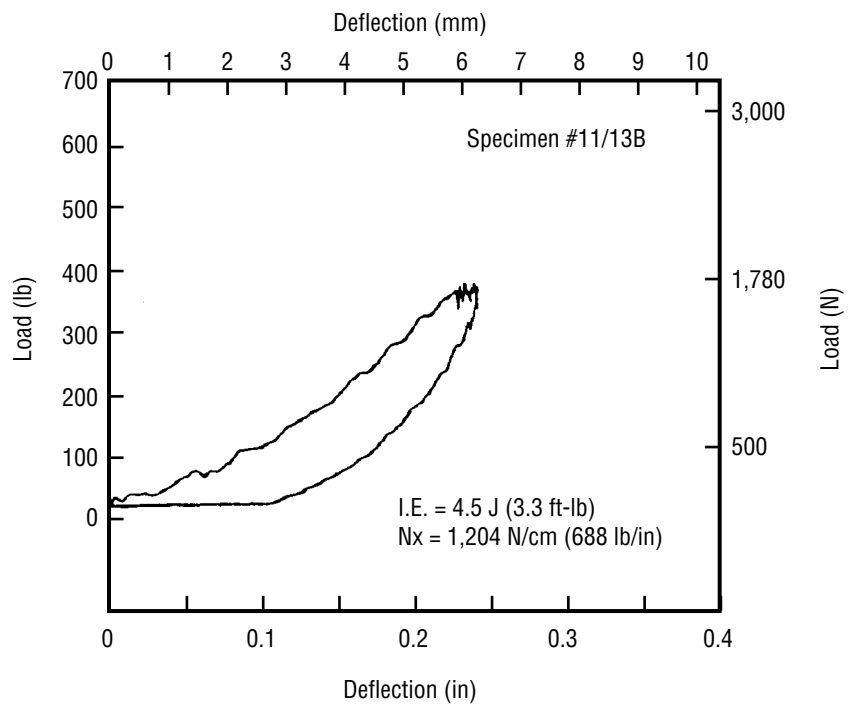
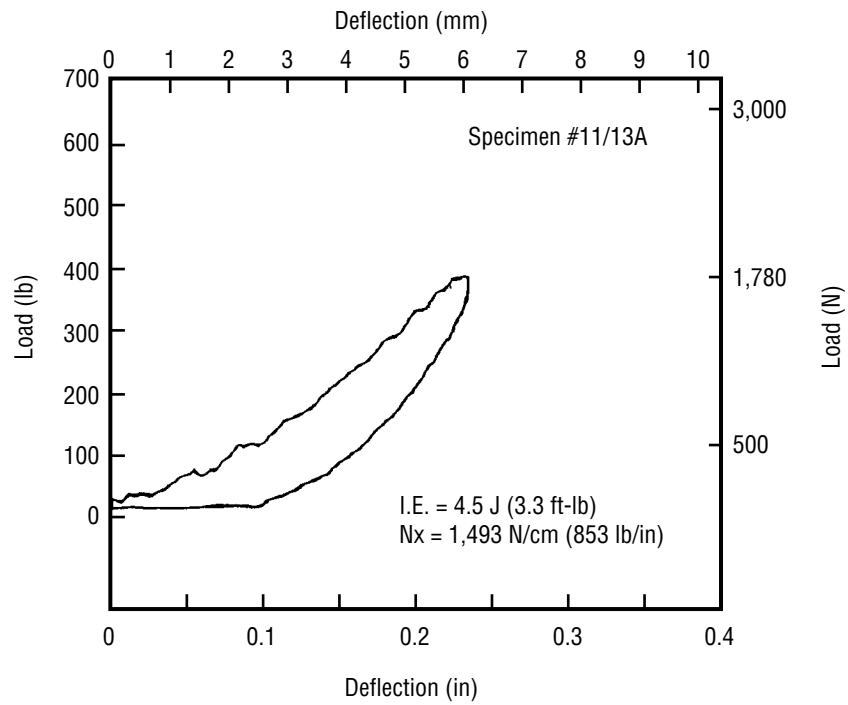
Contact stresses are very important, even when the specimen is flexible and allowed to deform many times its thickness. Static indentation and “quasi-static” impact tests show the same basic behavior and damage formation, but subtle differences do exist.

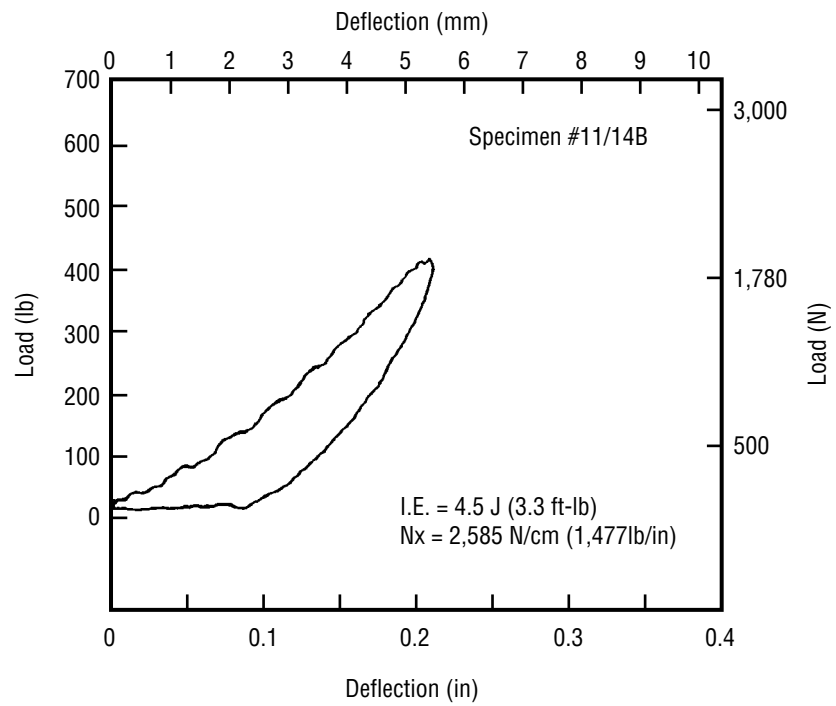
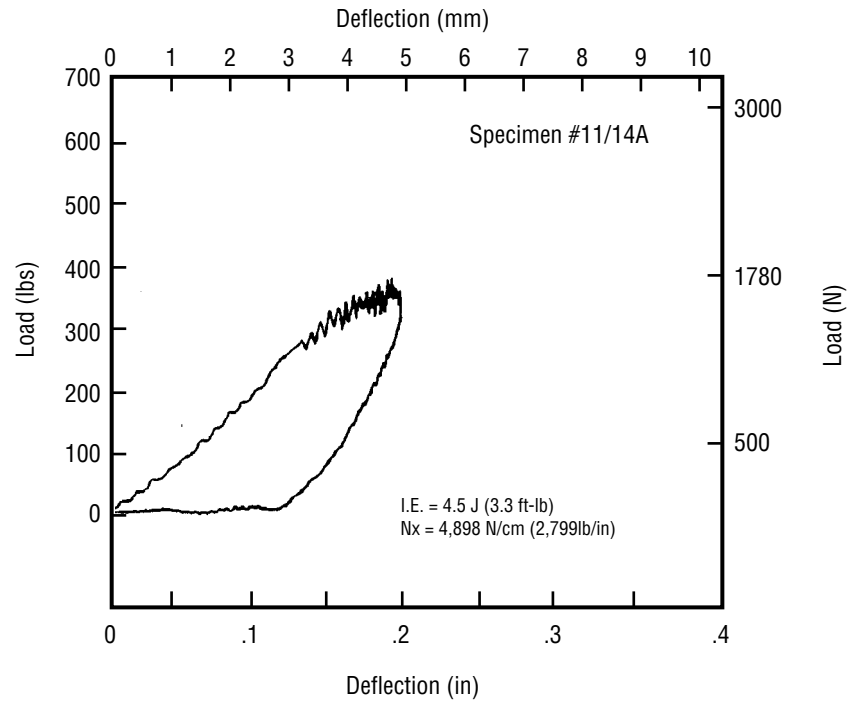
APPENDIX A—LOAD-DEFLECTION DATA FROM INSTRUMENTED IMPACT TESTS

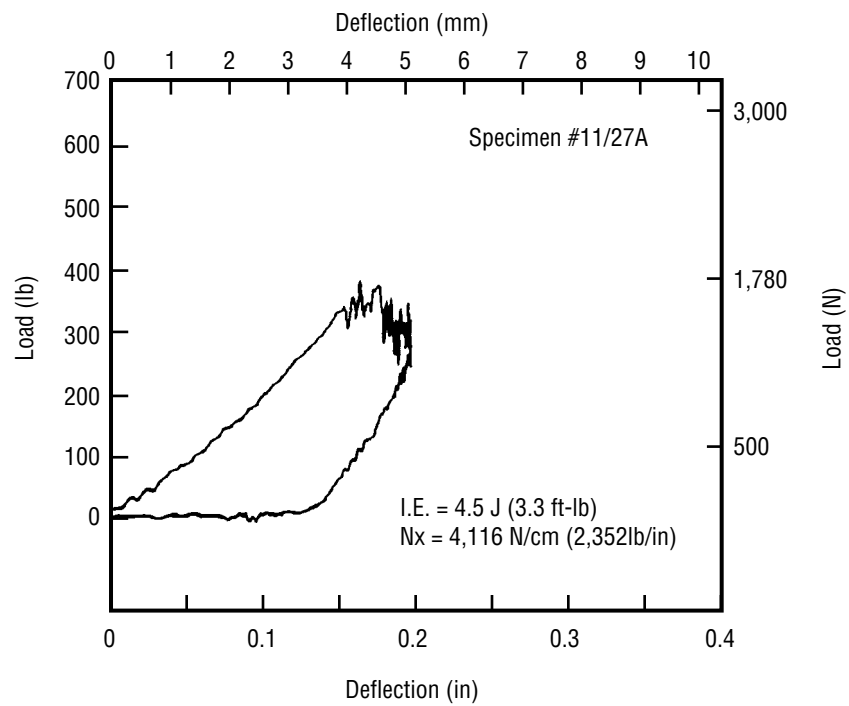
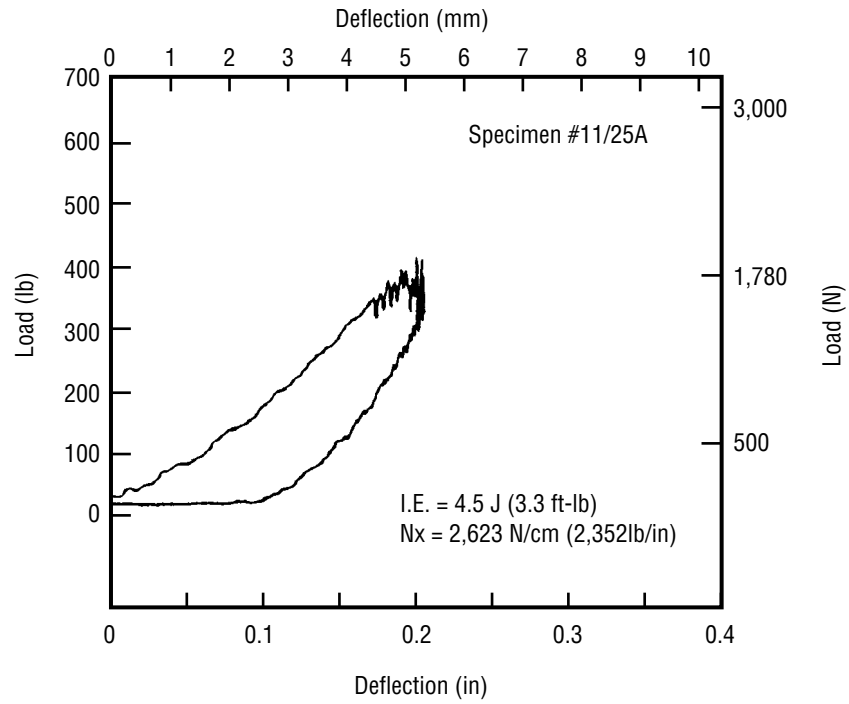


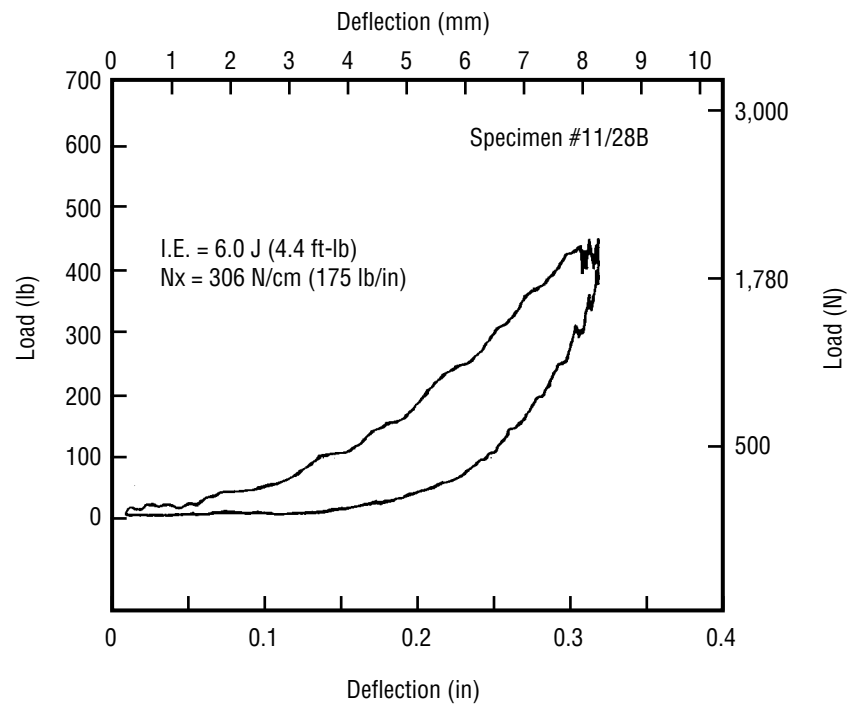
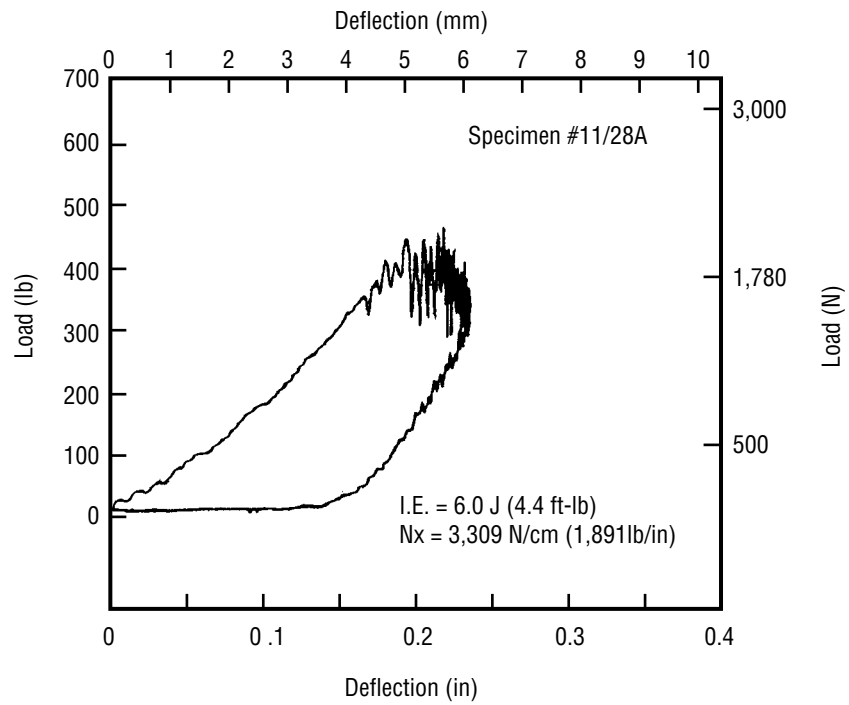


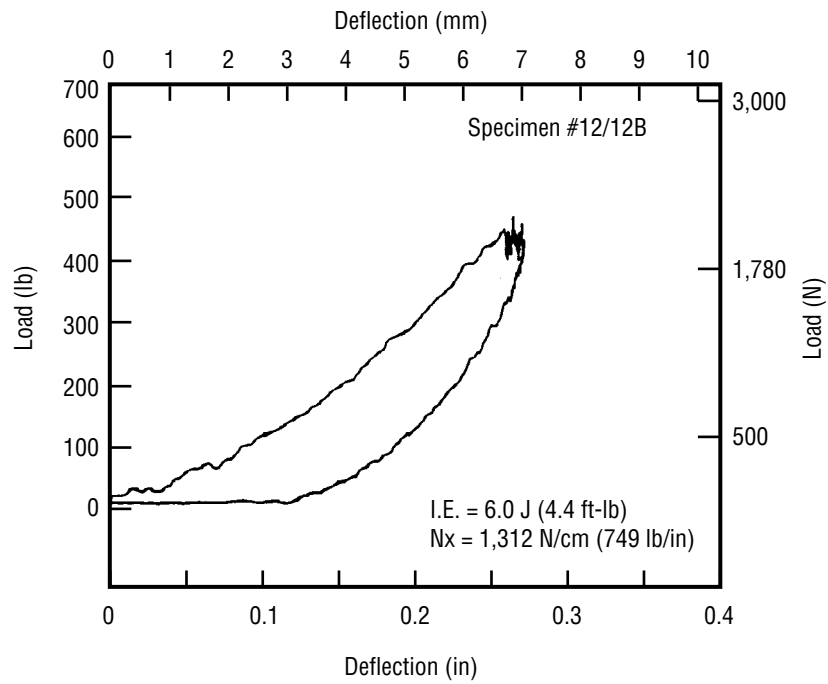
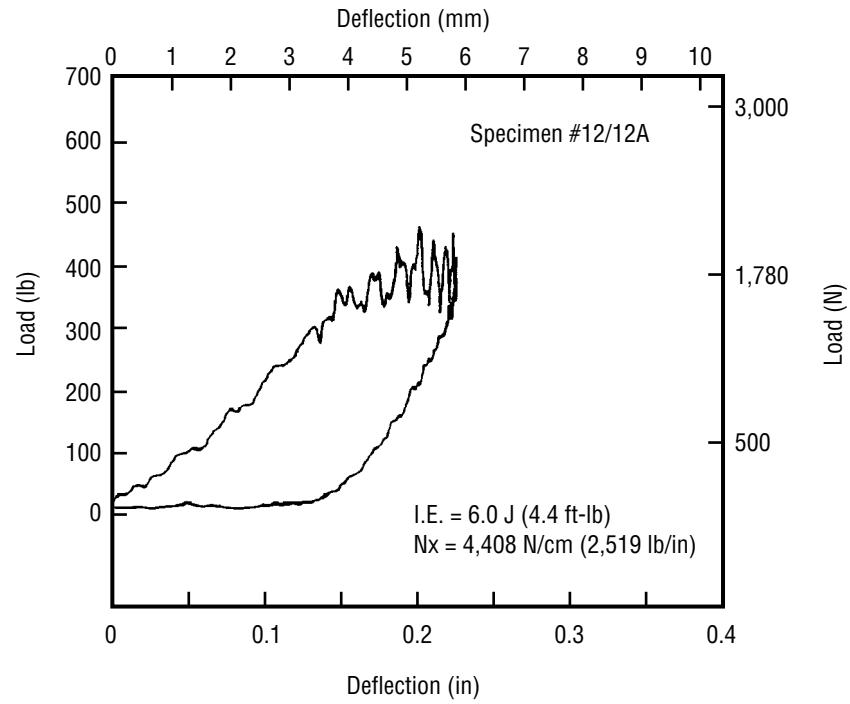


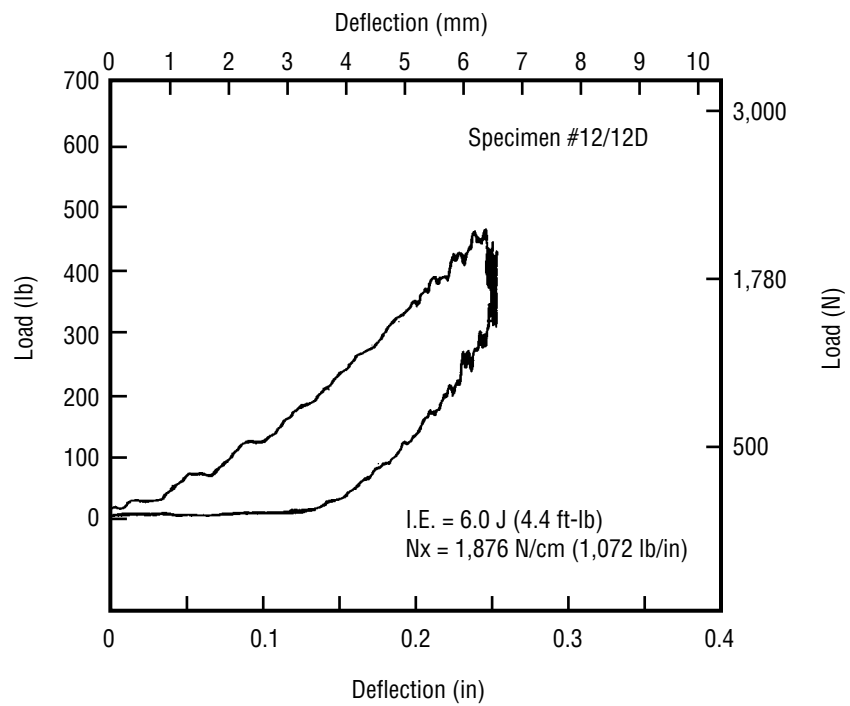
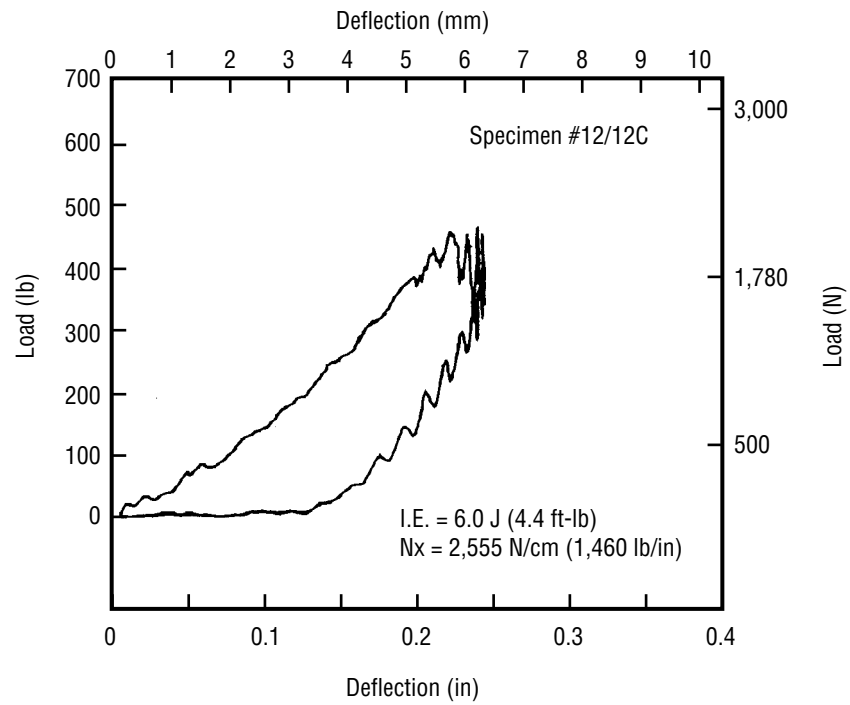


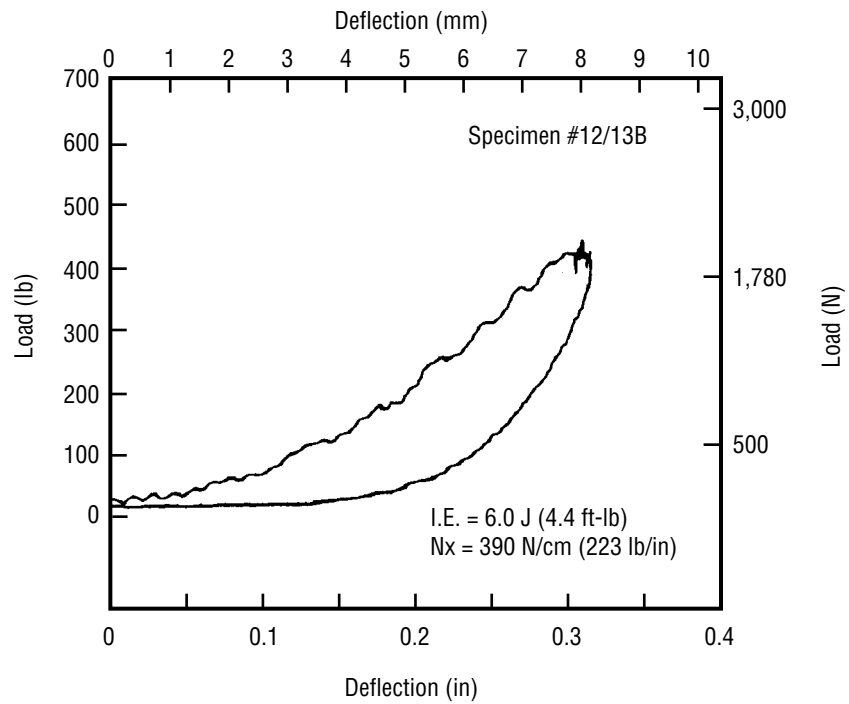
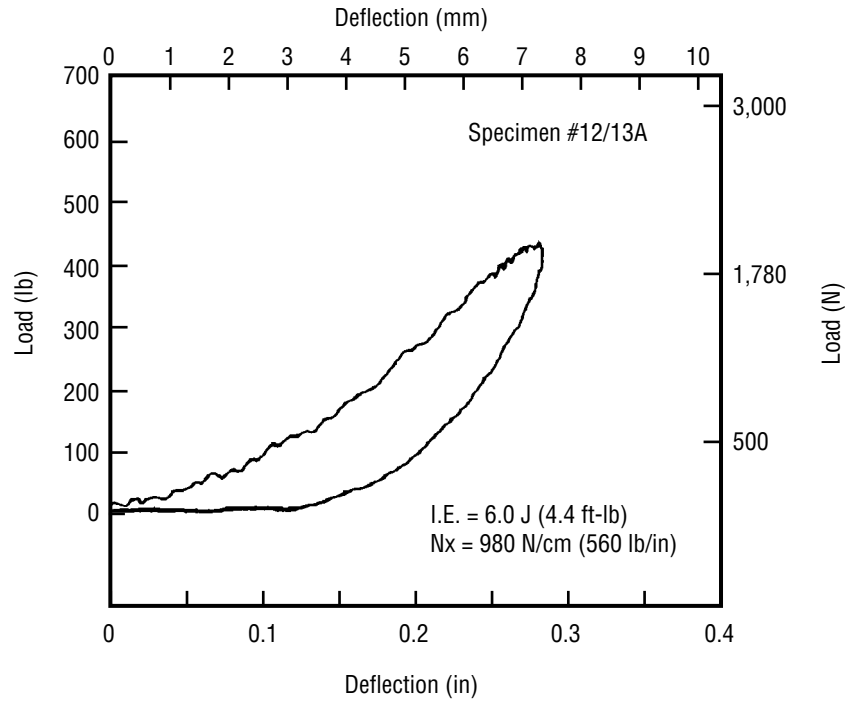


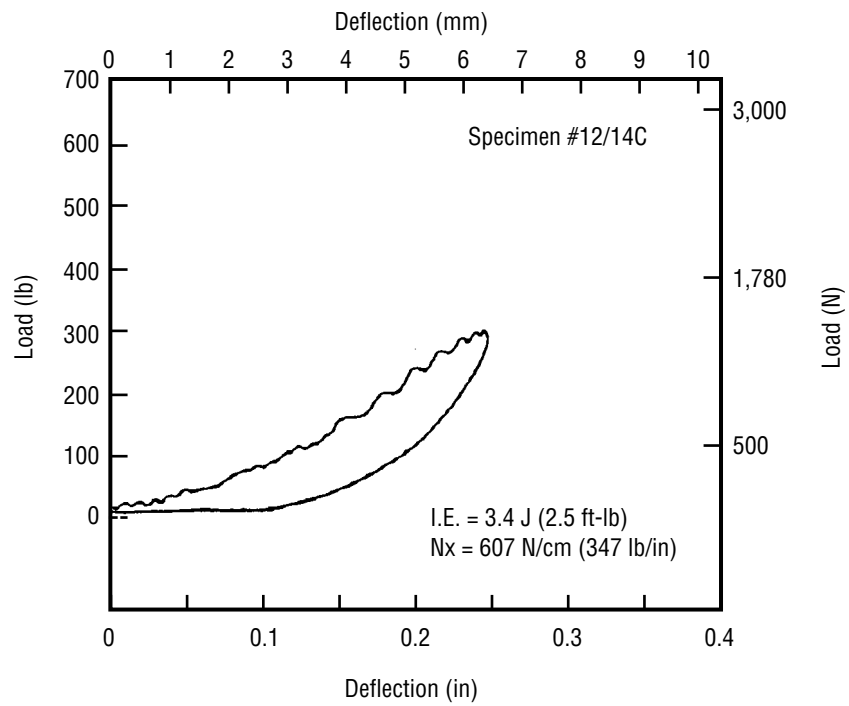
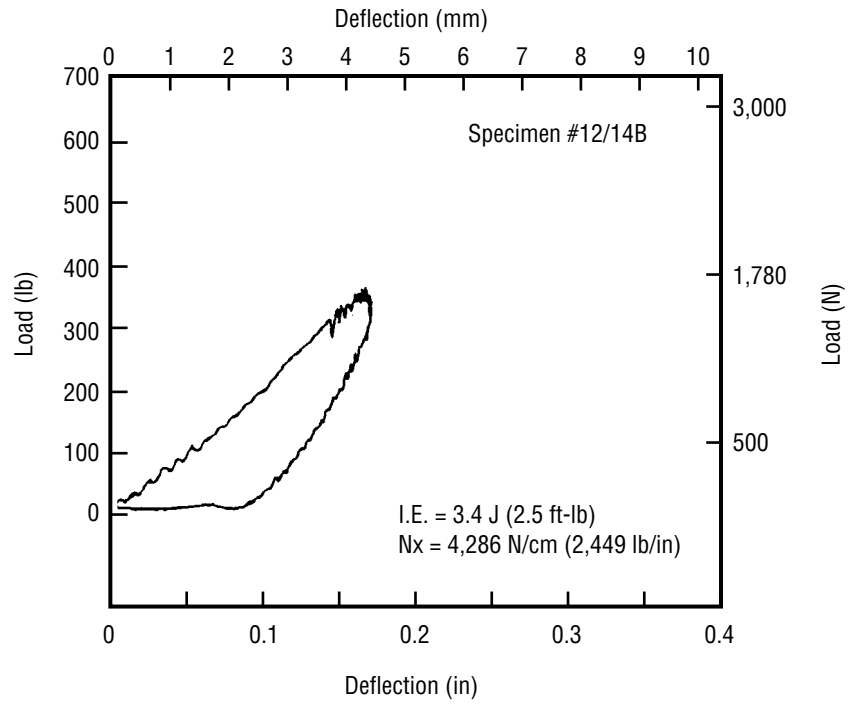


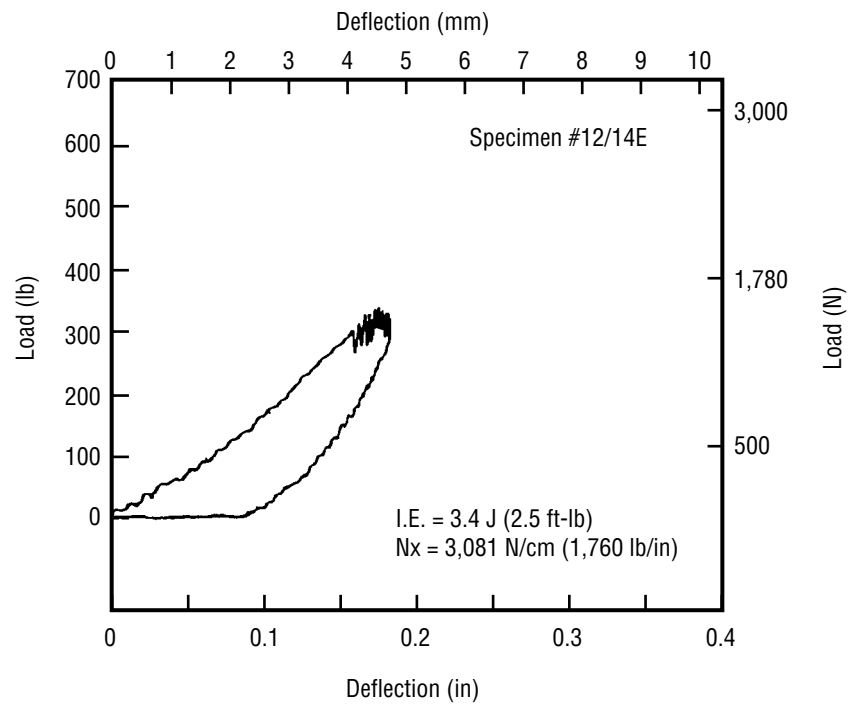
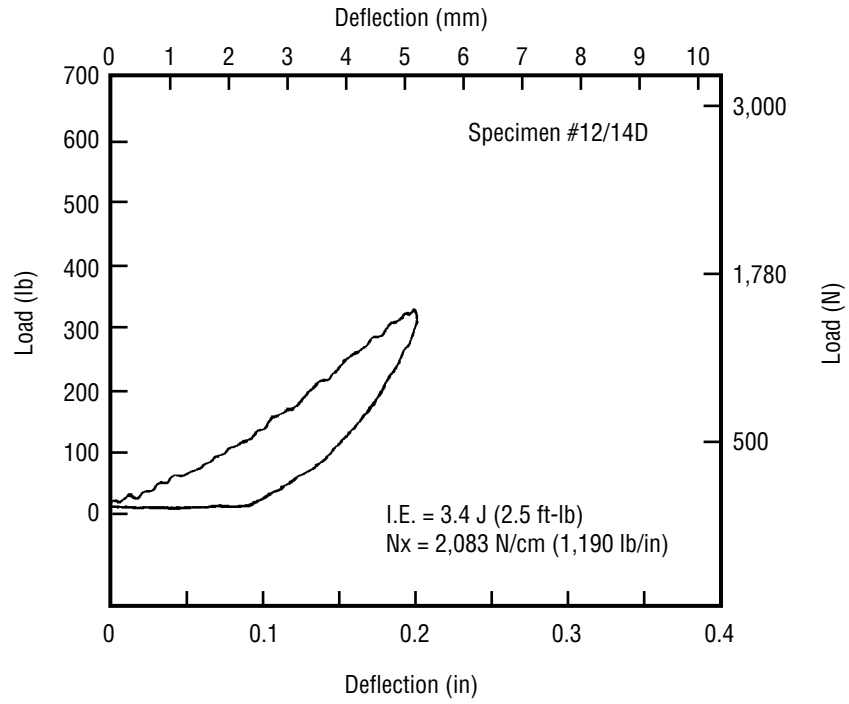


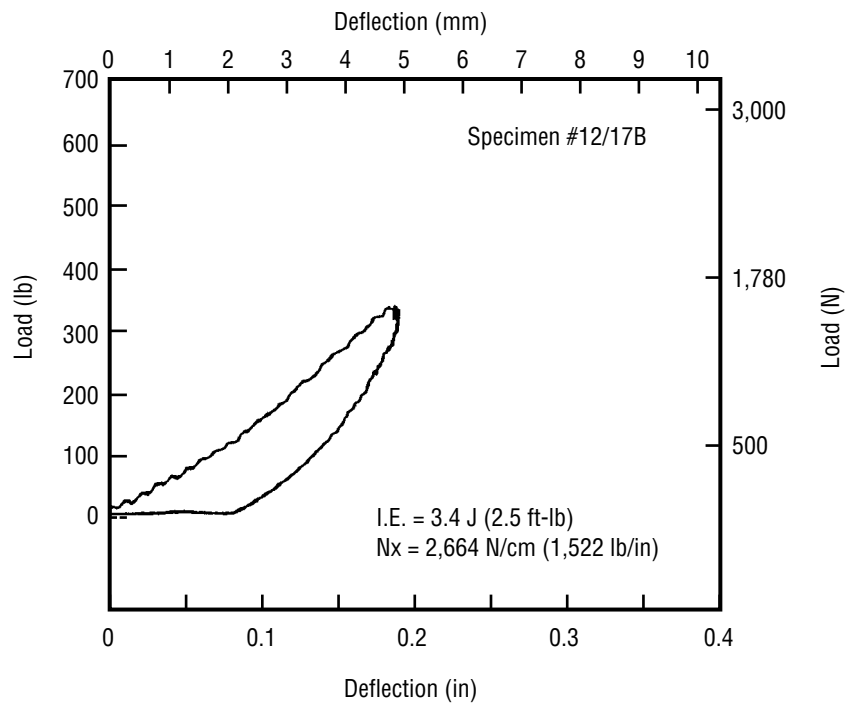
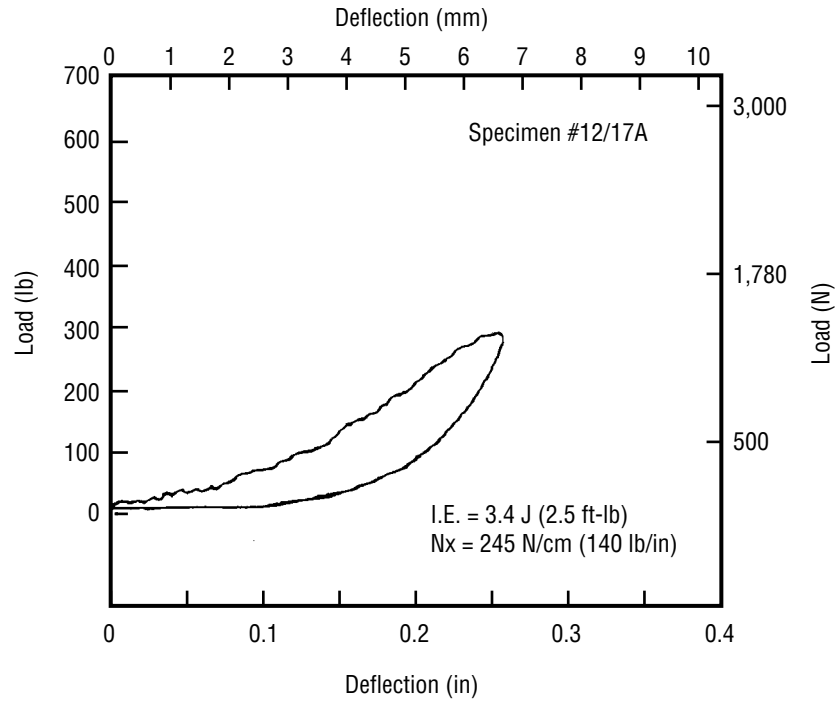


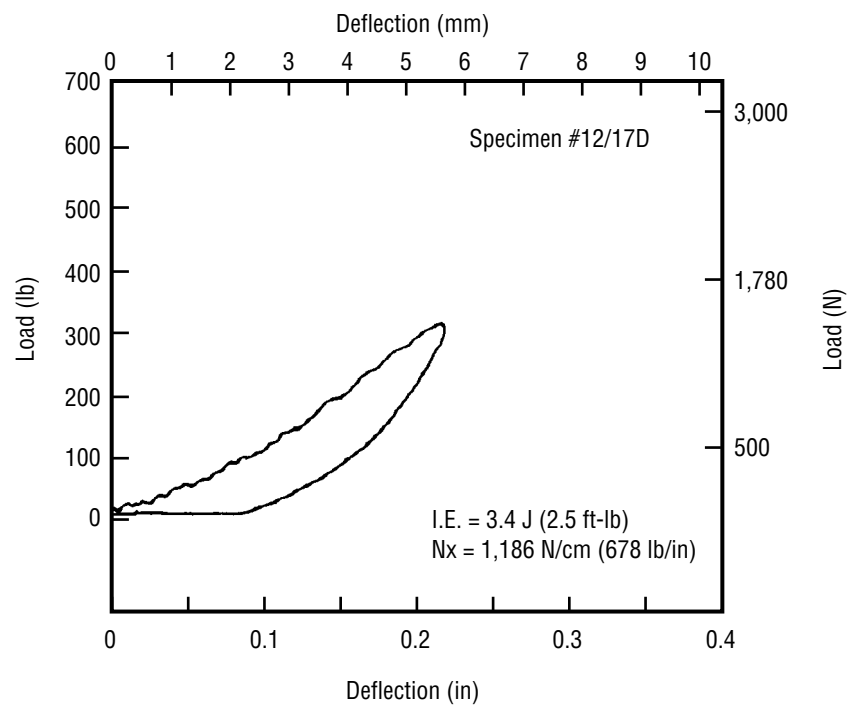
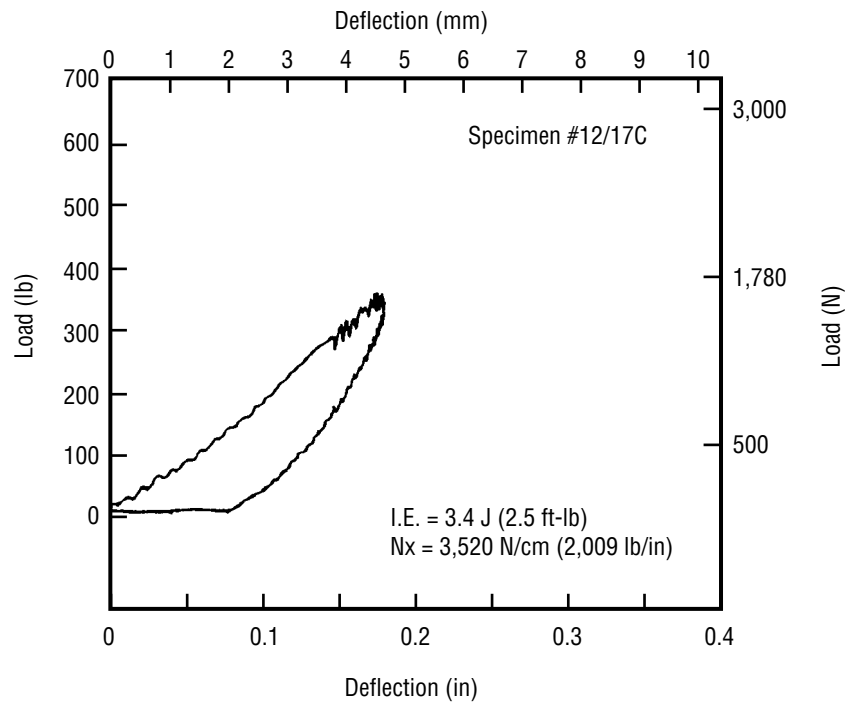




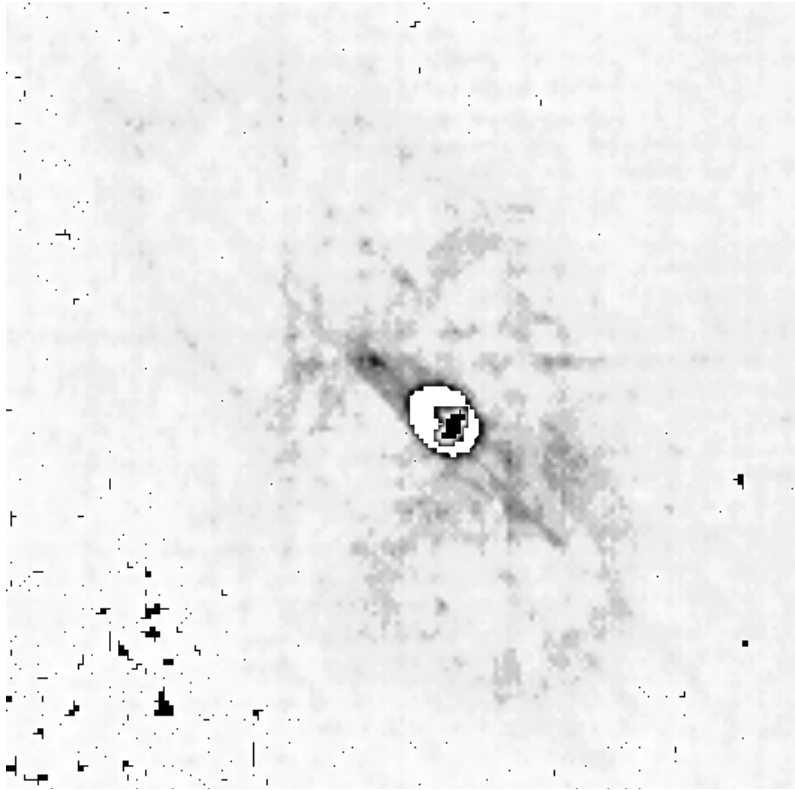




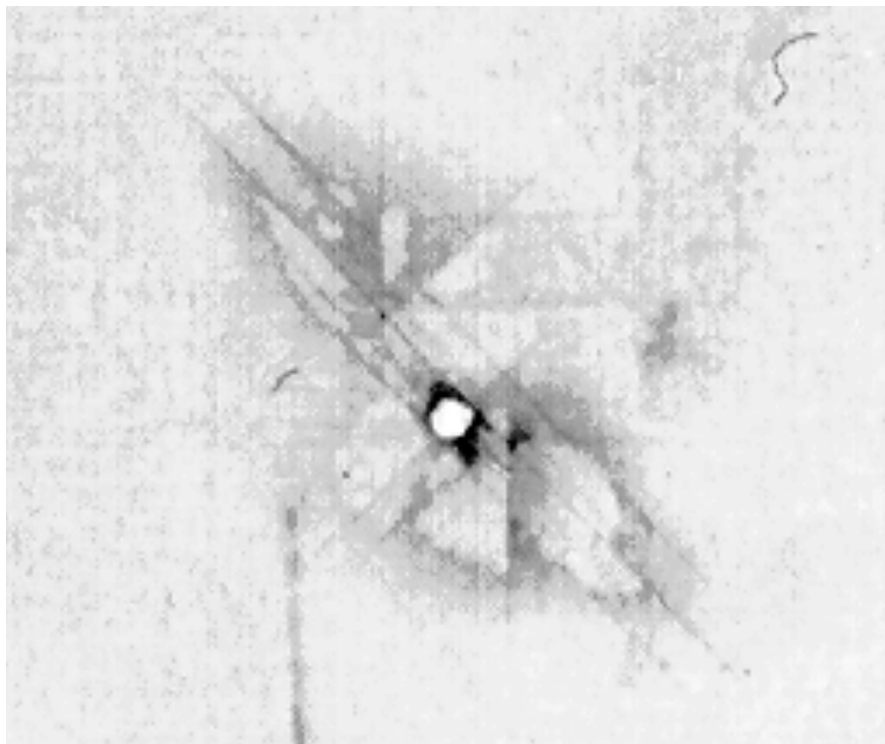




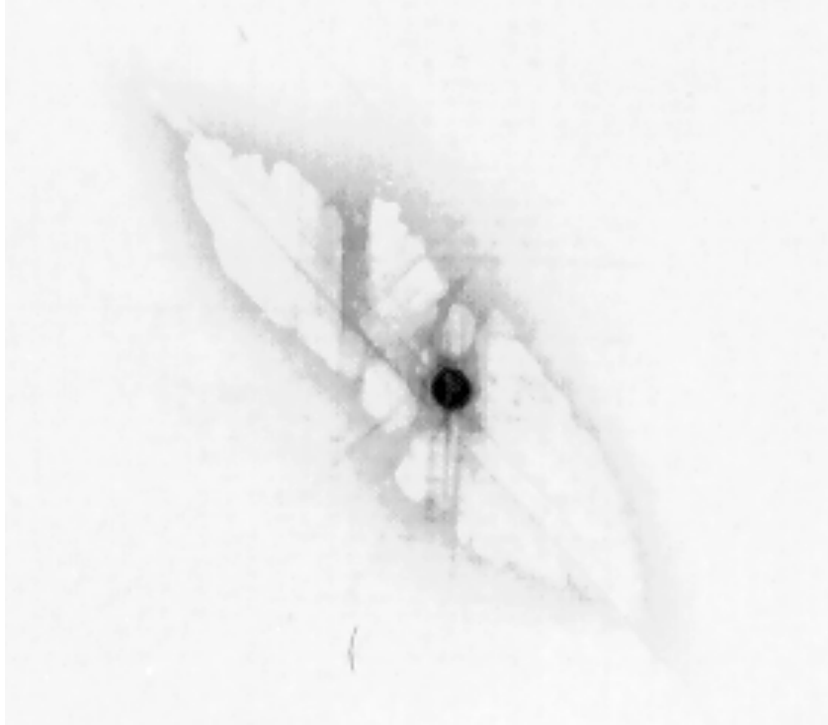
**APPENDIX B—X-RAY SIGNATURES OF STATIC INDENTATION
AND IMPACTED SPECIMENS**



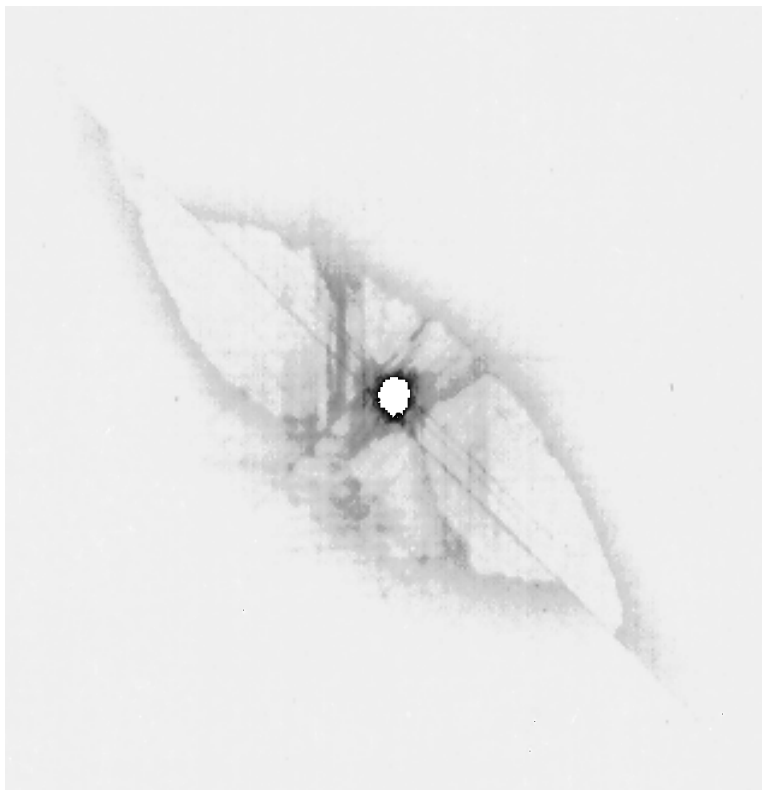
Static indentation specimen # 1.



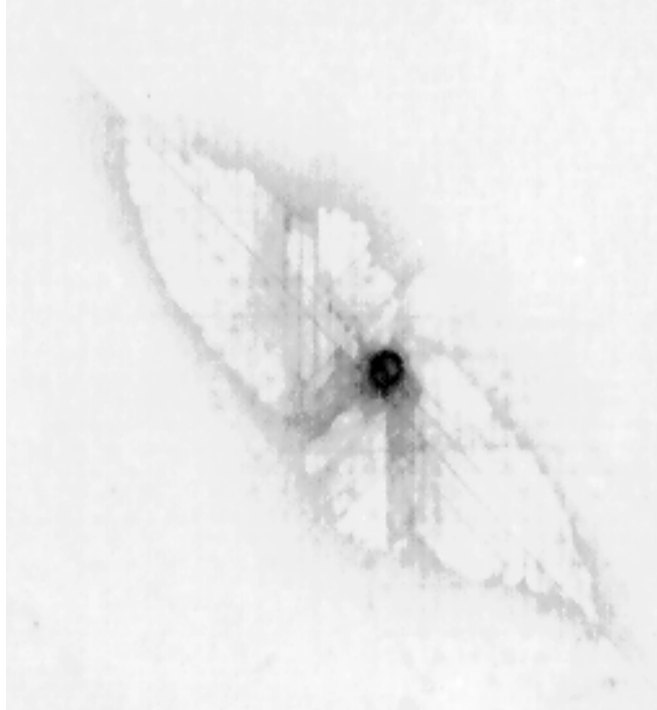
Static indentation specimen # 3.



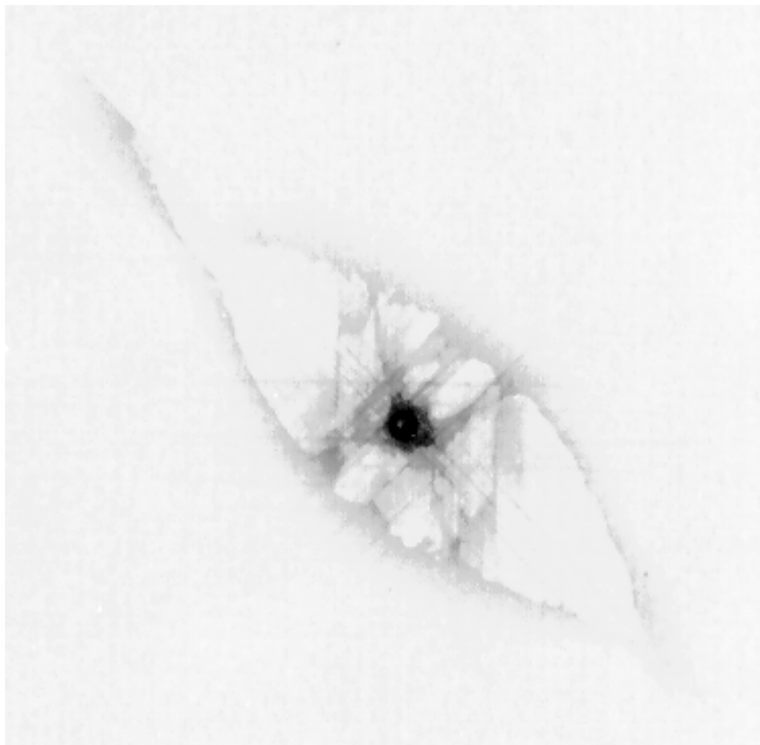
Static indentation specimen # 4.



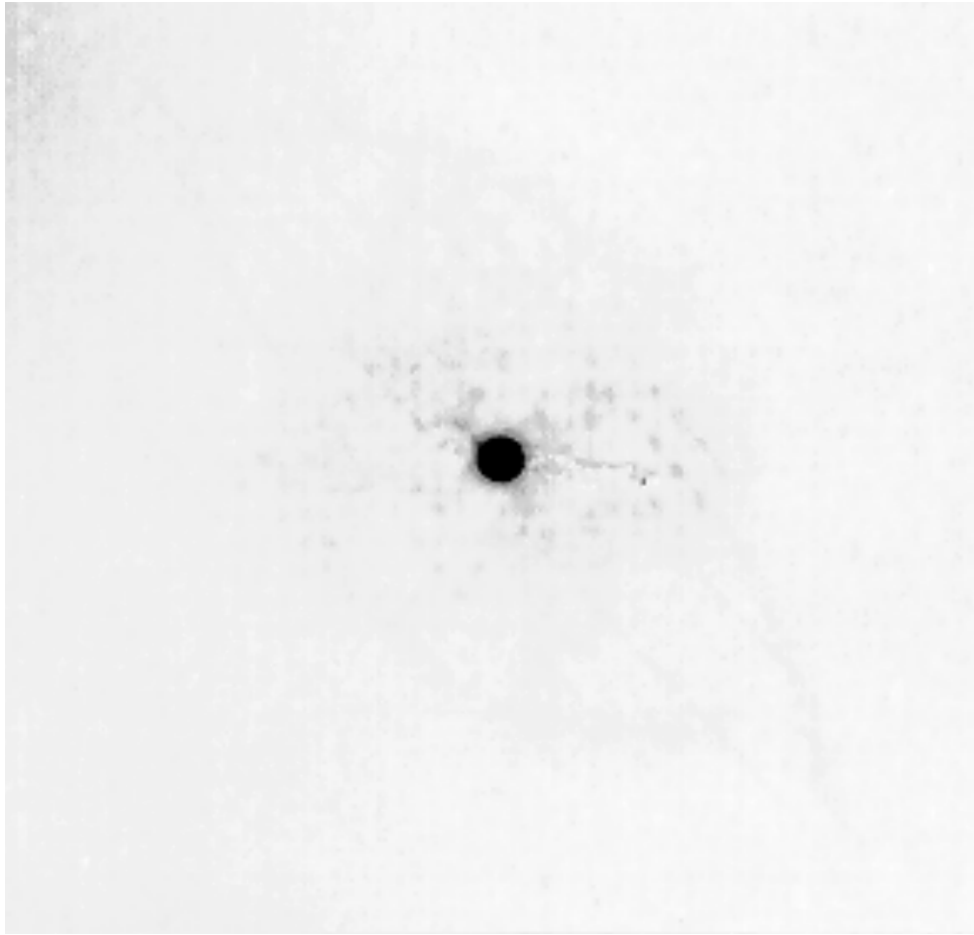
Static indentation specimen # 4.



Static indentation specimen # 7.



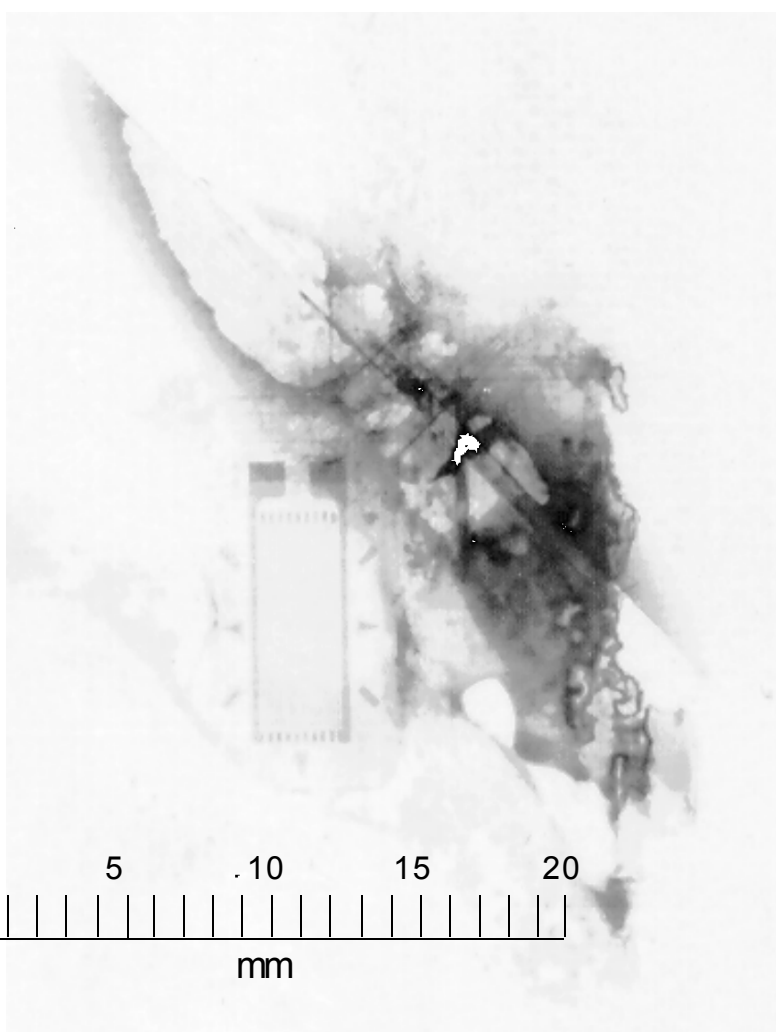
Static indentation specimen # 9.



Static indentation specimen # 10.

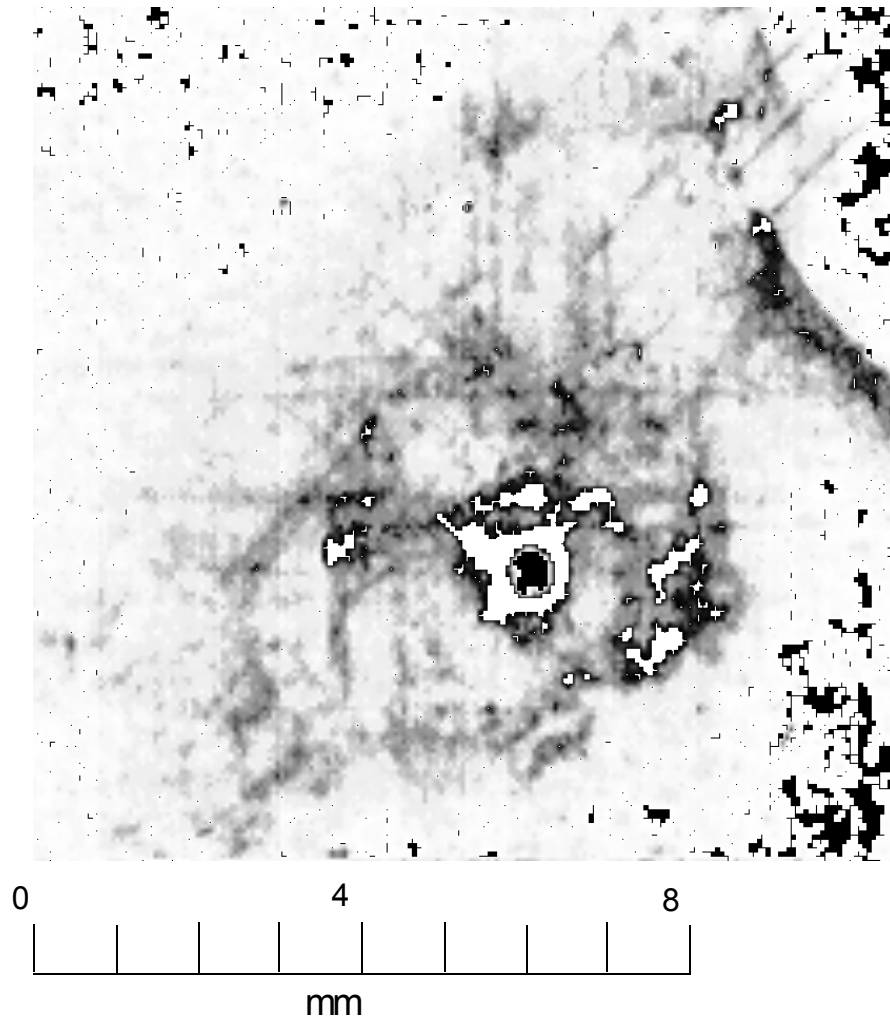
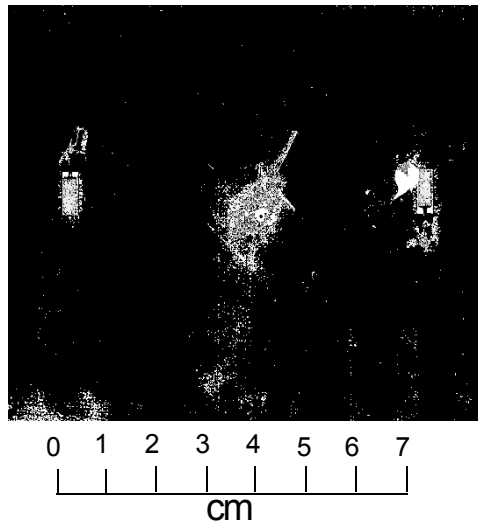


0 1 2 3 4 5 6 7
cm

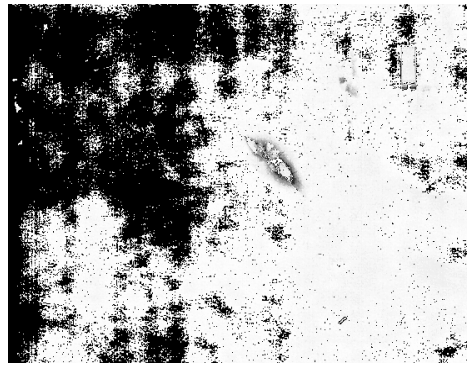


0 5 10 15 20
mm

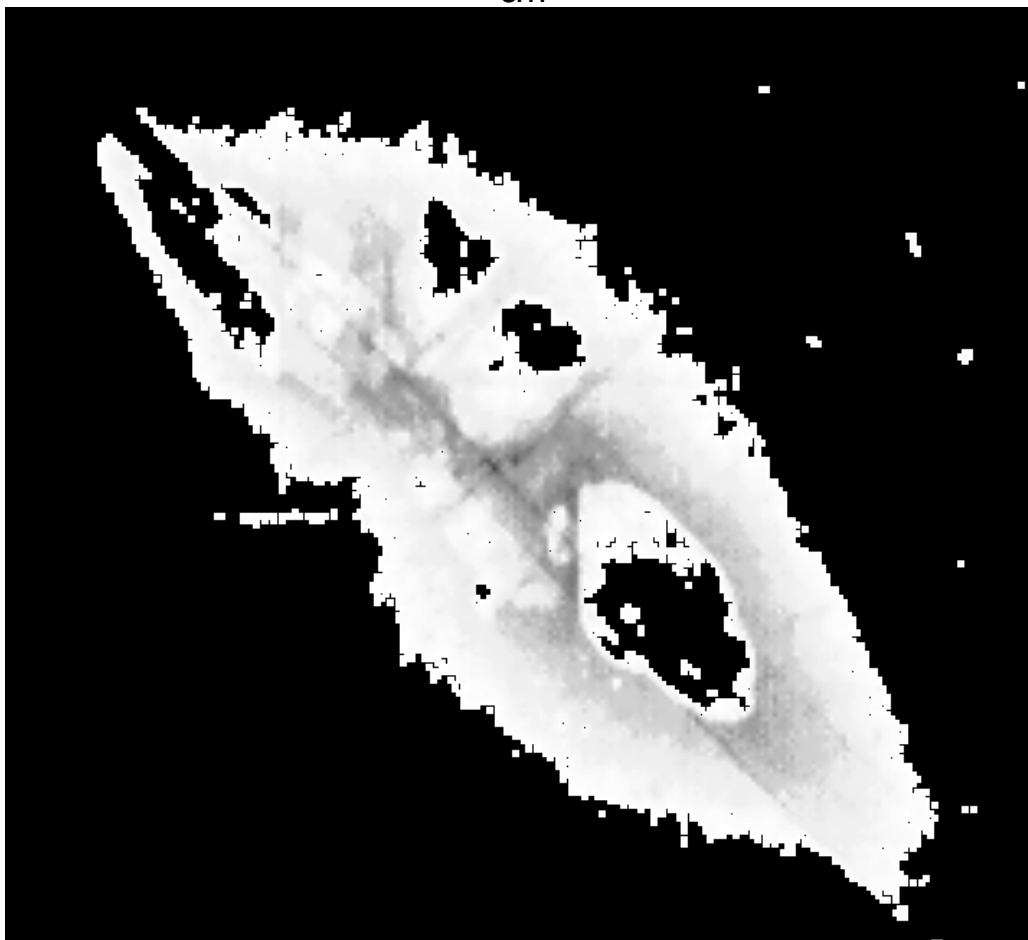
Specimen # L1.



Specimen # L2

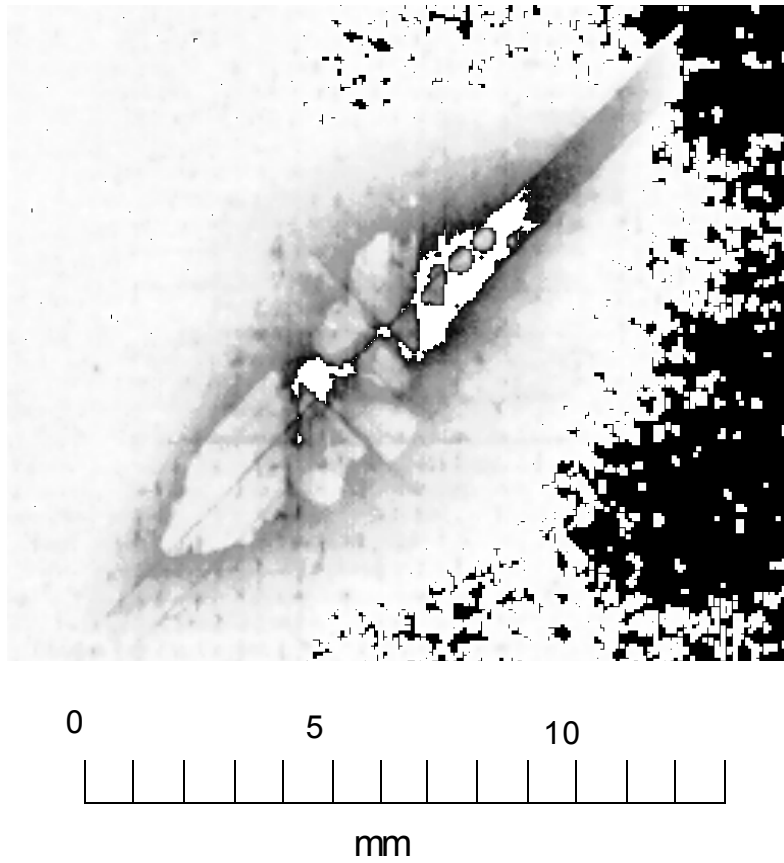
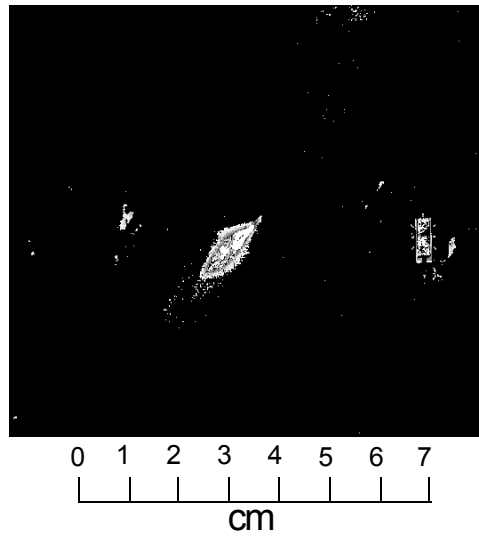


0 1 2 3 4 5 6 7
cm

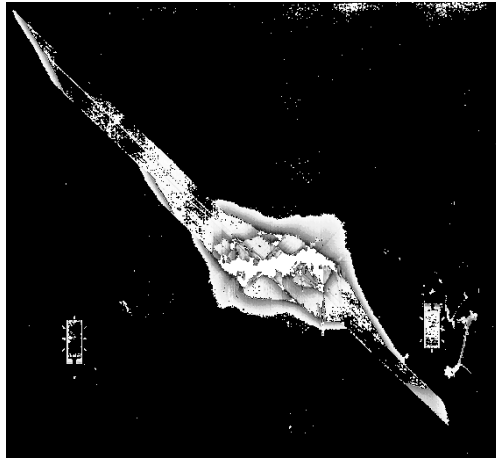


0 5 10
mm

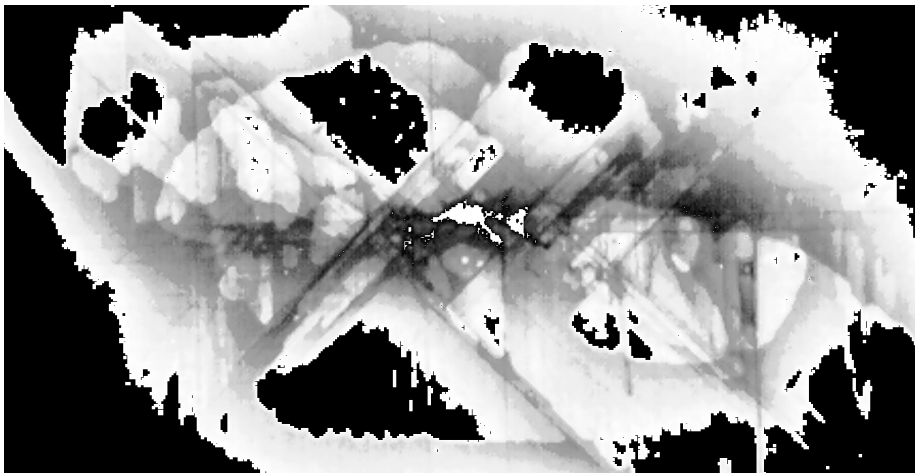
Specimen # L3



Specimen # L4\

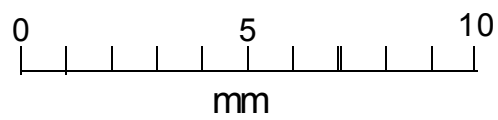
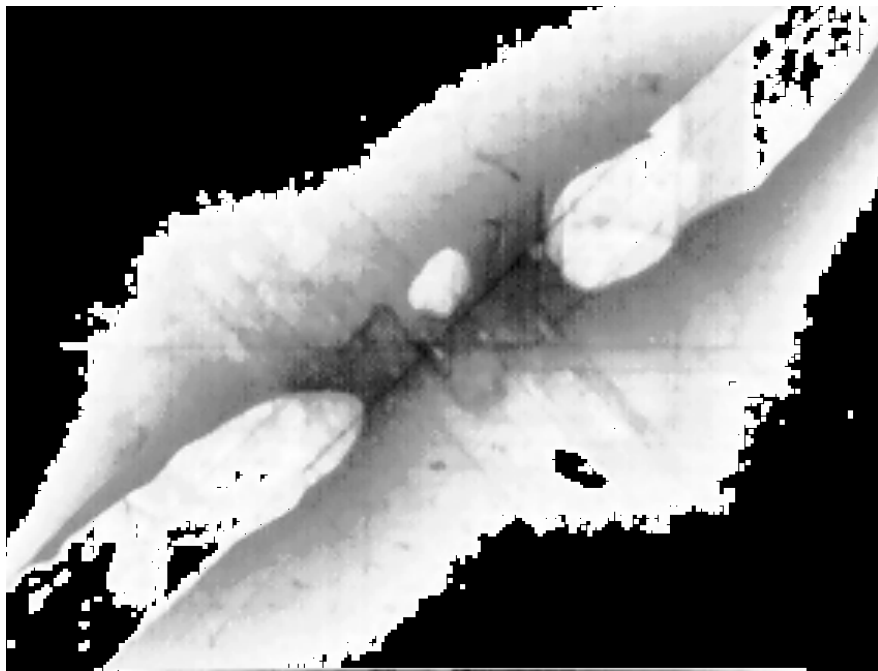
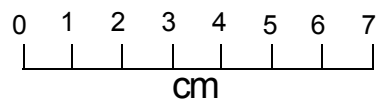
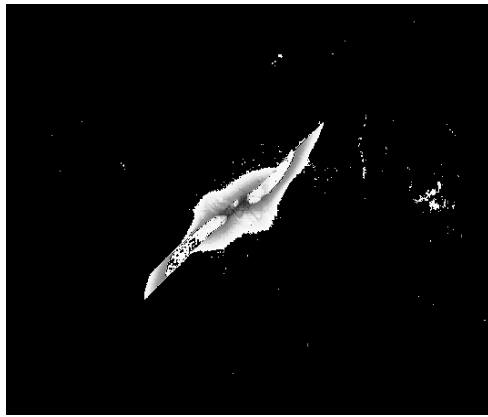


0 1 2 3 4 5 6 7
cm



0 5 10 15 20
mm

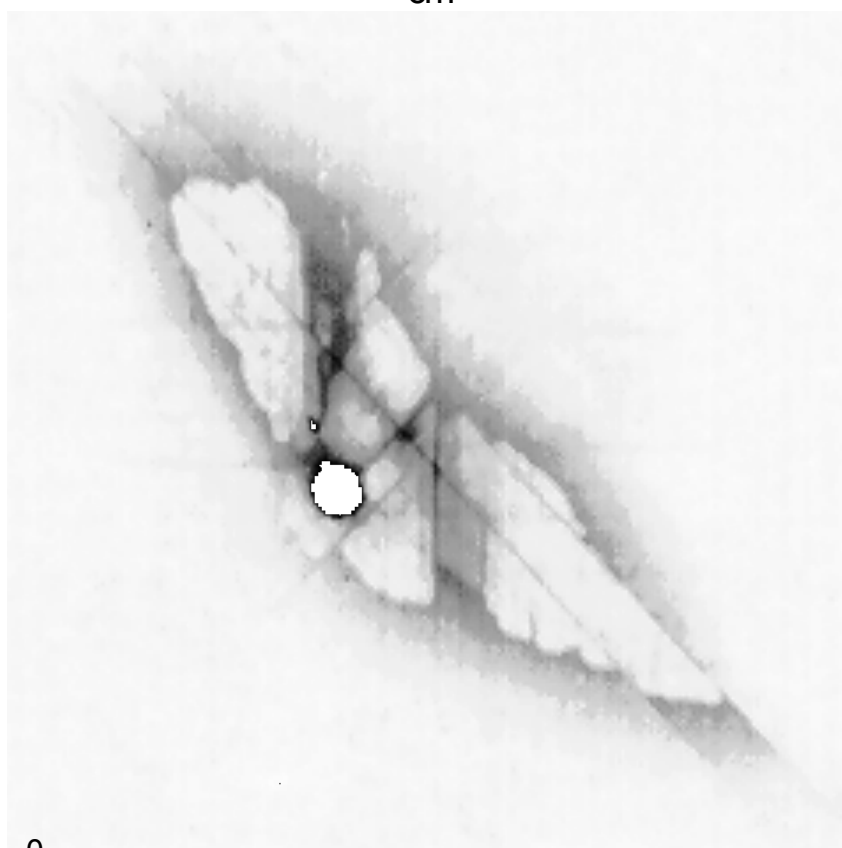
Specimen # L5



Specimen # L6

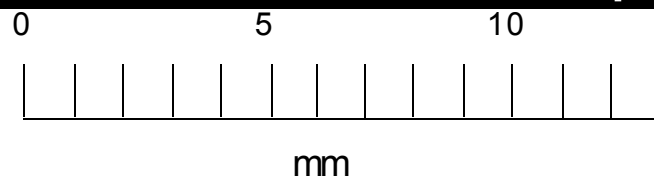
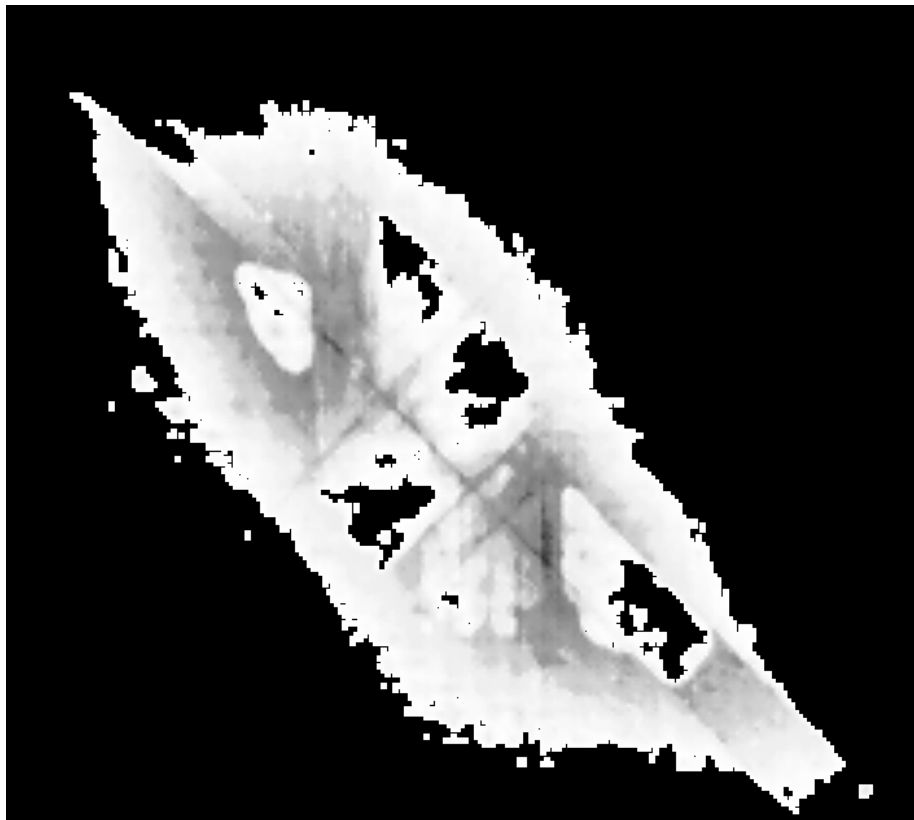
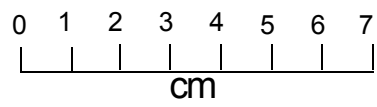
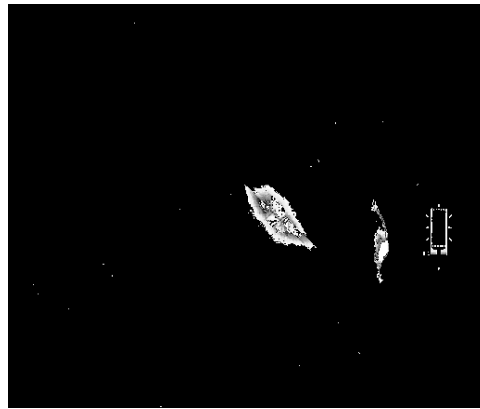


0 1 2 3 4 5 6 7
cm

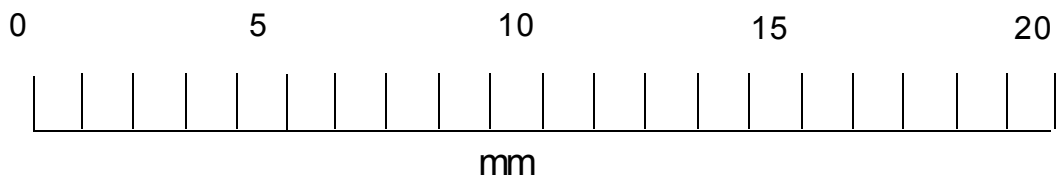
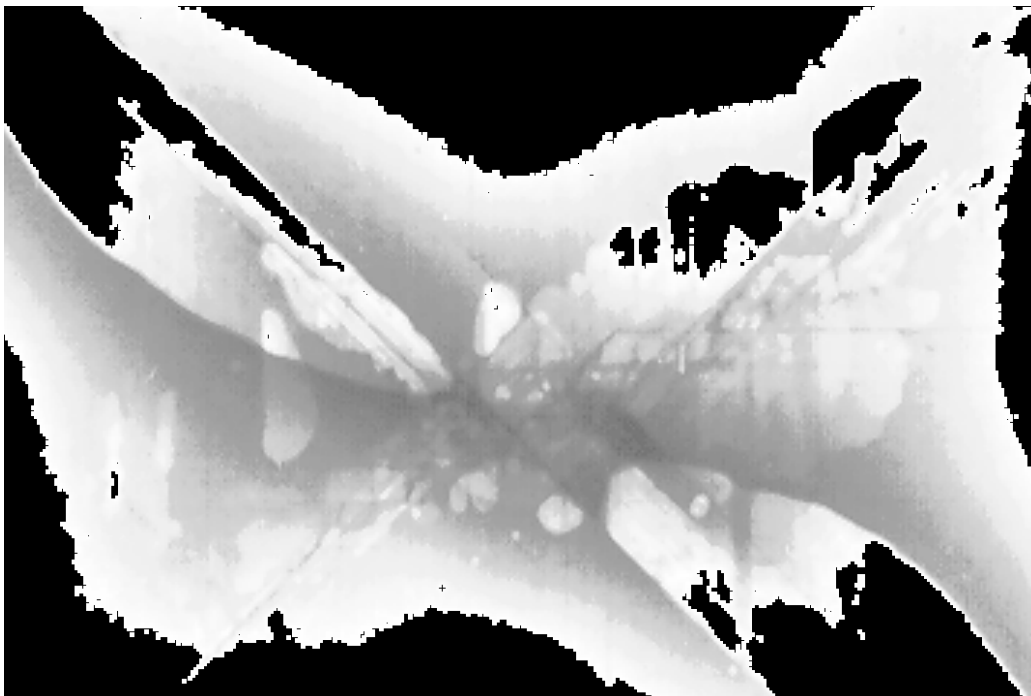
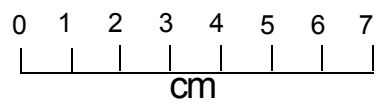
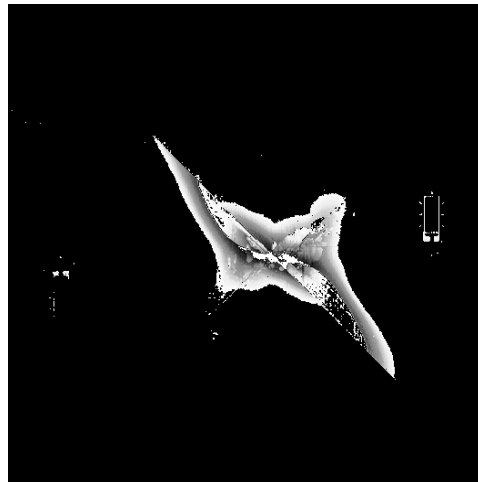


0 5 10
mm

Specimen # 11/13A



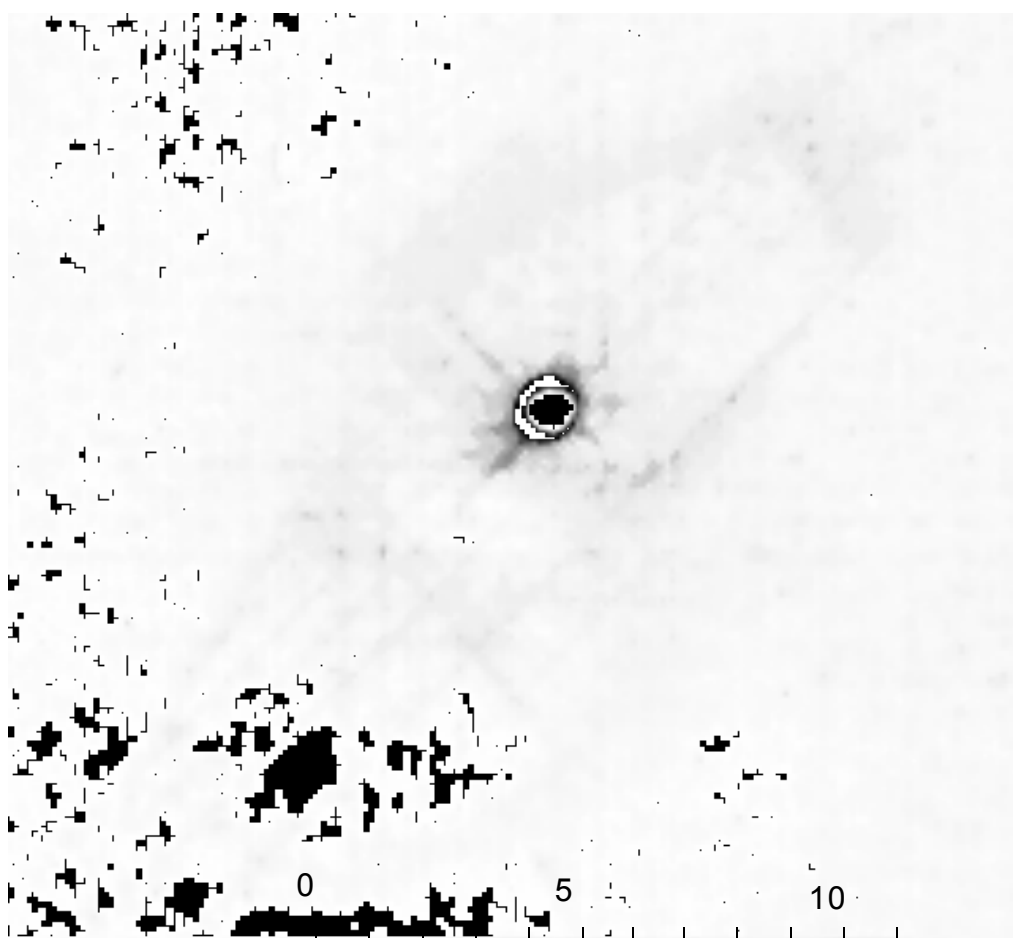
Specimen # 11/13B



Specimen # 11/14A

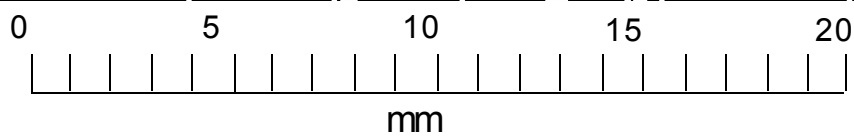
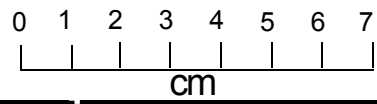
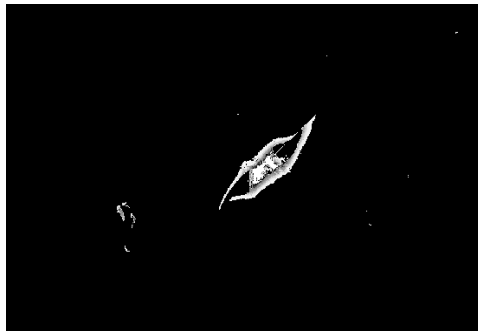


0 1 2 3 4 5 6 7
cm

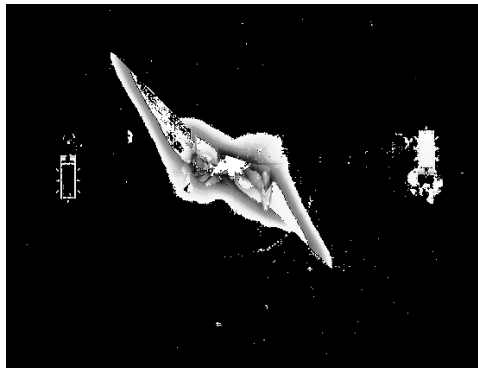


0 5 10
mm

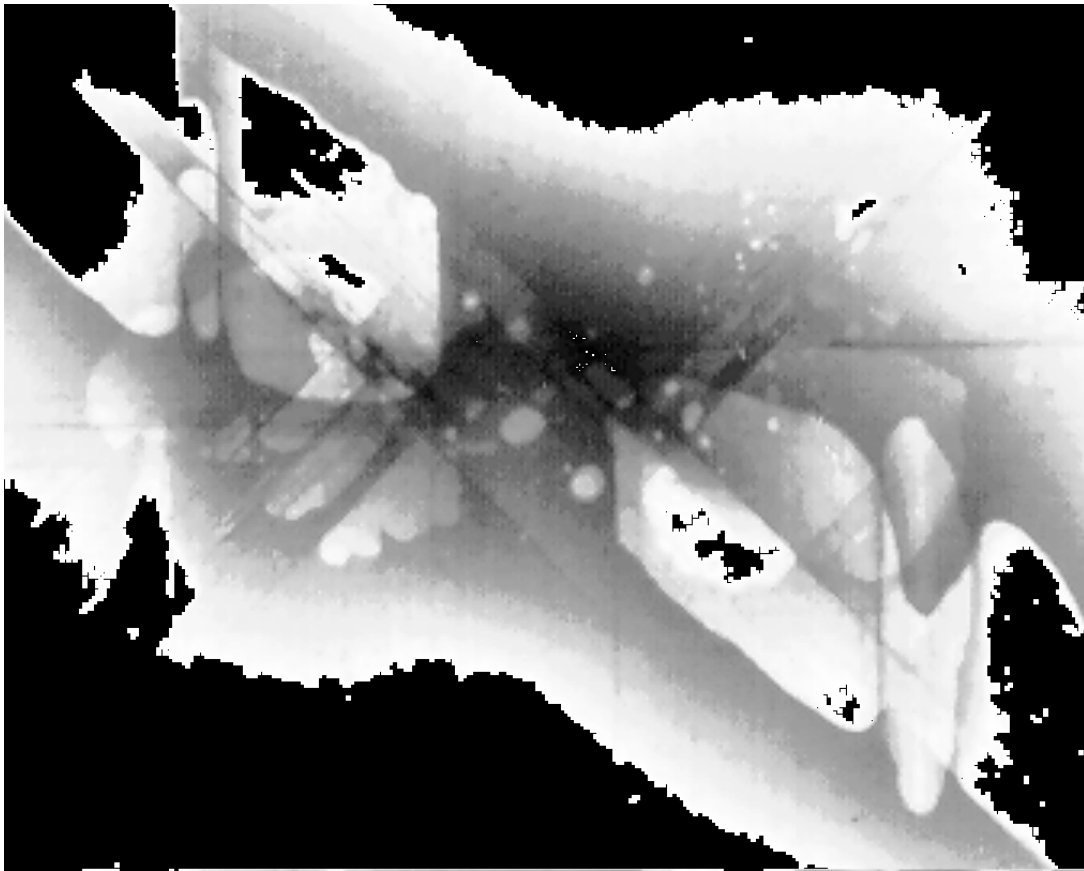
Specimen # 11/14B



Specimen # 11/25A



0 1 2 3 4 5 6 7
cm

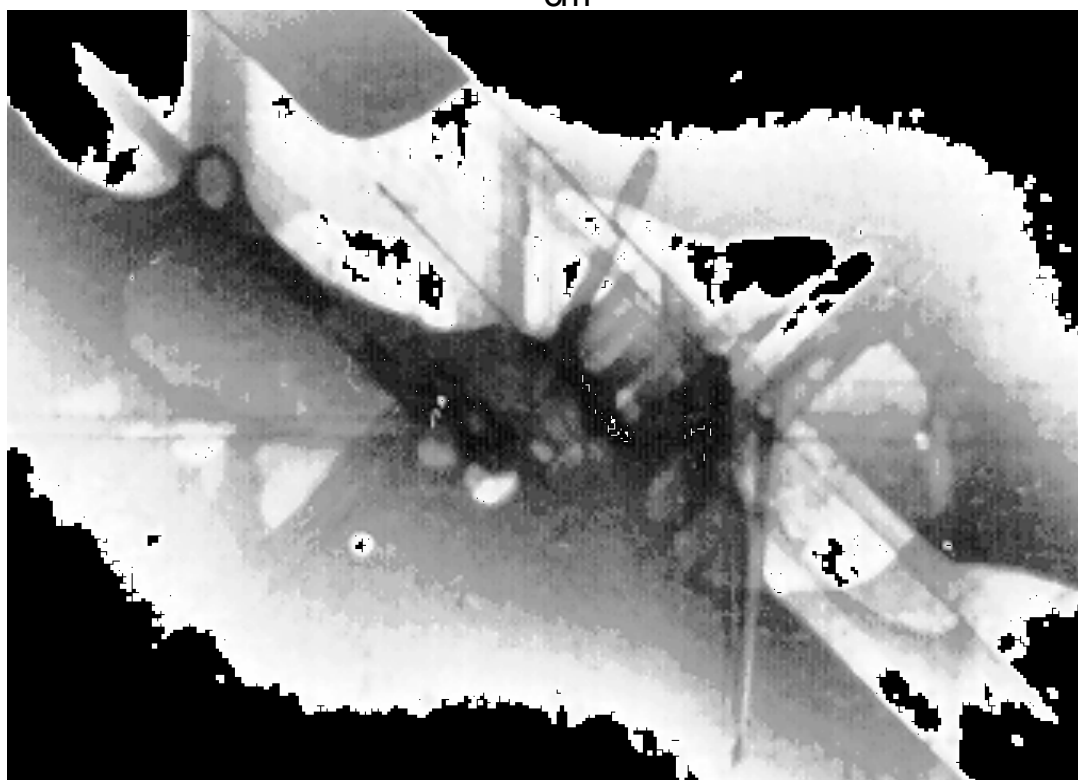


0 5 10 15 20
mm

Specimen # 11/27A

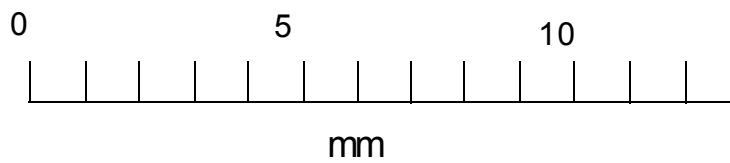
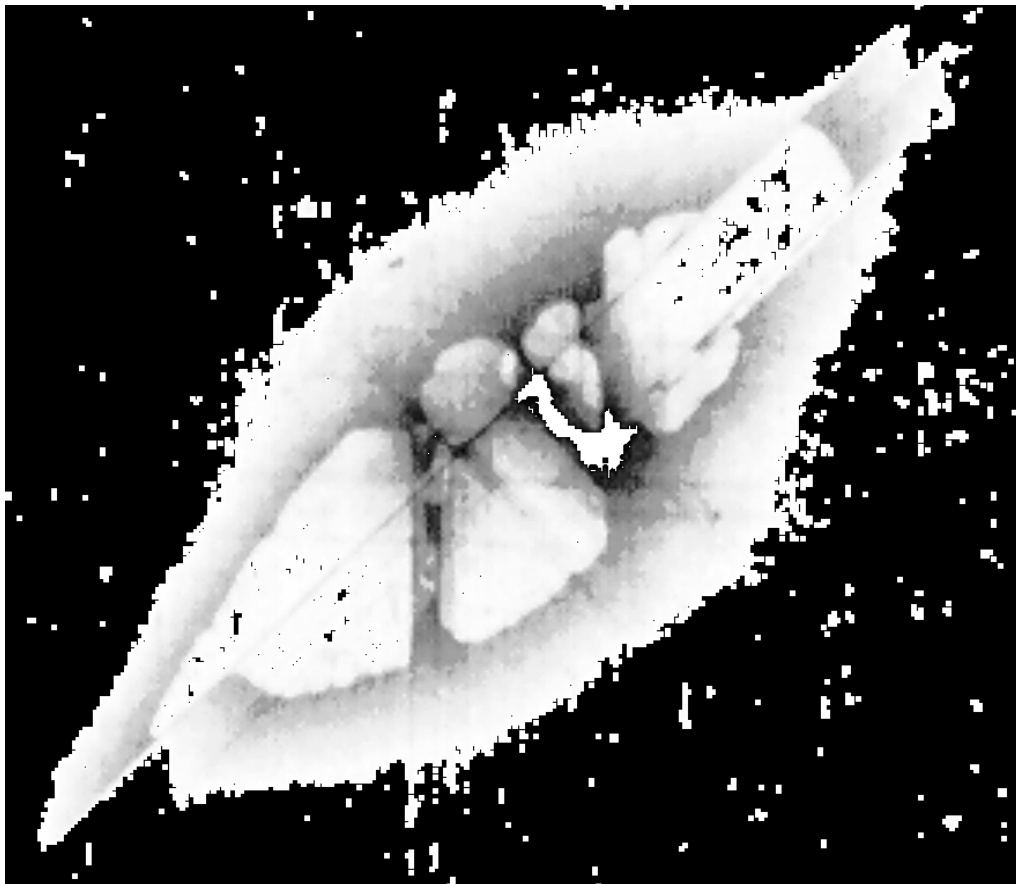
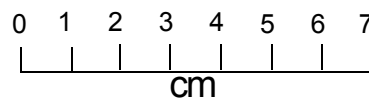
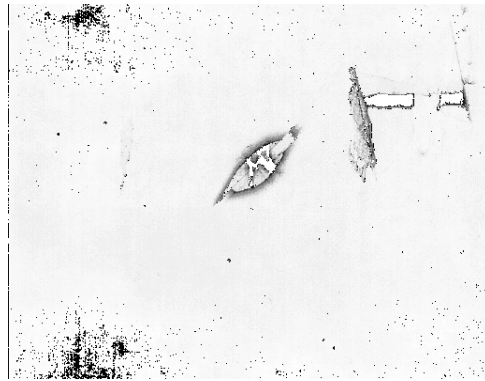


0 1 2 3 4 5 6 7
cm

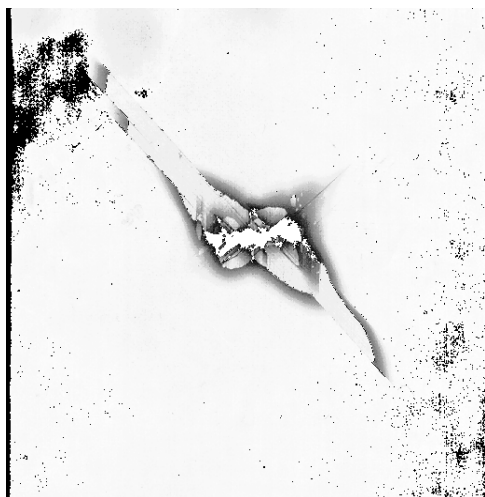


0 5 10 15 20
mm

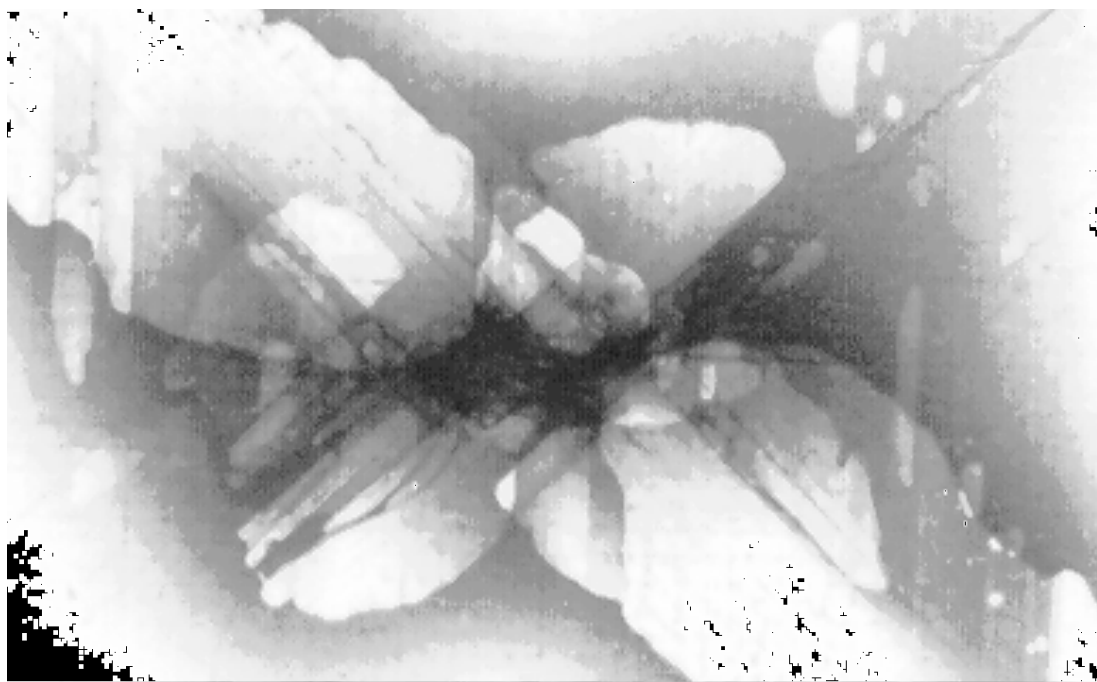
Specimen # 11/28A



Specimen # 11/28B

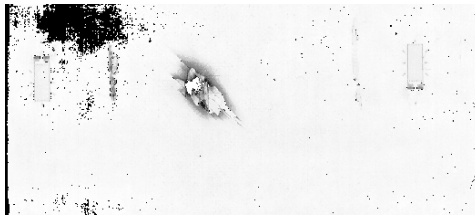


0 1 2 3 4 5 6 7
cm

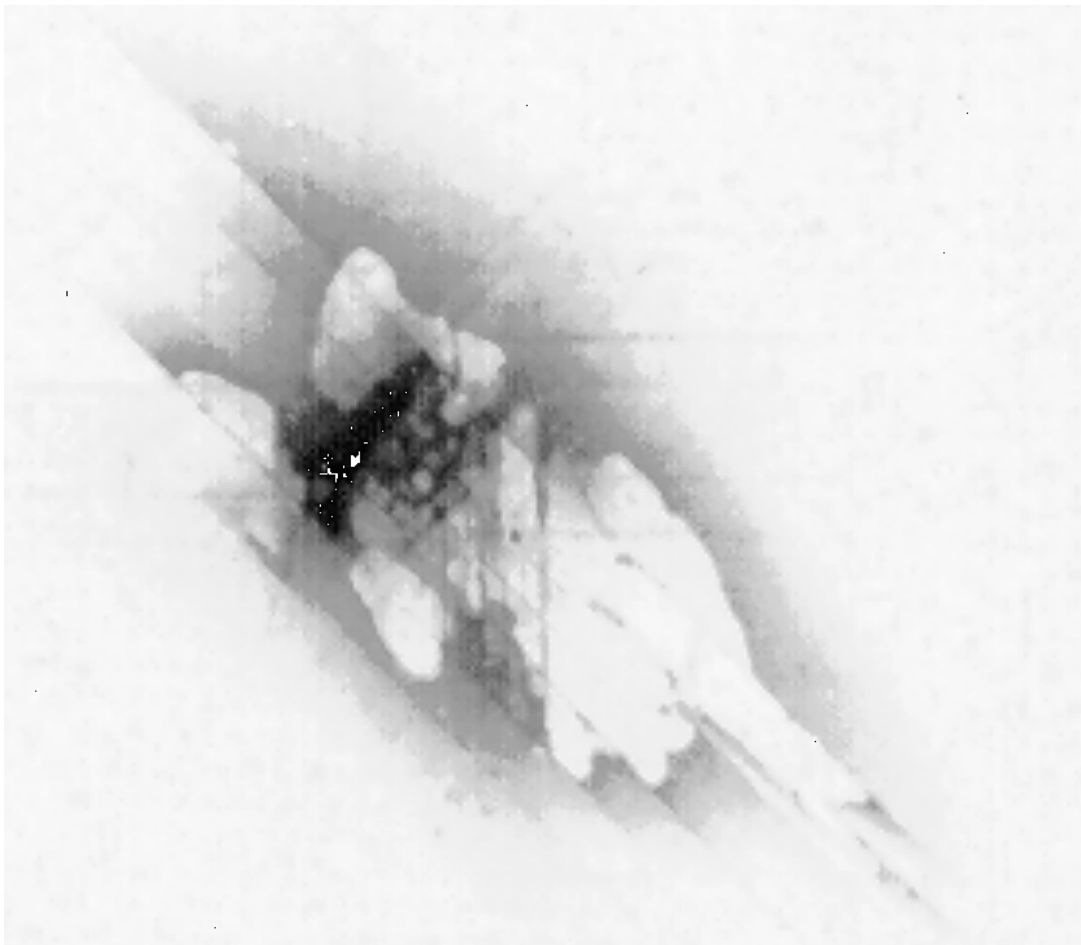


0 5 10 15 20
mm

Specimen # 12/12A

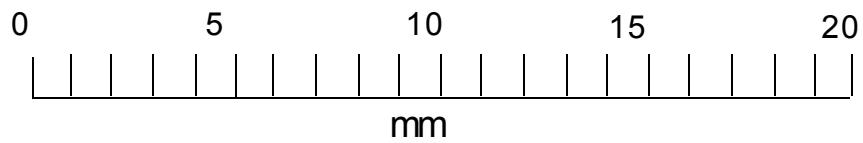
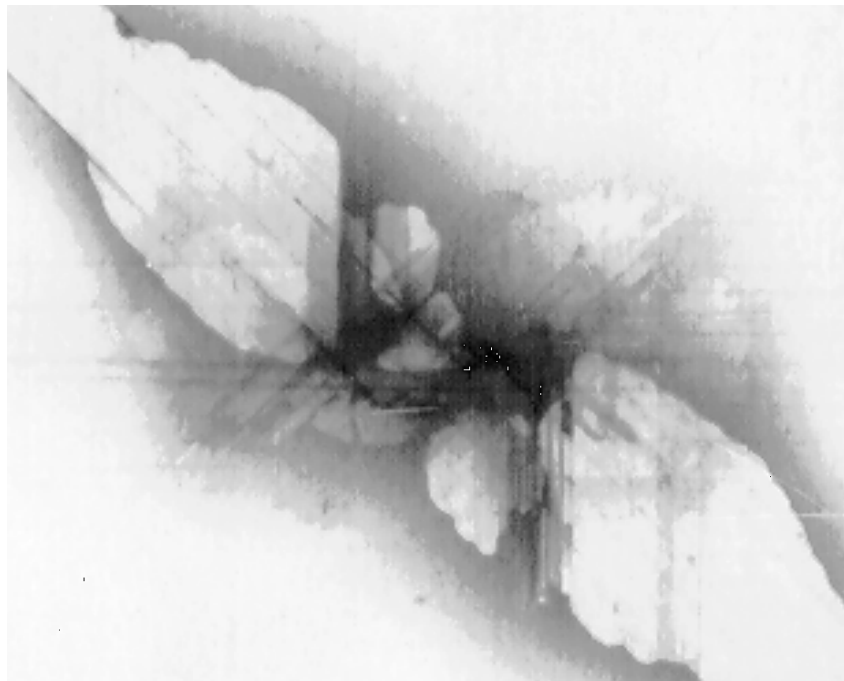
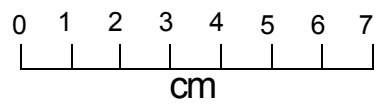
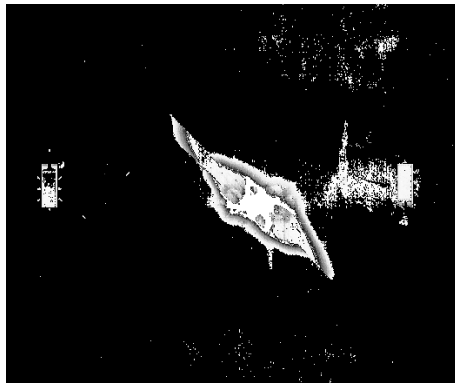


0 1 2 3 4 5 6 7
cm

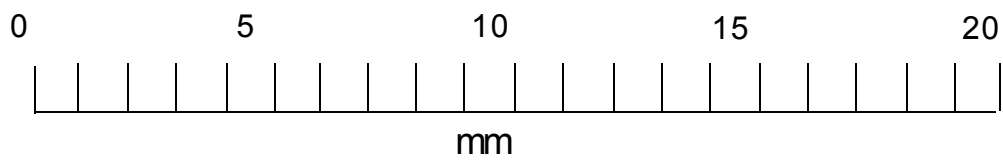
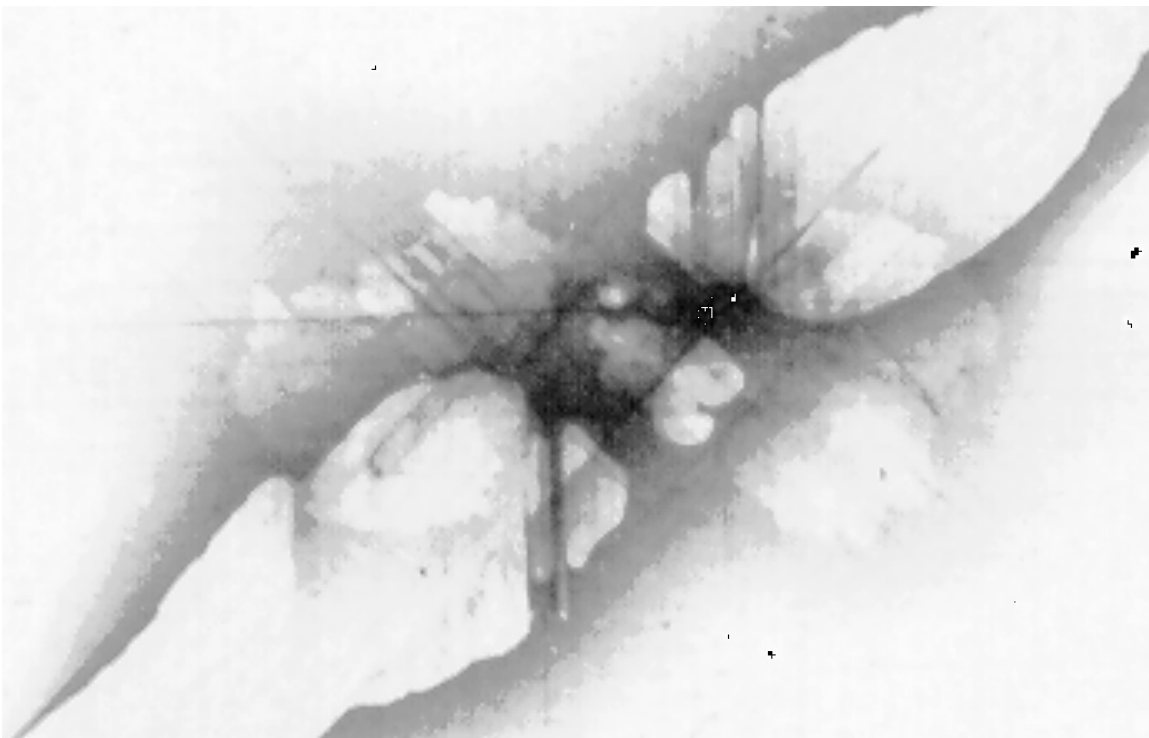
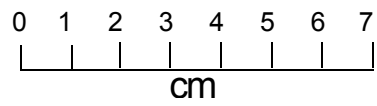
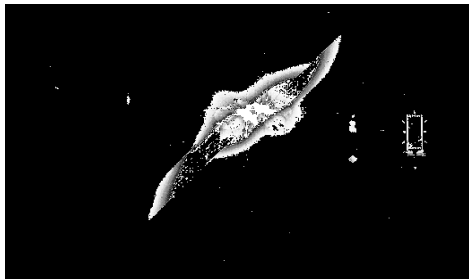


0 5 10 15
mm

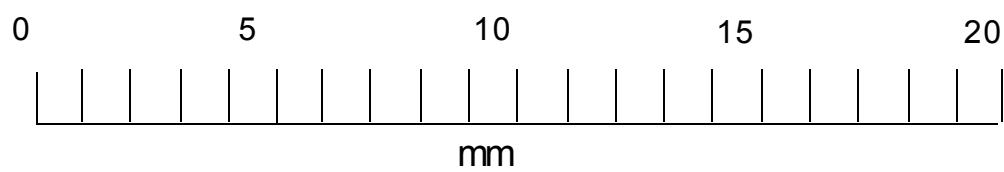
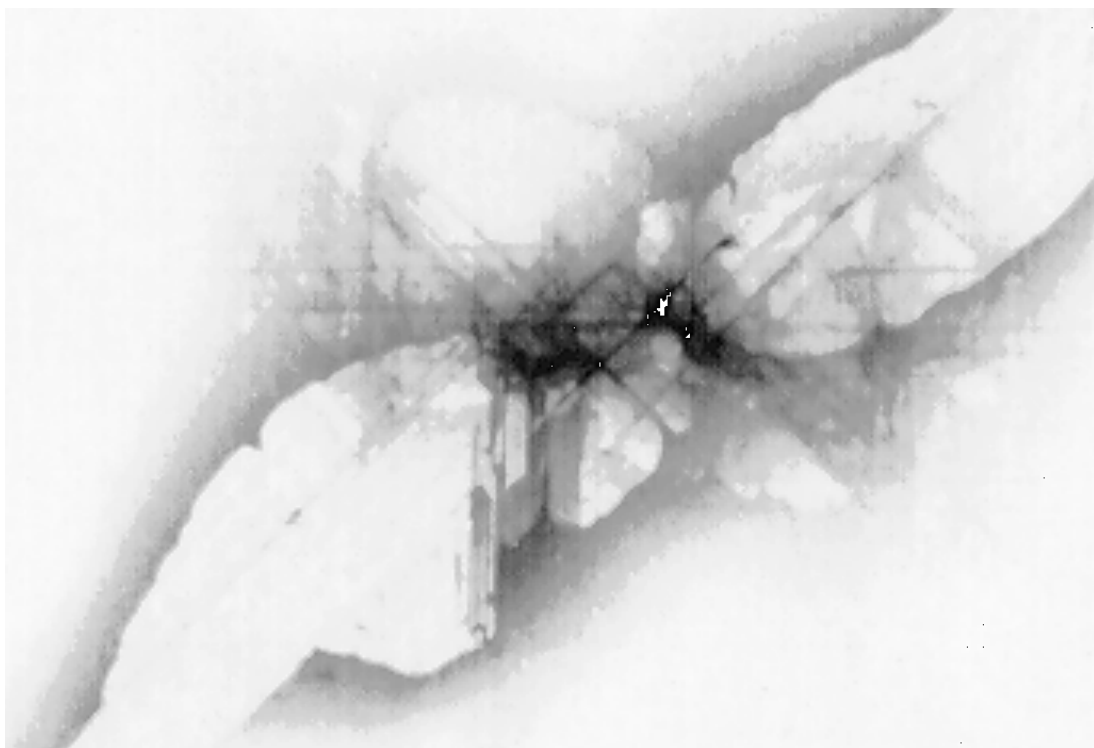
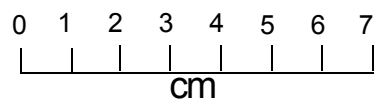
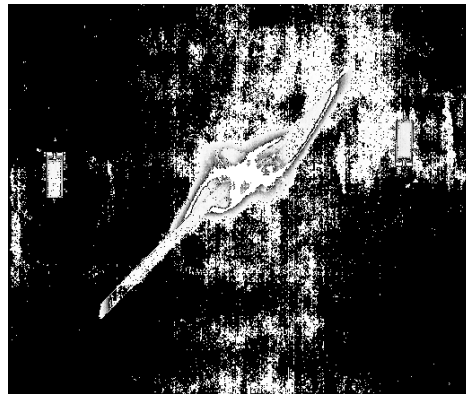
Specimen # 12/12B



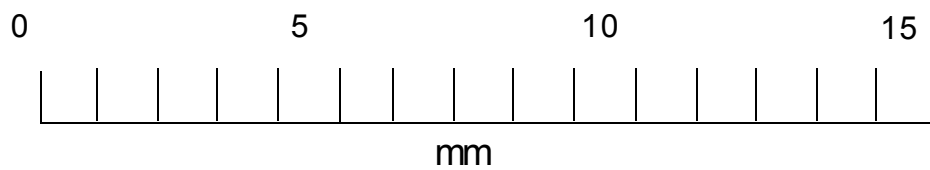
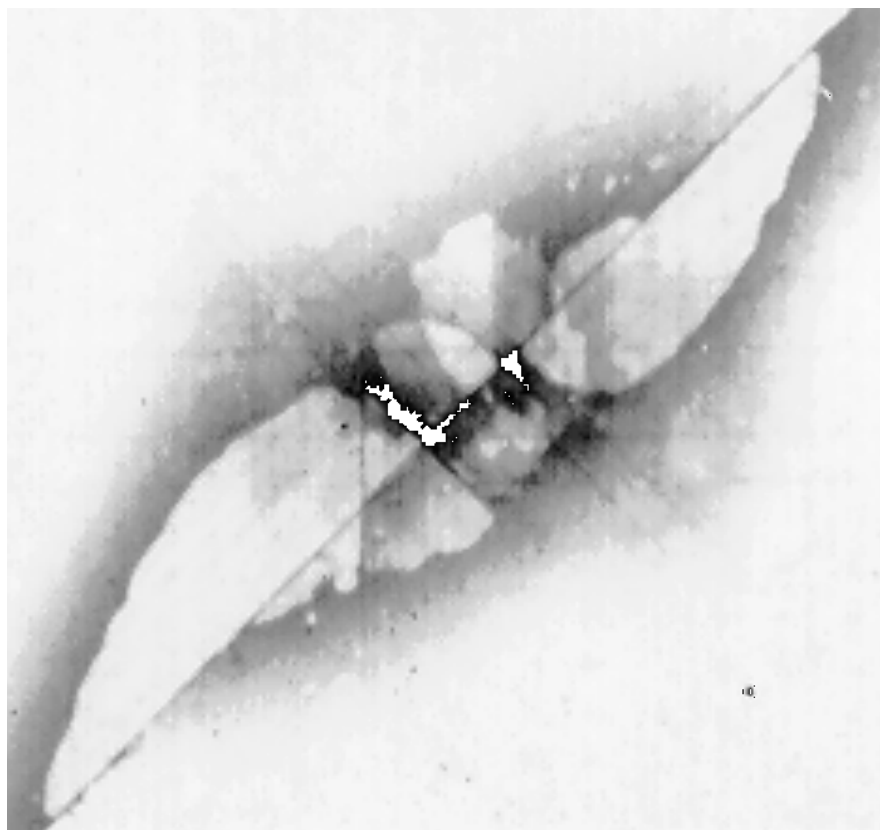
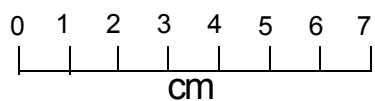
Specimen # 12/12C



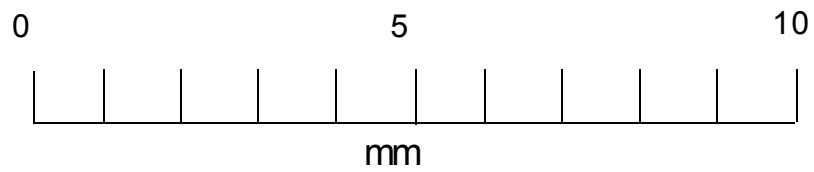
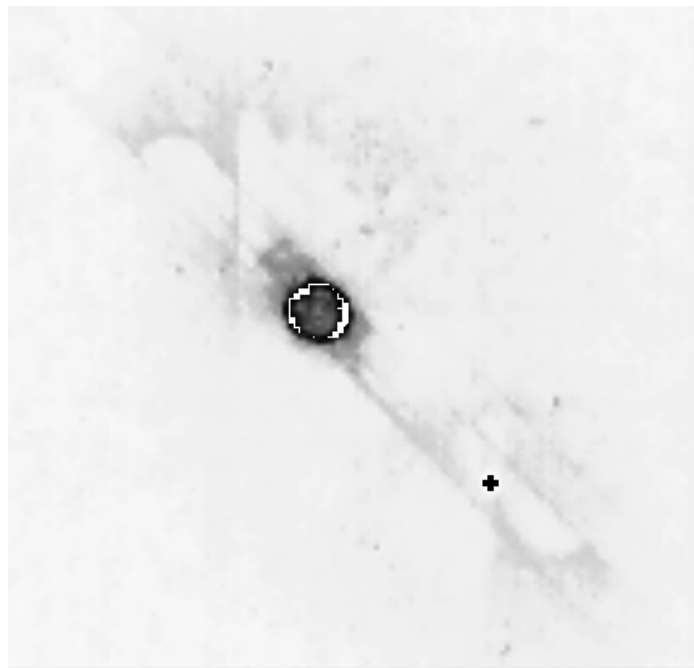
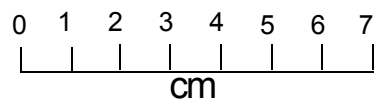
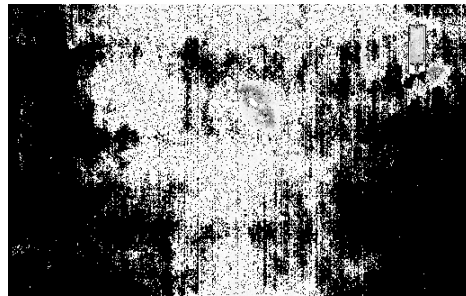
Specimen # 12/12D



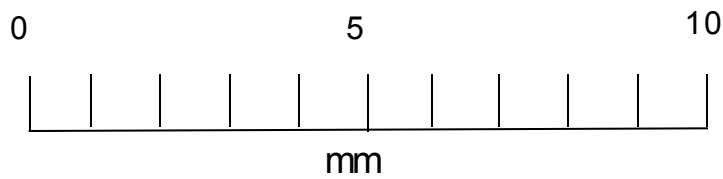
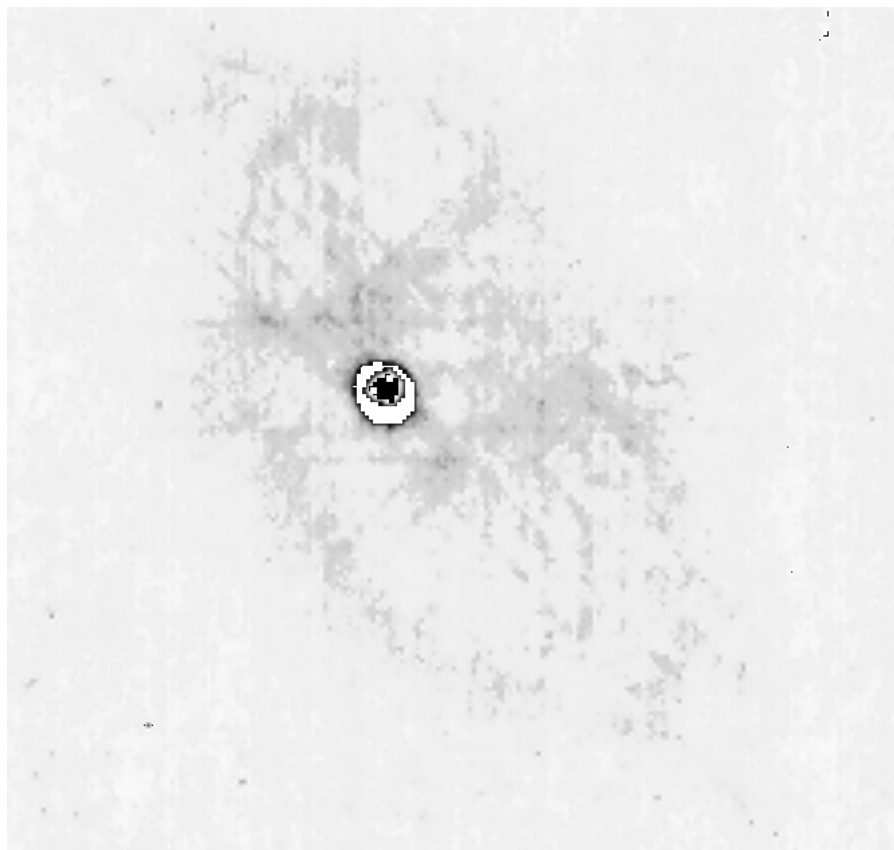
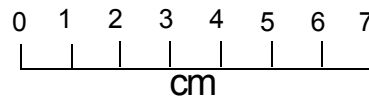
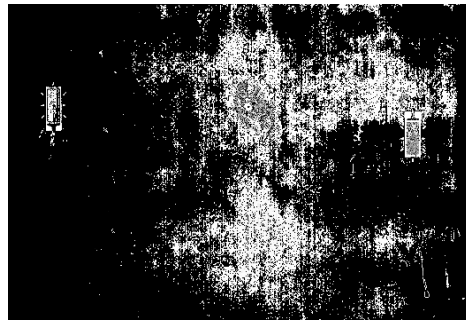
Specimen # 12/14A



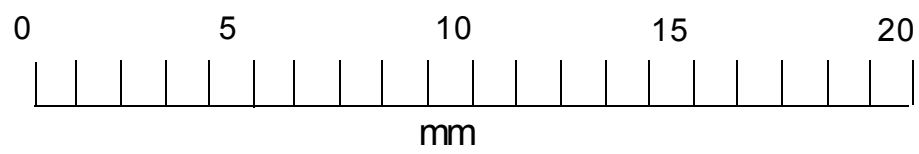
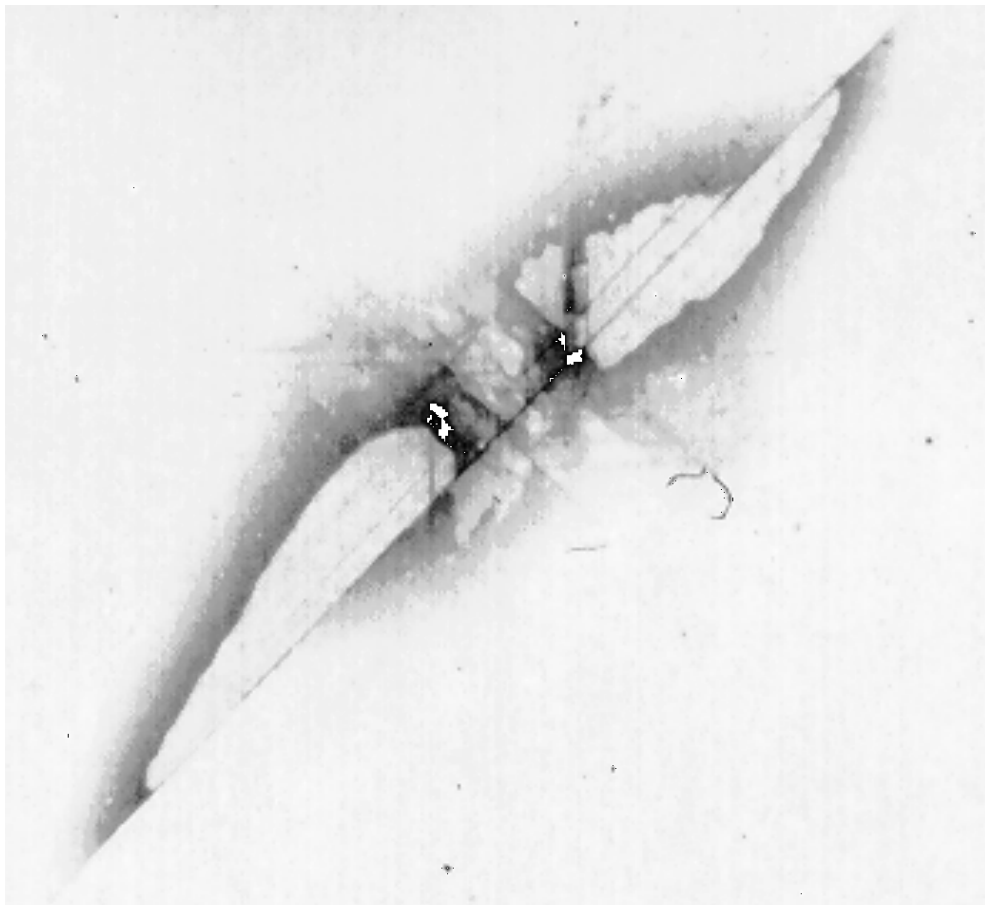
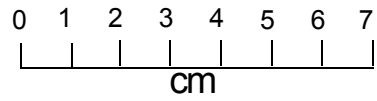
Specimen # 12/14B



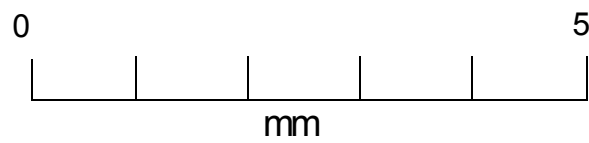
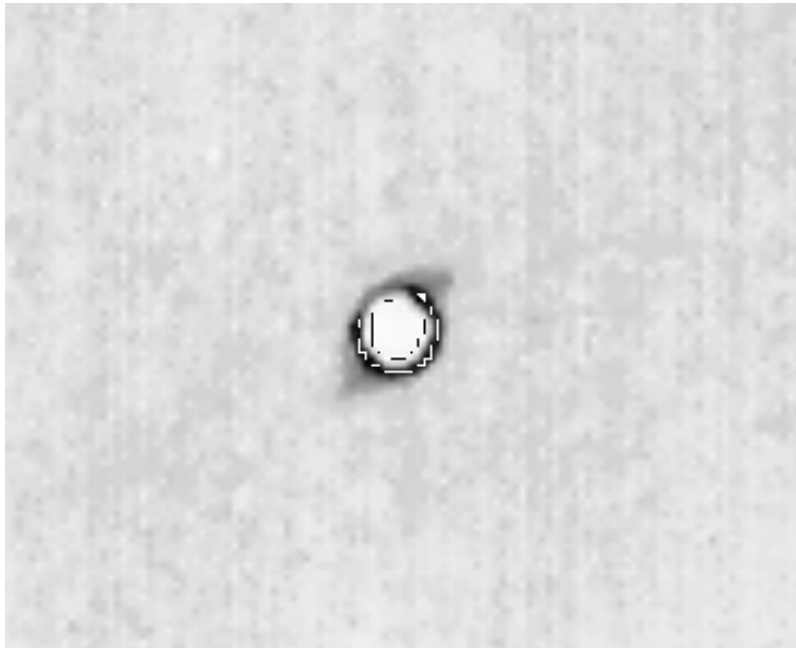
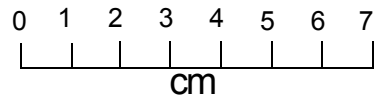
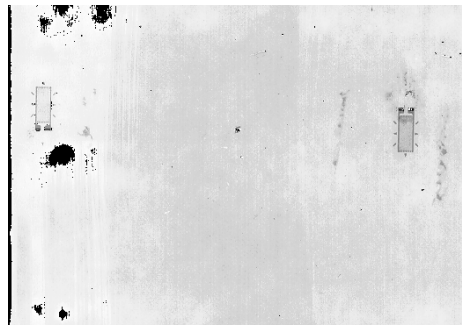
Specimen # 12/14C



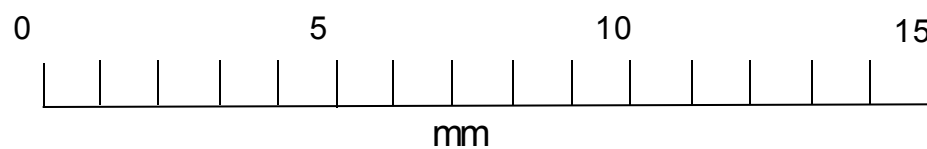
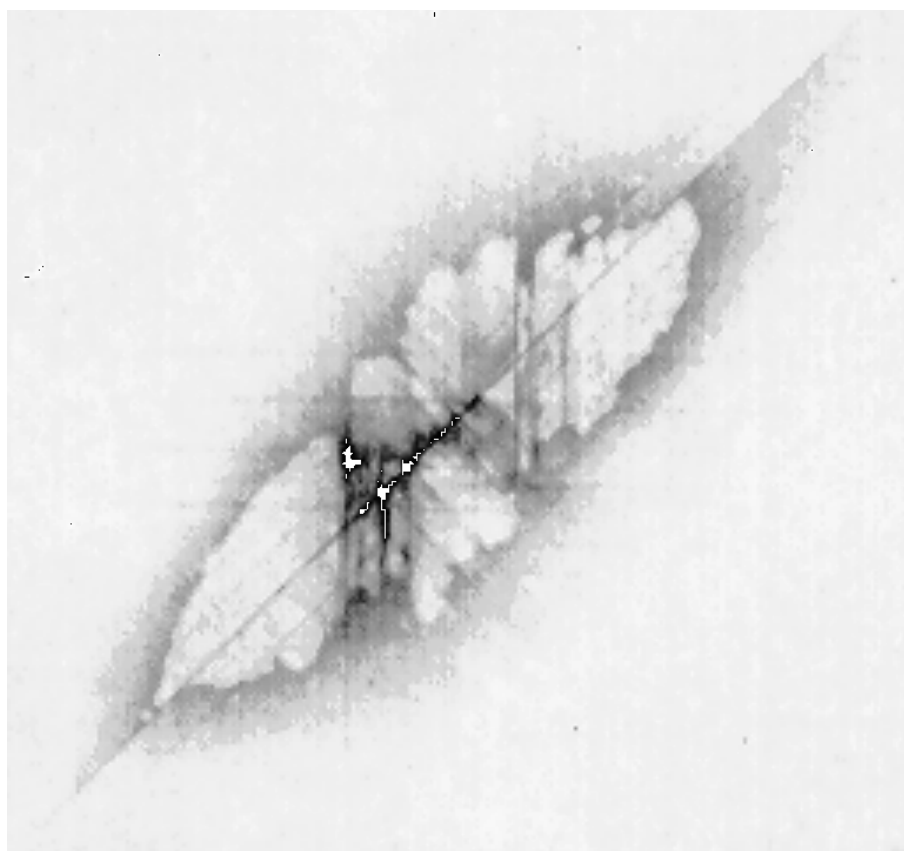
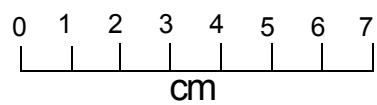
Specimen # 12/14D



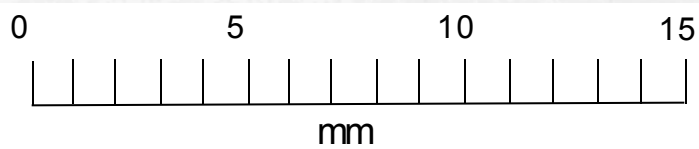
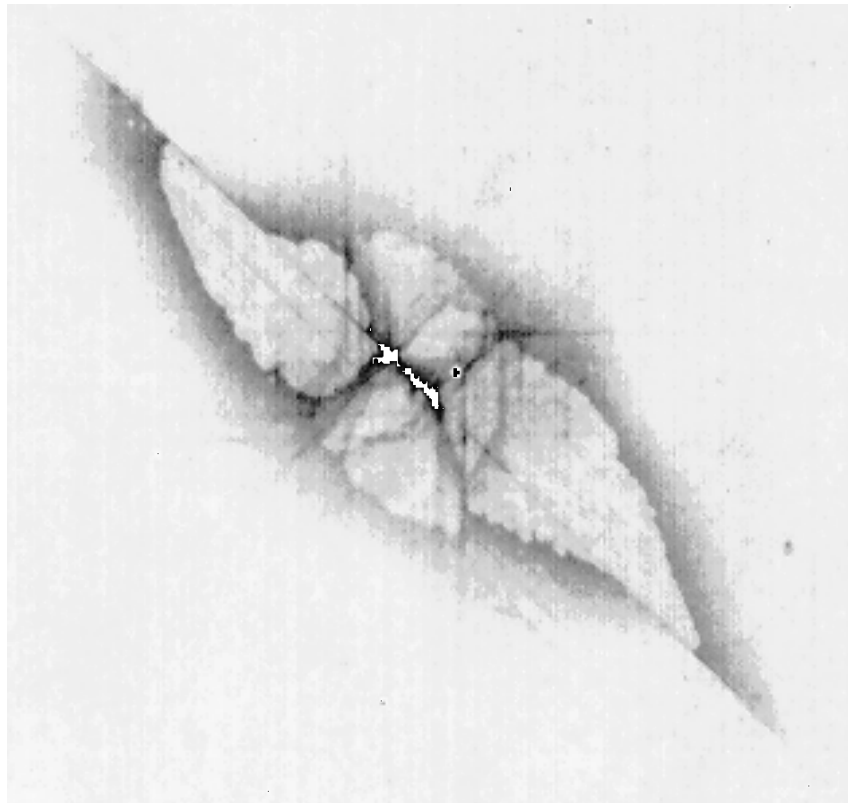
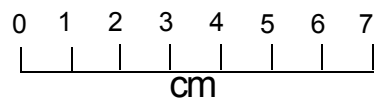
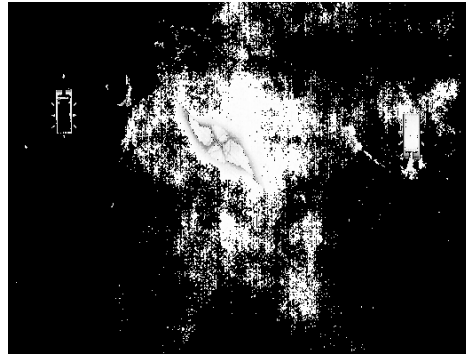
Specimen 12/14E



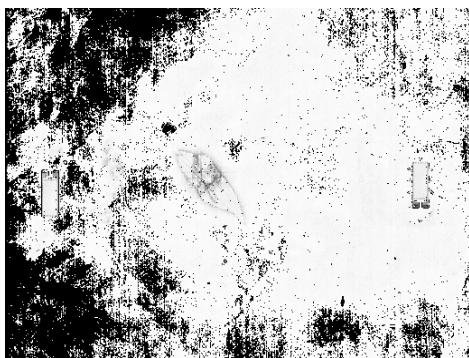
Specimen # 12/17A



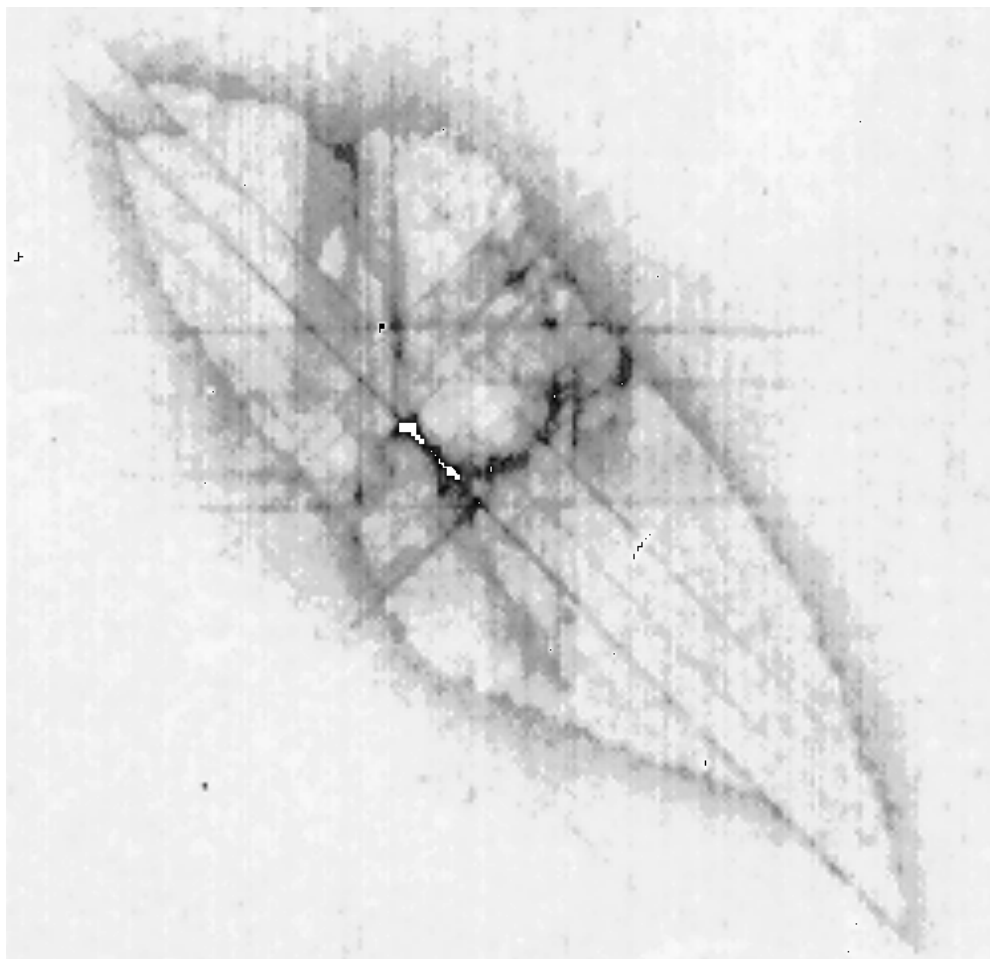
Specimen # 12/17B



Specimen # 12/17C

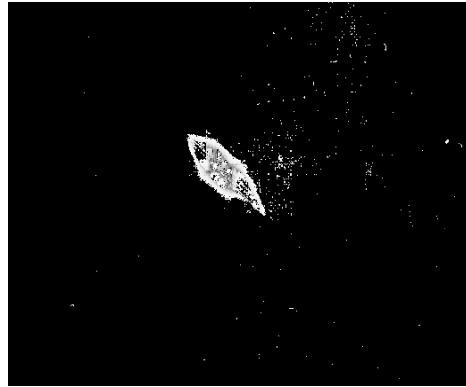


0 1 2 3 4 5 6 7
cm

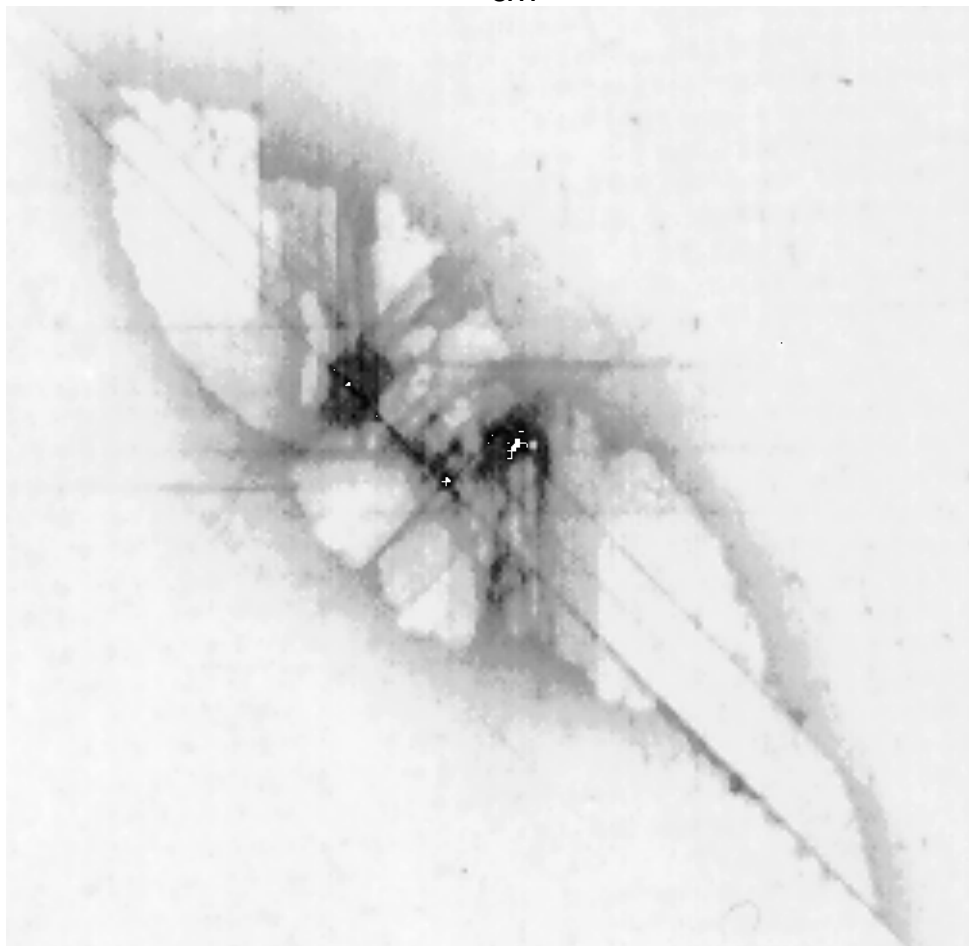


0 5 10 15
mm

Specimen # 12/13B

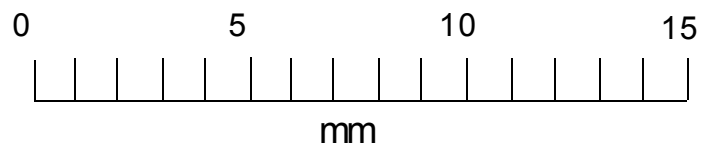
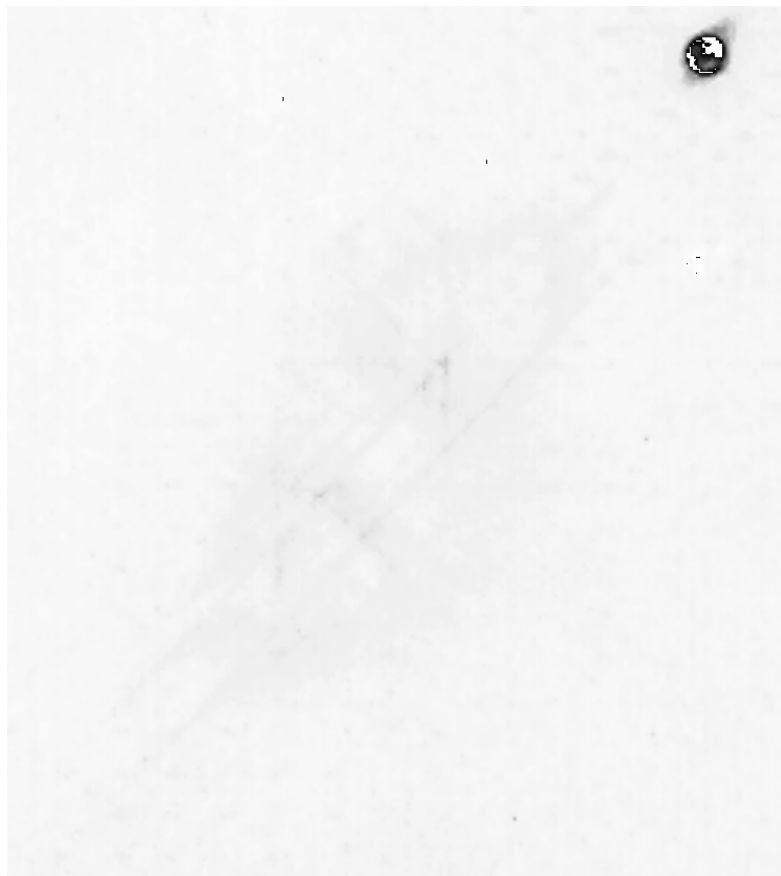
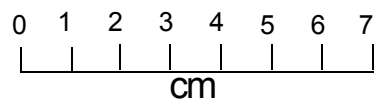


0 1 2 3 4 5 6 7
cm



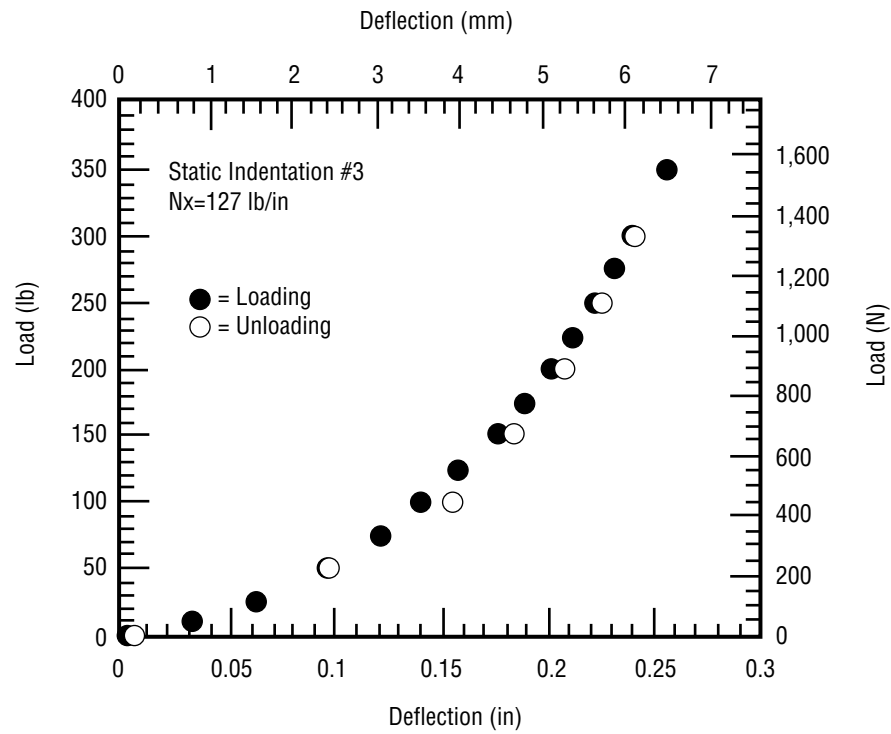
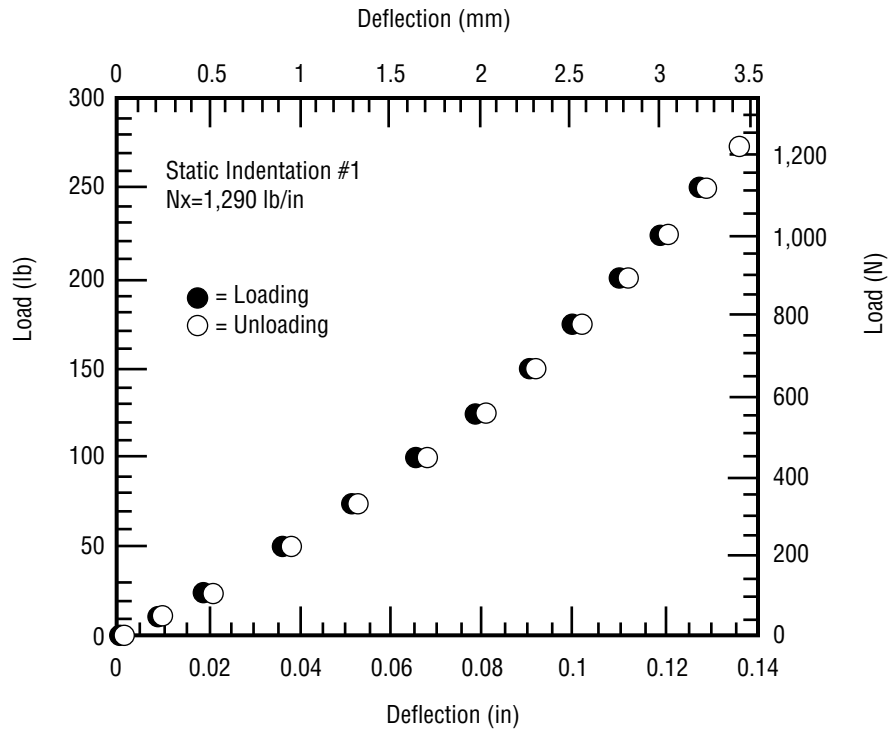
0 5 10 15
mm

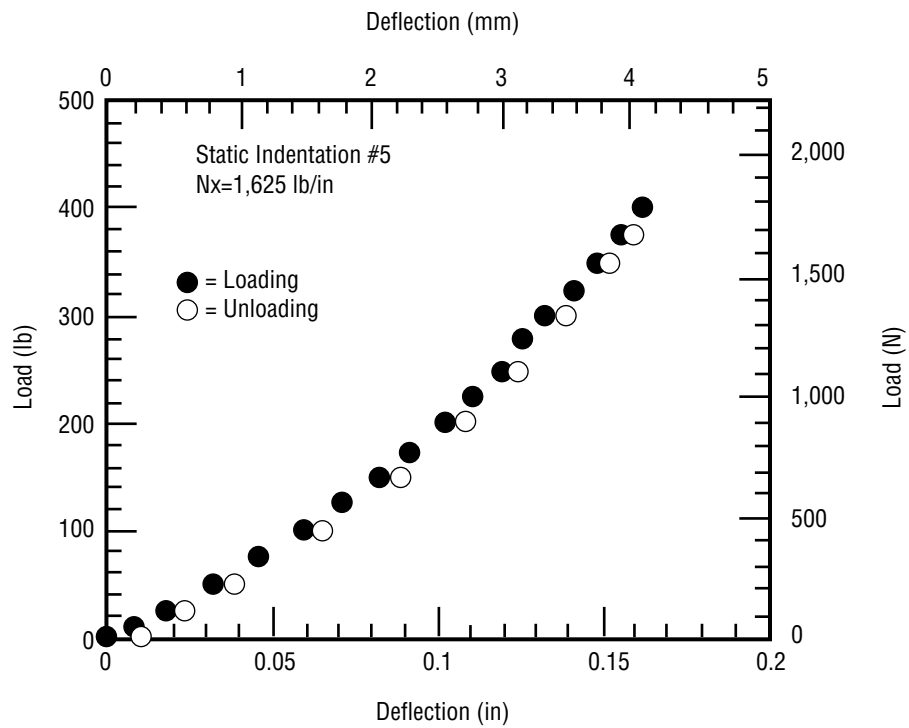
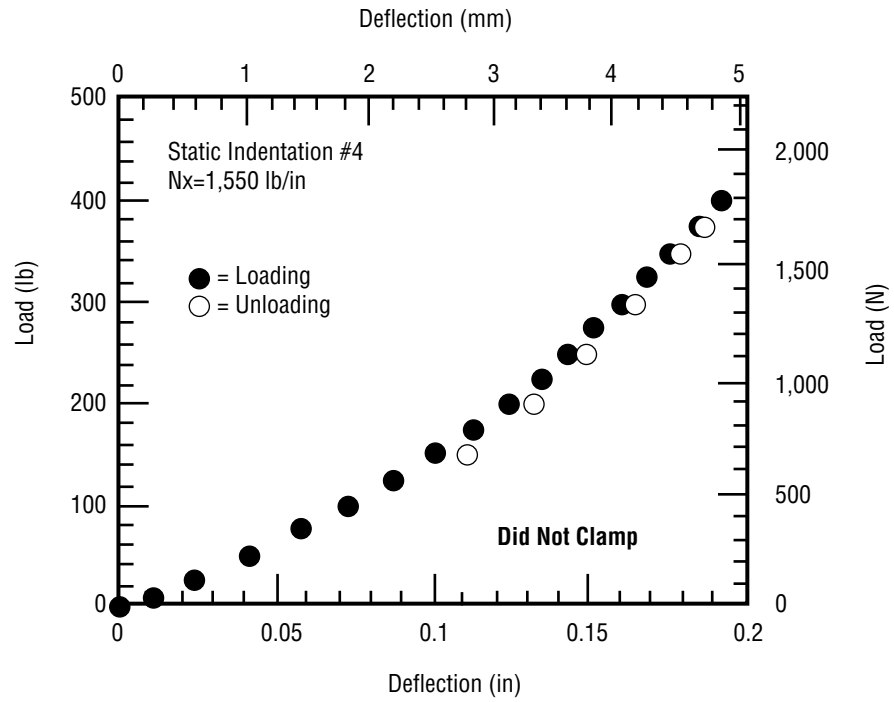
Specimen # 12/13A

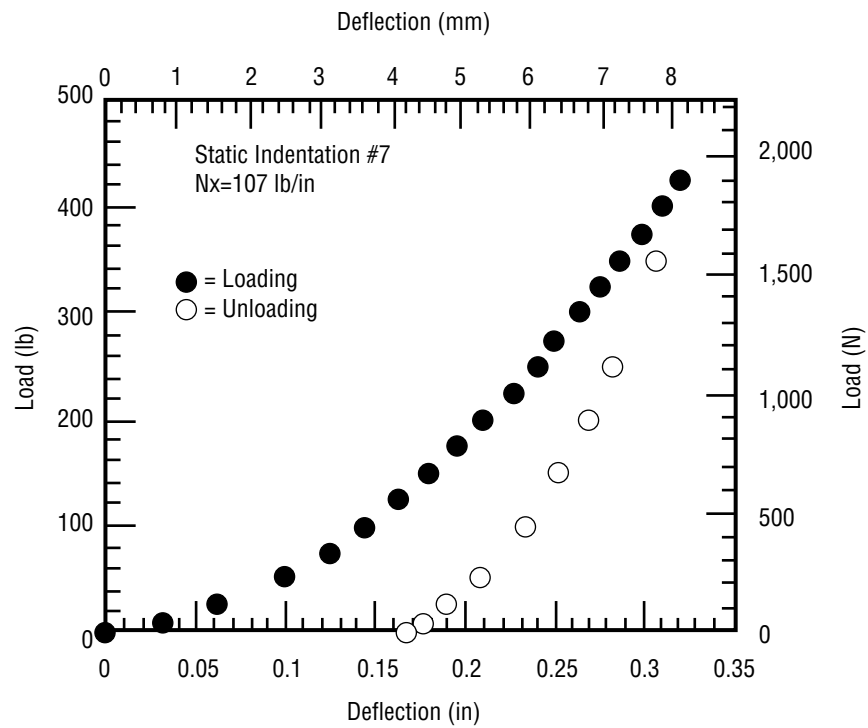
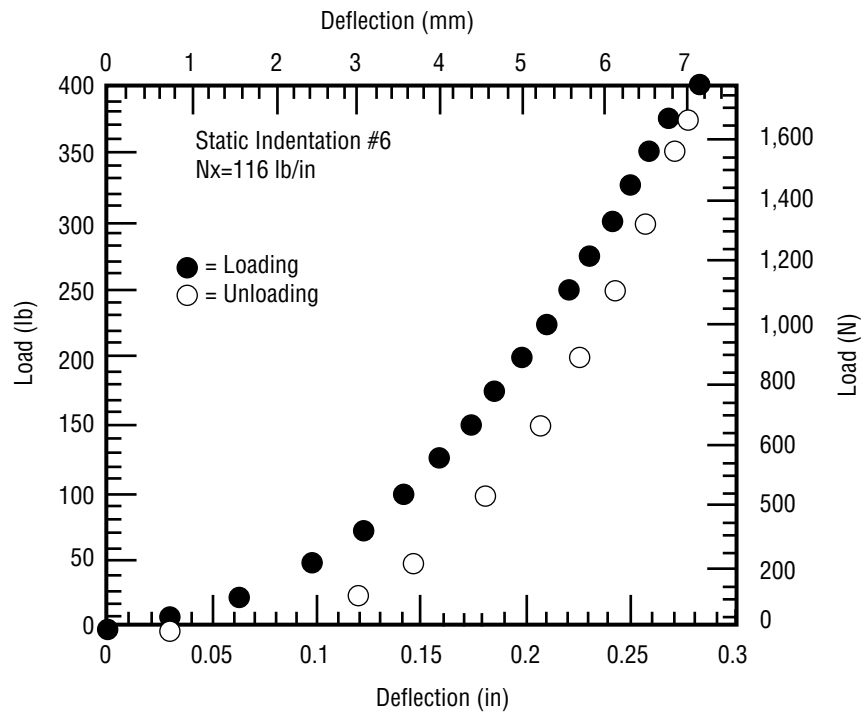


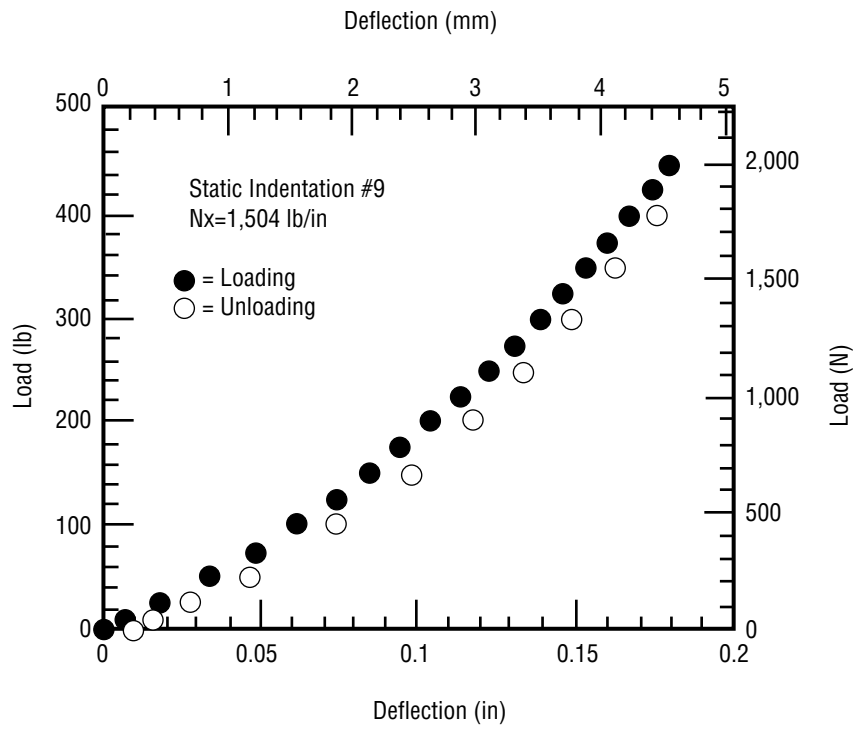
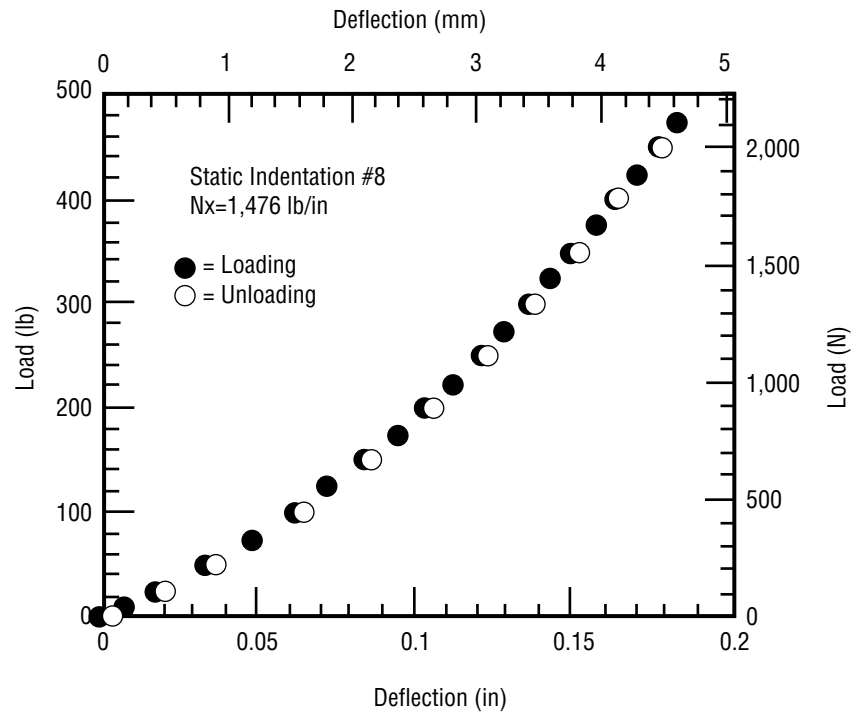
Specimen # 12/17D

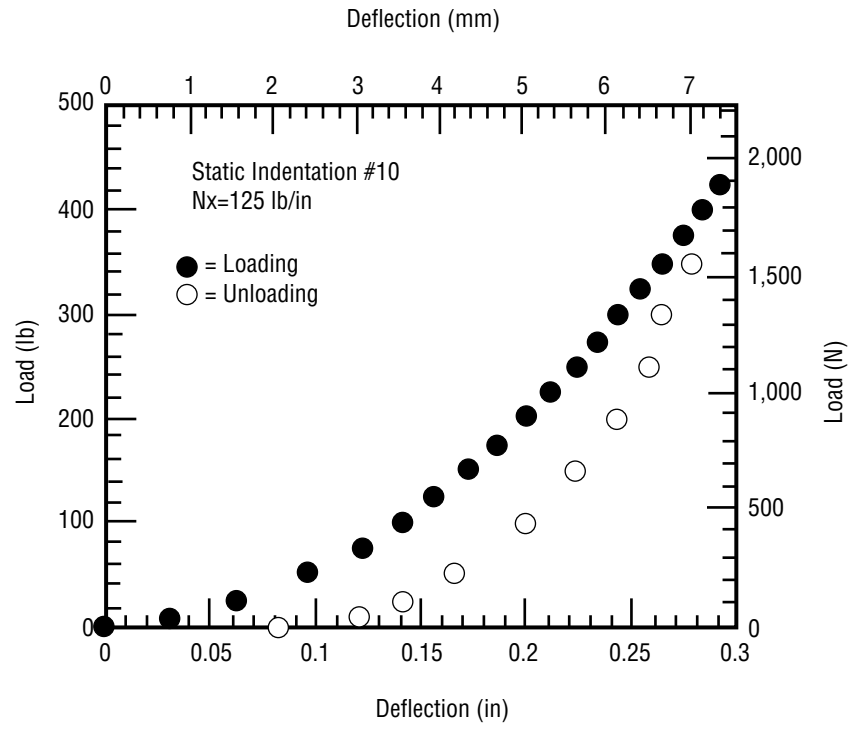
APPENDIX C—LOAD-DISPLACEMENT CURVES FROM STATIC INDENTATION TESTS



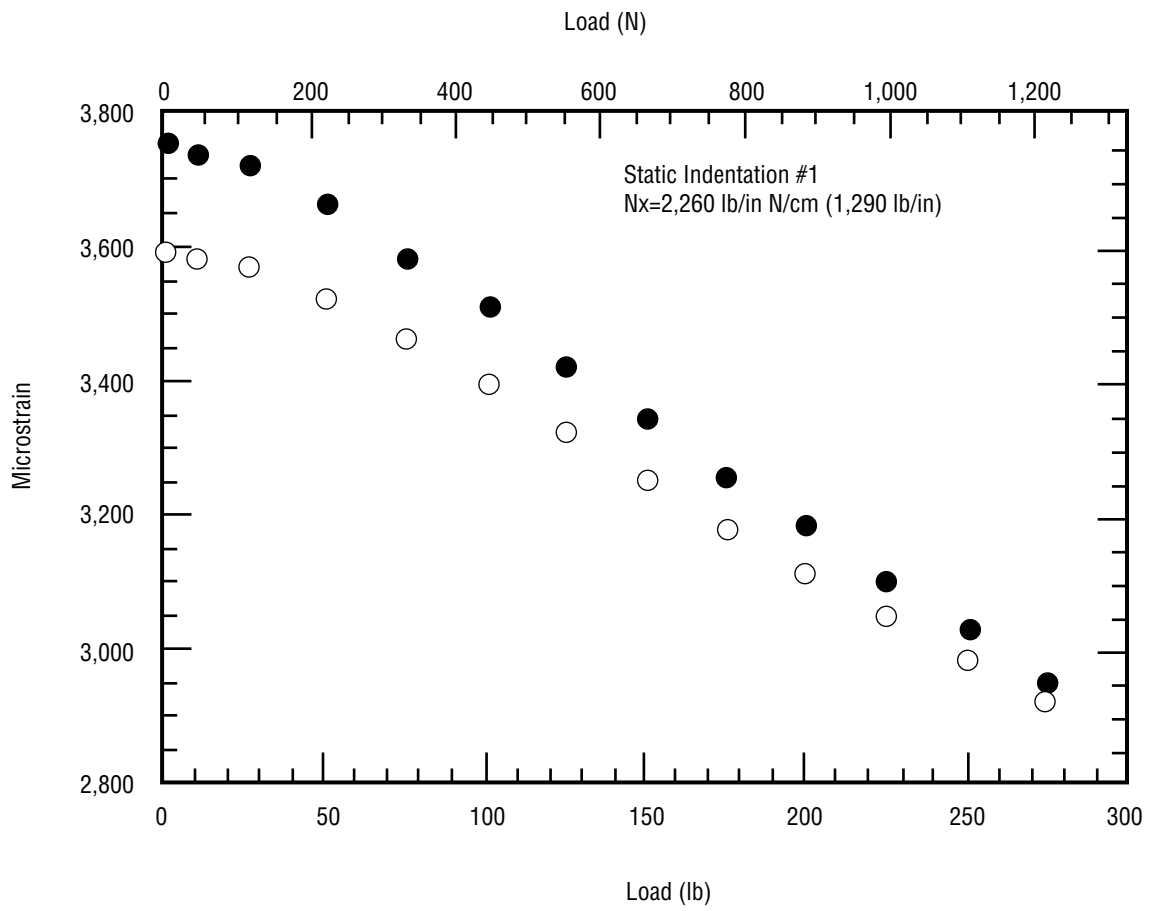
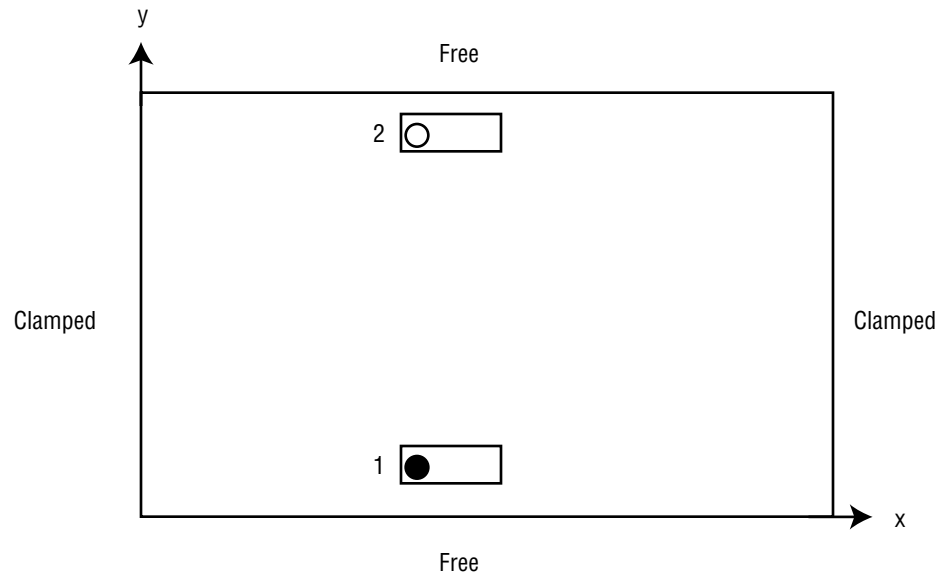


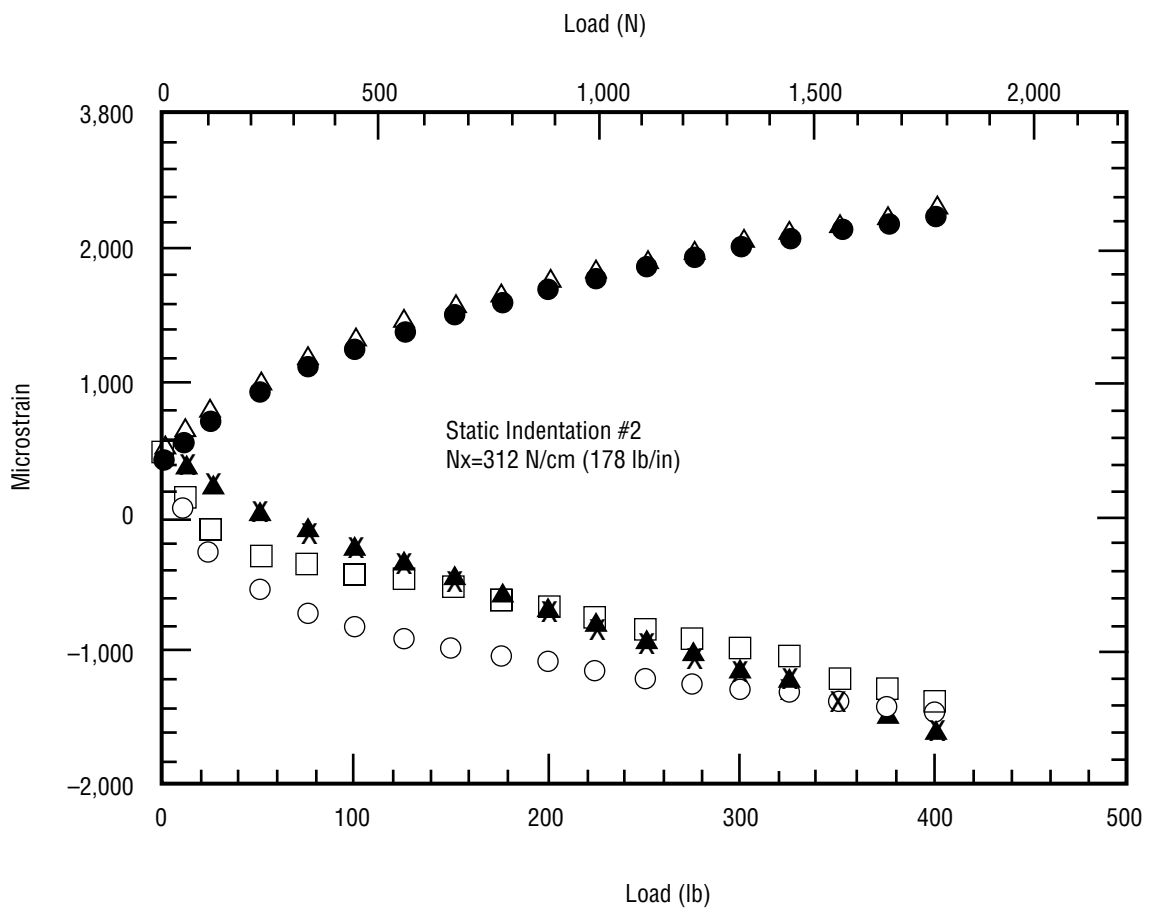
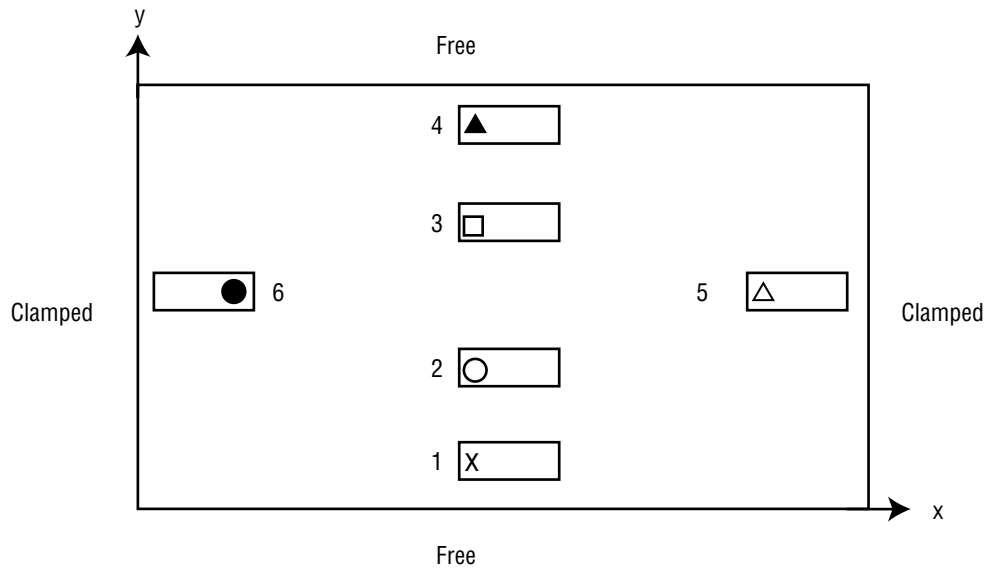


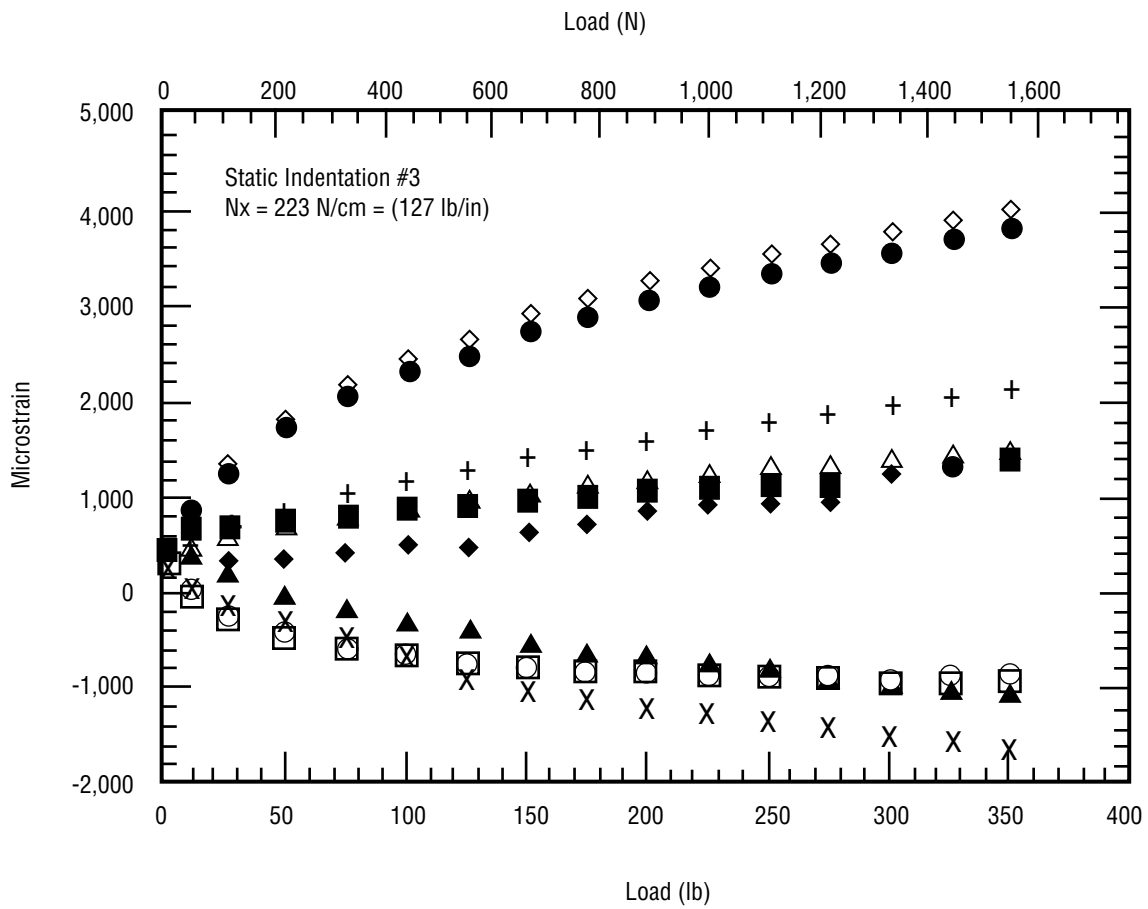
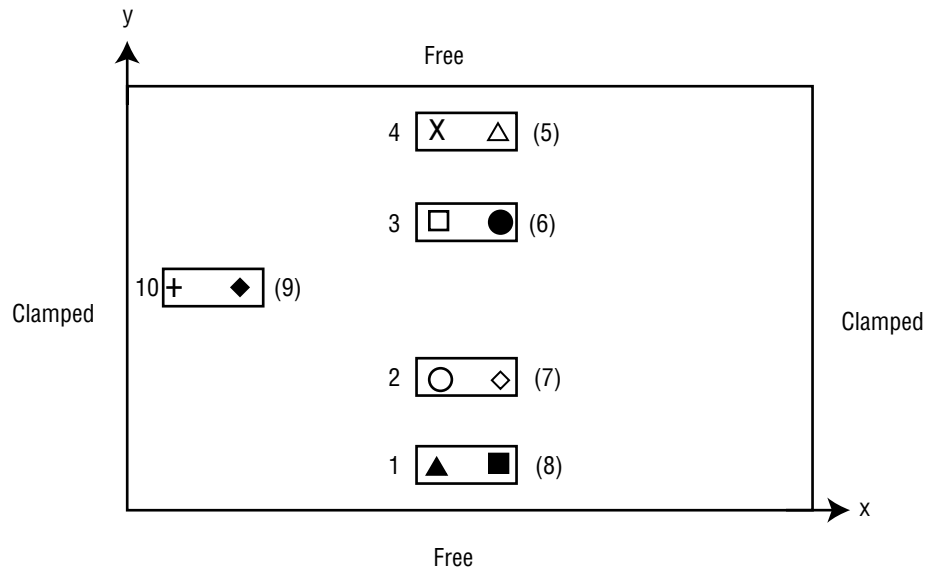


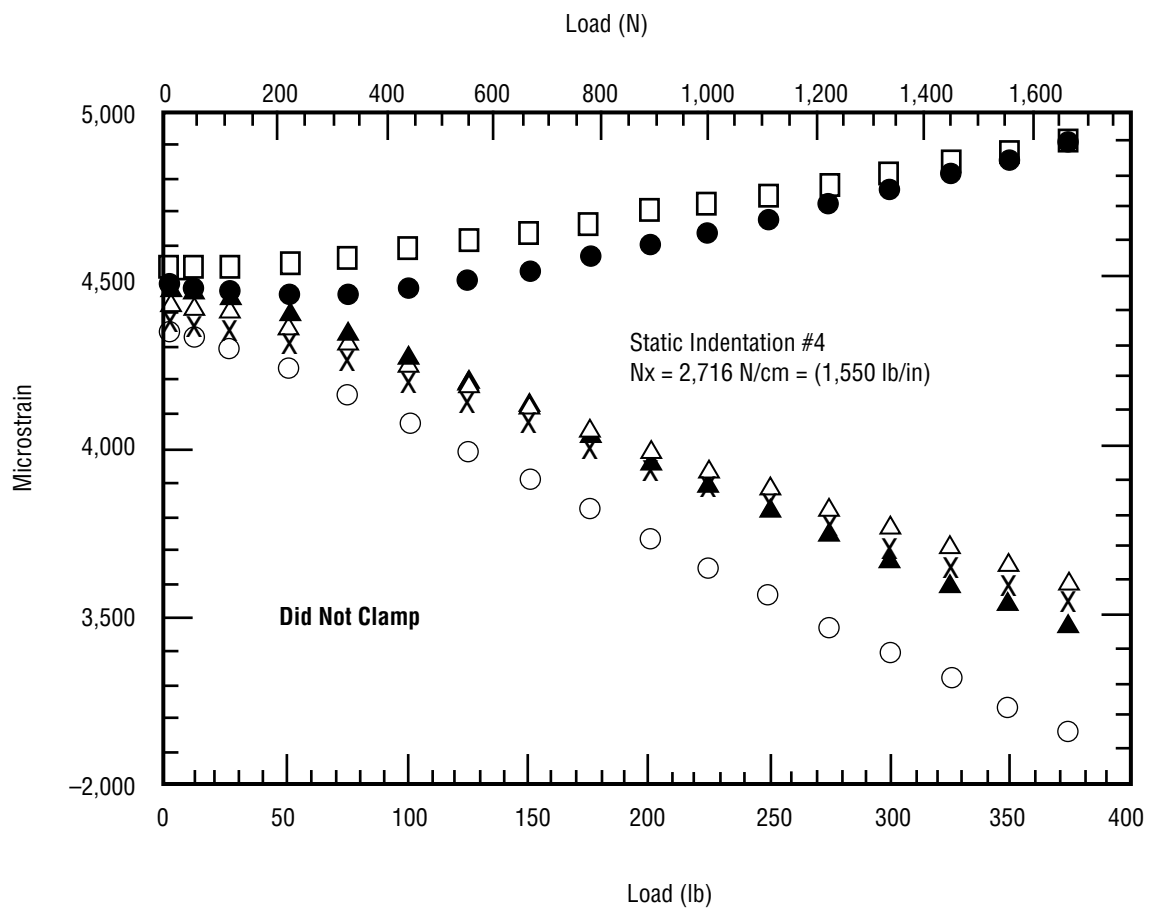
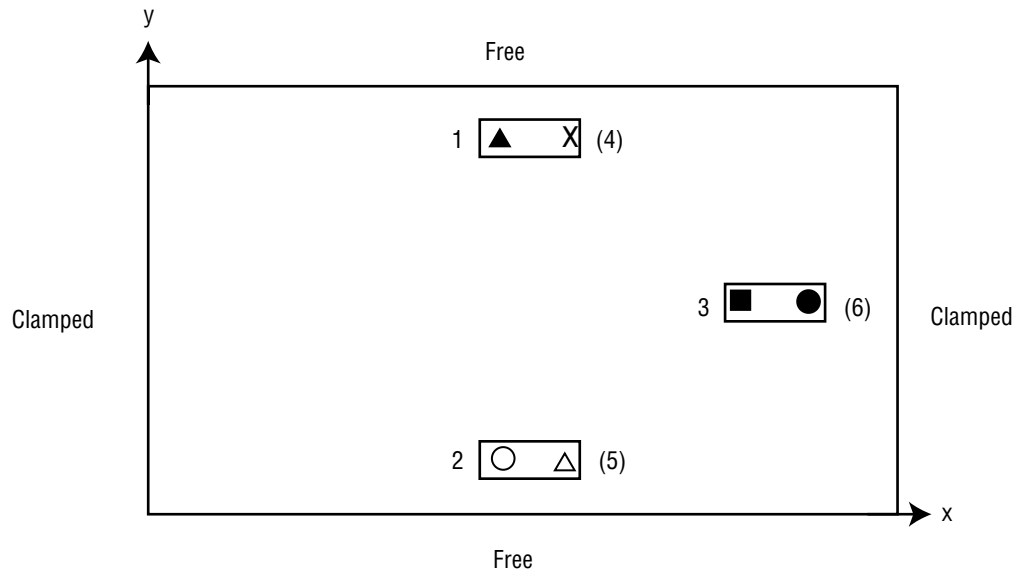


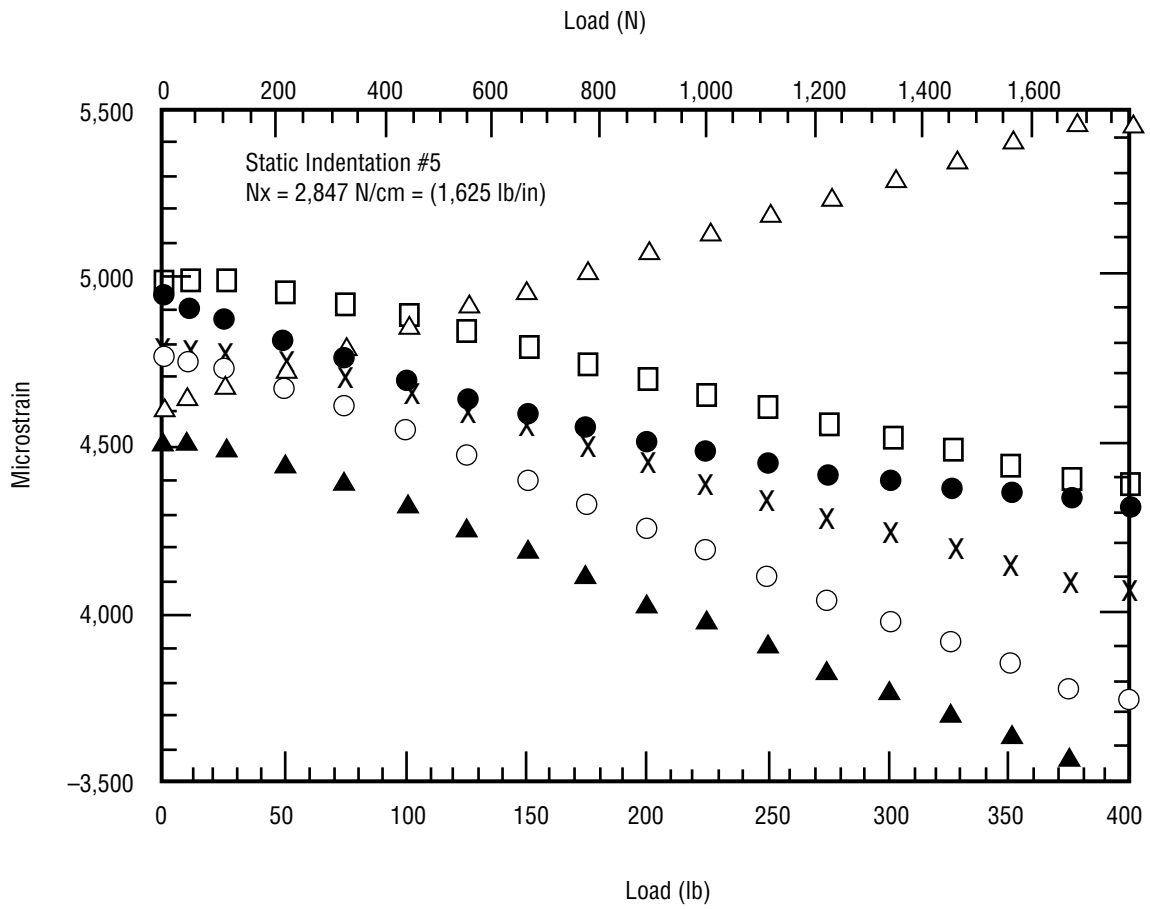
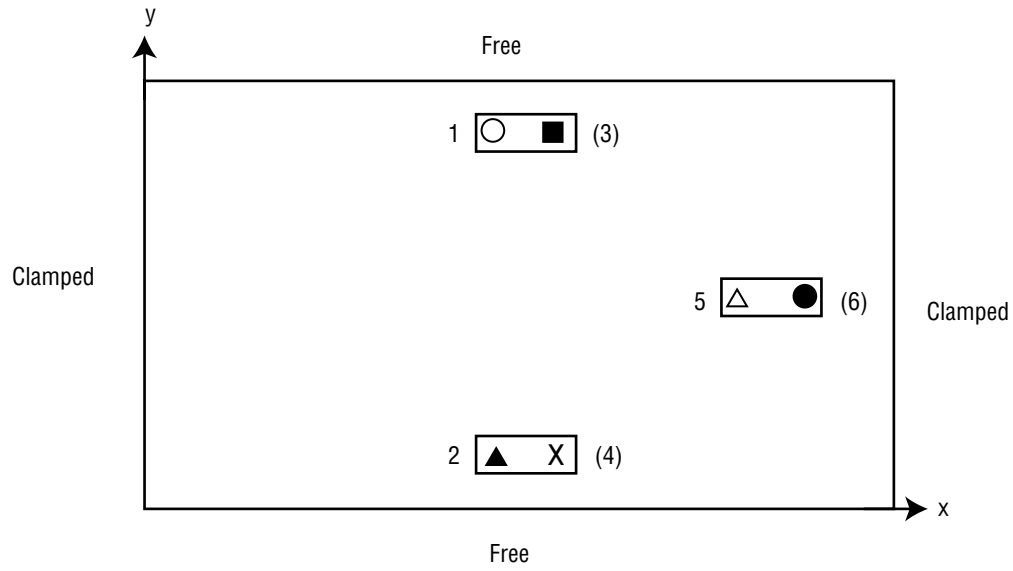
APPENDIX D—STRAIN GAUGE READINGS FROM STATIC INDENTATION TESTS

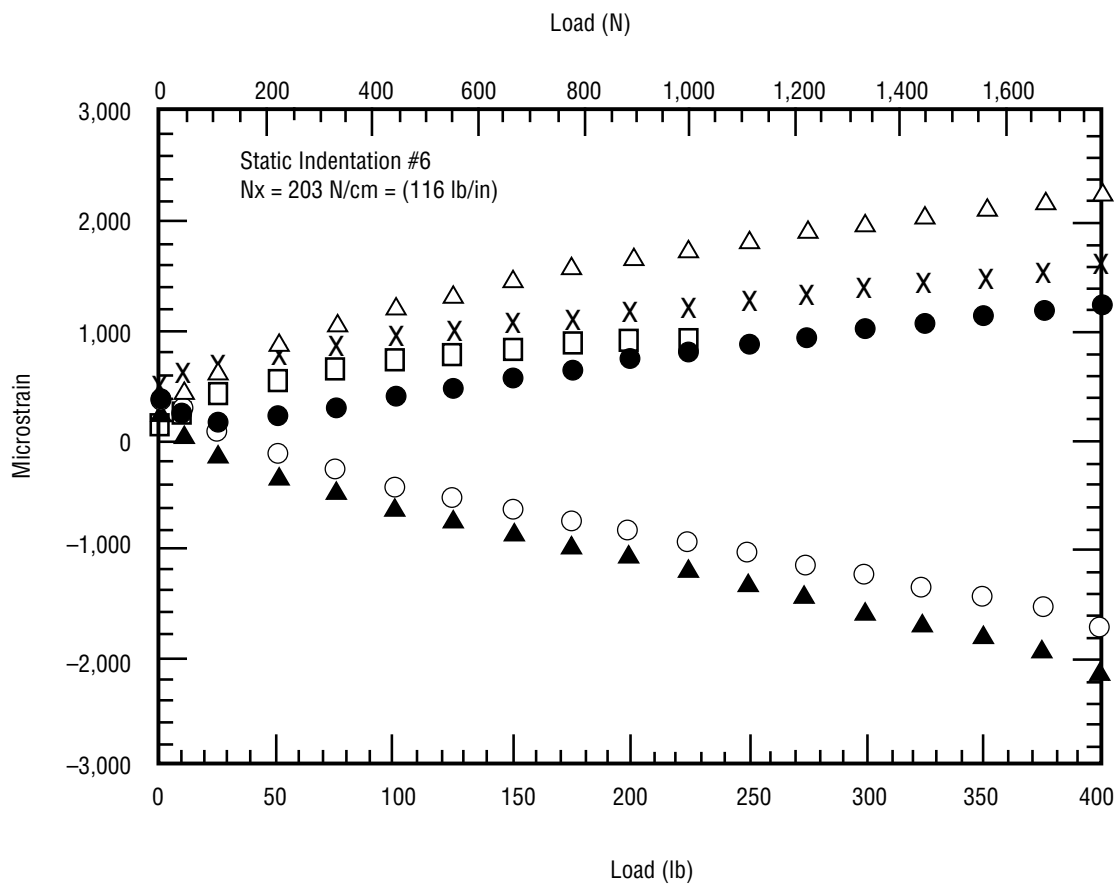
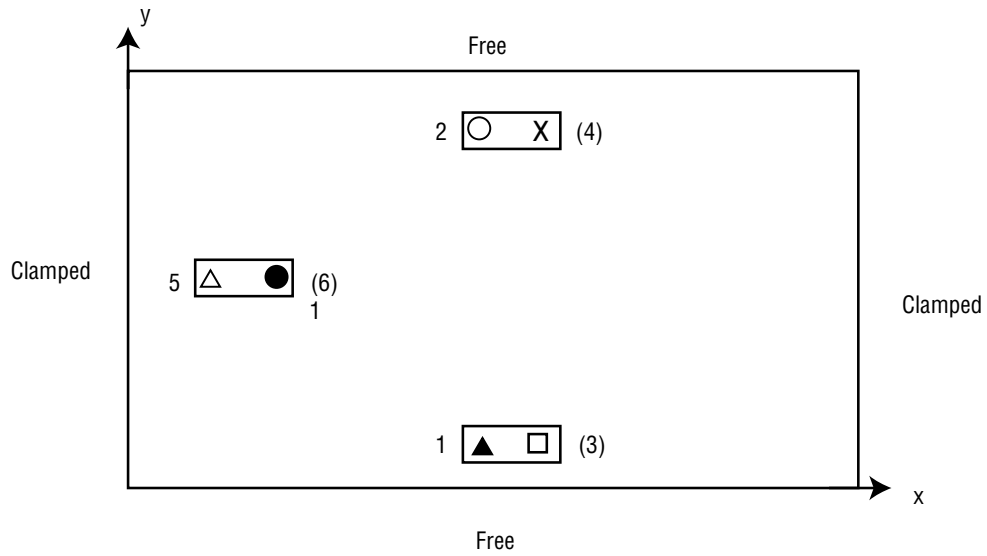


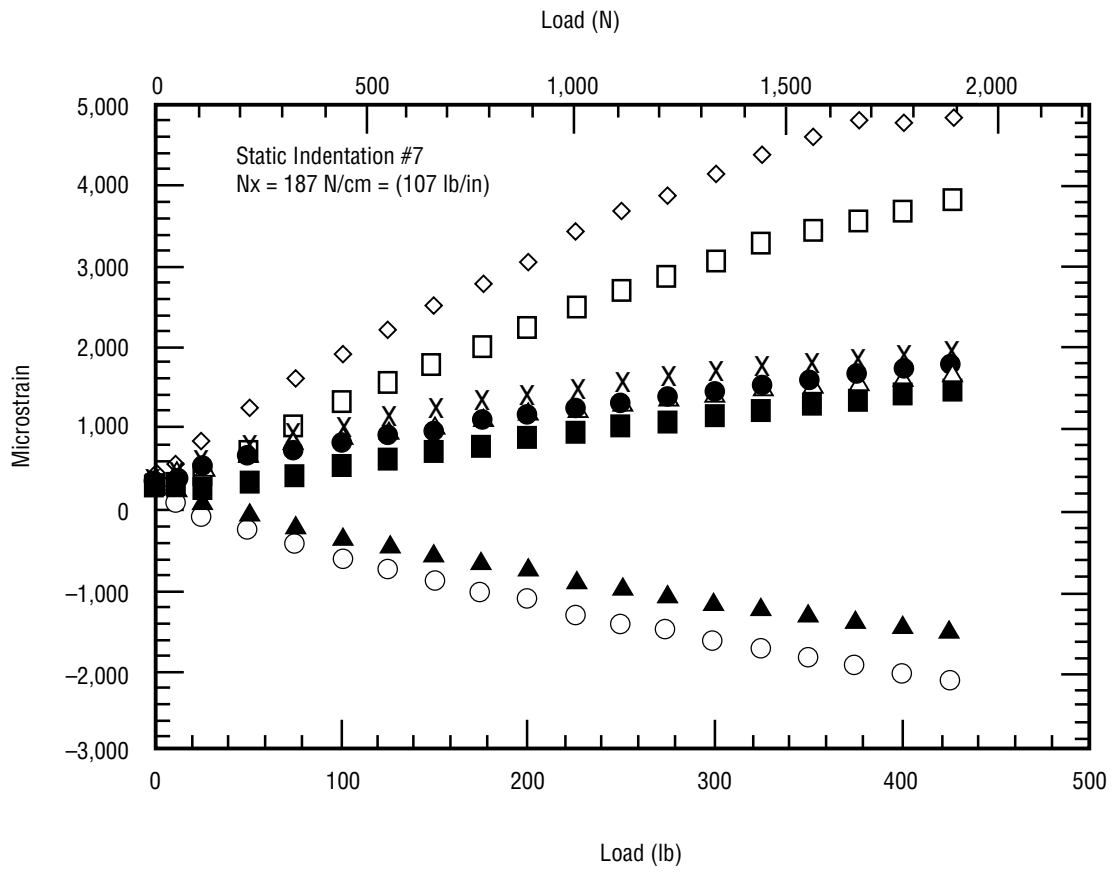
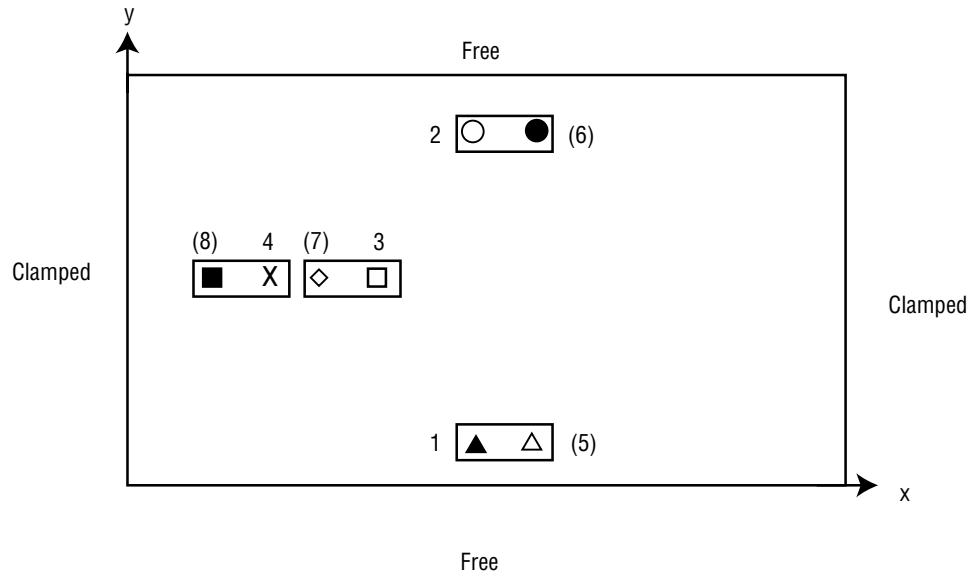


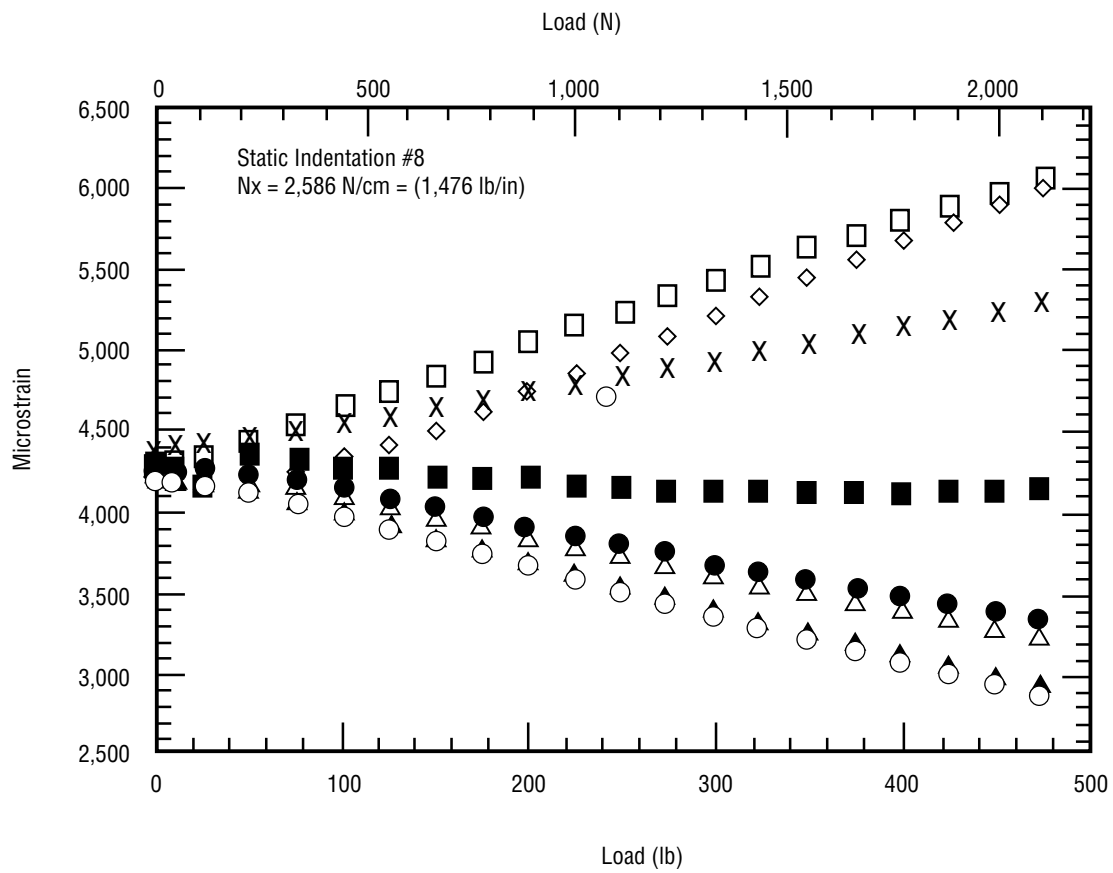
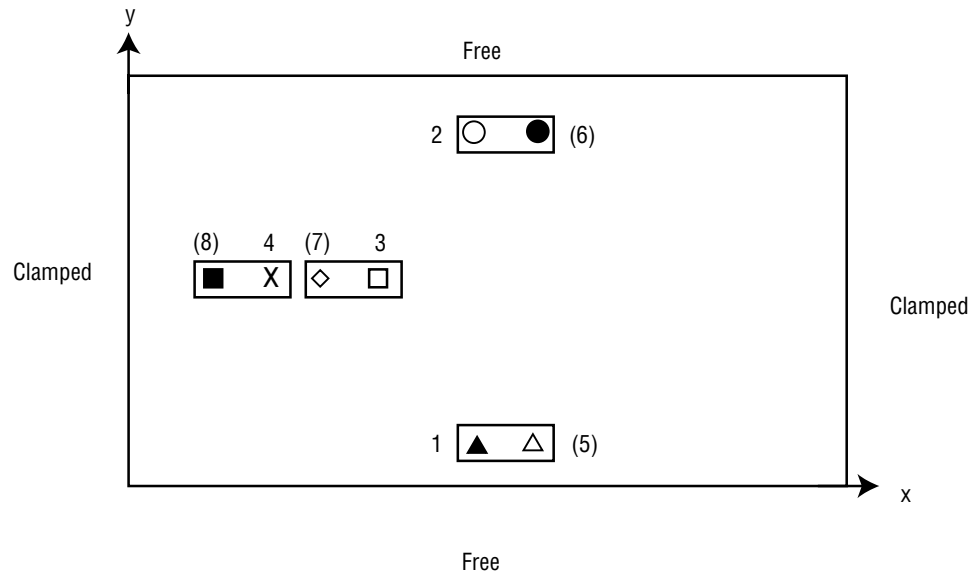


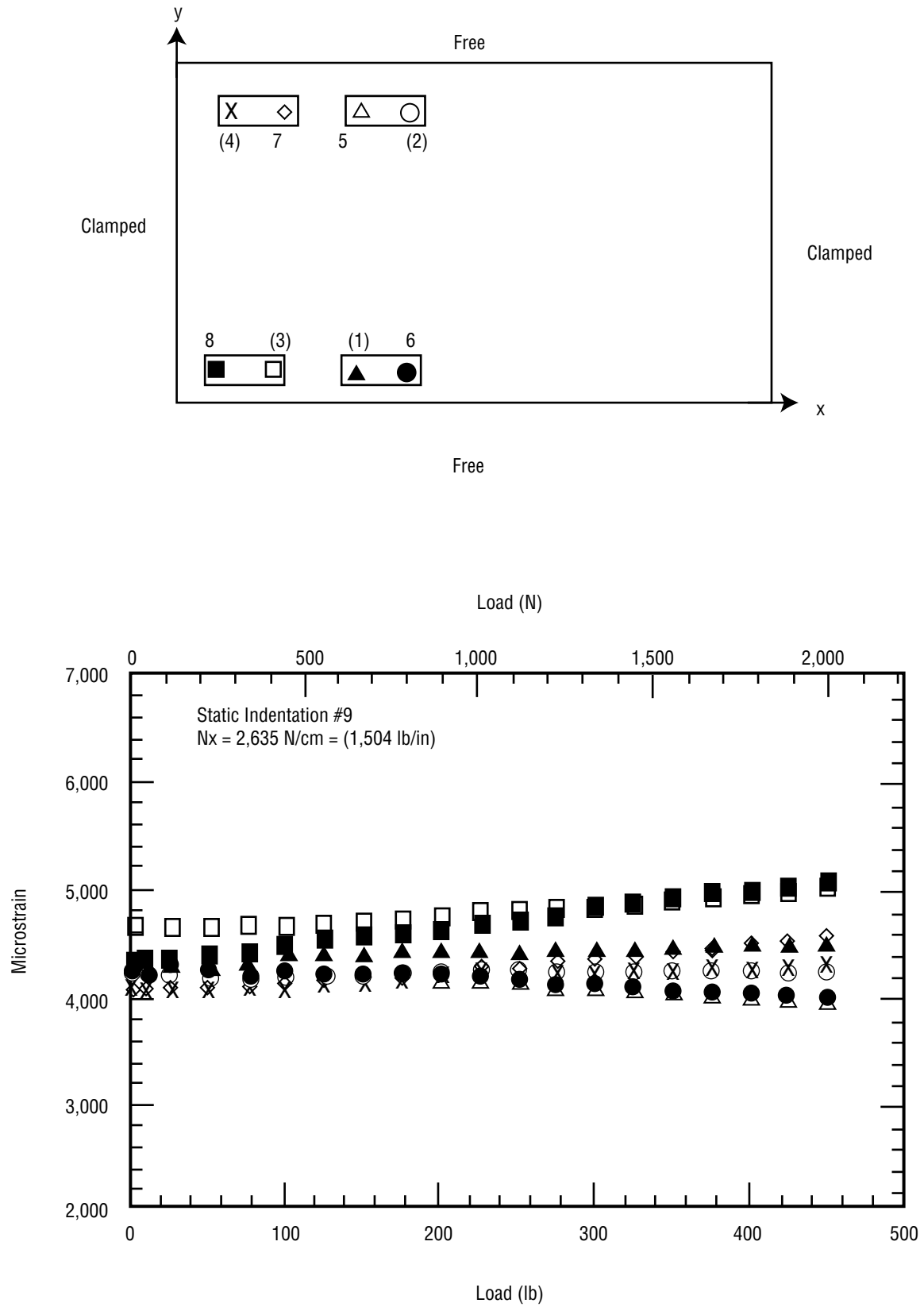


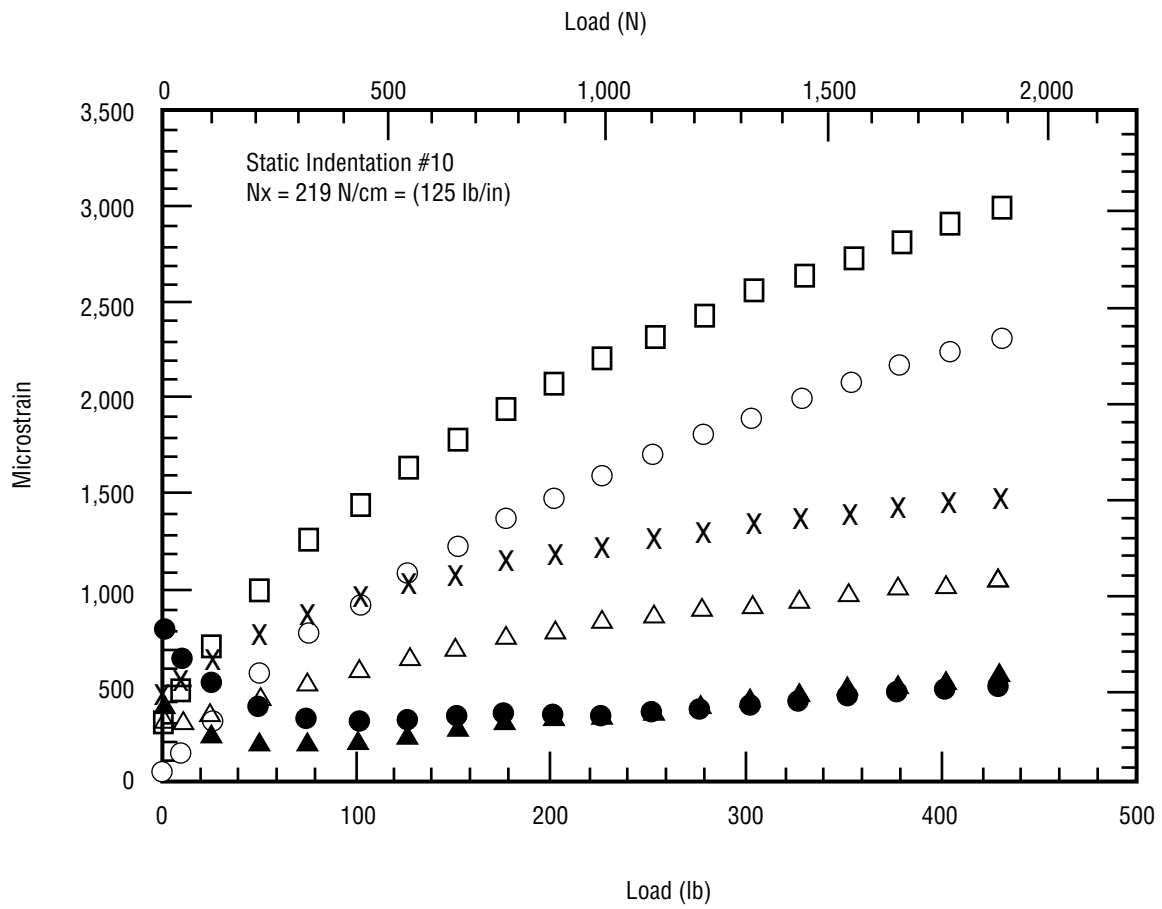
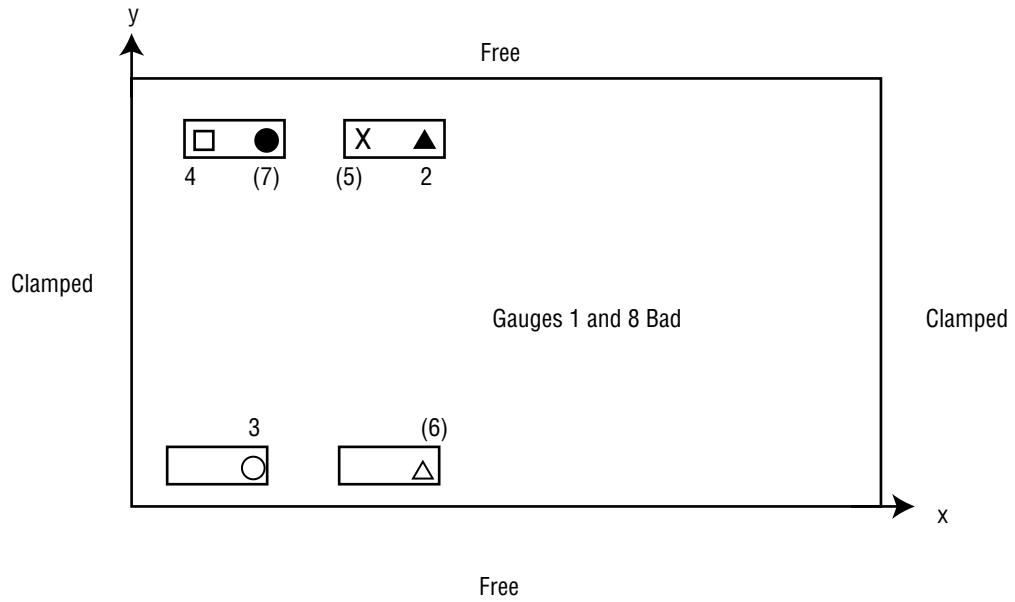












REFERENCES

1. Johnson, W.: Oak Targets and Navel Gunnery in the Early 19th Century,” *Proceedings of International Symposium on Composite Materials and Structures*, Beijing, China, pp. 667–675, June 10–13, 1986.
2. Paul, B; and Zaid, M.: “Penetration of a Thin Plate,” *Journal of the Franklin Institute*, Vol. 265, No. 4, pp. 317–335, 1948.
3. Gupta, B.P.; and Davids, N.: “Penetration Experiments With Fiberglass-Reinforced Plastics,” *Experimental Mechanics*, pp. 445–450, September 1966.
4. Chamis, C.C.; Hanson, M.P.; and Serafini, T.T.: “Impact Resistance of Unidirectional Fiber Composites,” *Composite Materials: Testing and Design (Second Conference)*, *ASTM STP 497*, pp. 324–349, 1972.
5. Novak, R.C.; and DeCrescente, M.A.: “Impact Behavior of Unidirectional Resin Matrix Composites Tested in the Fiber Direction,” *Composite Materials: Testing and Design (Second Conference)*, *ASTM STP 497*, pp. 311–323, 1972.
6. Cotterell, B.: “Fracture Toughness and the Charpy V-Notch Impact Test,” *British Welding Journal*, pp. 83–89, February 1962.
7. Toland, R.H.: “Instrumented Impact Testing of Composite Materials,” *Instrumented Impact Testing*, *ASTM STP 563*, pp. 133–145, 1974.
8. Phillips, D.C.; and Tetelman, A.S.: “The Fracture Toughness of Fibre Composites,” *Composites*, Vol. 3, pp. 216–223, September 1972.
9. Oplinger, D.W.; and Slepetz, J.M.: “Impact Damage Tolerance of Graphite/Epoxy Sandwich Panels,” *Foreign Object Impact Damage to Composites*, *ASTM STP 568*, pp. 30–48, 1975.
10. *Foreign Object Impact Damage to Composites*, *ASTM STP 568*, American Society for Testing and Materials, Philadelphia, PA, 1975.
11. Preston, J.L.; Jr., and Cook, T.S., “Impact Response of Graphite-Epoxy Flat Laminates Using Projectiles That Simulate Aircraft Engine Encounters,” *Foreign Object Impact Damage to Composites*, *ASTM STP 568*, pp. 49–71, 1975.
12. Husman, G.E.; Whitney, J.M.; and Halpin, J.C.: “Residual Strength Characterization of Laminated Composites Subjected to Impact Loading,” *Foreign Object Impact Damage to Composites*, *ASTM STP 568*, pp. 92–113, 1975.

13. Moon, F.C.; “Wave Surfaces Due to Impact of Anisotropic Plates,” *Journal of Composite Materials*, Vol. 6, pp. 306–319, 1972.
14. Mortimer, R.W.; Chou, P.C.; and Carleone, J.: “Behavior of Laminated Composite Plates Subjected to Impact,” Foreign Object Impact Damage to Composites, *ASTM STP 568*, pp. 173–182, 1975.
15. Sun, C.T.; Achenbach, J.D.; and Herrmann, G.; “Continuum Theory for a Laminated Medium,” *Journal of Applied Mechanics*, pp. 467–475, September 1968.
16. Greszczuk, L.B.: “Response of Isotropic and Composite Materials to Particle Impact,” Foreign Object Impact Damage to Composites, *ASTM STP 568*, pp. 183–211, 1975.
17. Pintado, P.; Vogler, T.J.; and Morton, J.: “Impact Damage Development in Thick Composite Laminates,” *Composites Engineering*, Vol. 1, No. 4, pp. 195–210, 1991.
18. Kaczmarek, H.; and Maison, S.: “Comparative Ultrasonic Analysis of Damage in CFRP Under Static Indentation and Low-Velocity Impact,” *Composites Science and Technology*, Vol. 51, pp. 11–26, 1994.
19. Madsen, C.B.; Morgan, M.E.; and Nuismer, R.J.: “Scaling Impact Response and Damage in Composites. Damage Assessment for Composite Cases,” *Aeronautical Laboratories—Technical Report 90–037*, 1990.
20. Swanson, S.R.: “Limits of Quasi-Static Solutions in Impact of Composite Structures,” *Composites Engineering*, Vol. 2, No. 4, pp. 261–267, 1992.
21. Highsmith, A.L.: “A Study of the Use of Contact Loading to Simulate Low Velocity Impact,” *Final Report, NASA Grant No. NASA NCC8–23*, 1993.
22. Jackson, W.C.; and Poe, C.C., Jr.: “The Use of Impact Force as a Scale Parameter for the Impact Response of Composite Laminates,” *Journal of Composites Technology and Research*, Vol. 15, No. 4, pp. 282–289, Winter 1993.
23. Joshi, S.P.; and Sun, C.T.: “Impact Induced Fracture in a Laminated Composite,” *Journal of Composite Materials*, Vol. 19, pp. 51–66, January 1985.
24. Srinivasan, K.; Jackson, W.C.; Smith, B.T.; and Hinkley, J.A.: “Characterization of Damage Modes in Impacted Thermoset and Thermoplastic Composites,” *Journal of Reinforced Plastics and Composites*, Vol. 11, pp. 1111–1126, October 1992.

25. Salpekar, S.A.: "Analysis of Delamination in Cross-Ply Laminates Initiating from Impact Induced Matrix Cracking," *Journal of Composites Technology and Research*, Vol. 15, No. 2, pp. 88–94, 1993.
26. Cantwell, W.J.; and Morton, J.: "Detection of Impact Damage in CFRP Laminates." *Composite Structures*, Vol. 3, pp. 241–257, 1985.
27. Kwon, Y.S.; and Sankar, B.V.: "Indentation-Flexure and Low-Velocity Impact Damage in Graphite Epoxy Laminates," *Journal of Composites Technology and Research*, Vol. 15, No. 2, pp. 101–111, 1993.
28. Dost, E.F.; Avery, W.B.; Ilcewicz, L.B.; Grande, D.H.; and Coxon, B.R.: "Impact Damage Resistance of Composite Fuselage Structure, Part I," *Proceedings of the Ninth DoD/NASA/FAA Conference on Fibrous Composites in Structural Design*, pp. 1037–1069, 1991.
29. Hull, D.; and Shi, Y.B.: "Damage Mechanism Characterization in Composite Damage Tolerance Investigations," *Composite Structures*, Vol. 23, pp. 99–120, 1993.
30. Choi, H.Y.; Downs, R.J.; and Chang, F.K.: "A New Approach Toward Understanding Damage Mechanisms and Mechanics of Laminated Composites Due to Low-Velocity Impact: Part I—Experiments," *Journal of Composite Materials*, Vol. 25, pp. 992–1011, August 1991.
31. Choi, H.Y.; Wu, H.Y.T.; and Chang, F.K.: "A New Approach Toward Understanding Damage Mechanisms and Mechanics of Laminated Composites Due to Low-Velocity Impact: Part II—Analysis," *Journal of Composite Materials*, Vol. 25, pp. 1012–1038, August 1991.
32. Lammerant, L.; and Verpoest, I.: "The Interaction Between Matrix Cracks and Delaminations During Quasi-Static Impact of Composites," *Composites Science and Technology*, Vol. 51, pp. 505–516, 1994.
33. Doucet, A.B.; and Qin, J.: "Microstructural Analysis of Impact Damage in Two Glass/Epoxy Composite Laminates," *Composites Engineering*, Vol. 3, No. 1, pp. 55–68, 1993.
34. Liu, D.; and Malvern, L.E.: "Matrix Cracking in Impacted Glass/Epoxy Plates," *Journal of Composite Materials*, Vol. 21, pp. 594–609, July 1987.
35. Liu, D.: "Impact-Induced Delamination—A View of Bending Stiffness Mismatching," *Journal of Composite Materials*, Vol. 22, pp. 674–692, July 1988.
36. Kumar, P.; and Rai, B.: "Reduction of Impact Damage in KFRP through Replacement of Surface Plies with Glass Fabric Plies," *Journal of Composite Materials*, Vol. 25, pp. 694–702, June 1991.

37. Clarke, M.P.; and Pavier, M.J.: "Artificial Damage Techniques for Low Velocity Impact in Carbon Fibre Composites," *Composite Structures*, Vol. 25, pp. 113–120, 1993.
38. Hitchen, S.A.; and Kemp, R.M.: "The Effect of Stacking Sequence on Impact Damage in a Carbon Fiber/Epoxy Composite," *Composites*, Vol. 26, No. 3, pp. 207–214, 1995.
39. Choi, H.Y.; and Chang, F.K.: "A Model for Predicting Damage in Graphite/Epoxy Laminated Composites Resulting from Low-Velocity Point Impact," *Journal of Composite Materials*, Vol. 26, No. 14, pp. 2134–2169, 1992.
40. Cantwell, W.J., "The Influence of Target Geometry on the High Velocity Impact Response of CFRP," *Composite Structures*, Vol. 10, pp. 247–265, 1988.
41. Wyrick, D.A.; and Adams, D.F.: "Damage Sustained by a Carbon/Epoxy Composite Material Subjected to Repeated Impact," *Composites*, Vol. 19, No. 1, pp. 19–27, January 1988.
42. Wang, H.; and Vu-Khanh, T.: "Damage Extension in Carbon Fiber/PEEK Crossply Laminates Under Low Velocity Impact," *Journal of Composite Materials*, Vol. 28, No. 8, pp. 684–707, 1994.
43. Elber, W., "Failure Mechanics in Low-Velocity Impacts on Thin Composite Plates," *NASA Technical Paper 2152*, 1983.
44. Dorey, G.: "Impact and Crashworthiness of Composite Structures." Structural Impact and Crashworthiness, Vol. 1, J. Morton, ed., Elsevier Applied Science Publishers, London and New York, 1984.
45. Cantwell, W.; Curtis, P.; and Morton, J., "Post-Impact Fatigue Performance of Carbon Fibre Laminates With Non-Woven and Mixed-Woven Layers," *Composites*, Vol. 14, No. 3, pp. 301–305, July 1983.
46. Avery, W.B.; and Grande, D.H.: "Influence of Materials and Lay-up Parameters on Impact Damage Mechanisms," *Proceedings of the 22nd International SAMPE Technical Conference*, pp. 470–483, November 1990.
47. Choi, H.Y.; Wang, H.S.; and Chang, F.K.: "Effect of Laminate Configuration and Impactor's Mass on the Initial Impact Damage of Graphite/Epoxy Composite Plates Due to Line-Loading Impact," *Journal of Composite Materials*, Vol. 26, No. 6, pp. 804–827, 1992.
48. Finn, S.R.; He, Y.F.; Springer, G.S.; and Lee, H.J.: "Compressive Strength of Damaged and Repaired Composite Plates," *Journal of Composite Materials*, Vol. 26, No. 12, pp. 1796–1825, 1992.

49. Kim, C.G.; and Jun, E.J.: "Impact Resistance of Composite Laminated Sandwich Plates," *Journal of Composite Materials*, Vol. 26, No. 15, pp. 2247–2261, 1992.
50. Rhodes, M.D.: Impact Tests on Fibrous Composite Sandwich Structures," *NASA Technical Memorandum 78719*, 1978.
51. Avva, V.S.; Vala, J.R.; and Jeyaseelan, M.: "Effect of Impact and Fatigue Loads on the Strength of Graphite/Epoxy Composites," Composite Materials: Testing and Design (Seventh Conference), *ASTM STP 893*, pp. 196–206, 1986.
52. Jegley, D.: "Effect of Low-Speed Impact Damage and Damage Location on Behavior of Composite Panels," *Proceedings of the Ninth DoD/NASA/FAA Conference On Fibrous Composites In Structural Design*, pp. 1013–1036, November 1991.
53. Dow, M.B.; and Smith, D.L.: "Properties of Two Composite Materials Made of Toughened Epoxy Resin and High-Strain Graphite Fiber," *NASA Technical Paper 2826*, 1988.
54. Jenq, S.T.; Wang, S.B.; and Sheu, L.T.: "A Model for Predicting the Residual Strength of GFRP Laminates Subject to Ballistic Impact," *Journal of Reinforced Plastics and Composites*, Vol. 11, pp. 1127–1141, October 1992.
55. Cairns, D.S.: "Impact and Post-Impact Response of Graphite/Epoxy and Kevlar/Epoxy Structures," Ph.D. Dissertation, M.I.T., 1987.
56. Adsit, N.R.; and Waszczak, J.P.: "Effect of Near-Visual Damage on the Properties of Graphite/Epoxy," Composite Materials: Testing and Design (Fifth Conference), *ASTM STP 674*, pp. 101–117, 1979.
57. Dorey, G.: "Impact Damage in Composites—Development, Consequences and Prevention," *Proceedings of the Sixth International Conference on Composite Materials, Second European Conference on Composite Materials*, Vol. 3, pp. 3.1–3.26, 1986.
58. Cantwell, W.J.; Morton, J.; and Curtis, P.: "A Study of the Impact Resistance and Subsequent 0-Compression Fatigue Performance of Non-Woven and Mixed-Woven Composites," in *Structural Impact and Crashworthiness, Vol. 2 Conference Papers*, J. Morton Ed., Elsevier Applied Science Publishers, London and New York, pp. 521–531, 1985.
59. Dorey, G.; Bishop, S.M.; and Curtis, P.T.: "On the Impact Performance of Carbon Fiber Laminates with Epoxy and PEEK Matrices," *Composites Science and Technology*, Vol. 23, pp. 221–237, 1985.
60. Morton, J.; and Godwin, E.W.: "Impact Response of Tough Carbon Fibre Composites," *Composite Structures*, Vol. 13, pp. 1–19, 1989.

61. Caprino, G.: "Residual Strength Prediction of Impacted CFRP Laminates," *Journal of Composite Materials*, Vol. 18, pp. 508–518, November 1984.
62. Nettles, A.T.: "Instrumented Impact and Residual Tensile Strength Testing of Eight-Ply Carbon/Epoxy Specimens," *NASA Technical Paper 2981*, 1990.
63. Bishop, S.M.: "The Mechanical Performance and Impact Behavior of Carbon-Fibre Reinforced PEEK," *Composite Structures*, Vol. 3, pp. 295–318, 1985.
64. Lal, K.M.: "Residual Strength Assessment of Low Velocity Impact Damage of Graphite-Epoxy Laminates," *Journal of Reinforced Plastics and Composites*, Vol. 2, pp. 226–238, October 1983.
65. Poe, C.C., Jr.: "Summary of a Study to Determine Low-Velocity Impact Damage and Residual Tension Strength for a Thick Graphite/Epoxy Motor Case," *Proceedings of the 17th Congress of the International Council of the Aeronautical Sciences*, pp. 1005–1016, 1990.
66. Cantwell, W.J.; Curtis, P.T.; and Morton, J.: "An Assessment of the Impact Performance of CFRP Reinforced with High-Strain Carbon Fibers," *Composites Science and Technology*, Vol. 25, pp. 133–148, 1986.
67. Prichard, J.C.; and Hogg, P.J.: "The Role of Impact Damage in Post-Impact Compression Testing," *Composites*, Vol. 21, No. 6, pp. 503–511, November 1990.
68. Teh, K.T.; and Morton, J.: "Impact Damage Development and Residual Compression Performance of Advanced Composite Material Systems," *American Institute for Aeronautics and Astronautics Paper 93-1401-CP*, 1993.
69. Srinivasan, K.; Jackson, W.C.; and Hinkley, J.A.: "Response of Composite Materials to Low Velocity Impact," *Proceedings of the 36th International SAMPE Symposium*, pp. 850–862, 1991.
70. Sjoblom, P.; and Hwang, B.: "Compression-After-Impact: The \$5,000 Data Point!," *Proceedings of the 34th International SAMPE Symposium*, pp. 1411–1421, 1989.
71. Nettles, A.T.; and Hodge, A.J.: "Compression-After-Impact Testing of Thin Composite Materials," *Proceedings of the 23rd International SAMPE Technical Conference*, pp. 177–183, 1991.
72. Manders, P.W.; and Harris, W.C.: "A Parametric Study of Composite Performance in Compression-After-Impact Testing," *SAMPE Journal*, Vol. 22, No. 6, pp. 47–51, November/December 1986.

73. Tsai, X.; and Tang, J.: "The Impact Behavior of Laminated Glass Fiber Composites by Weight Dropping Testing Method," *Proceedings of the 36th International SAMPE Symposium*, pp. 1118–1127, 1991.
74. Kinsey, A.; Saunders, D.E.J.; and Soutis, C.: "Post-Impact Compressive Behavior of Low Temperature Curing Woven CFRP Laminates," *Composites*, Vol. 26, No. 9, pp. 661–667, 1995.
75. Dempsey, R.L.; and Horton, R.E.: "Damage Tolerance Evaluation of Several Elevated Temperature Graphite Composite Materials," *Proceedings of the 35th International SAMPE Symposium*, pp. 1292–1305, 1990.
76. Starnes, J.H., Jr.; Rhodes, M.D.; and Williams, J.G.: "The Effect of Impact Damage and Circular Holes on the Compressive Strength of a Graphite-Epoxy Laminate," *NASA Technical Memorandum 78796*, 1978.
77. Byers, B.A.: "Behavior of Damaged Graphite/Epoxy Laminates Under Compression Loading," *NASA CR 159293*, 1980.
78. Moon, D.; and Shively, J.H.: "Towards a Unified Method of Causing Impact Damage in Thick Laminated Composites," *Proceedings of the 35th International SAMPE Symposium*, pp. 1466–1478, 1990.
79. Nettles, A.T.; Lance, D.G.; and Hodge, A.J.: "Damage Tolerance of Candidate Thermoset Composites for Use on Single Stage to Orbit Vehicles," *NASA Technical Paper 3506*, 1994.
80. Jones, R., "Residual Strength of Composites With Multiple Impact Damage," *Composite Structures*, Vol. 28, pp. 347–356, 1994.
81. Gong, J.C.; and Sankar, B.V.: "Impact Properties of Three-Dimensional Braided Graphite/Epoxy Composites," *Journal of Composite Materials*, Vol. 25, pp. 715–731, June 1991.
82. Evans, D.A.; and Boyce, J.S.: "Transverse Reinforcement Methods for Improved Delamination Resistance," *Proceedings of the 34th International SAMPE Symposium*, pp. 271–282, 1989.
83. Yamashita, S.; Hatta, H.; Takei, T.; and Sugano, T.: "Interlaminar Reinforcement of Laminated Composites by Addition of Oriented Whiskers in the Matrix," *Journal of Composite Materials*, Vol. 26, No. 9, pp. 1254–1268, 1992.
84. Ko, F.K.; and Hartman, D.: "Impact Behavior of 2-D and 3-D Glass/Epoxy Composites," *Sampe Journal*, Vol. 22, No. 4, pp. 26–30, July/August 1986.
85. Dransfield, K.; Baillie, C.; and Mai, Y.W.: "Improving the Delamination Resistance of CFRP by Stitching—A Review," *Composites Science and Technology*, Vol. 50, pp. 305–317, 1994.

86. Lu, W.H.; Liao, F.S.; Su, A.C.; Kao, P.W.; and Hsu, T.J.: "Effect of Interleaving on the Impact Response of a Unidirectional Carbon/Epoxy Composite," *Composites*, Vol. 26, No. 3, pp. 215–222, 1995.
87. Elber, W.: "Toughening of Graphite/Epoxy Composites by Interlaminar Perforated Mylar Films," *NASA Technical Memorandum 78643*, 1978.
88. Norman, T.L.; and Sun, C.T.: "Delamination Growth in Composite Laminates with Adhesive Strips Subjected to Static and Impact Loading," *Composites Science and Technology*, Vol. 46, pp. 203–211, 1993.
89. Marom, G.; Drukker, E.; Weinberg, A.; and Banbaji, J.: "Impact Behavior of Carbon/Kevlar Hybrid Composites," *Composites*, Vol. 17, No. 2, pp. 150–153, April 1986.
90. Adams, D.F.; and Zimmerman, R.S.: "Static and Impact Performance of Polyethylene Fiber/Graphite Fiber Hybrid Composites," *SAMPE Journal*, Vol. 22, No. 6, pp. 10–16, November/December 1986.
91. Phillips, M.G.: "Fracture and Fatigue of Hybrid Composites," in *Fibre Composite Hybrid Materials*, N.L. Hancox, ed., MacMillan Publishing Co., Inc., NY, pp. 119–162, 1981.
92. Peijs, A.A.J.M.; Venderbosch, R.W.; and Lemstra, P.J.: "Hybrid Composites Based on Polyethylene and Carbon Fibers, Part 3: Impact Resistant Structural Composites Through Damage Management," *Composites*, Vol. 21, No. 6, pp. 522–530, November 1990.
93. Busgen, A.W.; Effing, M.; and Scholle, M.: "Improved Damage Tolerance of Carbon Fibre Composites by Hybridization with Polyethylene Fibre, Dyneema SK60," *Proceedings of the American Society for Composites Fourth Technical Conference*, pp. 418–423, 1989.
94. Nettles, A.T.; and Lance, D.G.: "On the Enhancement of Impact Damage Tolerance of Composite Laminates," *Composites Engineering*, Vol. 3, No. 5, pp. 383–394, 1993.
95. Jang, B.Z.; Chen, L.C.; Wang, C.Z.; Lin, H.T.; and Zee, R.H.: "Impact Resistance and Energy Absorption Mechanisms in Hybrid Composites," *Composites Science and Technology*, Vol. 34, pp. 305–335, 1989.
96. Demuts, E.; and Sharpe, P.: "Tougher Advanced Composite Structures," *American Institute for Aeronautics and Astrionics Paper 87-0794*.
97. Ghasemi Nejhad, M.N.; and Parvizi-Majidi, A.: "Impact Behavior and Damage Tolerance of Woven Carbon Fibre-Reinforced Thermoplastic Composites," *Composites*, Vol. 21, No. 2, pp. 155–168, March 1990.

98. Recker, H.G.; Altstadt, V.; Eberle, W.; Folda, T.; Gerth, D.; Heckmann, W.; Ittemann, P.; Tesch, H.; and Weber, T.: "Toughened Thermosets for Damage Tolerant Carbon Fiber Reinforced Composites," *SAMPE Journal*, Vol. 26, No. 2, pp. 73–78, March/April 1990.
99. Lance, D.G.; and Nettles, A.T.: "Low Velocity Instrumented Impact Testing of Four New Damage Tolerant Carbon/Epoxy Composite Systems," *NASA Technical Paper 3029*, 1990.
100. Cantwell, W.J.; and Morton, J.: "Comparison of the Low and High Velocity Impact Response of CFRP," *Composites*, Vol. 20, No. 6, pp. 545–551, November 1989.
101. Cantwell, W.J.; and Morton, J.: "Geometrical Effects in the Low Velocity Impact Response of CFRP," *Composite Structures*, Vol. 12, pp. 39–59, 1989.
102. Verpoest, I.; Marien, J.; Devoes, J.; and Wevers, M.: "Is Absorbed Energy a Test Independent Parameter for Damage and Residual Strength After Impact?," *Proceedings of the Second International Conference on Testing, Evaluation and Quality Control of Composites—TEQC 87*, pp. 69–77, September 1987.
103. Robinson, P.; and Davies, G.A.O.: "Impactor Mass and Specimen Geometry Effects in Low Velocity Impact of Laminated Composites," *International Journal of Impact Engineering*, Vol. 12, No. 2, pp. 189–207, 1992.
104. Shivakumar, K.N.; Elber, W.; and Illg, W.: "Prediction of Impact Force and Duration Due to Low-Velocity Impact on Circular Composite Laminates," *Transactions of the ASME*, Vol. 52, pp. 674–680, September 1985.
105. Poe, C.C., Jr.: "Relevance of Impacter Shape to Nonvisible Damage and Residual Tensile Strength of a Thick Graphite/Epoxy Laminate," *NASA Technical Memorandum 102599*, 1990.
106. Morton, J.: "Scaling of Impact Loaded Carbon Fiber Composites," *AIAA Journal*, Vol. 26, No. 8, pp. 989–994, 1988.
107. Swanson, S.R.: "Scaling of Impact Damage in Fiber Composites from Laboratory Specimens to Structures," *Composite Structures*, Vol. 25, pp. 249–255, 1993.
108. Bucinell, R.B.; Madsen, C.B.; Nuismer, R.J.; Benzinger, S.T.; and Morgan, M.E.: "Experimental Investigation of Scaling Impact Response and Damage in Composite Rocket Motor Cases," *Proceedings, JANNAF Composite Motor Case and Structures and Mechanical Behavior Meeting*, Jet Propulsion Laboratory, Anaheim, CA, November 7–9, 1989.
109. Chen, V.L.; Wu, H.Y.T.; and Yeh, H.Y.: "A Parametric Study of Residual Strength and Stiffness for Impact Damaged Composites," *Composite Structures*, Vol. 25, pp. 267–275, 1993.

110. Horton, R.E.; and McCarty, J.E.: "Damage Tolerance of Composites," in *Engineered Materials Handbook, Vol. 1—Composites*. ASME International, Metals Park, OH, pp. 264–270, 1988.
111. Olster, E.F.; and Roy, P.A.: "Tolerance of Advanced Composites to Ballistic Damage," *Composite Materials: Testing and Design (Third Conference)*, *ASTM STP 546*, pp. 583–603, 1974.
112. Sharma, A.V.: "Low-Velocity Impact Tests on Fibrous Composite Sandwich Structures," *Test Methods and Design Allowables for Fibrous Composites*, *ASTM STP 734*, pp. 54–70, 1981.
113. Avva, V.S.: "Impact Initiated Damage in Laminated Composites," *AFOSR TR 82-1038*, 1982.
114. Avva, V.S.: "Fatigue/Impact Studies on Laminated Composites," *AFWAL TR 83-3060*, May 1983.
115. Avva, V.S.; Vala, J.R.; and Jeyaseelan, M.: "Effect of Impact and Fatigue Loads on the Strength of Graphite/Epoxy Composites," *Composite Materials: Testing and Design (Seventh Conference)*, *ASTM STP 893*, pp. 196–206, 1986.
116. Rhodes, M.D.; Williams, J.G.; and Starnes, J.H., Jr.: "Low-Velocity Impact Damage in Graphite-Fiber Reinforced Epoxy Laminates," *Polymer Composites*, Vol. 2, No. 1, pp. 36–44, January 1981.
117. Starnes, J.H.; Rhodes, M.D.; and Williams, J.G.: "Effect of Impact Damage and Holes on the Compressive Strength of a Graphite/Epoxy Laminate," *Nondestructive Evaluation and Flaw Criticality for Composite Materials*, *ASTM STP 696*, pp. 145–171, 1979.
118. Park, N.: "The Impact Response of Composites Under Stress," *IMEchE Paper No. C400/019*, pp. 137–142, 1990.
119. Sankar, B.V.; and Sun, C.T.: "Low-Velocity Impact Damage in Graphite-Epoxy Laminates Subjected to Tensile Initial Stresses," *AIAA Journal*, Vol. 24, No. 3, pp. 470–471, 1985.
120. Nettles, A.T.; and Lance, D.G.: "The Effects of Compressive Preloads on the Compression-After-Impact Strength of Carbon Epoxy," *NASA Technical Paper 3303*, 1992.
121. Robb, M.D.; Arnold, W.S.; and Marshall, I.H.: "The Damage Tolerance of GRP Laminates Under Biaxial Prestress," *Composite Structures*, Vol. 32, pp. 141–149, 1995.
122. Sun, C.T.; and Chen, J.K.: "On the Impact of Initially Stressed Composite Laminates," *Journal of Composite Materials*, Vol. 19, pp. 490–504, November 1985.

123. Chen, J.K.; and Sun, C.T.: "Dynamic Large Deflection Response of Composite Laminates Subjected to Impact," *Composite Structures*, Vol. 4, pp. 59–73, 1985.
124. Sun, C.T.; and Chattopadhyay, S.: "Dynamic Response of Anisotropic Laminated Plates Under Initial Stress to Impact of a Mass," *Journal of Applied Mechanics*, pp. 693–698, September 1975.
125. Bert, C.W.; and Birman, V.: "Response of Prestressed Cylindrically Curved Composite Structures Subjected to Low-Velocity Impact," *Proceedings of the Fourth Japan–U.S. Conference on Composite Materials*, American Society for Composites, pp. 43–52, 1988.
126. Pipes, R.B.; and Pagano, N.J.: "Interlaminar Stresses in Composite Laminates Under Uniform Axial Extension," *Journal of Composite Materials*, Vol. 4, pp. 538–548, October 1970.
127. Pipes, R.B.; and Daniel, I.M.: "Moire Analysis of the Interlaminar Shear Edge Effect in Laminated Composites," *Journal of Composite Materials*, Vol. 5, pp. 255–259, April 1971.
128. Pagano, N.J.; and Pipes, R.B.: "The Influence of Stacking Sequence on Laminate Strength," *Journal of Composite Materials*, Vol. 5, pp. 50–57, January 1971.
129. Madsen, C.B.; Morgan, M.E.; and Nuismer, R.J.: "Subelement Validation for Damage Assessment for Composite Cases," *Phillips Laboratory Technical Report #93–3015*, April 1993.

APPROVAL

THE IMPACT RESPONSE OF CARBON/EPOXY LAMINATES (MSFC Center Director's Discretionary Fund Final Report, Project No. 94-13)

A.T. Nettles and A.J. Hodge

The information in this report has been reviewed for technical content. Review of any information concerning Department of Defense or nuclear energy activities or programs has been made by the MSFC Security Classification Officer. This report, in its entirety, has been determined to be unclassified.



Dr. A.F. Whitaker
DIRECTOR, MATERIALS and PROCESSES LABORATORY

REPORT DOCUMENTATION PAGE			Form Approved OMB No. 0704-0188	
Public reporting burden for this collection of information is estimated to average 1 hour per response, including the time for reviewing instructions, searching existing data sources, gathering and maintaining the data needed, and completing and reviewing the collection of information. Send comments regarding this burden estimate or any other aspect of this collection of information, including suggestions for reducing this burden, to Washington Headquarters Services, Directorate for Information Operation and Reports, 1215 Jefferson Davis Highway, Suite 1204, Arlington, VA 22202-4302, and to the Office of Management and Budget, Paperwork Reduction Project (0704-0188), Washington, DC 20503				
1. AGENCY USE ONLY (Leave Blank)		2. REPORT DATE November 1997		3. REPORT TYPE AND DATES COVERED Technical Memorandum
4. TITLE AND SUBTITLE The Impact Response of Carbon/Epoxy Laminates MSFC Center Director's Discretionary Fund Final Report, Project No. 94-13			5. FUNDING NUMBERS	
6. AUTHORS A.T. Nettles and A.J. Hodge				
7. PERFORMING ORGANIZATION NAME(S) AND ADDRESS(ES) George C. Marshall Space Flight Center Marshall Space Flight Center, Alabama 35812			8. PERFORMING ORGANIZATION REPORT NUMBER M-844	
9. SPONSORING/MONITORING AGENCY NAME(S) AND ADDRESS(ES) National Aeronautics and Space Administration Washington, DC 20546-0001			10. SPONSORING/MONITORING AGENCY REPORT NUMBER NASA/TM-97-206317	
11. SUPPLEMENTARY NOTES Prepared by Materials and Processes Laboratory, Science and Engineering Directorate				
12a. DISTRIBUTION/AVAILABILITY STATEMENT Subject Category 39 Unclassified-Unlimited Nonstandard Distribution			12b. DISTRIBUTION CODE	
13. ABSTRACT (Maximum 200 words) Low velocity dropweight impact tests were conducted on carbon/epoxy laminates under various boundary conditions. The composite plates were 8-ply (+45,0,-45,90)s laminates supported in a clamped-clamped/free-free configuration with varying amounts of in-plane load, Nx, applied. Specimens were impacted at energies of 3.4, 4.5, and 6 Joules (2.5, 3.3, and 4.4 ft-lb). The amount of damage induced into the specimen was evaluated using instrumented impact techniques, x-ray inspection, and cross-sectional photomicroscopy. Some static indentation tests were performed to examine if the impact events utilized in this study were of a quasi-static nature and also to gain insight into the shape of the deflected surface at various impact load combinations. Load-displacement curves from these tests were compared to those of the impact tests, as was damage determined from x-ray inspection. The finite element technique was used to model the impact event and determine the stress field within the laminae. Results showed that for a given impact energy level, more damage was induced into the specimen as the external in-plane load, Nx, was increased. The majority of damage observed consisted of back face splitting of the matrix parallel to the fibers in that ply, associated with delaminations emanating from these splits. The analysis showed qualitatively the results of impact conditions on maximum load of impact, maximum transverse deflection, and first failure mode and location.				
14. SUBJECT TERMS composite materials, impact, damage tolerance			15. NUMBER OF PAGES 176	
			16. PRICE CODE A09	
17. SECURITY CLASSIFICATION OF REPORT Unclassified	18. SECURITY CLASSIFICATION OF THIS PAGE Unclassified	19. SECURITY CLASSIFICATION OF ABSTRACT Unclassified	20. LIMITATION OF ABSTRACT Unlimited	